SCUOLA INTERNAZIONALE SUPERIORE DI STUDI AVANZATI
INTERNATIONAL SCHOOL FOR ADVANCED STUDIES
Physics Area
Astroparticle Physics Curriculum

The Nature of Massive Neutrinos and Unified Theories of Flavour

Thesis submitted for the degree of
Doctor Philosophiæ

SUPERVISOR:
Prof. S. T. Petcov

CANDIDATE:
A. Meroni

September 2013

To the memory of Francesco Caracciolo

Natura Artis Magistra

Abstract

The present Ph.D. thesis is devoted to two fundamental unsolved problems of neutrino physics, which are intimately connected: determining the nature - Dirac or Majorana - of massive neutrinos, which is related with the possibility of existence of New Physics beyond that predicted by the Standard Model (SM) of particle interactions, and, discovering the origin of the patterns of neutrino masses and of leptonic mixing, stemming from new underlying symmetries in the neutrino, charged lepton and quark sectors. The remarkable experimental efforts of the last 15 years or so have delivered an enormous amount of data that have to be explained in terms of possibly economic and simple theoretical models. Moreover, exciting times are ahead of us. Currently running and future upcoming experiments under construction aim at i) high precision measurement of the parameters characterizing the neutrino oscillations, ii) identifying the neutrino mass hierarchy, and iii) establishing the status of the CP symmetry in the leptonic sector by searching for CP violation effects in neutrino oscillations. In addition, significant experimental efforts are been made to unveil the possible Majorana nature of massive neutrinos by searching for neutrinoless double beta ($(\beta\beta)_{0\nu}$-) decay with increasing sensitivity. Unique data on the absolute scale of neutrino masses, which is unknown at present, is expected to be provided by β-decay experiments under preparation. The first part of the Ph.D. thesis is devoted to the problem of extracting information about the New Physics if it will be experimentally established via the observation of the $(\beta\beta)_{0\nu}$-decay that the massive neutrinos are Majorana particles. In this case new couplings, changing the total lepton charge $L = L_e + L_\mu + L_\tau$ by two units, must be admitted in the Lagrangian of particle interactions and there is the possibility that more than one such coupling is operative in $(\beta\beta)_{0\nu}$-decay. We discuss four such couplings (arising in seesaw and Right-Left (L-R) symmetric models and in supersymmetric extensions of the SM with R-parity nonconservation) and analyze in detail the possibility to determine which couplings, if any, might be involved in $(\beta\beta)_{0\nu}$-decay from data on the $(\beta\beta)_{0\nu}$-decay half-lives of several different isotopes. In the second part of the Ph.D thesis we analyze the neutrino flavour problem in connection with new underlying symmetries in the leptonic sector. The existence of an organizing principle which could explain the pattern of masses and mixing of the neutrinos is explored in two different approaches based on the use of finite discrete non-Abelian groups. A unified model of flavour based on the symmetry group $SU(5) \times T'$, incorporating the seesaw mechanism of neutrino mass generation is constructed and the predictions of this model for the neutrino mixing angles, the Dirac and Majorana CP violation phases in the neutrino mixing matrix, the sum of neutrino masses and for the $(\beta\beta)_{0\nu}$-decay effective Majorana mass are derived. The model can be tested in the future planned neutrino physics experiments.

Contents

Chapter 1

Motivations and Goals

Measure what can be measured, and make measurable what it is not.

G. Galileo

The present Ph. D. Thesis is devoted to aspects of the physics of massive neutrinos and neutrino mixing and to the problem of flavour in particle physics.

There has been an extraordinary progress in the field of neutrino physics in the last 15 years or so. In this period compelling experimental evidences for flavour neutrino oscillations [1–4], transitions in flight between the different flavour neutrinos ν_e, ν_μ, ν_τ (antineutrinos $\bar{\nu}_e$, $\bar{\nu}_\mu$, $\bar{\nu}_\tau$), caused by nonzero neutrino masses and neutrino mixing, were obtained, and the parameters which characterize the oscillations were determined with a relatively high precision. As a consequence, the existence of nonzero neutrino masses and neutrino mixing was firmly established.

In spite of this impressive progress we still do not know what is the origin of neutrino masses and mixing and we are completely ignorant about some of the fundamental aspects of neutrino mixing. More specifically, we still do not have even lightest hints about

- whether the massive neutrinos are Dirac or Majorana particles [5],
- what kind of spectrum —normal hierarchical, inverted hierarchical, with partial hierarchy, or quasi-degenerate— the neutrino masses obey,
- what is the absolute scale of neutrino masses,
- what is the status of the CP symmetry in the lepton sector.

Determining the nature —Dirac or Majorana— of massive neutrinos is one of the most pressing and challenging problems in the field of neutrino physics (see, e.g., [6–8]). It is also one of the fundamental problems of contemporary particle physics. Establishing whether the neutrinos with definite mass ν_j are Dirac fermions possessing distinct antiparticles, or Majorana fermions, i.e., spin 1/2 particles that are identical with their antiparticles, is of fundamental importance for understanding the origin of ν-masses and mixing and the underlying symmetries of the Lagrangian of particle interactions. The neutrinos ν_j with definite mass m_j will be Dirac fermions if particle interactions conserve some additive lepton number, e.g., the total lepton charge $L = L_e + L_\mu + L_\tau$. If no lepton charge is conserved, the neutrinos ν_j will be Majorana fermions (see, e.g.,

[9]). One of the simplest realization in which the massive neutrinos are predicted to be of Majorana nature is the see-saw mechanism of neutrino mass generation [10–13], which also provides an attractive explanation of the smallness of neutrino masses and, through the leptogenesis theory [14, 15] (see also, e.g., [16, 17]), of the observed baryon asymmetry of the Universe. The observed patterns of neutrino mixing and of neutrino mass squared differences driving, e.g., the solar and the dominant atmospheric neutrino oscillations, can be related to Majorana massive neutrinos and to the existence of an *approximate* symmetry in the lepton sector, which can be continuous (corresponding, e.g., to the conservation of the *non-standard* lepton charge $L' = L_e - L_\mu - L_\tau$ [18]), or discrete (see, e.g., [8, 19, 20]).

Determining the type of spectrum the neutrino masses obey is also of crucial importance for making progress in our understanding of the origin of neutrino masses and mixing. Getting information about the status of CP symmetry in the lepton sector might allow us to make progress in the understanding of the origin of the observed matter-antimatter asymmetry of the Universe.

This is an exciting time in neutrino physics. Answering the fundamental questions about the nature of massive neutrinos, the type of neutrino mass spectrum, the status of the CP symmetry in the lepton sector and and absolute neutrino mass scale is the main goal of the programme of worldwide future research in neutrino physics. We have entered the "golden age" of high precision measurements, tests and searches in this field.

In the next 10-15 years or so, even more precise measurements of the neutrino oscillation parameters will be performed. There is a remarkable experimental effort aiming to establish whether the massive neutrinos are Dirac or Majorana particles by searching for neutrinoless double beta ($(\beta\beta)_{0\nu}$-) decay, $(A, Z) \to (A, Z+2) + e^- + e^-$, with increasing sensitivity and variety of isotopes. We will discuss this effort in detail in Part I.

A rich experimental activity is under preparation for determination of the neutrino mass hierarchy. This includes:
i) long base-line neutrino oscillation experiments at existing accelerators (e.g., T2K (which is operational), NOνVA (under construction), etc.);
ii) reactor neutrino oscillation experiments (Daya Bay II and RENO50 projects) with a base-line of $\sim (50 - 60)$ km;
iii) the next generation of atmospheric neutrino oscillation experiments (INO-ICAL in India, the PINGU project within the IceCube experiment at the South Pole, the planned Hyper Kamiokande experiment in Japan, etc.);
iv) the planned (very) Long Base-Line (LBL) neutrino Oscillation experiments (such as the LBNE in U.S.A. and the mostly European LAGUNA-LBNO projects).
Searches for CP violation effects in neutrino oscillations are planned to be performed by the T2K, NOνVA, LBNO and LBNE experiments. These experiments will provide important information about the status of the CP symmetry in the lepton sector.
Unique data on the absolute scale of neutrino masses is expected to be provided by the ^3H β-decay experiments like KATRIN, which is under preparation.

In the next Section we give a more detailed overview of the status of research in neutrino physics and describe the implications in neutrino physics (and in particle physics, in general) of the data which are and will be available from the past, the currently running and future experiments. We first describe the three neutrino mixing framework, introducing the notation used in the Ph. D. Thesis. We then review the

current experimental data on the oscillation parameters and the existing limits on the absolute scale of masses of the three light neutrinos. We introduce next two of the main fundamental problems in neutrino physics that are addressed in this Thesis: the problem of the nature of massive neutrinos and the origin of the absolute scale of neutrino masses.

I The three neutrino mixing framework

In the formalism used to construct the Standard Model (SM), the existence of a non-trivial neutrino mixing and massive neutrinos implies that the left-handed (LH) flavour neutrino fields $\nu_{l\mathrm{L}}(x)$, which enter into the expression for the lepton current in the charged current weak interaction Lagrangian, are linear combinations of the fields of three (or more) neutrinos ν_j, having masses $m_j \neq 0$:

$$\nu_{l\mathrm{L}}(x) = \sum_j U_{lj}\, \nu_{j\mathrm{L}}(x), \quad l = e, \mu, \tau, \tag{1.1}$$

where $\nu_{j\mathrm{L}}(x)$ is the LH component of the field of ν_j possessing a mass $m_j \geq 0$ and U is a unitary matrix —the Pontecorvo-Maki-Nakagawa-Sakata (PMNS) neutrino mixing matrix [3, 4, 9], $U \equiv U_{\mathrm{PMNS}}$. Similarly to the Cabibbo-Kobayashi-Maskawa (CKM) quark mixing matrix, the leptonic matrix U_{PMNS}, is described (to a good approximation) by a 3×3 unitary mixing matrix. In the widely used standard parametrization [6], U_{PMNS} is expressed in terms of the solar, atmospheric and reactor neutrino mixing angles θ_{12}, θ_{23} and θ_{13}, respectively, and one Dirac - δ, and two (eventually) Majorana [21] - α_{21} and α_{31}, CP violating phases:

$$U_{\mathrm{PMNS}} \equiv U = V(\theta_{12}, \theta_{23}, \theta_{13}, \delta)\, Q(\alpha_{21}, \alpha_{31})\,, \tag{1.2}$$

where

$$V = \begin{pmatrix} 1 & 0 & 0 \\ 0 & c_{23} & s_{23} \\ 0 & -s_{23} & c_{23} \end{pmatrix} \begin{pmatrix} c_{13} & 0 & s_{13}e^{-i\delta} \\ 0 & 1 & 0 \\ -s_{13}e^{i\delta} & 0 & c_{13} \end{pmatrix} \begin{pmatrix} c_{12} & s_{12} & 0 \\ -s_{12} & c_{12} & 0 \\ 0 & 0 & 1 \end{pmatrix}, \tag{1.3}$$

and we have used the standard notation $c_{ij} \equiv \cos\theta_{ij}$, $s_{ij} \equiv \sin\theta_{ij}$, the allowed range for the values of the angles being $0 \leq \theta_{ij} \leq \pi/2$, and

$$Q = \mathrm{Diag}(1, e^{i\alpha_{21}/2}, e^{i\alpha_{31}/2})\,. \tag{1.4}$$

The neutrino oscillation data, accumulated over many years, allowed to determine the frequencies and the amplitudes (i.e. the angles and the mass squared differences) which drive the solar and atmospheric neutrino oscillations, with a rather high precision (see, e.g., [6]). Furthermore, there were spectacular developments in the period June 2011 - June 2012 year in what concerns the CHOOZ angle θ_{13}. In June of 2011 the T2K collaboration reported [22] evidence at 2.5σ for a non-zero value of θ_{13}. Subsequently the MINOS [23] and Double Chooz [24] collaborations also reported evidence for $\theta_{13} \neq 0$, although with a smaller statistical significance. Global analysis of the neutrino oscillation data, including the data from the T2K and MINOS experiments, performed in [25], showed that actually $\sin\theta_{13} \neq 0$ at $\geq 3\sigma$. In March of 2012 the first data of the Daya Bay reactor antineutrino experiment on θ_{13} were published [26]. The value

of $\sin^2 2\theta_{13}$ was measured with a rather high precision and was found to be different from zero at 5.2σ:

$$\sin^2 2\theta_{13} = 0.092 \pm 0.016 \pm 0.005\,. \tag{1.5}$$

Subsequently, the RENO experiment reported a 4.9σ evidence for a non-zero value of θ_{13} [27], compatible with the Day Bay result:

$$\sin^2 2\theta_{13} = 0.113 \pm 0.013 \pm 0.019\,. \tag{1.6}$$

The results on θ_{13} described above will have far reaching implications for the program of future research in neutrino physics (see, e.g., [28]). In Table 1.1 we list the best fit values of the angles parametrising the PMNS mixing matrix with 1σ uncertainty coming form two of the latest global fits analysis which combine results from several experiments [29, 30]. From the 3σ allowed intervals obtained in [29] we can write the numerical expression for $|U_{\rm PMNS}|$:

$$|U_{\rm PMNS}| = \begin{pmatrix} 0.788 - 0.853 & 0.505 - 0.590 & 0.130 - 0.177 \\ 0.474 - 0.481 & 0.398 - 0.666 & 0.570 - 0.785 \\ 0.201 - 0.393 & 0.549 - 0.703 & 0.593 - 0.811 \end{pmatrix}. \tag{1.7}$$

Parameter	Fogli et al. [29]	Gonzalez-Garcia et al. [30]
$\Delta m^2_{21}[10^{-5}\text{eV}^2]$	$7.54^{+0.26}_{-0.22}$	7.50 ± 0.185
$\Delta m^2_{31}[10^{-3}\text{eV}^2]$	$2.43^{+0.06}_{-0.10}$ $-2.42^{+0.11}_{-0.07}$	$2.47^{+0.069}_{-0.067}$ $-2.43^{+0.042}_{-0.065}$
$\sin^2\theta_{12}$	$0.307^{+0.018}_{-0.016}$	0.30 ± 0.013
$\sin^2\theta_{23}$	$0.386^{+0.024}_{-0.021}$ $0.392^{+0.039}_{-0.022}$	$0.41^{+0.037}_{-0.025}$ $0.41^{+0.037}_{-0.025} \oplus 0.59^{+0.021}_{-0.022}$
$\sin^2\theta_{13}$	0.0241 ± 0.0025 $0.0244^{+0.0023}_{-0.0025}$	0.023 ± 0.0023

Table 1.1: The table summarizes two recent global fit analysis for the neutrino oscillation parameters corresponding to 1σ uncertainty. For Δm^2_{31}, $\sin^2\theta_{23}$ and $\sin^2\theta_{13}$ the upper (lower) row corresponds to normal (inverted) neutrino mass ordering. These values and the methods to extract them from experimental data are discussed in respectively in [29] and [30].

The experimental data we have summarized in Table 1.1 are compatible with different neutrino mass patterns (see Figure 1.1):

- *spectrum with normal ordering (NO)*, $m_1 < m_2 < m_3$, corresponding to $\Delta m^2_{\odot} \equiv \Delta m^2_{21} > 0$ and $\Delta m^2_A \equiv \Delta m^2_{31} > 0$;
- *spectrum with inverted ordering (IO)*, $m_3 < m_1 < m_2$, corresponding to $\Delta m^2_{\odot} \equiv \Delta m^2_{21} > 0$ and $\Delta m^2_A \equiv \Delta m^2_{32} < 0$.

Depending on the value of the light neutrino mass $min(m_j)$, the neutrino mass spectrum can be:

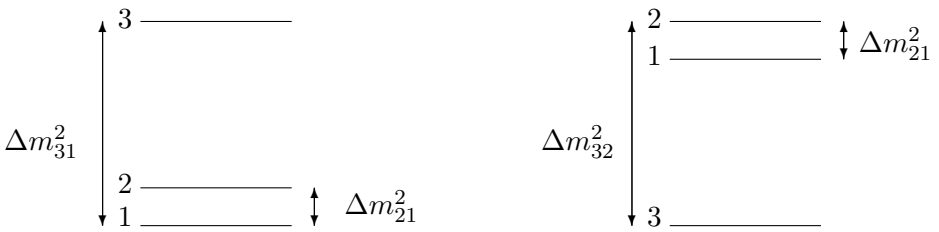

Figure 1.1: The two possible neutrino mass spectra: with normal ordering (NO, left) and with inverted ordering (IO, right).

- *normal hierarchical (NH)*: $m_1 \ll m_2 < m_3$ so $m_2 \sim \sqrt{\Delta m^2_{\odot}}$, $m_3 \sim \sqrt{\Delta m^2_A}$
- *inverted hierarchical (IH)*: $m_3 \ll m_1 < m_2$ so $m_{1,2} \sim \sqrt{\Delta m^2_A}$
- *quasi-degenerate (QD)*: $m_1 \cong m_2 \cong m_3 \cong m_0$, $m_j^2 \gg |\Delta m^2_A|$, i.e. $m_0 > 0.1eV$

It is worth noticing that the global fit analyses we are referring to, [29] and [30], which are performed within the framework of the 3-neutrino mixing, suggest that $\sin^2\theta_{23} \lesssim 1/2$ in the case of NO neutrino mass spectrum. In the IO case the authors of [29] find that $\sin^2\theta_{23} \gtrsim 1/2$, while in [30] two different solutions for $\sin^2\theta_{23}$, slightly below and above the value of 1/2, are found. These results have important consequences from a theoretical point of view in view of the need of finding an economic and simple principle which could explain the patterns of the masses and of the mixing in the neutrino sector.

All the possible types of neutrino mass spectrum are compatible with the experimental constrains on the absolute scale of neutrino masses coming from ^3H β-decay experiments and cosmological/astrophysical data. From ^3H β-decay ($^3H \to {}^3He\ e^-\bar{\nu}_e$ with $Q = m_{^3He} - m_{^3H} = 18.6$ keV), one can measure the spectrum of the electron energy near the end-point and extract the value of $m_{\bar{\nu}_e} \cong \sqrt{\sum_i |U_{ei}|^2 m_i^2}$.

The most stringent upper limit on $m_{\bar{\nu}_e}$ was obtained by the Mainz and Troitzk experiments [31]:

$$m_{\bar{\nu}_e} < 2.3\,eV \quad \text{at } 95\% \text{ C.L.}, \tag{1.8}$$

while the KArlsruhe TRItium Neutrino experiment (KATRIN), which is expected to start the data taking in 2015, will provide data on the absolute scale of neutrino masses with a sensitivity to $m_j \sim 0.2$ eV [32].

Information on the masses of light neutrinos can be obtained also from cosmological observations. In particular the total mass of light active neutrinos, $\Sigma\, m_i$, can be constrained from measurements of the matter power spectrum, $P(\vec{k})$, i.e., a measure of the the variance of the distribution of density fluctuations. An upper bound for the sum of the masses can be obtained from the lack of the suppression of the power spectrum at small scales. This bound is model dependent and varies with the assumptions used in the analysis of the data. The Planck Collaboration [33] recently presented the first cosmological results based on Planck measurements of the cosmic microwave background

(CMB) temperature and lensing-potential power spectra. In [34] the Collaboration provided constraints assuming three species of degenerate massive neutrinos and a ΛCDM model. We give here some results reported in [34] based on the combination of the Planck temperature power spectrum with a WMAP polarization low-multipole ($\ell \leq 23$) and ACT high-multipole ($\ell \geq 2500$) data. We refer to this CMB data combination as Planck+WP. In this case the upper limit on the sum of the neutrino mass reads:

$$\Sigma\, m_i < 0.66\,\text{eV at } 95\%\,\text{C.L. (Planck + WP)}, \tag{1.9}$$

Combining the latter with the Barion Acoustic Oscillation data (BAO), the limit is significantly lowered at

$$\Sigma\, m_i < 0.23\,\text{eV at } 95\%\,\text{C.L. (Planck + WP + BAO)}. \tag{1.10}$$

The above upper limits can be converted into limits on the absolute scale of neutrino masses that read respectively $m_{min} \lesssim 0.22$ eV in the more conservative case (eq. 1.9) and $m_{min} \lesssim 0.07$ eV in the more stringent case (eq. 1.10). This is depicted in Figure 1.2.

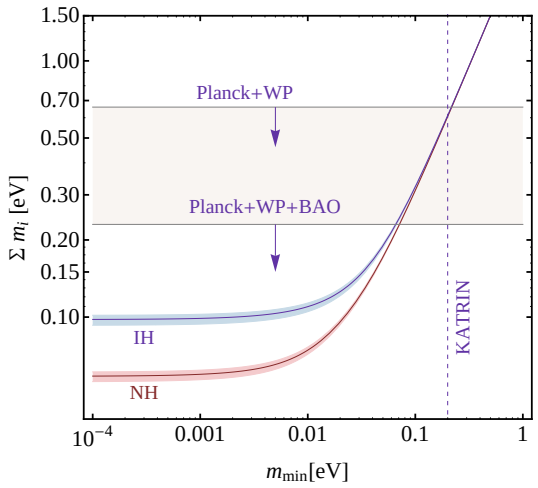

Figure 1.2: The sum of the light neutrino masses plotted as function of the lightest neutrino mass considering the 3σ uncertainty in the atmospheric and solar Δm^2 given in [29]. The horizontal solid lines represent the recent Planck limits. The allowed area is indicated by the arrows.

We have to add that in addition to the Planck Collaboration also the South Pole Telescope (SPT) Collaboration released in December 2012 a fit analysis that indicated a preferred value for the sum of the light neutrino, being the latter $\Sigma\, m_i = 0.32 \pm 0.11$ eV, with a 3σ detection of positive neutrino mass in the range $[0.01, 0.63]$eV at 99.7 % C.L. [35].

Clearly, all these bounds are not definitive and they will be improved by current or forthcoming observations. For instance, the EUCLID survey [36], approved in 2012, will be able most likely to measure the neutrino mass sum at the 0.01 eV level of precision by combining their data with measurements of the CMB anisotropies by the Planck mission [33]. Such an outstanding precision will be able to provide unique information

on, and possibly determine, the absolute scale of neutrino masses [37]: the minimum of the sum compatible with current neutrino oscillation data being $\Sigma_{min} = 5.87 \times 10^{-2}$ eV for a normal hierarchical (NH) spectrum and $\Sigma_{min} = 9.78 \times 10^{-2}$ eV for an inverted hierarchical spectrum (IH). This information could be used in synergy with $(\beta\beta)_{0\nu}$-decay data to test the nature —Dirac or Majorana— of massive neutrinos.

II On the origin of neutrino masses

One of the unsolved issues in neutrino physics is the origin of the scale of the masses of the three light active neutrinos [6]. The evidence of neutrino oscillations, and thus the existence of at least three neutrino states, impose to include them in the SM. Their tiny masses make them unique when compared to the masses of the charged leptons and quarks. Taking, for instance, the indicative neutrino mass upper limit of $m_j < 0.5$ eV, one finds that the neutrino masses are at least 10^6 times smaller than the mass of the lightest charged fermion in the SM - the electron. This enormous disparity between the neutrino masses and the masses of the charged leptons and quarks suggests that the neutrino masses might be related to the existence of new fundamental mass scale in particle physics, associated with the existence of New Physics (NP) beyond that predicted by the SM. This idea has a number of natural realizations in the case when that massive neutrinos are Majorana particles. In this case one can generate the neutrino masses, e.g., through the effective five-dimension operator, the so-called Weinberg operator [38]:

$$\delta\mathcal{L}^{d=5} \supset C_{l'l}^{d=5} \frac{(\overline{\psi^c_{l'L}}\tilde{\phi}^*)(\tilde{\phi}^\dagger \psi_{lL})}{\Lambda} \xrightarrow{SSB} \quad C_{l'l}^{d=5} v^2 \frac{\overline{(\nu_{l'L})^c}\nu_{lL}}{\Lambda}, \tag{1.11}$$

where ψ_{lL} is the SM left-handed doublet $\psi_{lL}^T = (\nu_{lL}, l_L)^T$, $C_{l'l}^{d=5}$ are constants and $\phi^T = (\phi^0, \phi^-)$ is the SM Higgs doublet field with $\tilde{\phi} = i\sigma_2\phi$ with $v = 174$ GeV being the Higgs doublet vacuum expectation value (vev). The operator is suppressed at the scale Λ which can be identified with the scale of New Physics.

If we do not want to spoil the Lorentz invariance, the gauge invariance and the renormalizability of the SM, the only way to generate the operator in eq. (1.11) is to enlarge the field content of the SM. Possible relevant extensions of the SM can be, for instance, i) in the Higgs sector only, ii) in the lepton sector only, and ii) in both the lepton and the Higgs sectors. These extension are generally called see-saw mechanisms and provide a Majorana mass term for the light neutrinos and, most importantly, a natural explanation of the smallness of the neutrino masses. The basic see-saw scenarios have different realizations depending on the nature of the heavy fields present.

- SM fermion $SU(2)$ singlet (called see-saw type I) [10–13, 39]
- SM $SU(2)$ triplet scalars (sometimes called see-saw type II) [40–43]
- SM $SU(2)$ triplet fermion (called see-saw type III) [44]

We will focus here on the first possibility, i.e., introducing three SM $SU(2)$ singlets - sterile right-handed (RH) neutrino states N_{Ri} with $i = 1, 2, 3$. Then, a simple realization of the operator in eq. (1.11) is through the following Dirac—Majorana renormalizable mass terms:

$$\mathcal{L}_{Y+M} = -(M_D)_{l'l}(\bar{\nu}_{l'L}\tilde{\phi})N_{lR} - \frac{1}{2}\overline{(N_{l'R})^c}(M^R)_{l'l}N_{lR} + h.c. \tag{1.12}$$

here $M_D = Y_\nu v$ where Y_ν is the matrix of neutrino Yukawa coupling, v is the Higgs vev and M^R is the Majorana mass term for the RH neutrino states.

When the electroweak symmetry is spontaneously broken, the neutrino Yukawa coupling generates a neutrino Dirac mass term. For $|M_D| \ll |M_R|$ the iterplay of the neutrino Dirac mass term and the Majorana mass term of the RH neutrinos induces effectively a Majorana mass term for the LH flavour neutrinos:

$$M_\nu = -v^2 Y_\nu (M^R)^{-1} Y_\nu^T \equiv -M_D (M^R)^{-1} M_D^T. \tag{1.13}$$

In grand unified theories (GUTs), M_D is typically of the order of the charged fermion masses. For example in theories based on the gauge group SO(10), M_D coincides with the up-quark mass matrix. Taking indicatively $M_\nu \sim 0.1$ eV, $M_D \sim 100$ GeV, one gets $M_R \sim 10^{14}$ GeV. This value is close to the scale of unification of the electroweak and strong interactions, $M_{GUT} \backsimeq 2 \times 10^{16}$ GeV. In GUT theories with RH neutrinos one finds that indeed the heavy Majorana neutrinos N_R naturally obtain masses which are by few to several orders of magnitude smaller than M_{GUT} . Thus, the enormous disparity between the neutrino and charged fermion masses is explained in this approach by the huge difference between effectively the electroweak symmetry breaking scale and M_{GUT}.

This mechanism is therefore a very elegant way to explain the smallness of the neutrino masses in a natural way and their eventual Majorana nature. Another attractive feature of the see-saw scenario is that this mechanism can relate the smallness of neutrino masses and the generation of the baryon asymmetry of the Universe [14, 15] (see also, e.g., [16, 17]). This is due to the fact the the Dirac Yukawa coupling in eq. (1.12) is, in general, CP nonconserving, so the rates of the decays $N_j \to l^+ + \phi^-$ and $N_j \to l^- + \phi^+$ are different. When the temperature of the Universe drops below the mass of the lightest heavy RH neutrino, so that the latter is out of equilibrium, the decays of the heavy neutrino states mentioned above might generate a CP asymmetries for the individual lepton charges, L_ℓ and for the total lepton charge L. The final lepton number asymmetry can be partially converted into a non-zero baryon asymmetry by the fast spahleron interactions in the thermal bath in the Early Universe. Therefore in this scenario the smallness of the neutrino masses and the baryon asymmetry have the same origin.

III Are massive neutrinos Majorana particles?

The Majorana nature of massive neutrinos manifests itself in the existence of processes in which the total lepton charge L changes by two units: $K^+ \to \pi^- + \mu^+ + \mu^+$, $\mu^- + (A, Z) \to \mu^+ + (A, Z-2)$, etc. Extensive studies have shown that the only feasible experiments having the potential of establishing that the massive neutrinos are Majorana particles are at present the experiments searching for neutrinoless double beta $(\beta\beta)_{0\nu}$-decay [45]: $(A, Z) \to (A, Z+2) + e^- + e^-$. Under the assumptions of 3-ν mixing, for which we have compelling evidence, of massive neutrinos ν_j being Majorana particles, and of $(\beta\beta)_{0\nu}$-decay generated only by the $(V-A)$ charged current weak interaction via the exchange of the three Majorana neutrinos ν_j having masses $m_j \lesssim$ a

few MeV, the $(\beta\beta)_{0\nu}$-decay amplitude of interest has the form (see, e.g. [7, 46]):

$$\mathcal{A}(\beta\beta)_{0\nu} = \langle m \rangle \, M(A, Z) \, , \tag{1.14}$$

where $M(A, Z)$ is the nuclear matrix element (NME) of the decay $(A, Z) \to (A, Z + 2) + e^- + e^-$ which does not depend on the neutrino mass and mixing parameters, and

$$|\langle m \rangle| \ = \left| m_1 \, |U_{\rm e1}|^2 + m_2 \, |U_{\rm e2}|^2 \, e^{i\alpha_{21}} + m_3 |U_{\rm e3}|^2 e^{i\alpha_{31}} \right| \, , \tag{1.15}$$

is the $(\beta\beta)_{0\nu}$-decay effective Majorana mass. In eq. (1.15), U_{ej}, $j = 1, 2, 3$, are the elements of the first row of the PMNS matrix U, and α_{21} and α_{31} are the two Majorana CP violation (CPV) phases which U contains. In the standard parametrization of the PMNS matrix U (see, e.g., [6]), the phase α_{31} in eq. (1.15) must be replaced by $(\alpha_{31} - 2\delta)$, δ being the Dirac CPV phase present in U, and $|U_{\rm e1}| = \cos\theta_{12} \cos\theta_{13}$, $|U_{\rm e2}| = \sin\theta_{12} \cos\theta_{13}$, $|U_{\rm e3}| = \sin\theta_{13}$, where θ_{12} and θ_{13} are the solar and reactor neutrino mixing angles, respectively.

The $(\beta\beta)_{0\nu}$-decay rate depends on the type of neutrino mass spectrum which can be, as we have seen in section I, hierarchical, with partial hierarchy or quasi-degenerate. Using the data on the neutrino oscillation parameters it is possible to show (see, e.g., [6]) that in the case of normal hierarchical spectrum one has $|\langle m \rangle| \lesssim 0.005$ eV, while if the spectrum is with inverted hierarchy, 0.01 eV $\lesssim |\langle m \rangle| \lesssim 0.05$ eV (see Figure 1.3). A larger value of $|\langle m \rangle|$ up to approximately 0.5 eV is possible if the light neutrino mass spectrum is with partial hierarchy or is of quasi-degenerate type. In the latter case $|\langle m \rangle|$ can be close to the existing upper limits. The $(\beta\beta)_{0\nu}$ experimental decay search can therefore have an enormous impact in constraining or even determining the spectrum of the light neutrino masses, the absolute scale of neutrino masses and together with other sources of information coming form cosmology could provide a unique insight on the value of the CP violating phases appearing in the leptonic mixing matrix, U_{PMNS}. In the following we will comment in details all the constrains that are now collected both from the $(\beta\beta)_{0\nu}$-decay search and from the cosmological observations.

The most stringent upper limits on $|\langle m \rangle|$ were set by the IGEX (^{76}Ge), CUORICINO (^{130}Te), NEMO3 (^{100}Mo) and more recently by EXO-200 , KamLAND-ZEN (^{136}Xe) and GERDA (^{76}Ge) experiments (see e.g. [49] for a summary). In Table 1.2 we report the current 90% C.L. experimental lower limits on the $(\beta\beta)_{0\nu}$-decay half-lives of different isotopes and the corresponding upper limits on $|\langle m \rangle|$, obtained using the NMEs - including the relevant uncertainties —from [50].

The best lower limit on the half-life of ^{76}Ge, $\mathrm{T}^{0\nu}_{1/2} > 1.9 \times 10^{25}$ yr (90% C.L.), was found in the Heidelberg-Moscow ^{76}Ge experiment (HdM) [52]. It corresponds to the upper limit [50] $|\langle m \rangle| < (0.20 - 0.35)$ eV. A positive $(\beta\beta)_{0\nu}$-decay signal at $> 3\sigma$, corresponding to $\mathrm{T}^{0\nu}_{1/2} = (0.69 - 4.18) \times 10^{25}$ yr (99.73% C.L.) and implying $|\langle m \rangle| = (0.1 - 0.9)$ eV, is claimed to have been observed in [53], while a later analysis reports evidence for $(\beta\beta)_{0\nu}$-decay at 6σ corresponding to $|\langle m \rangle| = 0.32 \pm 0.03$ eV [47].

Most importantly, a large number of projects, or already running experiments, aim at a sensitivity to $|\langle m \rangle| \sim (0.01 - 0.05)$ eV, i.e., to probe the range of values of $|\langle m \rangle|$ corresponding to IH neutrino mass spectrum [49]: CUORE (^{130}Te), GERDA (^{76}Ge), SuperNEMO, EXO (^{136}Xe), MAJORANA (^{76}Ge), MOON (^{100}Mo), COBRA (^{116}Cd), XMASS (^{136}Xe), CANDLES (^{48}Ca), KamLAND-Zen (^{136}Xe), SNO+ (^{150}Nd), etc.

Specifically among these, GERDA (GERmanium Detector Array) at the Gran Sasso Laboratory (Italy)(^{76}Ge), EXO-200 (Enriched Xenon Observatory) in New Mexico

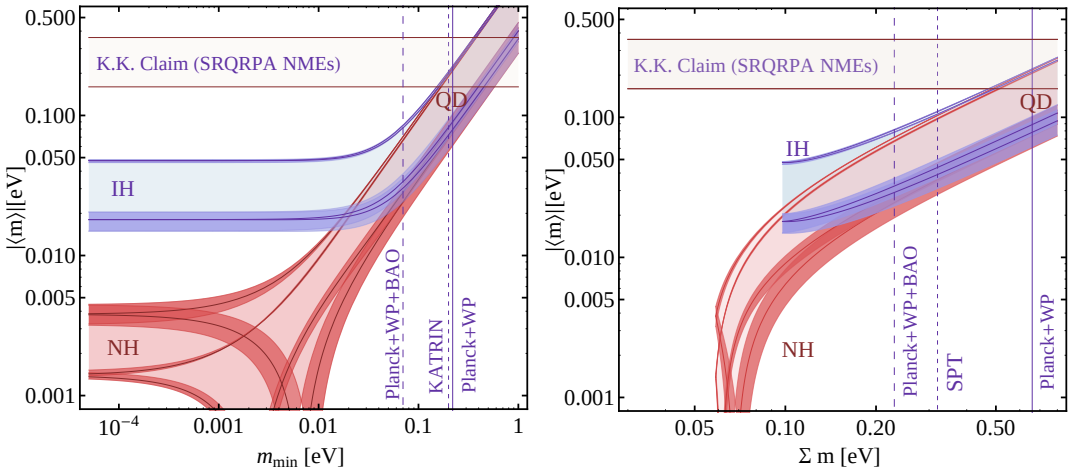

Figure 1.3: (Left Panel) The plot indicates the values of $|\langle m\rangle|$ as function of the lightest neutrino mass exploiting its dependence on the neutrino masses and oscillation parameters (amplitudes and frequencies). The light and strong shaded region indicate respectively the 2σ allowed CP-nonconserving and CP-conserving values of $|\langle m\rangle|$. The claim in [47] is given by the horizontal band. The vertical solid, dashed and dotted lines represent respectively the constrains on m_{min} obtained by the Planck Collaboration and the perspective upper limits of the β-decay experiment KATRIN [48]. (Right Panel) Values of $|\langle m\rangle|$ as function of the sum of the light neutrino masses. The vertical dashed line here represents the best fit value obtained by the SPT team. (See the text for details).

(^{136}Xe) and KamLAND-Zen in Japan (^{136}Xe) are operational and in particular, they are testing the positive result claimed in [47]. In 2012 the experiment EXO-200 has obtained a lower limit on the half-life of ^{136}Xe [54],

$$\mathrm{T}(^{136}\mathrm{Xe}) > 1.6 \times 10^{25}\mathrm{yr\ at\ 90\%\ C.L.} \tag{1.16}$$

while later the experiment KamLAND-Zen reported the lower bound [55];

$$\mathrm{T}(^{136}\mathrm{Xe}) > 1.9 \times 10^{25}\mathrm{yr\ at\ 90\%\ C.L.} \tag{1.17}$$

In the latter work a combined analysis between the EXO-200 and KamLAND-Zen limits is also presented, $\mathrm{T}(^{136}\mathrm{Xe}) > 3.4 \times 10^{25}$ yr. Although this results would exclude the claimed observation in [47], as can be seen from Table 1.3, the latter is not confirmed by the EXO-200 collaboration due to the difficulties to combine data with different systematic uncertainties (BLV Conference 2013).

In July 2013 also the GERDA collaboration reported the results from Phase I searches for $(\beta\beta)_{0\nu}$decay of the isotope ^{76}Ge. No signal was observed and a lower limit has been derived for T(^{76}Ge) [56]:

$$\mathrm{T}(^{76}\mathrm{Ge}) > 2.1 \times 10^{25}\mathrm{yr\ at\ 90\%\ C.L.}. \tag{1.18}$$

The Collaboration reported also a combined limit using the limits obtained by the HdM and IGEX experiments which is:

$$\mathrm{T}(^{76}\mathrm{Ge}) > 3.0 \times 10^{25}\mathrm{yr\ at\ 90\%\ C.L.}. \tag{1.19}$$

Isotope	$T^{0\nu}_{1/2}$ [yrs]	Experiment	$\lvert\langle m\rangle\rvert$ [eV]
^{48}Ca	5.8×10^{22}	CANDLES	3.55-9.91
^{76}Ge	1.57×10^{25}	IGEX	0.22-0.35
^{82}Se	3.2×10^{25}	NEMO-3	0.85-2.08
^{100}Mo	5.8×10^{23}	NEMO-3	0.25-0.45
^{116}Cd	1.7×10^{23}	SOLOTVINO	1.22-2.30
^{130}Te	3.0×10^{24}	CUORICINO	0.50-0.96
^{136}Xe	1.6×10^{25}	EXO-200	0.14-0.38
^{150}Nd	1.8×10^{22}	NEMO-3	2.35-5.08

Table 1.2: Experimental lower limits at 90% C.L. on the $(\beta\beta)_{0\nu}$-decay half-lives of different isotopes and the corresponding upper limits on $\lvert\langle m\rangle\rvert$, obtained using the NMEs (including the relevant uncertainties) from [51].

In Table 1.3 we present the constrains on $\lvert\langle m\rangle\rvert$ obtained by the $(\beta\beta)_{0\nu}$-decay experiments mentioned above. In order to extract these constrains we use the four sets of NMEs used in [57] of the decays of the nuclei of interest, ^{76}Ge and ^{136}Xe, derived within the Self-consistent Renormalized Quasiparticle Random Phase Approximation (SRQRPA) [58, 59]. In this approach, the particle-particle strength parameter g_{pp} of the SRQRPA [60–62] is fixed by the recent data on the two-neutrino double beta decays of EXO-200. In the calculation of the $(\beta\beta)_{0\nu}$-decay NMEs were considered the two-nucleon short-range correlations derived from same potential as residual interactions, namely from the Argonne or CD-Bonn potentials [50] and two values of the axial-vector constant are used, $g_A = 1.0, 1.25$.

Isotope	$T^{0\nu}_{1/2}$ [10^{25} yr]	Experiment	$\lvert\langle m\rangle\rvert$ [eV] (Arg.)	$\lvert\langle m\rangle\rvert$ [eV] (Cd-Bonn)
^{76}Ge	> 1.9	HdM	$< 0.24(0.30)$	$< 0.23(0.28)$
^{76}Ge	$2.23^{+0.44}_{-0.31}$	Klapdor-K.	0.18-0.29 (0.22-0.36)	0.16-0.27 (0.20-0.34)
^{136}Xe	> 1.6	EXO-200	$< 0.19(0.24)$	$< 0.16(0.20)$
^{136}Xe	> 1.9	KamLAND-ZEN	$< 0.18(0.22)$	$< 0.14(0.18)$
^{136}Xe	> 3.4	EXO-200+KamLAND-ZEN	$< 0.13(0.16)$	$< 0.11(0.14)$
^{76}Ge	> 2.1	GERDA	$< 0.23(0.28)$	$< 0.21(0.27)$
^{76}Ge	> 3.0	GERDA+IGEX+HdM	$< 0.19(0.24)$	$< 0.18(0.22)$

Table 1.3: In the Table we show the experimental lower limits at 90% C.L. on the $(\beta\beta)_{0\nu}$-decay half-lives of different isotopes and the corresponding upper limits or range on $\lvert\langle m\rangle\rvert$ assuming that the exchange of light Majorana neutrinos is the leading mechanism. The range for $\lvert\langle m\rangle\rvert$ are obtained using the correlated uncertainties associated to the NMEs within the SRQRPA method i.e. the use of different nucleon-nucleon potential such as the Argonne and Cd-Bonn potentials and the value of g_A=1.25 (1.0 in parenThesis)— for the numerical values of NMEs see [57].

Figure 1.3 shows the combinations of all the available present data using the best fit values of one of the most recent global fit analysis on the neutrino oscillation parameters

[29] and considering a 2σ uncertainty on the latter. An horizontal band corresponding to the claim in [47] and it corresponds to the NMEs obtained using the correlated uncertainties associated to the NMEs within the SRQRPA method (Argonne or Cd-Bonn potentials and $g_A = 1.25, 1.0$). From the Figure we can see that the cosmological bounds reported by the Planck Collaboration strongly disfavor the claim in [47] in the most conservative case. Nevertheless It seems from Figure 1.3 and Table 1.3 that the less stringent cosmological bound obtained combining BAO with Planck data together with the unofficial combination of $(\beta\beta)_{0\nu}$-decay results of EXO-200 and KamLAND-ZEN and the GERDA results pinpoint to disfavour (if not exclude) the Klapdor-K. Claim.

However, the experimental searches for $(\beta\beta)_{0\nu}$-decay are not restricted only to test the claim in [47]. The latter is only part of a more general programme of research which aims to probe values of the effective Majorana mass $|\langle m \rangle| \geq 0.01$ eV, thus covering the range predicted in the case of IH neutrino mass spectru. If the $(\beta\beta)_{0\nu}$-decay will be observed, the corresponding data will be used to constrain or even determining the possible mechanism(s) generating the decay. Indeed, the observation of the $(\beta\beta)_{0\nu}$-decay would not guarantee that the dominant mechanism inducing the decay is the light Majorana neutrino exchange [63]. The results of the $(\beta\beta)_{0\nu}$-decay searches will play a very important role in testing and constraining i) theories of neutrino mass generation predicting massive Majorana neutrinos, and ii) the existence of new $|\Delta L| = 2$ couplings in the effective weak interaction Lagrangian, which could induce the decay. The existence of such couplings would have enormous impact from the model-building point of view.

IV In this Thesis

This Thesis is focused on some aspects of neutrino phenomenology and is an attempt to incorporate and explain the recent experimental results clearly indicating the beginning of the precise measurement era for neutrino physics. As we said, oscillation measurements and $(\beta\beta)_{0\nu}$-decay experiments are going to give important results to the scientific community in the next years. Due to its deep interdisciplinary character, it seems natural to consider neutrino physics from different points of view. This Thesis is mainly organized in two parts.

The first one is devoted to the phenomenological study of $(\beta\beta)_{0\nu}$-decay i.e. to the possible determination of the nature —Dirac or Majorana— of massive neutrinos and establishing the status of the symmetry, associated with the total lepton charge conservation, in particle physics. More specifically, this part of the Thesis aims to explore New Physics contributions in $(\beta\beta)_{0\nu}$-decay. If the $(\beta\beta)_{0\nu}$-decay will be observed, it will be of crucial importance to identify the mechanism(s) triggering the decay. This will help identify the New Physics beyond that predicted by the Standard Model associated with lepton charge nonconservation and the $(\beta\beta)_{0\nu}$-decay. At present we do not have evidence for the existence of $\Delta L \neq 0$ terms in the Lagrangian describing the particle interactions. Nevertheless, such terms can exist and they can be operative in the $(\beta\beta)_{0\nu}$-decay. Moreover, it is impossible to exclude the hypoThesis that, if observed, the $(\beta\beta)_{0\nu}$-decay is triggered by more than one competing mechanisms. Given the experimental observation of the $(\beta\beta)_{0\nu}$-decay of sufficient number of nuclei, one can determine and/or sufficiently constrain the fundamental parameters associated with

the lepton charge non-conserving couplings generating the $(\beta\beta)_{0\nu}$-decay. This topic has been developped in [64] and [57], where we considered the possibility of several different Lepton Number Violating (LNV) mechanisms contributing to the $(\beta\beta)_{0\nu}$-decay amplitude in the general case of CP non-conservation.

The aim of the second part of this Thesis is to investigate and propose possible solutions to the flavour problem in the neutrino sector and more generally, in the neutrino, charged lepton and quark sectors. This includes, in particular, studying the origin of the patterns of neutrino masses and mixing, and of the flavour structure in the lepton sector. The method enployed is the analysis of possible symmetries and frameworks, within which one can have realistic patterns of lepton (neutrino) mixing and, in a unified model of flavour, of quark and lepton masses and mixings. One of the requirements used is to reproduce the relatively large value of the angle θ_{13} and at the same time have possibly sizable deviations of the angle θ_{23} from the value $\pi/4$. These studies are related to the problem of understanding the fundamental mechanism giving rise to neutrino masses and mixing and possibly to L_ℓ non-conservation. The second part of the Thesis is based on the articles [65] and [66], in which two different approaches based on the use of discrete finite non-Abelian symmetries are developed.

IV In this Thesis

This Ph.D. Thesis is based on the following papers and proceedings:

1. A. Faessler, A. Meroni, S.T. Petcov, F. Simkovic, and J. Vergados, *Uncovering Multiple CP-Nonconserving Mechanisms of $(\beta\beta)_{0\nu}$-Decay*, Phys.Rev. D**83** (2011) 113003

2. A. Meroni, S. T. Petcov and M. Spinrath, *A SUSY $SU(5) \times T'$ Unified Model of Flavour with large θ_{13}* Phys.Rev. D**86** (2012) 113003

3. A. Meroni, S.T. Petcov, F. Simkovic, *Multiple CP Non-conserving Mechanisms of $(\beta\beta)_{0\nu}$-Decay and Nuclei with Largely Different Nuclear Matrix Elements* JHEP **1302** (2013) 025

4. C. Hagedorn, A. Meroni and L. Vitale, *Mixing Patterns from the Groups Sigma $(n\phi)$*, arXiv:1307.5308 Submitted to J. Phys. A

5. A. Meroni and S.T. Petcov, *On Multiple CP Nonconserving Mechanisms of $\beta\beta_{0\nu}$-Decay*, Published in "Venice 2011, Neutrino Telescopes" 401-403, NeuTel 2011, XIV International Workshop on Neutrino Telescopes - Venice, Italy.

6. A. Meroni and S.T. Petcov, *Multiple CP nnoconserving mechanisms in $\beta\beta_{0\nu}$ decay*, in Proceedings of the International School of Physics "Enrico Fermi", Course CLXXXII, "Neutrino Physics and Astrophysics", (IOS Press, Amsterdam and SIF, Bologna), 2012, pp. 315-319.

7. A. Meroni, *Multiple mechanisms in $\beta\beta_{0\nu}$ decay*, Proceeding for "Rencontres de Moriond 2012", ElectroWeak Interactions and Unified Theories, La Thuile (Italy), 3-10/03/12.

8. A. Meroni, *A SUSY $SU(5) \times T'$ Unified Model of Flavour with large θ_{13}*, Proceedings of the 2nd Workshop on Flavor Symmetries and Consequences in Accelerators and Cosmology (FLASY12), Dortmund (Germany), 30/06-4/07/12.

Part I

Neutrinoless Double β-Decay and $\Delta L = 2$ Couplings

Chapter 2

Overview

If neutrinoless double beta $(\beta\beta)_{0\nu}$-decay will be observed, it will be of fundamental importance to determine the mechanism which induces the decay. We know that neutrinos have mass and mix, and if they are Majorana particles they should trigger the decay at some probability level. As we have mentioned in the Introduction, the fundamental parameter which controls the $(\beta\beta)_{0\nu}$-decay rate in this case is the effective Majorana mass:

$$\langle m \rangle = \sum_{j}^{light} (U_{ej})^2 \, m_j \ , \ (\text{all } m_j \geq 0) \ , \tag{2.1}$$

where U is the PMNS neutrino mixing matrix and m_j are the light Majorana neutrino masses, $m_j \lesssim 1$ eV (see [6]). The $(\beta\beta)_{0\nu}$-decay rate depends on the type of neutrino mass spectrum which can be hierarchical, with partial hierarchy or quasi-degenerate. Using the data on the neutrino oscillation parameters it is possible to show that in the case of normal hierarchical spectrum one has $|\langle m \rangle| \lesssim 0.005$ eV, while if the spectrum is with inverted hierarchy, $0.01 \text{ eV} \lesssim |\langle m \rangle| \lesssim 0.05$ eV. A larger value of $|\langle m \rangle|$ is possible if the light neutrino mass spectrum is with partial hierarchy or of quasi-degenerate type. In the latter case $|\langle m \rangle|$ can be close to the existing upper limits.

The fact that $max|\langle m \rangle|$ in the case of NH spectrum is considerably smaller than $min|\langle m \rangle|$ for the IH and QD spectrum opens the possibility to obtain information about the neutrino mass pattern from a measurement of $|\langle m \rangle| \neq 0$. More specifically a positive result in the future generation of $(\beta\beta)_{0\nu}$-decay experiments with $|\langle m \rangle| > 0.01$ eV would imply that the NH spectrum is strongly disfavored (if not excluded). If the future $(\beta\beta)_{0\nu}$-decay experiments show that $|\langle m \rangle| < 0.01$ eV both the IH and QD spectrum will be ruled out for massive Majorana neutrinos, if in addition, it is establish from oscillation experiment that $\Delta m^2_A < 0$ then one would be let to conclude that either the massive neutrino are Dirac fermions, or the neutrinos are Majorana particles but there are additional contributions to $(\beta\beta)_{0\nu}$-decay amplitude which interfere destructively [67].

Summarizing, the studies on $(\beta\beta)_{0\nu}$-decay and a measurement of a nonzero value of $|\langle m \rangle| \geq$ (of a few 10^{-2} eV) could:

- establish the Majorana nature of massive neutrinos; the $(\beta\beta)_{0\nu}$-decay experiments are presently the only feasible experiments capable of doing that;
- give information on the type of neutrino mass spectrum. More specifically, a measured value of $|\langle m \rangle| \sim$ few 10^{-2} eV can provide, in particular, unique constraints

on, or even can allow one to determine, the type of neutrino mass spectrum if neutrinos ν_i are Majorana particles [46, 68–70];

- provide also unique information on the absolute scale of neutrino masses or on the lightest neutrino mass (see e.g. [71]);

- with additional information from other sources (^3H β-decay experiments or cosmological and astrophysical data considerations) on the absolute neutrino mass scale, the $(\beta\beta)_{0\nu}$-decay experiments can provide unique information on the Majorana CP-violation phases α_{31} and/or α_{21} [46, 72, 73].

An observation of $(\beta\beta)_{0\nu}$-decay would imply that the total lepton charge L is not conserved. This of course implies that the massive neutrinos get a Majorana mass [74, 75] and therefore are Majorana particles (see, e.g. [9]). However, the latter does not guarantee that the dominant mechanism inducing the $(\beta\beta)_{0\nu}$-decay is the light Majorana neutrino exchange (that we will call the "standard" mechanism of the $(\beta\beta)_{0\nu}$-decay) since the Majorana mass thus generated is exceedingly small. The $(\beta\beta)_{0\nu}$-decay can well be due to the existence of interactions which do not conserve the total lepton charge L, specifically $\Delta L = \pm 2$. A number of such interactions have been proposed in the literature: heavy Majorana neutrinos coupled to the electron in the $V - A$ charged current weak interaction Lagrangian, supersymmetric (SUSY) theories with R-parity breaking terms which do not conserve the total lepton charge L, L-nonconserving couplings in the Left-Right symmetric theories, etc. At present we do not have evidence for the existence of $\Delta L \neq 0$ terms in the Lagrangian describing the particle interactions. Nevertheless, such terms can exist and they can be operative in the $(\beta\beta)_{0\nu}$-decay. Moreover, it is impossible to exclude the hypothesis that, if observed, the $(\beta\beta)_{0\nu}$-decay is triggered by more than one competing mechanisms.

The possibility of several different mechanisms contributing to the $(\beta\beta)_{0\nu}$-decay amplitude was considered in [76] assuming that the corresponding $\Delta L = \pm 2$ couplings are CP conserving.

The analysis presented in this part of the thesis is a natural continuation of the study performed in [76]. We consider the possibility of several different mechanisms contributing to the $(\beta\beta)_{0\nu}$-decay amplitude in the general case of CP nonconservation: light Majorana neutrino exchange, heavy left-handed (LH) and heavy right-handed (RH) Majorana neutrino exchanges, lepton charge non-conserving couplings in SUSY theories with R-parity breaking. These different mechanisms can interfere only if the electron current structure coincides and hence it can be factorized. If, on the contrary, these are not-interfering mechanisms, i.e., the electron currents have different chiralities, then the interference term is suppressed by a factor which depends on the considered nucleus. [77]. If the $(\beta\beta)_{0\nu}$-decay is induced by, e.g., two "non-interfering" mechanisms (e.g. light Majorana neutrino and heavy RH Majorana neutrino exchanges), one can determine the absolute values of the two fundamental parameters, characterizing these mechanisms, from data on the half-lives of two nuclear isotopes. In the case when two "interfering" mechanisms are responsible for the $(\beta\beta)_{0\nu}$-decay, the absolute values of the two relevant parameters and the interference term can be uniquely determined from data on the half-lives of three nuclei. We present in chapter 3 illustrative examples of determination of the relevant fundamental parameters and of possible tests of the hypothesis that more than one mechanism is responsible for the $(\beta\beta)_{0\nu}$-decay, using as input hypothetical half-lives of ^{76}Ge, ^{130}Te and ^{100}Mo and considering two "nonin-

terfering" and two "interfering" mechanisms, namely, the light Majorana neutrino and the heavy RH Majorana neutrino exchanges, and the light Majorana neutrino and the dominant gluino exchanges. The effects of the uncertainties in the values of the nuclear matrix elements (NMEs) on the results of the indicated analyzes are also discussed and illustrated.
The method considered by us can be generalized to the case of more than two $(\beta\beta)_{0\nu}$-decay mechanisms. It has also the advantage that it allows to treat the cases of CP conserving and CP nonconserving couplings generating the $(\beta\beta)_{0\nu}$-decay in a unique way. In chapter 4 we will investigate also the potential of combining data on one or more of the five nuclei ^{76}Ge, ^{82}Se, ^{100}Mo, ^{130}Te and ^{136}Xe, for discriminating between different pairs of non-interfering or interfering mechanisms of $(\beta\beta)_{0\nu}$-decay. Before going into the details of such analysis we briefly describe the mechanisms that can trigger the $(\beta\beta)_{0\nu}$-decay considered in this part of the thesis.

I Possible $\Delta L = 2$ coupligs in $(\beta\beta)_{0\nu}$-Decay

As we have said, $(\beta\beta)_{0\nu}$-decay is allowed by a number of models, from the standard mechanism of light Majorana neutrino exchange [45] to those such as Left-Right Symmetry [43, 78] or R-parity violating Supersymmetry (SUSY) [79]. These mechanisms might trigger $(\beta\beta)_{0\nu}$-decay individually or together. In Left-Right Symmetric models, for example, there is an additional contribution from the exchange of heavy right-handed neutrinos. In R-parity violating SUSY, on the other hand, $(\beta\beta)_{0\nu}$-decay can be mediated by heavy particles such as neutralino or gluino. The $(\beta\beta)_{0\nu}$-decay half-life of a certain nucleus can therefore be written as function of some lepton number violating (LNV) parameters, each of them connected with a different mechanism i:

$$[T^{0\nu}_{1/2}]^{-1} = G^{0\nu}(E, Z)|\sum_i \eta^{LNV}_i M^{0\nu}_i|^2 \tag{2.2}$$

where $G^{0\nu}(E_0, Z)$ and $M'^{0\nu}_{\kappa}$ are, respectively, the known phase-space factor (E_0 is the energy release) and the NMEs of the decay. The latter depends on the mechanism generating the decay and on the nuclear structure of the specific isotopes (A, Z), $(A, Z+1)$ and $(A, Z+2)$ under study.

The phase space factors $G^{0\nu}(E_0, Z)$, which include the fourth power of the "standard" value of the axial-coupling constant $g_A = 1.25$, are tabulated in reference [80]; for ^{76}Ge, ^{82}Se, ^{100}Mo and ^{130}Te are given in Table I. For a given isotope (A, Z), $G^{0\nu}(E_0, Z)$ contains the inverse square of the nuclear radius $R(A)$ of the isotope, $R^{-2}(A)$, compensated by the factor $R(A)$ in $M'^{0\nu}_{\kappa}$. The assumed value of the nuclear radius is $R(A) = r_0 A^{1/3}$ with $r_0 = 1.1\ fm$. The NME $M'^{0\nu}_{\kappa}$ is defined as

$$M'^{0\nu}_{\kappa} = \left(\frac{g_A}{1.25}\right)^2 M^{0\nu}_{\kappa}. \tag{2.3}$$

This definition of $M'^{0\nu}_{\kappa}$ [60, 61] allows to display the effects of uncertainties in g_A and to use the same phase factor $G^{0\nu}(E_0, Z)$ when calculating the $(\beta\beta)_{0\nu}$-decay rate.

We outline below the LNV mechanisms we will consider in the analysis.

I.I Light Majorana Neutrino exchange mechanism

The standard scenario to allow $(\beta\beta)_{0\nu}$-decay is the exchange of a light Majorana left-handed neutrino, χ_{jL}, via $V-A$ weak interactions. The following term in the S-matrix (or scattering matrix) gives the contribution to the matrix element of the process in second order of perturbation theory in G_F:

$$\begin{aligned} S^{(2)} &= T\left(e^{-i\int \mathcal{H}_I^{w.i.}(x)dx} e^{-i\int \mathcal{H}_I^{S.I.}(x)dx}\right) \\ &\propto G_F^2 \frac{(-i)^2}{2!}\int dx_1^4 dx_2^4 N\left[\mathcal{L}_I^{w.i.}(x_1)\mathcal{L}_I^{w.i.}(x_2)\right] T\left(j_\alpha^h(x_1) j_\beta^h(x_2) e^{-i\int \mathcal{H}_I^{S.I.}(x)dx}\right) \end{aligned} \tag{2.4}$$

where

$$\mathcal{L}_I^{w.i.} = \bar{e}_L \gamma_\alpha \nu_{eL}. \tag{2.5}$$

We can recast the weak lepton current part using the Majorana properties $-\chi_j^T C^\dagger = \overline{\chi_j^c} = \xi_j \chi_j$, $C^{-1}\gamma_\alpha C = -\gamma_\alpha^T$ and $\nu_{eL} = \sum_{j=1}^3 U_{ej}\chi_{jL}$ with U_{ej} being the elements of the first row of the PMNS mixing matrix.

Thus we get[1]:

$$\begin{aligned} (\bar{e}_L\gamma_\alpha\nu_{eL})(\bar{e}_L\gamma_\beta\nu_{eL}) &= -\sum_j (U_{ej})^2 \bar{e}\gamma_\alpha P_L \chi_j \chi_j^T C^\dagger C P_L \gamma_\beta^T C^\dagger C \bar{e}^T \\ &= -\sum_j \xi_j (U_{ej})^2 \bar{e}\gamma_\alpha P_L \underbrace{\chi_j \overline{\chi_j}} P_L \gamma_\beta C \bar{e}^T \\ &= -\sum_j \xi_j (U_{ej})^2 \bar{e}\gamma_\alpha P_L S(x_1-x_2) P_L \gamma_\beta C \bar{e}^T \end{aligned} \tag{2.6}$$

where $S(x_1 - x_2)$ is the propagator:

$$P_L S(x_1-x_2) P_L = P_L(-i)\frac{\int e^{iq(x_1-x_2)}(\not{q}+m_k)dq}{q^2-m_k^2} P_L = P_L(-i)(m_k)\frac{\int e^{iq(x_1-x_2)}}{q^2-m_k^2} P_L \tag{2.7}$$

Therefore one can define the effective Majorana mass $|\langle m\rangle|$ corresponding to the contribution from standard $(V-A)$ charged current (CC) weak interaction as follows:

$$|\langle m\rangle| \equiv \left|\sum_j^3 (U_{ej})^2 m_j\right| = |m_1 U_{e1}^2 + m_2 U_{e2}^2 + m_3 U_{e3}^2| \ , \ (\text{all } m_j \geq 0). \tag{2.8}$$

One can show (appendix of [9]) that taking some approximations, that usually are made in calculating $(\beta\beta)_{0\nu}$-decay amplitudes, the hadron current is a symmetric operator:

$$A_{\alpha\beta} \equiv J_\alpha(x_1) J_\beta(x_2) = J_\beta(x_2) J_\alpha(x_1), \tag{2.9}$$

therefore in the matrix element the product of the hadron part and the weak V-A current can be written as:

$$-\bar{e}\gamma_\alpha P_L \gamma_\beta C \bar{e}^T A_{\alpha\beta} = \bar{e}\gamma_\alpha\gamma_\beta P_R C \bar{e}^T A_{\alpha\beta} = \bar{e}(g_{\alpha\beta} + \frac{1}{2}(\gamma_\alpha\gamma_\beta - \gamma_\beta\gamma_\alpha)) P_R C \bar{e}^T A_{\alpha\beta}, \tag{2.10}$$

[1] We define the chiral projectors as $P_{L,R} = (1 \mp \gamma_5)/2$

so finally the contribution to $(\beta\beta)_{0\nu}$-decay is given by:

$$\mathcal{A}(\beta\beta)_{0\nu} = \langle m \rangle [\bar{e}(1+\gamma_5)e^c] A_{\alpha\beta}, \tag{2.11}$$

where $|\langle m \rangle|$ is the effective Majorana neutrino mass. The basic diagram corresponding to this mechanism is drawn in Fig. 2.1. In the case of the light Majorana neutrino exchange mechanism of $(\beta\beta)_{0\nu}$-decay, we can define a LNV parameter which is given by:

$$\eta_\nu = \frac{\langle m \rangle}{m_e}. \tag{2.12}$$

I.II Right Heavy Neutrino exchange mechanism

We assume that the neutrino mass spectrum includes, in addition to the three light Majorana neutrinos, heavy Majorana states N_k with masses M_k much larger than the typical energy scale of the $(\beta\beta)_{0\nu}$-decay, $M_k \gg 100$ MeV; we will consider the case of $M_k \gtrsim 10$ GeV. Such a possibility arises if the weak interaction Lagrangian includes right-handed (RH) sterile neutrino fields which couple to the LH flavour neutrino fields via the neutrino Yukawa coupling and possess a Majorana mass term. The heavy Majorana neutrinos N_k can mediate the $(\beta\beta)_{0\nu}$-decay similar to the light Majorana neutrinos via the $V-A$ charged current weak interaction. The difference between the two mechanisms is that, unlike in the light Majorana neutrino exchange which leads to a long range inter-nucleon interactions, in the case of $M_k \gtrsim 10$ GeV of interest the momentum dependence of the heavy Majorana neutrino propagators can be neglected (i.e., the N_k propagators can be contracted to points) and, as a consequence, the corresponding effective nucleon transition operators are local. The LNV parameter in the case when the $(\beta\beta)_{0\nu}$-decay is generated by the $(V-A)$ CC weak interaction due to the exchange of N_k can be written as:

$$\eta_N^L \quad = \quad \sum_k^{heavy} U_{ek}^2 \frac{m_p}{M_k}\,, \tag{2.13}$$

where m_p is the proton mass and U_{ek} is the element of the neutrino mixing matrix through which N_k couples to the electron in the weak charged lepton current.

The weak interaction Lagrangian might contains also, in theories like Left-Right Symmetric models, $(V+A)$ (i.e., right-handed (RH)) charged currents coupled to a RH charged weak boson W_R, as,

$$\mathcal{L}_{L+R} = \frac{g}{2\sqrt{2}}[(\bar{e}\gamma_\alpha(1-\gamma_5)\nu_{eL})W_\mu^- + (\bar{e}\gamma_\alpha(1+\gamma_5)\nu_{eR})W_{\mu R}^-] \tag{2.14}$$

where $\nu_{eR} = \sum_k V_{ek} N_{kR}$, $C\bar{N}_k^T = \xi N_k$. Here V_{ek} are the elements of a mixing matrix by which N_k couple to the electron in the $(V+A)$ charged lepton current, M_W is the mass of the Standard Model charged weak boson, $M_W \cong 82$ GeV, and M_{WR} is the mass of W_R. It follows from the existing data that [43, 78] $W_R \gtrsim 2.5$ TeV.

For instance, in the $SU(2)_L \times SU(2)_R \times U(1)$ theories we can have also a contribution to the $(\beta\beta)_{0\nu}$-decay amplitude generated by the exchange of virtual N_k coupled to the electron in the hypothetical $(V+A)$ CC part of the weak interaction Lagrangian. In

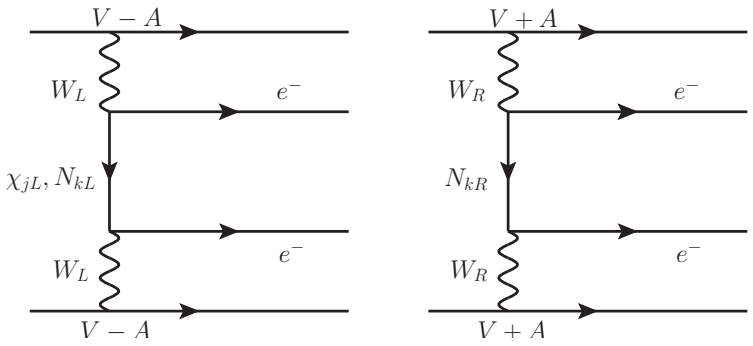

Figure 2.1: Feynman diagrams for the $(\beta\beta)_{0\nu}$-decay, generated by the light or heavy Majorana neutrino exchange (left panel) and the heavy (RH) Majorana neutrino exchange (right panel).

this case the corresponding LNV parameter can be written as:

$$\eta_N^R \quad = \quad \left(\frac{M_W}{M_{WR}}\right)^4 \sum_k^{heavy} V_{ek}^2 \frac{m_p}{M_k}. \tag{2.15}$$

If CP invariance does not hold, which we will assume to be the case in what follows, U_{ek} and V_{ek} will contain physical CP violating phases at least for some k and thus the parameters η_N^L and η_N^R will not be real.

As can be shown, the NMEs corresponding to the two mechanisms of $(\beta\beta)_{0\nu}$-decay with exchange of heavy Majorana neutrinos N_k, described in the present subsection, are the same and are given in [80]. We will denote them by $\mathcal{M}_N^{0\nu}$.

Finally, it is important to note that the current factor in the $(\beta\beta)_{0\nu}$-decay amplitude describing the two final state electrons, has different forms in the cases of $(\beta\beta)_{0\nu}$-decay mediated by $(V-A)$ and $(V+A)$ CC weak interactions[2], namely, $\bar{e}(1+\gamma_5)e^c \equiv 2\bar{e_L}\,(e^c)_R$ and $\bar{e}(1-\gamma_5)e^c \equiv 2\bar{e_R}\,(e^c)_L$, respectively, where $e^c = C(\bar{e})^T$, C being the charge conjugation matrix.

The difference in the chiral structure of the two currents leads to a relatively strong suppression of the interference between the terms in the $(\beta\beta)_{0\nu}$-decay amplitude involving the two different electron current factors (see further).

I.III SUSY Models with R-Parity Non-conservation

The SUSY models with R-parity non-conservation include LNV couplings which can trigger the $(\beta\beta)_{0\nu}$-decay. Let us recall that the R-parity is a multiplicative quantum number defined by $R = (-1)^{2S+3B+L}$, where S, B and L are the spin, the baryon and lepton numbers of a given particle. The ordinary (Standard Model) particles have $R = +1$, while their superpartners carry $R = -1$.

The LNV couplings emerge in this class of SUSY models from the R-parity breaking ($\not{R}_p$) part of the superpotential

$$W_{\not{R}_p} \;=\; \lambda_{ijk} L_i L_j E_k^c + \lambda'_{ijk} L_i Q_j D_k^c + \mu_i L_i H_2, \tag{2.16}$$

[2]The procedure is the same defined in the light neutrino exchange section. One has in this case $\bar{e}\gamma_\alpha P_R \gamma_\beta C \bar{e}^T A_{\alpha\beta} = \bar{e} P_L e^c A_{\alpha\beta}$

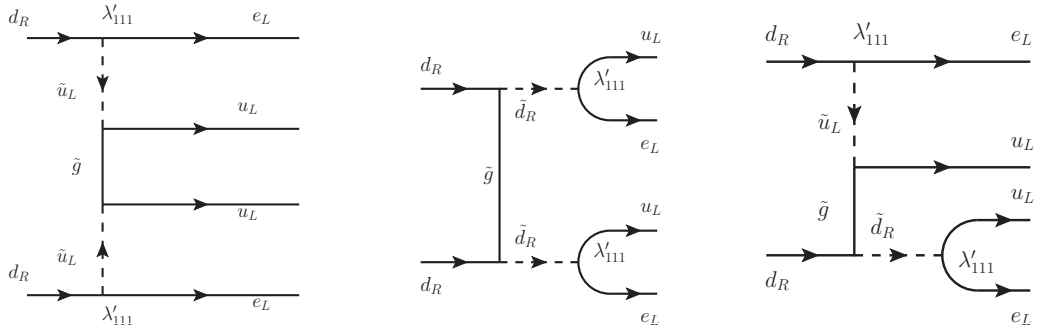

Figure 2.2: Feynman diagrams for $(\beta\beta)_{0\nu}$-decay due to the gluino exchange mechanism.

where L, Q stand for lepton and quark $SU(2)_L$ doublet left-handed superfields, while E^c, D^c for lepton and down quark singlet superfields. Here we concentrate only on the trilinear λ'-couplings. The λ'-couplings of the first family of particles and sparticles relevant for $(\beta\beta)_{0\nu}$-decay are given in terms of the fields of the LH electron, electron neutrino ν_{eL}, LH selectron $\tilde{e}_L$ and sneutrino $\tilde{\nu}_{eL}$, LH and RH u- and d-quarks, $u_{L,R}$ and $d_{L,R}$, and LH and RH u- and d-squarks, $\tilde{u}_{L,R}$, $\tilde{d}_{L,R}$, by:

$$\mathcal{L}_{\not R_p} = \lambda'_{111}\left[(\bar{u}_L\ \bar{d}_L)\begin{pmatrix} e^c_R \\ -\nu^c_{eR}\end{pmatrix}\tilde{d}_R + (\bar{e}_L\ \bar{\nu}_{eL})d_R\begin{pmatrix}\tilde{u}^*_L \\ -\tilde{d}^*_L\end{pmatrix} + (\bar{u}_L\ \bar{d}_L)d_R\begin{pmatrix}\tilde{e}^*_L \\ -\tilde{\nu}^*_{eL}\end{pmatrix}\right] + h.c. \tag{2.17}$$

At the quark-level there are basically two types of $\not R_p$ SUSY mechanisms of $(\beta\beta)_{0\nu}$-decay: a short-range one with exchange of heavy Majorana and scalar SUSY particles (gluinos and squarks, and/or neutralinos and selectrons) [79, 81–88], and a long-range mechanism involving the exchange of both heavy squarks and light Majorana neutrinos [79, 89–94]. We will call the latter the "squark-neutrino" mechanism.

The Case of Gluino Exchange Dominance

Assuming the dominance of the gluino exchange in the short-range mechanism, one obtains the following expression for the corresponding LNV parameter (see the Feynmann diagrams in Fig. 2.2):

$$\eta_{\lambda'} = \frac{\pi\alpha_s}{6}\frac{\lambda'^2_{111}}{G_F^2 m^4_{\tilde{d}_R}}\frac{m_p}{m_{\tilde{g}}}\left[1 + \left(\frac{m_{\tilde{d}_R}}{m_{\tilde{u}_L}}\right)^2\right]^2. \tag{2.18}$$

Here, G_F is the Fermi constant, $\alpha_s = g_3^2/(4\pi)$, g_3 being the $\mathrm{SU(3)_c}$ gauge coupling constant. $m_{\tilde{u}_L}$, $m_{\tilde{d}_R}$ and $m_{\tilde{g}}$ are masses of the LH u-squark, RH d-squark and gluino, respectively.

The NMEs associated with the gluino exchange mechanism, $M^{0\nu}_{\lambda'}$, was calculated in [84, 85, 95]. The electron current factor in the term of the $(\beta\beta)_{0\nu}$-decay amplitude corresponding to the gluino exchange mechanism under discussion has the form $\bar{e}(1+\gamma_5)e^c \equiv 2\bar{e_L}\,(e^c)_R$, i.e., it coincides with that of the light (or heavy LH) Majorana neutrino exchange. Thus, when calculating the $(\beta\beta)_{0\nu}$-decay rate, the interference between the two terms present in the $(\beta\beta)_{0\nu}$-decay amplitude, corresponding to the

indicated two mechanisms, has the same phase space factor as the contributions due to each of the two mechanisms. As a consequence, the interference term will not suffer from phase space suppression.

The Squark-Neutrino Mechanism

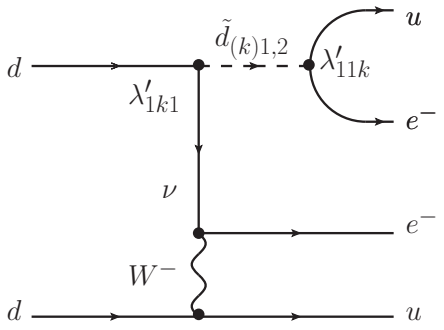

Figure 2.3: Feynman diagrams for $(\beta\beta)_{0\nu}$-decay due to the squark-neutrino mechanism at the quark-level [94].

In the case of squark-neutrino exchange [94], the $(\beta\beta)_{0\nu}$-decay amplitude does not vanish in the limit of zero Majorana neutrino mass, in contrast to the case of the "standard" light (LH) Majorana neutrino exchange (see Figure 2.3). This is a consequence of the chiral structure of the corresponding $\not{R}_p$ SUSY couplings. The contribution due to the squark-neutrino exchange to the $(\beta\beta)_{0\nu}$-decay amplitude is roughly proportional to the momentum of the virtual neutrino, which is of the order of the Fermi momentum of the nucleons inside of nucleus, $p_F \approx 100$ MeV. The corresponding LNV parameter is defined as [94]

$$\eta_{\tilde{q}} \;=\; \sum_k \frac{\lambda'_{11k}\lambda'_{1k1}}{2\sqrt{2}G_F} \sin 2\theta^d_{(k)} \left(\frac{1}{m^2_{\tilde{d}_1(k)}} - \frac{1}{m^2_{\tilde{d}_2(k)}} \right) . \tag{2.19}$$

Here we use the notations $d_{(k)} = d, s, b$ and assumed that there are 3 light Majorana neutrinos. This LNV parameter vanishes in the absence of $\tilde{d}_{kL} - \tilde{d}_{kR}$ - mixing, i.e., when $\theta^d = 0$. The NME for the squark-neutrino mechanism, $M^{0\nu}_{\tilde{q}}$, is given in [94].

II Nuclear Structure Calculations

In the following chapters the $(\beta\beta)_{0\nu}$-decay NMEs for the standard light Majorana neutrino, heavy RH and LH Majorana neutrino, gluino and squark exchange mechanisms will be denoted respectively as $M'^{0\nu}_{\nu}$, $M'^{0\nu}_{N}$, $M'^{0\nu}_{\lambda'}$ and $M'^{0\nu}_{\tilde{q}}$. We will use the following isotopes: ^{76}Ge, ^{82}Se, ^{100}Mo, ^{130}Te and ^{136}Xe. These nuclei are considered as most probable candidate sources for the next generation of the experiments searching for $(\beta\beta)_{0\nu}$-decay.

We note that the NMEs used in this part of the Thesis were calculated by F. Simkovic for the studies published in [57, 64] using the Self-consistent Renormalized Quasiparticle Random Phase Approximation (SRQRPA) [58]. The SRQRPA method

takes into account the Pauli exclusion principle and conserves the mean particle number in correlated ground state.

For each of the four nuclei, two choices of single-particle basis are considered. The intermediate size model space has 12 levels (oscillator shells $N = 2 - 4$) for ^{76}Ge and ^{82}Se, 16 levels (oscillator shells $N = 2 - 4$ plus the f+h orbits from $N = 5$) for ^{100}Mo and 18 levels (oscillator shells $N = 3, 4$ plus f+h+p orbits from $N = 5$) for ^{130}Te and ^{136}Xe. The large size single particle space contains 21 levels (oscillator shells $N = 0-5$) for ^{76}Ge, ^{82}Se and ^{100}Mo, and 23 levels for ^{130}Te and ^{136}Xe ($N = 1 - 5$ and i orbits from $N = 6$). In comparison with previous studies [60, 61], we omitted the small space model which is not sufficient to describe realistically the tensor part of the $(\beta\beta)_{0\nu}$-decay NMEs.

Table 2.1: Nuclear matrix elements $M'^{0\nu}_{\nu}$ (light neutrino mass mechanism), $M'^{0\nu}_{N}$ (heavy neutrino mass mechanism), $M'^{0\nu}_{\lambda'}$ (trilinear R-parity breaking SUSY mechanism) and $M'^{0\nu}_{\tilde{q}}$ (squark mixing mechanism) for the $0\nu\beta\beta$-decays of ^{76}Ge, ^{82}Se, ^{100}Mo, ^{130}Te and ^{136}Xe within the Selfconsistent Renormalized Quasiparticle Random Phase Approximation (SRQRPA). $G^{0\nu}(E_0, Z)$ is the phase-space factor. We notice that all NMEs given in Table 2.1 are real and positive. The nuclear radius is R = 1.1 fm $A^{1/3}$.

Nuclear transition	$G^{0\nu}(E_0,Z)$ $[y^{-1}]$			$\lvert M'^{0\nu}_{\nu}\rvert$		$\lvert M'^{0\nu}_{N}\rvert$		$\lvert M'^{0\nu}_{\lambda'}\rvert$		$\lvert M'^{0\nu}_{\tilde{q}}\rvert$	
				$g_A =$		$g_A =$		$g_A =$		$g_A =$	
		NN pot.	m.s.	1.0	1.25	1.0	1.25	1.0	1.25	1.0	1.25
$^{76}Ge \rightarrow {}^{76}Se$	7.98 10^{-15}	Argonne	intm.	3.85	4.75	172.2	232.8	387.3	587.2	396.1	594.3
			large	4.39	5.44	196.4	264.9	461.1	699.6	476.2	717.8
		CD-Bonn	intm.	4.15	5.11	269.4	351.1	339.7	514.6	408.1	611.7
			large	4.69	5.82	317.3	411.5	392.8	595.6	482.7	727.6
$^{82}Se \rightarrow {}^{82}Kr$	3.53 10^{-14}	Argonne	intm.	3.59	4.54	164.8	225.7	374.5	574.2	379.3	577.9
			large	4.18	5.29	193.1	262.9	454.9	697.7	465.1	710.2
		CD-Bonn	intm.	3.86	4.88	258.7	340.4	328.7	503.7	390.4	594.5
			large	4.48	5.66	312.4	408.4	388.0	594.4	471.8	719.9
$^{100}Mo \rightarrow {}^{100}Ru$	5.73 10^{-14}	Argonne	intm.	3.62	4.39	184.9	249.8	412.0	629.4	405.1	612.1
			large	3.91	4.79	191.8	259.8	450.4	690.3	449.0	682.6
		CD-Bonn	intm.	3.96	4.81	298.6	388.4	356.3	543.7	415.9	627.9
			large	4.20	5.15	310.5	404.3	384.4	588.6	454.8	690.5
$^{130}Te \rightarrow {}^{130}Xe$	5.54 10^{-14}	Argonne	intm.	3.29	4.16	171.6	234.1	385.1	595.2	382.2	588.9
			large	3.34	4.18	176.5	239.7	405.5	626.0	403.1	620.4
		CD-Bonn	intm.	3.64	4.62	276.8	364.3	335.8	518.8	396.8	611.1
			large	3.74	4.70	293.8	384.5	350.1	540.3	416.3	640.7
$^{136}Xe \rightarrow {}^{136}Ba$	5.92 10^{-14}	Argonne	intm.	2.30	2.29	119.2	163.5	275.0	425.3	270.5	417.2
			large	2.19	2.75	117.1	159.7	276.7	428.0	271.0	418.0
		CD-Bonn	intm.	2.32	2.95	121.4	166.7	274.4	424.3	267.4	412.1
			large	2.61	3.36	125.4	172.1	297.2	460.0	297.0	458.8

The single particle energies were obtained by using a Coulomb–corrected Woods–Saxon potential. Two-body G-matrix elements we derived from the Argonne and the

Charge Dependent Bonn (CD-Bonn) one-boson exchange potential within the Brueckner theory. The schematic pairing interactions have been adjusted to fit the empirical pairing gaps [96]. The particle-particle and particle-hole channels of the G-matrix interaction of the nuclear Hamiltonian H are renormalized by introducing the parameters g_{pp} and g_{ph}, respectively. The calculations have been carried out for $g_{ph} = 1.0$. The particle-particle strength parameter g_{pp} of the SRQRPA is fixed by the data on the two-neutrino double beta decays [60–62]. In the calculation of the $(\beta\beta)_{0\nu}$-decay NMEs, the two-nucleon short-range correlations derived from same potential as residual interactions, namely from the Argonne or CD-Bonn potentials, were considered [50].

The calculated NMEs $M'^{0\nu}_{\nu}$, $M'^{0\nu}_{N}$, $M'^{0\nu}_{\lambda'}$ and $M'^{0\nu}_{\tilde{q}}$ are listed in Table 2.1. We see that a significant source of uncertainty is the value of the axial-vector coupling constant g_A. Further, the NMEs associated with heavy neutrino exchange are sensitive also to the choice of the NN interaction, the CD-Bonn or Argonne potential. These types of realistic NN interaction differ mostly by the description of the short-range interactions.

Finally, we notice that all NMEs given in Table 2.1 are real and positive.

Chapter 3

Uncovering Multiple CP non-conserving Mechanisms in $(\beta\beta)_{0\nu}$-Decay

In this chapter we are going to illustrate the possibility to get information about the different LNV parameters when two or more mechanisms are operative in $(\beta\beta)_{0\nu}$-decay, analyzing the following two cases. First we consider two competitive "not-interfering" mechanisms of $(\beta\beta)_{0\nu}$-decay: light left-handed Majorana neutrino exchange and heavy right-handed Majorana neutrino exchange. In this case the interference term arising in the $(\beta\beta)_{0\nu}$-decay half-life from the product of the contributions due to the two mechanisms in the $(\beta\beta)_{0\nu}$-decay amplitude, is strongly suppressed [77] as a consequence of the different chiral structure of the final state electron current in the two amplitudes. The latter leads to a different phase-space factor for the interference term, which is typically by a factor of 10 smaller than the standard one (corresponding to the contribution to the $(\beta\beta)_{0\nu}$-decay half-life of each of the two mechanisms). More specifically, the suppression factors for ^{76}Ge, ^{82}Se, ^{100}Mo and ^{130}Te read, respectively [77]: 0.13; 0.08; 0.075 and 0.10. It is particularly small for ^{48}Ca: 0.04. In the analysis which follows we will neglect the contribution of the interference term in the $(\beta\beta)_{0\nu}$-decay half-life. The effect of taking into account the interference term on the results thus obtained, as our numerical calculations have shown, does not exceed approximately 10%.

In the case of negligible interference term, the inverse value of the $(\beta\beta)_{0\nu}$-decay half-life for a given isotope (A,Z) is given by:

$$\frac{1}{T^{0\nu}_{1/2,i} G^{0\nu}_i(E,Z)} \cong |\eta_\nu|^2 |M'^{0\nu}_{i,\nu}|^2 + |\eta_R|^2 |M'^{0\nu}_{i,N}|^2 \,, \tag{3.1}$$

where the index i denotes the isotope. The values of the phase space factor $G^{0\nu}_i(E,Z)$ and of the NMEs $M'^{0\nu}_{i,\nu}$ and $M'^{0\nu}_{i,N}$ are listed in Table 2.1. The parameters $|\eta_\nu|$ and $|\eta_R|$ are defined in eqs. (2.12) and (2.15). In this chapter we will work with the following isotopes: ^{76}Ge, ^{82}Se, ^{100}Mo and ^{130}Te.

In the second illustrative case we consider $(\beta\beta)_{0\nu}$-decay triggered by two active and "interfering" mechanisms: the light Majorana neutrino exchange and the gluino exchange. In this case, for a given nucleus, the inverse of the $(\beta\beta)_{0\nu}$-decay half-life is

given by:

$$\frac{1}{T^{0\nu}_{1/2,i} G^{0\nu}_i(E,Z)} = |\eta_\nu|^2 |M'^{0\nu}_{i,\nu}|^2 + |\eta_{\lambda'}|^2 |M'^{0\nu}_{i,\lambda'}|^2 + 2\cos\alpha |M'^{0\nu}_{i,\lambda'}||M'^{0\nu}_{i,\nu}||\eta_\nu||\eta_{\lambda'}|\,. \quad (3.2)$$

Here $|\eta_{\lambda'}|$ is the basic parameter of the gluino exchange mechanism defined in eq. (2.18) and α is the relative phase of $\eta_{\lambda'}$ and η_ν. The values of the NMEs of the mechanisms considered are listed in Table 2.1.

In the illustrative examples of how one can extract information about $|\eta_\nu|$, $|\eta_R|$, etc. we use as input hypothetical values of the $(\beta\beta)_{0\nu}$-decay half-life of ^{76}Ge satisfying the existing lower limits and the value claimed in ref. [47] [97], as well as the following hypothetical ranges for $T^{0\nu}_{1/2}(^{100}\mathrm{Mo})$ and $\mathrm{T}^{0\nu}_{1/2}(^{130}\mathrm{Te})$:

$$\begin{aligned} T^{0\nu}_{1/2}(^{76}Ge) \geq 1.9\times 10^{25} y, \quad T^{0\nu}_{1/2}(^{76}Ge) = 2.23^{+0.44}_{-0.31}\times 10^{25} y \\ 5.8\times 10^{23} y \leq T^{0\nu}_{1/2}(^{100}Mo) \leq 5.8\times 10^{24} y, \quad 3.0\times 10^{24} y \leq T^{0\nu}_{1/2}(^{130}Te) \leq 3.0\times 10^{25} y \end{aligned} \quad (3.3)$$

Let us note that 5.8×10^{23} y and 3.0×10^{24} y are the existing lower bounds on the half-lives of ^{100}Mo and ^{130}Te [98, 99].

In the analysis which follows we will present numerical results first for $g_A = 1.25$ and using the NMEs calculated with the large size single particle basis ("large basis") and the Charge Dependent Bonn (CD-Bonn) potential. Later results for $g_A = 1.0$, as well as for NMEs calculated with the Argonne potential, will also be reported.

As we will see, in certain cases of at least one more mechanism being operative in $(\beta\beta)_{0\nu}$-decay beyond the light neutrino exchange, one has to take into account the upper limit on the absolute scale of neutrino masses set by the ^3H β-decay experiments [31,48]: $m(\bar{\nu}_e) < 2.3$ eV. In the case of $(\beta\beta)_{0\nu}$-decay, this limit implies a similar limit on the effective Majorana mass [1] $|\langle m\rangle| < 2.3$ eV. The latter translates into the following limit on the conveniently rescaled parameter $|\eta_\nu|^2$:

$$|\eta_\nu|^2 \times 10^{10} < 0.21\,. \quad (3.4)$$

A more stringent limit on the absolute neutrino mass scale and therefore on $|\langle m\rangle|$ is planned to be obtained in the KATRIN experiment [48]: $|\langle m\rangle| < 0.2$ eV (90% C.L.). This corresponds to the following prospective limit on $|\eta_\nu|^2$:

$$|\eta_\nu|^2 \times 10^{10} < 1.6\times 10^{-3}\,. \quad (3.5)$$

As the results presented in Section 6 indicate, if the limit of 0.2 eV will be reached in the KATRIN experiment, this will lead to severe constraints on some of the solutions for $|\eta_\nu|^2$ obtained in the case of two "interfering" mechanisms, one of which is the light neutrino exchange.

I Two "Non-Interfering" Mechanisms

In the case of two active non-interfering $(\beta\beta)_{0\nu}$-decay generating mechanisms, which we will assume to be the light LH and heavy RH Majorana neutrino exchanges [77], it

[1] We remind the reader that for $m_{1,2,3} \gtrsim 0.1$ eV the neutrino mass spectrum is quasi-degenerate (QD), $m_1 \cong m_2 \cong m_3 \equiv m$, $m_j^2 \gg \Delta m^2_{21}, |\Delta m^2_{31}|$. In this case we have $m(\bar{\nu}_e) \cong m$ and $|\langle m\rangle| \lesssim m$.

is possible to extract the absolute values of the corresponding two LNV fundamental parameters $|\eta_\nu|$ and $|\eta_R|$, using the "data" on the half-lives of two different nuclei undergoing the $(\beta\beta)_{0\nu}$-decay. Indeed, using eq. (4.3) we can set a system of two linear equations for two unknowns using as input the two half-lives:

$$\frac{1}{T_1 G_1} = |\eta_\nu|^2 |M'^{0\nu}_{1,\nu}|^2 + |\eta_R|^2 |M'^{0\nu}_{1,N}|^2, \quad \frac{1}{T_2 G_2} = |\eta_\nu|^2 |M'^{0\nu}_{2,\nu}|^2 + |\eta_R|^2 |M'^{0\nu}_{2,N}|^2. \quad (3.6)$$

The solutions read:

$$|\eta_\nu|^2 = \frac{|M'^{0\nu}_{2,N}|^2/T_1 G_1 - |M'^{0\nu}_{1,N}|^2/T_2 G_2}{|M'^{0\nu}_{1,\nu}|^2 |M'^{0\nu}_{2,N}|^2 - |M'^{0\nu}_{1,N}|^2 |M'^{0\nu}_{2,\nu}|^2}, \quad |\eta_R|^2 = \frac{|M'^{0\nu}_{1,\nu}|^2/T_2 G_2 - |M'^{0\nu}_{2,\nu}|^2/T_1 G_1}{|M'^{0\nu}_{1,\nu}|^2 |M'^{0\nu}_{2,N}|^2 - |M'^{0\nu}_{1,N}|^2 |M'^{0\nu}_{2,\nu}|^2}. \quad (3.7)$$

Obviously, solutions giving $|\eta_\nu|^2 < 0$ and/or $|\eta_R|^2 < 0$ are unphysical. Given a pair of nuclei (A_1, Z_1), (A_2, Z_2) of the three ^{76}Ge, ^{100}Mo and ^{130}Te we will be considering, and T_1, and choosing (for convenience) always $A_1 < A_2$, positive solutions for $|\eta_\nu|^2$ and $|\eta_R|^2$ are possible for the following range of values of T_2:

$$\frac{T_1 G_1 |M'^{0\nu}_{1,N}|^2}{G_2 |M'^{0\nu}_{2,N}|^2} \leq T_2 \leq \frac{T_1 G_1 |M'^{0\nu}_{1,\nu}|^2}{G_2 |M'^{0\nu}_{2,\nu}|^2}\,, \quad (3.8)$$

where we have used the fact that $|M'^{0\nu}_{1,\nu}|^2/|M'^{0\nu}_{2,\nu}|^2 > |M'^{0\nu}_{1,N}|^2/|M'^{0\nu}_{2,N}|^2$ (see Table 2.1) [2]. Using the values of the phase-space factors and the two relevant NME given in Table I in the columns "CD-Bonn, large, $g_A = 1.25$", we get the positivity conditions for the ratio of the half-lives of the different pairs of the three nuclei of interest:

$$0.15 \leq \frac{T^{0\nu}_{1/2}(^{100}Mo)}{T^{0\nu}_{1/2}(^{76}Ge)} \leq 0.18\,, 0.17 \leq \frac{T^{0\nu}_{1/2}(^{130}Te)}{T^{0\nu}_{1/2}(^{76}Ge)} \leq 0.22\,, 1.14 \leq \frac{T^{0\nu}_{1/2}(^{130}Te)}{T^{0\nu}_{1/2}(^{100}Mo)} \leq 1.24\,. \quad (3.9)$$

In the case of $g_A = 1.0$ we find:

$$0.15 \leq \frac{T^{0\nu}_{1/2}(^{100}Mo)}{T^{0\nu}_{1/2}(^{76}Ge)} \leq 0.17\,, 0.17 \leq \frac{T^{0\nu}_{1/2}(^{130}Te)}{T^{0\nu}_{1/2}(^{76}Ge)} \leq 0.23\,, 1.16 \leq \frac{T^{0\nu}_{1/2}(^{130}Te)}{T^{0\nu}_{1/2}(^{100}Mo)} \leq 1.30\,. \quad (3.10)$$

It is quite remarkable that the physical solutions are possible only if the ratio of the half-lives of all the pairs of the three isotopes considered take values in very narrow intervals. This result is a consequence of the values of the phase space factors and of the NME for the two mechanisms considered. In the case of the Argonne potential, "large basis" and $g_A = 1.25$ (1.0) (see Table 2.1) we get very similar results:

$$0.15 \leq \frac{T^{0\nu}_{1/2}(^{100}Mo)}{T^{0\nu}_{1/2}(^{76}Ge)} \leq 0.18\,, 0.18 \leq \frac{T^{0\nu}_{1/2}(^{130}Te)}{T^{0\nu}_{1/2}(^{76}Ge)} \leq 0.24\,(0.25)\,, 1.22 \leq \frac{T^{0\nu}_{1/2}(^{130}Te)}{T^{0\nu}_{1/2}(^{100}Mo)} \leq 1.36\,(1.42)\,. \quad (3.11)$$

[2] This condition will exhibit a relatively weak dependence on the value of g_A in the cases of mechanisms in which the Gamow-Teller term in the NMEs dominates (as in the gluino exchange dominance and the squark-neutrino exchange mechanisms). Indeed, the factor $(1.25)^4$ (corresponding to $g_A = 1.25$) and included in the definition of the phase space terms $G_{1,2}$, cancels in the ratio G_1/G_2, and $|M'_{1,\nu(N)}|^2/|M'_{2,\nu(N)}|^2 = |M^{0\nu}_{1,\nu(N)}|^2/|M^{0\nu}_{2,\nu(N)}|^2$ (see eq. (2.3)).

If it is experimentally established that any of the three ratios of half-lives considered lies outside the interval of physical solutions of $|\eta_\nu|^2$ and $|\eta_R|^2$, obtained taking into account all relevant uncertainties, one would be led to conclude that the $(\beta\beta)_{0\nu}$-decay is not generated by the two mechanisms under discussion. In order to show that the constraints given above are indeed satisfied, the relevant ratios of $(\beta\beta)_{0\nu}$-decay half-lives should be known with a remarkably small uncertainty (not exceeding approximately 5% of the central values of the intervals).

Obviously, given the half-life of one isotope, constraints similar to those described above can be derived on the half-life of any other isotope beyond those considered by us. Similar constraints can be obtained in all cases of two "non-interfering" mechanisms generating the $(\beta\beta)_{0\nu}$-decay. The predicted intervals of half-lives of the various isotopes will differ, in general, for the different pairs of "non-interfering" mechanisms. However, these differences in the cases of the of the $(\beta\beta)_{0\nu}$-decay triggered by the exchange of heavy Majorana neutrinos coupled to (V+A) currents and i) the gluino exchange mechanism, or ii) the squark-neutrino exchange mechanism, are extremely small. One of the consequences of this feature of the different pairs of "non-interfering" mechanisms considered by us is that if it will be possible to rule out one of them as the cause of $(\beta\beta)_{0\nu}$-decay, most likely one will be able to rule out all three of them. The set of constraints under discussion will not be valid, in general, if the $(\beta\beta)_{0\nu}$-decay is triggered by two "interfering" mechanisms with a non-negligible interference term, or by more than two mechanisms with significant contributions to the $(\beta\beta)_{0\nu}$-decay rates of the different nuclei.

Evidently, if one of the two solutions is zero, for example $|\eta_R|^2 = 0$, then only one of the two $(\beta\beta)_{0\nu}$-decay mechanisms is active. Since for the two mechanisms considered we have $(M'^{0\nu}_{1,\nu})^2(M'^{0\nu}_{2,N})^2 - (M'^{0\nu}_{1,N})^2(M'^{0\nu}_{2,\nu})^2 \neq 0$, the condition that $|\eta_R|^2 = 0$ reads:

$$|M'^{0\nu}_{1,\nu}|^2\, T_1\, G_1 = |M'^{0\nu}_{2,\nu}|^2\, T_2\, G_2\,, \quad |\eta_R|^2 = 0\,. \tag{3.12}$$

The condition that $|\eta_\nu|^2 = 0$ has a similar form:

$$|M'^{0\nu}_{1,N}|^2\, T_1\, G_1 = |M'^{0\nu}_{2,N}|^2\, T_2\, G_2\,, \quad |\eta_\nu|^2 = 0\,. \tag{3.13}$$

If only the light neutrino exchange mechanism is present and the NME are correctly calculated, the $(\beta\beta)_{0\nu}$-decay effective Majorana mass (and $|\eta_\nu|^2$) extracted from all three (or any number of) $(\beta\beta)_{0\nu}$-decay isotopes must be the same (see, e.g., [71,100]). Similarly, if the heavy RH Majorana neutrino exchange gives the dominant contribution, the extracted value $|\eta_R|^2$ must be the same for all three (or more) $(\beta\beta)_{0\nu}$-decay nuclei.

We analyze next the possible solutions for different combinations of the half-lives of the following isotopes: ^{76}Ge, ^{100}Mo and ^{130}Te. Assuming the half-lives of two isotopes to be known and using the physical solutions for $|\eta_\nu|^2$ and $|\eta_R|^2$ obtained using these half-lives, one can obtain a prediction for the half-life of the third isotope. The predicted half-life should satisfy the existing lower limits on it. In the calculations the results of which are reported here, we fixed the half-life of one of the two isotopes and assumed the second half-life lies in an interval compatible with the existing constraints. We used the value of $\mathrm{T}^{0\nu}_{1/2}(^{76}Ge)$ and values of $\mathrm{T}^{0\nu}_{1/2}(^{100}Mo)$ and $\mathrm{T}^{0\nu}_{1/2}(^{130}Te)$ from the intervals given in (4.2). The system of two equations is solved and the values of $|\eta_\nu|^2 > 0$ and $|\eta_R|^2 > 0$ thus obtained were used to obtained predictions for the half-life of the third

Table 3.1: The predictions for the half-life of a third nucleus (A_3, Z_3), using as input in the system of equations for $|\eta_\nu|^2$ and $|\eta_R|^2$, eq. (3.6), the half-lives of two other nuclei (A_1, Z_1) and (A_2, Z_2). The three nuclei used are ^{76}Ge, ^{100}Mo and ^{130}Te. The results shown are obtained for a fixed value of the half-life of (A_1, Z_1) and assuming the half-life of (A_2, Z_2) to lie in a certain specific interval. The physical solutions for $|\eta_\nu|^2$ and $|\eta_R|^2$ and then used to derive predictions for the half-life of the third nucleus (A_3, Z_3). The latter are compared with the lower limits given in eq. (4.2). The results quoted are obtained for NMEs given in the columns "CD-Bonn, large, $g_A = 1.25$" in Table 2.1. One star beside the isotope pair whose half-lives are used as input for the system of equations (3.6), indicates predicted ranges of half-lives of the nucleus (A_3, Z_3) that are not compatible with the lower bounds given in (4.2).

Pair	$\mathtt{T}^{0\nu}_{1/2}(A_1, Z_1)$[yr]	$\mathtt{T}^{0\nu}_{1/2}[A_2, Z_2]$[yr]	Prediction on $[A_3, Z_3]$[yr]
$^{76}Ge - ^{100}Mo$	$\mathtt{T}(Ge) = 2.23 \cdot 10^{25}$	$3.23 \cdot 10^{24} \leq T(Mo) \leq 3.97 \cdot 10^{24}$	$3.68 \cdot 10^{24} \leq T(Te) \leq 4.93 \cdot 10^{24}$
$^{76}Ge - ^{130}Te$	$\mathtt{T}(Ge) = 2.23 \cdot 10^{25}$	$3.68 \cdot 10^{24} \leq T(Te) \leq 4.93 \cdot 10^{24}$	$3.23 \cdot 10^{24} \leq T(Mo) \leq 3.97 \cdot 10^{24}$
$^{76}Ge - ^{100}Mo$	$\mathtt{T}(Ge) = 10^{26}$	$1.45 \cdot 10^{25} \leq T(Mo) \leq 1.78 \cdot 10^{25}$	$1.65 \cdot 10^{25} \leq T(Te) \leq 2.21 \cdot 10^{25}$
$^{76}Ge - ^{130}Te$	$\mathtt{T}(Ge) = 10^{26}$	$1.65 \cdot 10^{25} \leq T(Te) \leq 2.21 \cdot 10^{25}$	$1.45 \cdot 10^{25} \leq T(Mo) \leq 1.78 \cdot 10^{25}$
$^{100}Mo - ^{130}Te$ $\star$	$\mathtt{T}(Mo) = 5.8 \cdot 10^{23}$	$6.61 \cdot 10^{23} \leq T(Te) \leq 7.20 \cdot 10^{23}$	$3.26 \cdot 10^{24} \leq T(Ge) \leq 4.00 \cdot 10^{24}$
$^{100}Mo - ^{130}Te$	$\mathtt{T}(Mo) = 4 \cdot 10^{24}$	$4.56 \cdot 10^{24} \leq T(Te) \leq 4.97 \cdot 10^{24}$	$2.25 \cdot 10^{25} \leq T(Ge) \leq 2.76 \cdot 10^{25}$
$^{100}Mo - ^{130}Te$	$\mathtt{T}(Mo) = 5.8 \cdot 10^{24}$	$6.61 \cdot 10^{24} \leq T(Te) \leq 7.20 \cdot 10^{24}$	$3.26 \cdot 10^{25} \leq T(Ge) \leq 4.00 \cdot 10^{25}$
$^{100}Mo - ^{130}Te$ $\star$	$\mathtt{T}(Te) = 3 \cdot 10^{24}$	$2.42 \cdot 10^{24} \leq T(Mo) \leq 2.63 \cdot 10^{24}$	$1.36 \cdot 10^{25} \leq T(Ge) \leq 1.82 \cdot 10^{25}$
$^{100}Mo - ^{130}Te$	$\mathtt{T}(Te) = 1.65 \cdot 10^{25}$	$1.33 \cdot 10^{25} \leq T(Mo) \leq 1.45 \cdot 10^{25}$	$7.47 \cdot 10^{25} \leq T(Ge) \leq 1.00 \cdot 10^{26}$
$^{100}Mo - ^{130}Te$	$\mathtt{T}(Te) = 3 \cdot 10^{25}$	$2.42 \cdot 10^{25} \leq T(Mo) \leq 2.63 \cdot 10^{25}$	$1.36 \cdot 10^{26} \leq T(Ge) \leq 1.82 \cdot 10^{26}$

isotope. The results for NMEs corresponding to the case "CD-Bonn, large, $g_A = 1.25$" (see Table 2.1) are given in Table 3.1. We note that the experimental lower bounds quoted in eq. (4.2) have to be taken into account since they can further constrain the range of allowed values of $|\eta_\nu|^2$ and $|\eta_R|^2$. Indeed, an inspection of the values in Table 3.1 shows that not all the ranges predicted for the third half-life using the solutions obtained for $|\eta_R|^2$ and $|\eta_\nu|^2$ are compatible with the lower bounds on the half-live of the considered nuclear isotopes, given in (4.2). In this case, some or all "solution" values of $|\eta_R|^2$ and/or $|\eta_\nu|^2$ are ruled out. In Table 3.1 these cases are marked by a star.

The results reported in Table 3.1 are stable with respect to variations of the NMEs. If we use the NMEs corresponding to the case "CD-Bonn, large, $g_A = 1.0$" (see Table 2.1), the limits of the
intervals quoted in Table 3.1 change by $\pm 5\%$. If instead we use the NMEs corresponding to the Argonne potential, "large basis" and $g_A = 1.25$ ($g_A = 1.0$), the indicated limits change by $\pm 10\%$ ($\pm 14\%$).

These results and considerations are illustrated in Figs. 3.1-3.5. The horizontal dashed line in these figures corresponds to the prospective limit planned to be obtained in the upcoming KATRIN experiment [48]. In figure 3.1 we show the solutions for $|\eta_R|^2$ and/or $|\eta_\nu|^2$ (conveniently rescaled), obtained for two values of $T^{0\nu}_{1/2}(^{76}Ge) = 2.23 \times 10^{25}$ y and 10^{26} y, assuming $T^{0\nu}_{1/2}(^{100}Mo)$ has a value in a certain interval. In the case of $T^{0\nu}_{1/2}(^{76}Ge) = 2.23 \times 10^{25}$ and $T^{0\nu}_{1/2}(^{76}Ge) = 10^{26}$ y, the derived physical values of $|\eta_R|^2$ and $|\eta_\nu|^2$ lead to predictions for $T^{0\nu}_{1/2}(^{100}Te)$ which are compatible with the existing lower limit (Fig. 3.1, left and right panel). We get similar results using as input in the system of two equations for $|\eta_R|^2$ and $|\eta_\nu|^2$ the half-lives of different pairs of isotopes, and the lower limit of the half-life of the third as an additional constraint. They are presented in Figs. 3.2 - 3.4. In Fig. 3.5 we show the solutions for $|\eta_\nu|^2$ and $|\eta_R|^2$ for $T^{0\nu}_{1/2}(^{130}Te) = 3 \times 10^{24}$ y and $T^{0\nu}_{1/2}(^{100}Mo) = (2.42 - 2.63) \times 10^{24}$ y. In contrast to the

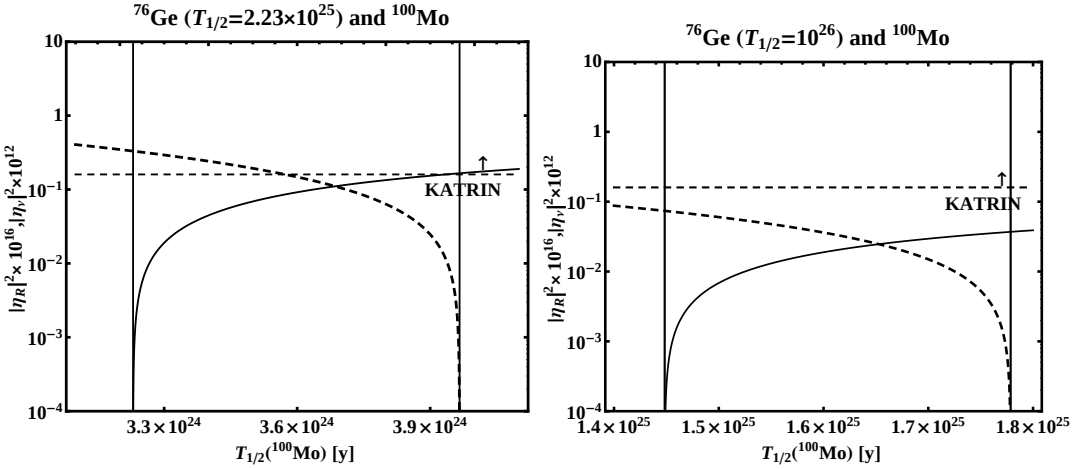

Figure 3.1: The values of the rescaled parameters $|\eta_\nu|^2$ (solid line) and $|\eta_R|^2$ (dashed lined), obtained as solutions of eq. (3.6) for two values of $T^{0\nu}_{1/2}(^{76}Ge)$ and values of $T^{0\nu}_{1/2}(^{100}Mo)$ lying in a specific interval. The physical (positive) solutions are delimited by the two vertical lines. The lower bound on $T^{0\nu}_{1/2}(^{130}Te)$ given in (4.2) does not lead to further constraints on $|\eta_\nu|^2$ and $|\eta_R|^2$. The horizontal dashed line corresponds to the prospective upper limit from the upcoming ^3H β-decay experiment KATRIN [48]. See text for further details.

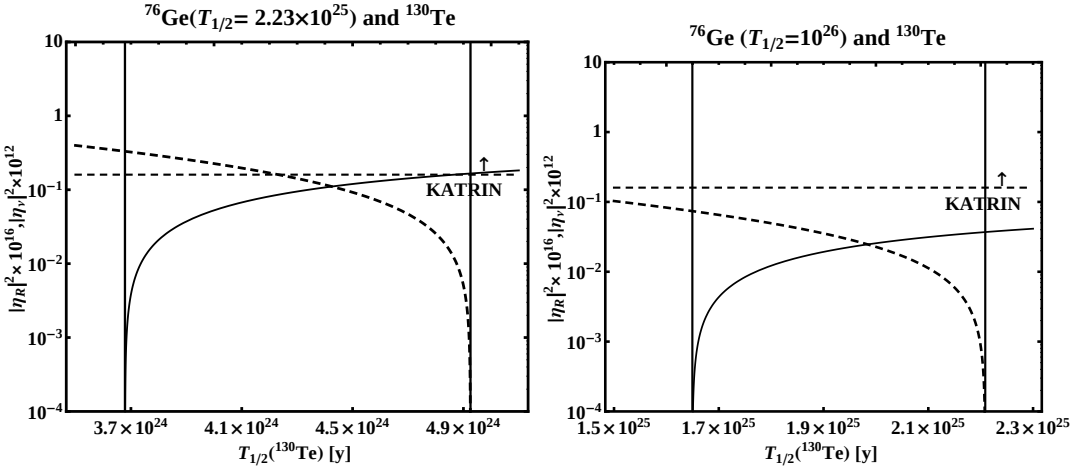

Figure 3.2: The same as in Fig. 3.1, but using as input hypothetical values of the half-lives of ^{76}Ge and ^{130}Te, $T^{0\nu}_{1/2}(^{76}Ge)$ and $T^{0\nu}_{1/2}(^{130}Te)$. The physical (positive) solutions are delimited by the two vertical lines. The lower bound on $T^{0\nu}_{1/2}(^{100}Mo)$ given in (4.2) does not lead to further constraints on $|\eta_{\nu,R}|^2$.

cases illustrated in Figs. 3.1 - 3.4, most of the solution values of $|\eta_\nu|^2$ and $|\eta_R|^2$ are excluded by taking into account the lower bound on $T^{0\nu}_{1/2}(^{76}Ge)$ given in eq. (4.2).

We have studied also the dependence of the results discussed above on the value of g_A and the NMEs used. This was done using the "large basis" NMEs, obtained with the CD-Bonn and Argonne potentials for the two values of $g_A = 1.25;\ 1.0$. Some of the results of this study are presented graphically in Figs. 3.6 and 4.6. The horizontal dashed line in these two figures corresponds again to the prospective limit from the

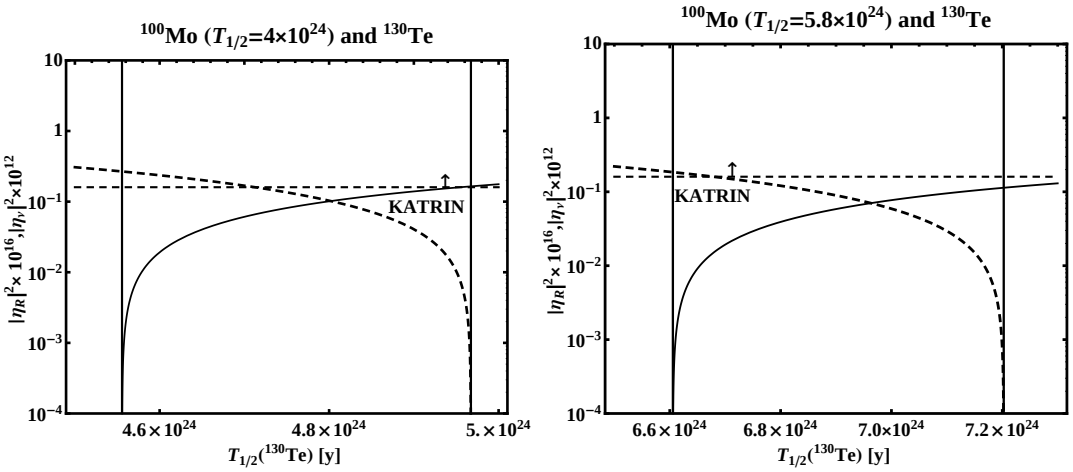

Figure 3.3: The same as in Fig. 3.1, but using as input two values of the half-life of ^{100}Mo and values of the half-life of ^{130}Te lying in a specific interval. The physical (positive) solutions are delimited by the two vertical lines. The lower bound on $T^{0\nu}_{1/2}(^{76}Ge)$ given in (4.2) does not lead to further constraints on $|\eta_\nu|^2$ and $|\eta_R|^2$.

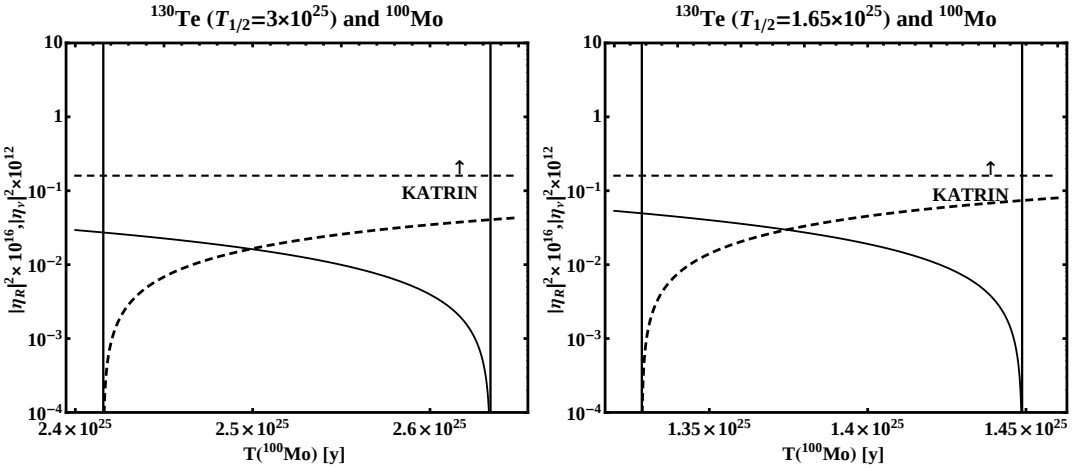

Figure 3.4: The same as in Fig. 3.3, but using as input two values of the half-life of ^{130}Te and values of the half-life of ^{100}Mo lying in a specific interval. The physical (positive) solutions are delimited by the two thick vertical lines. The lower bound on $T^{0\nu}_{1/2}(^{76}Ge)$ does not lead to further constraints on $|\eta_\nu|^2$ and $|\eta_R|^2$.

upcoming KATRIN experiment [48]. We note that in the cases studied by us, changing the value of g_A from 1.25 to 1.0 for a given potential (CD-Bonn or Argonne) does not lead to a significant change of the solutions for $|\eta_\nu|^2$ and $|\eta_R|^2$: the change is smaller than approximately 10%. The solutions exhibit a larger variation when for a given g_A and basis, the NMEs calculated with the CD-Bonn potential are replaced by the NME's obtained with the Argonne potential (Fig. 4.6, upper right and lower left panels). In this case, as we have mentioned earlier, given T_1, the interval of allowed values of the half-life of the second nucleus T_2 changes somewhat. In the specific cases shown, e.g., in Fig. 4.6 (upper right and lower left panels), $T_1 \equiv T^{0\nu}_{1/2}(^{76}Ge) = 2.23 \times 10^{25}$ y and the interval of interest of values of $T_2 \equiv T^{0\nu}_{1/2}(^{100}Mo)$ shifts to larger

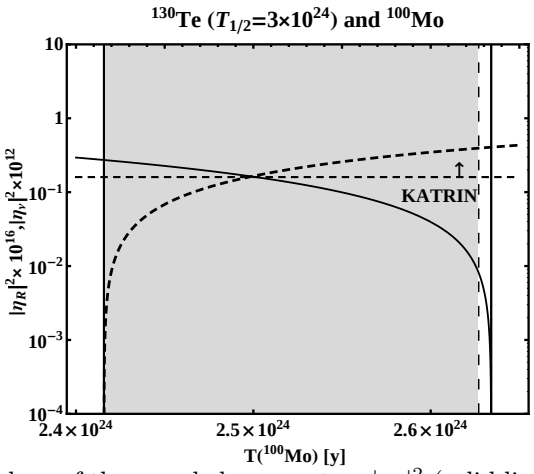

Figure 3.5: The values of the rescaled parameters $|\eta_\nu|^2$ (solid line) and $|\eta_R|^2$ (dashed lined), obtained as solutions of eq. (3.6) for the minimum value of $T^{0\nu}_{1/2}(^{130}Te)$ specified in eq. (4.2). The physical (positive) solutions are delimited by the two vertical lines. The gray region is an excluded due to the lower bound on $T^{0\nu}_{1/2}(^{76}Ge)$ quoted in (4.2).

values. Obviously, the solution values of the parameters $|\eta_\nu|^2$ and $|\eta_R|^2$, obtained with the two different sets of the NMEs, can differ drastically in the vicinity of the maximum and minimum values of T_2, as is also seen in Figs. 3.6 and 4.6. If a given extreme value of T_2, say $\max(T_2)$, obtained with one set of NMEs, belongs to the interval of allowed values of T_2, found with a second set of NMEs, one of the fundamental parameters, calculated at $\max(T_2)$ with the first set of NMEs can be zero, and can have a relatively large nonzero value when calculated with the second set of NMEs. Moreover, there are narrow intervals of values of T_2 for which there exist physical solutions for $|\eta_\nu|^2$ and $|\eta_R|^2$ if one uses the NMEs obtained with the CD-Bonn potential and there are no physical solutions for the NMEs derived with the Argonne potential. If the measured value of T_2 falls in such an interval, this can imply that either the two mechanisms considered are not at work in $(\beta\beta)_{0\nu}$-decay, or one of the two sets of NMEs does not describe correctly the nuclear transitions. As Figs. 3.6 and 4.6 indicate, the data from the KATRIN experiment can help limit further the solutions for $|\eta_\nu|^2$, obtained with NMEs calculated with the CD-Bonn potential and $g_A = 1.0$ or with the Argonne potential.

Let us note finally that Figs. 3.6 and 4.6 were obtained using hypothetical half-lives of ^{76}Ge and ^{100}Mo. We get similar results if we use as input hypothetical half-lives of a different pair of nuclei, ^{76}Ge and ^{130}Te, ^{130}Te and ^{100}Mo, etc.

II Two "Interfering" Mechanisms

Neutrinoless double beta decay can be triggered by two competitive mechanisms whose interference contribution to the $(\beta\beta)_{0\nu}$-decay rates is non-negligible. In this Section we analyze the case of light Majorana neutrino exchange and gluino exchange. From equation (4.4) it is possible to extract the values of $|\eta_\nu|^2$, $|\eta_{\lambda'}|^2$ and $\cos\alpha$ setting up a system of three equation with these three unknowns using as input the "data" on the

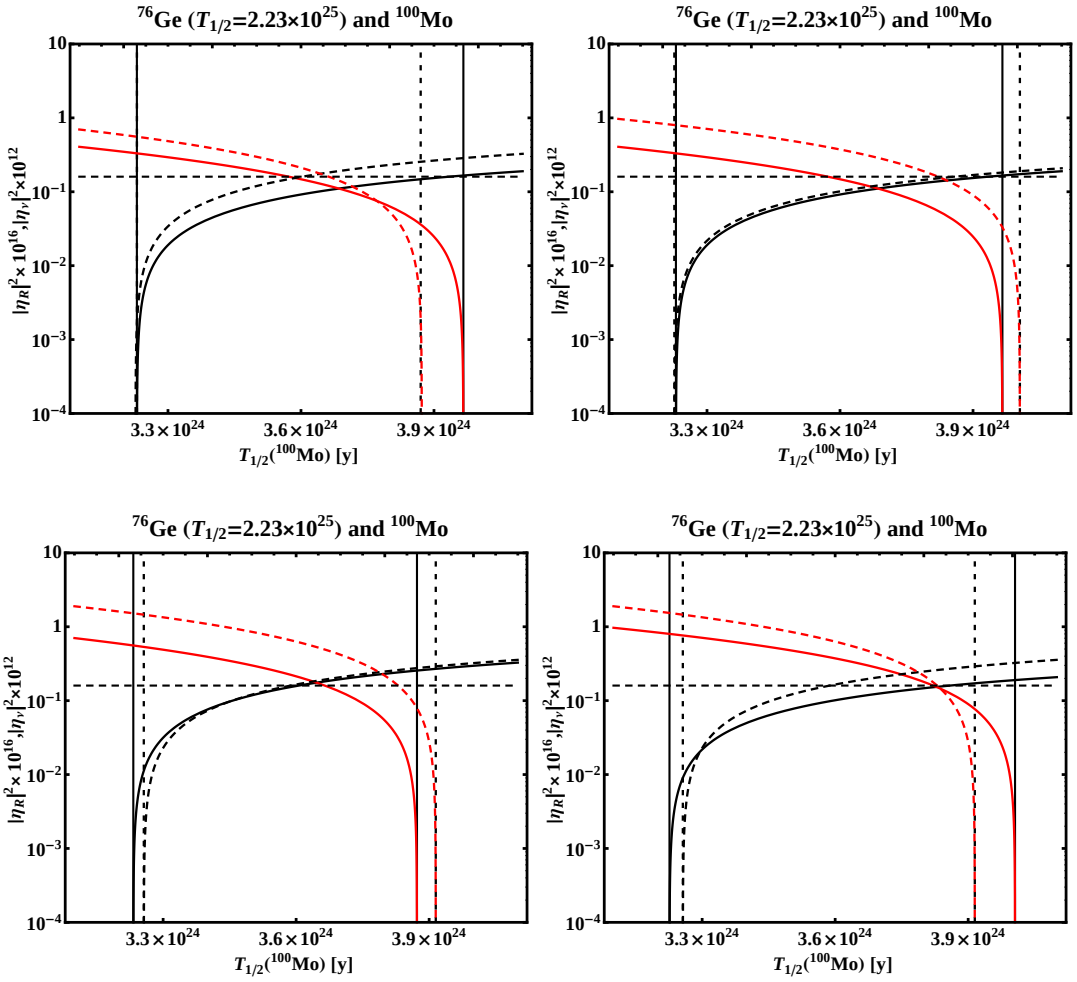

Figure 3.6: Solutions for $|\eta_\nu|^2$ (black lines) and $|\eta_R|^2$ (red lines), obtained by fixing $T_1 = T^{0\nu}_{1/2}(^{76}Ge) = 2.23 \times 10^{25}$ yr and $T_2 = T^{0\nu}_{1/2}(^{100}Mo)$ and using the sets of NMEs calculated using the "large basis" and i) CD-Bonn potential, $g_A = 1.25$ (solid lines) and $g_A = 1$ (dashed lines) (upper left panel); ii) CD-Bonn (solid lines) and Argonne (dashed lines) potentials with $g_A = 1.25$ (upper right panel); iii) CD-Bonn (solid lines) and Argonne (dashed lines) potentials with $g_A = 1.0$ (lower left panel); iv) Argonne potential with $g_A = 1.25$ (solid lines) and $g_A = 1$ (dashed lines) (lower right panel). The physical (positive) solutions for $|\eta_\nu|^2$ and $|\eta_R|^2$ shown with solid (dashed) lines are delimited by two vertical solid (dashed) lines. The horizontal dashed line corresponds to the prospective upper limit [48] $|\langle m\rangle|$ ¡ 0.2 eV.

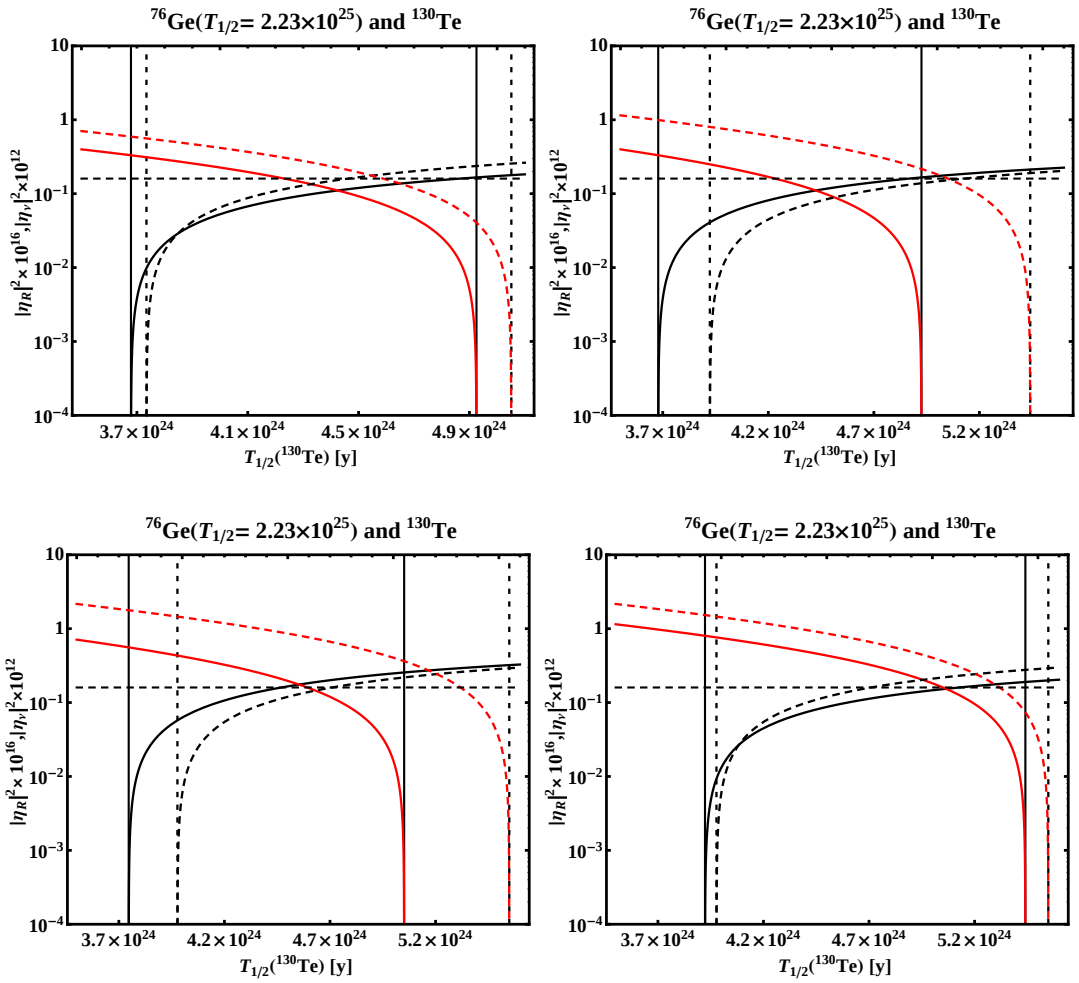

Figure 3.7: The same as in Fig. 3.6, but for $T_1 = T^{0\nu}_{1/2}(^{76}Ge) = 2.23 \times 10^{25}$ yr and $T_2 = T^{0\nu}_{1/2}(^{130}Te)$.

half-lives of three different nuclei. The solutions are given by:

$$|\eta_\nu|^2 = \frac{D_1}{D}\,, \quad |\eta_{\lambda'}|^2 = \frac{D_2}{D}\,, \quad z \equiv 2\cos\alpha|\eta_\nu||\eta_{\lambda'}| = \frac{D_3}{D}\,, \tag{3.14}$$

where D, D_1, D_2 and D_3 are the following determinants

$$D = \begin{vmatrix} (M'^{0\nu}_{1,\nu})^2 & (M'^{0\nu}_{1,\lambda'})^2 & M'^{0\nu}_{1,\lambda'}M'^{0\nu}_{1,\nu} \\ (M'^{0\nu}_{2,\nu})^2 & (M'^{0\nu}_{2,\lambda'})^2 & M'^{0\nu}_{2,\lambda'}M'^{0\nu}_{2,\nu} \\ (M'^{0\nu}_{3,\nu})^2 & (M'^{0\nu}_{3,\lambda'})^2 & M'^{0\nu}_{3,\lambda'}M'^{0\nu}_{3,\nu} \end{vmatrix}\,, \quad D_1 = \begin{vmatrix} 1/T_1G_1 & (M'^{0\nu}_{1,\lambda'})^2 & M'^{0\nu}_{1,\lambda'}M'^{0\nu}_{1,\nu} \\ 1/T_2G_2 & (M'^{0\nu}_{2,\lambda'})^2 & M'^{0\nu}_{2,\lambda'}M'^{0\nu}_{2,\nu} \\ 1/T_3G_3 & (M'^{0\nu}_{3,\lambda'})^2 & M'^{0\nu}_{3,\lambda'}M'^{0\nu}_{3,\nu} \end{vmatrix}\,, \tag{3.15}$$

$$D_2 = \begin{vmatrix} (M'^{0\nu}_{1,\nu})^2 & 1/T_1G_1 & M'^{0\nu}_{1,\lambda'}M'^{0\nu}_{1,\nu} \\ (M'^{0\nu}_{2,\nu})^2 & 1/T_2G_2 & M'^{0\nu}_{2,\lambda'}M'^{0\nu}_{2,\nu} \\ (M'^{0\nu}_{3,\nu})^2 & 1/T_3G_3 & M'^{0\nu}_{3,\lambda'}M'^{0\nu}_{3,\nu} \end{vmatrix}\,, \quad D_3 = \begin{vmatrix} (M'^{0\nu}_{1,\nu})^2 & (M'^{0\nu}_{1,\lambda'})^2 & 1/T_1G_1 \\ (M'^{0\nu}_{2,\nu})^2 & (M'^{0\nu}_{2,\lambda'})^2 & 1/T_2G_2 \\ (M'^{0\nu}_{3,\nu})^2 & (M'^{0\nu}_{3,\lambda'})^2 & 1/T_3G_3 \end{vmatrix}\,. \tag{3.16}$$

We must require that $|\eta_\nu|^2$ and $|\eta_{\lambda'}|^2$ be non-negative and that the factor $2\cos\alpha|\eta_\nu||\eta_{\lambda'}|$ in the interference term satisfies:

$$-2|\eta_\nu||\eta_{\lambda'}| \leq 2\cos\alpha|\eta_\nu||\eta_{\lambda'}| \leq 2|\eta_\nu||\eta_{\lambda'}|. \tag{3.17}$$

If we fix (i.e. have data on) the half-lives of two of the nuclei and combine these with the condition in eq. (4.35), we can obtain the interval of values of the half-life of the third nucleus, which is compatible with the data on the half-lives of the two other nuclei and the mechanisms considered. The minimal (maximal) value of this interval of half-lives of the third nucleus is obtained for $\cos\alpha = +1$ ($\cos\alpha = -1$). Examples of the intervals of half-life values of the third nucleus obtained using the half-life values of the other two nuclei [3] for the $(\beta\beta)_{0\nu}$-decay mechanisms discussed are listed in Table 3.2. The results reported in Table 3.2 are obtained with NMEs corresponding to the CD-Bonn potential, the "large basis" and $g_A = 1.25$.

Table 3.2: Ranges of half-lives of T_3 in the case of two interfering mechanisms: the light Majorana neutrino exchange and gluino exchange dominance.

$\mathtt{T}^{0\nu}_{1/2}$[y] (fixed)	$\mathtt{T}^{0\nu}_{1/2}$[y] (fixed)	Allowed
$\mathtt{T}(Ge) = 2.23 \cdot 10^{25}$	$\mathtt{T}(Mo) = 5.8 \cdot 10^{24}$	$5.99 \cdot 10^{24} \leq T(Te) \leq 7.35 \cdot 10^{24}$
$\mathtt{T}(Ge) = 2.23 \cdot 10^{25}$	$\mathtt{T}(Te) = 3 \cdot 10^{24}$	$2.46 \cdot 10^{24} \leq T(Mo) \leq 2.82 \cdot 10^{24}$
$\mathtt{T}(Ge) = 10^{26}$	$\mathtt{T}(Mo) = 5.8 \cdot 10^{24}$	$6.30 \cdot 10^{24} \leq T(Te) \leq 6.94 \cdot 10^{24}$
$\mathtt{T}(Ge) = 10^{26}$	$\mathtt{T}(Te) = 3 \cdot 10^{24}$	$2.55 \cdot 10^{24} \leq T(Mo) \leq 2.72 \cdot 10^{24}$
$\mathtt{T}(Ge) = 2.23 \cdot 10^{25}$	$\mathtt{T}(Te) = 3 \cdot 10^{25}$	$2.14 \cdot 10^{25} \leq T(Mo) \leq 3.31 \cdot 10^{25}$
$\mathtt{T}(Ge) = 10^{26}$	$\mathtt{T}(Te) = 3 \cdot 10^{25}$	$2.38 \cdot 10^{25} \leq T(Mo) \leq 2.92 \cdot 10^{25}$

We show in few illustrative figures (Figs. 3.8 - 3.11) the results of the determination of $|\eta_\nu|^2$, $|\eta_{\lambda'}|^2$ and $\cos\alpha$ using different values of half-lives of the three nuclei ^{76}Ge, ^{100}Mo and ^{130}Te from the intervals given in eq. (4.2). The lower bounds of the half-lives quoted in eq. (4.2) are taken into account. In these figures the physical allowed regions correspond to the areas shown in white, while the areas shown in gray are excluded.

[3] Technically this is done in the following way. Fixing the half-lives of two isotopes, T_1 and T_2, and varying the half-life of the third isotope T_3 in a certain interval, we obtained $|\eta_\nu|^2$, $|\eta_{\lambda'}|^2$ and $z = 2\cos\alpha|\eta_\nu||\eta_{\lambda'}|$ as a function of T_3. Requiring that $|\eta_\nu|^2 > 0$, $|\eta_{\lambda'}|^2 > 0$ and that $-2\eta_\nu||\eta_{\lambda'}| \leq z \leq 2\eta_\nu||\eta_{\lambda'}|$ determines the interval of physically allowed values of T_3 (given T_1, T_2 and the mechanisms of $(\beta\beta)_{0\nu}$-decay considered). This interval of physically allowed values of T_3 is shown in Table 3.2.

The allowed interval of values of the half-life of the 3rd nucleus, corresponding to the white areas, are listed in the 3rd column of Table 3.2. The results presented in Figs. 3.8 - 3.11 are derived using the NMEs, calculated with the CD-Bonn potential, the "large basis" and $g_A = 1.25$.

It is interesting to note that for the two fixed half-life values used to obtain Figs. 3.8, 3.9 and 3.10, the interference between the contributions of the two mechanisms considered is destructive: one finds using these values that for most of the physical (positive) solutions for $|\eta_\nu|^2$ and $|\eta_{\lambda'}|^2$, $\cos\alpha$ is negative. Moreover, the rescaled parameters $|\eta_\nu|^2 \times 10^{10}$ and $|\eta_{\lambda'}|^2 \times 10^{14}$ in most of the solution regions have very close values. This is due to the fact that for most of the physically allowed values of $|\eta_\nu|^2$ and $|\eta_{\lambda'}|^2$, each of the two terms including $|\eta_\nu|^2$ or $|\eta_{\lambda'}|^2$ as a factor in the right hand side of eq. (4.4) is much larger than the free term in the left hand side of eq. (4.4). As a consequence, in order to explain the "data" (i.e. the chosen values of the half-lives of the three isotopes) there should be a strong mutual compensation between the contributions due to the two mechanisms. This is possible only if $|\eta_\nu|^2 (M'^{0\nu}_{i,\nu})^2$ and $|\eta_{\lambda'}|^2 (M'^{0\nu}_{i,\lambda'})^2$ have close values and $\cos\alpha \cong -1$.

In the case of destructive interference between the two contributions, $|\langle m \rangle|$ can have values which exceed the limit on the absolute scale of neutrino masses set by the ^3H β-decay experiments [31,48], eq. (3.4). This limit is indicated as a horizontal solid line in Figs. 3.8 - 3.10. It leads to further constraints on the physical solution for $|\eta_\nu|^2$, and thus for $|\eta_{\lambda'}|^2$.

As we have already indicated, a more stringent limit on the absolute neutrino mass scale and therefore on $|\langle m \rangle|$ is planned to be obtained in the KATRIN experiment [48]: it is given in eq. (3.5). The KATRIN prospective upper bound is shown as a horizontal dashed line in Figs. 3.8 - 3.10. As the results presented in Figs. 3.8 - 3.10 indicate, if the limit of 0.2 eV will be reached in KATRIN experiment, if will lead to severe constraints on the solutions for $|\eta_\nu|^2$ obtained in the cases we have considered, strongly disfavoring (if not ruling out) essentially all of them.

In Fig. 3.11 we illustrate the possibility of constructive interference between the light neutrino and the gluino exchange contributions. The solutions shown in Fig. 3.11 are not constrained by the limits obtained in the ^3H β-decay experiments [31,48]; they also satisfy the prospective upper limit from KATRIN experiment.

It is not difficult to derive from eqs. (4.32) - (3.16) the general conditions under which $|\eta_\nu|^2$ and $|\eta_{\lambda'}|^2$ are positive and the interference between the light neutrino and gluino exchange contributions is constructive (destructive), i.e. $\cos\alpha$ (or z) is positive (negative). We will illustrate them later using again the NMEs calculated with the CD-Bonn potential, the "large basis" and $g_A = 1.25$.

Consider first the conditions for constructive interference. We will introduce a somewhat simplified notations in this part of the chapter: T_i, G_i, M_i and Λ_i for $i = 1, 2, 3$ will denote respectively the half-life, phase space factor, light neutrino and dominant gluino exchange NMEs for ^{76}Ge ($i = 1$), ^{100}Mo ($i = 2$) and ^{130}Te ($i = 3$). The first thing to notice is that it follows from Table 2.1 that the ratios of NMEs M_i/Λ_i satisfy the inequalities:

$$\frac{M_1}{\Lambda_1} > \frac{M_2}{\Lambda_2} > \frac{M_3}{\Lambda_3}\,. \tag{3.18}$$

This implies that the determinant D, defined in eq. (3.15), is negative:

$$D = \Lambda_1^2 \Lambda_2^2 \Lambda_3^2 (\frac{M_2}{\Lambda_2} - \frac{M_1}{\Lambda_1})(\frac{M_3}{\Lambda_3} - \frac{M_1}{\Lambda_1})(\frac{M_3}{\Lambda_3} - \frac{M_2}{\Lambda_2}), \tag{3.19}$$

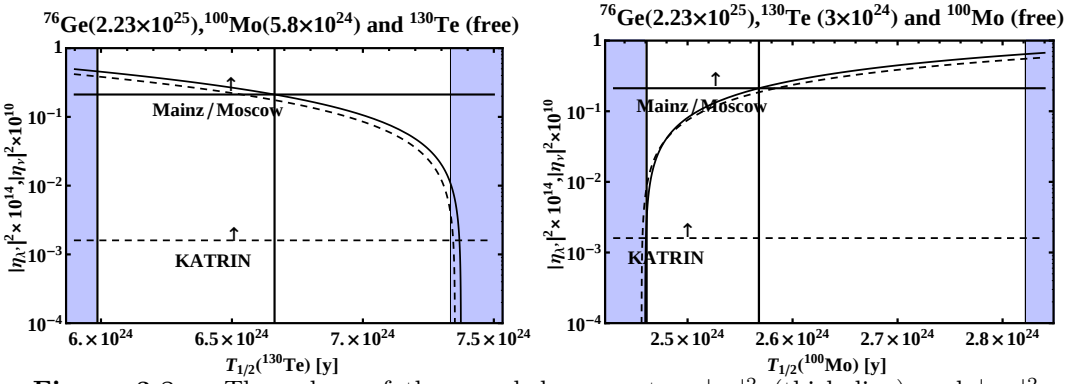

Figure 3.8: The values of the rescaled parameters $|\eta_\nu|^2$ (thick line) and $|\eta_{\lambda'}|^2$ (dashed lined), obtained as solutions of the system of equations (4.4) for fixed values of $T^{0\nu}_{1/2}(^{76}Ge)$ and $T^{0\nu}_{1/2}(^{100}Mo)$ and values of $T^{0\nu}_{1/2}(^{130}Te)$ lying in a specific interval. The physical allowed regions correspond to the areas shown in white, while the areas shown in gray are excluded. The horizontal solid (dashed) line corresponds to the upper limit [31, 48] $|\langle m\rangle|$ ¡ 2.3 eV (prospective upper limit [48] $|\langle m\rangle|$ ¡ 0.2 eV). See text for details.

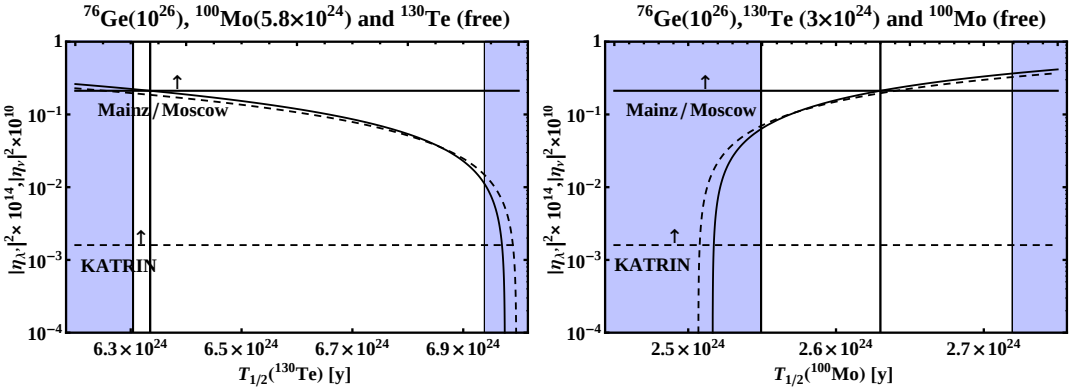

Figure 3.9: The same as in Fig. 3.8 for a different set of values of the three half-lives used as input in the analysis.

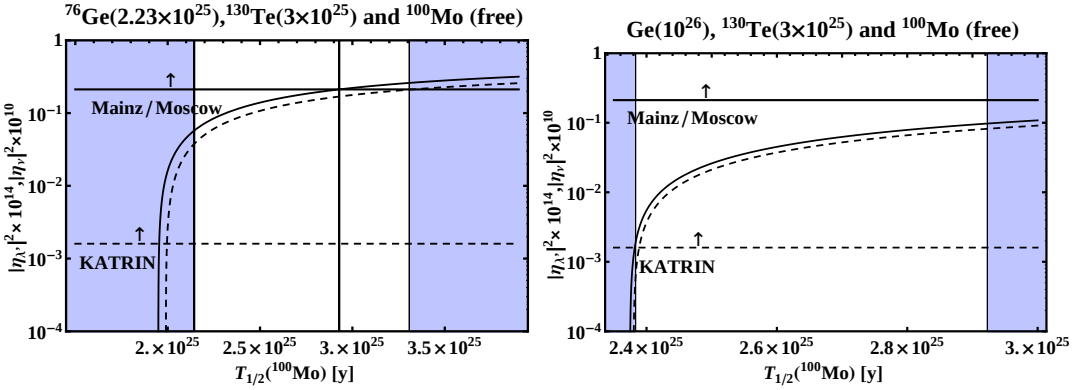

Figure 3.10: The same as in Figs. 3.8 and 3.9 for a different set of values of the three half-lives used as input in the analysis.

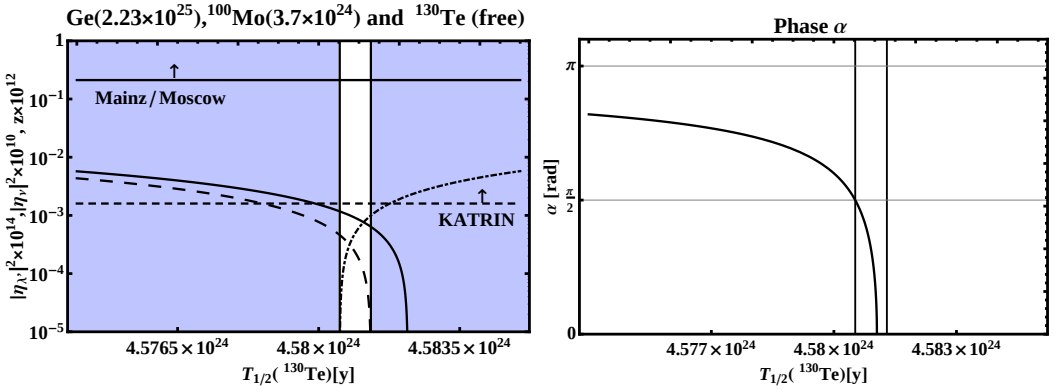

Figure 3.11: Left Panel: the values of $|\eta_\nu|^2 \times 10^{10}$ (thick line), $|\eta_{\lambda'}|^2 \times 10^{14}$ (dashed line) and $z = 2\cos\alpha|\eta_\nu||\eta_{\lambda'}| \times 10^{12}$ (dot-dashed line) corresponding to the half-lives of ^{76}Ge, ^{100}Mo and ^{130}Te indicated on the figure. The interval of values of $T^{0\nu}_{1/2}(^{130}\mathrm{Te})$ between the two vertical lines corresponds to physical (positive) solutions for $|\eta_\nu|^2$ and $|\eta_{\lambda'}|^2$ as well as to a positive z (i.e. to a constructive interference between the contributions due to the two mechanisms). The horizontal solid (dashed) line corresponds to the upper limit [31] [48] $|\langle m\rangle|$ ¡2.3 eV (prospective upper limit [48] $|\langle m\rangle|$ ¡ 0.2 eV). See text for details. Right Panel: the phase α.

Consequently, in order to have $|\eta_\nu|^2 >, |\eta_{\lambda'}|^2 > 0$ and constructive interference between the two contributions, i.e. $z > 0$, all three determinants D_1, D_2 and D_3, defined in eqs. (3.15) and (3.16), have to be negative: $D_a < 0$, $a = 1, 2, 3$. Given the half-life T_1 and the NMEs M_i and Λ_i, these three conditions are satisfied if each of the two half-lives T_2 and T_3 lies in specific intervals [4]:

$$A)\quad \begin{cases} \frac{\Lambda_1^2}{\Lambda_2^2}\,\frac{G_1}{G_2}\,T_1 < T_2 \leq \frac{M_1\Lambda_1}{M_2\Lambda_2}\,\frac{G_1}{G_2}\,T_1\,, \\ \frac{(M_2^2\Lambda_1^2 - M_1^2\Lambda_2^2)\,\frac{G_2}{G_3}\,T_2}{(M_3^2\Lambda_1^2 - M_1^2\Lambda_3^2) + \frac{T_2G_2}{T_1G_1}(M_2^2\Lambda_3^2 - M_3^2\Lambda_2^2)} < T_3 < \frac{(M_2\Lambda_2\Lambda_1^2 - M_1\Lambda_1\Lambda_2^2)\,\frac{G_2}{G_3}\,T_2}{(M_3\Lambda_3\Lambda_1^2 - M_1\Lambda_1\Lambda_3^2) + \frac{T_2G_2}{T_1G_1}(M_2\Lambda_2\Lambda_3^2 - M_3\Lambda_3\Lambda_2^2)}\,; \end{cases}$$

$$B)\quad \begin{cases} \frac{M_1\Lambda_1}{M_2\Lambda_2}\,\frac{G_1}{G_2}\,T_1 < T_2 < \frac{M_1^2}{M_2^2}\,\frac{G_1}{G_2}\,T_1\,, \\ \frac{(M_2^2\Lambda_1^2 - M_1^2\Lambda_2^2)\,\frac{G_2}{G_3}\,T_2}{(M_3^2\Lambda_1^2 - M_1^2\Lambda_3^2) + \frac{T_2G_2}{T_1G_1}(M_2^2\Lambda_3^2 - M_3^2\Lambda_2^2)} < T_3 < \frac{(M_2\Lambda_2M_1^2 - M_1\Lambda_1M_2^2)\,\frac{G_2}{G_3}\,T_2}{(M_3\Lambda_3M_1^2 - M_1\Lambda_1M_3^2) + \frac{T_2G_2}{T_1G_1}(M_2\Lambda_2M_3^2 - M_3\Lambda_3M_2^2)}\,; \end{cases} \tag{3.20}$$

For the NMEs calculated with the CD-Bonn potential, the "large basis" and $g_A = 1.25$ and given $T_1 \neq 0$, the conditions for constructive interference, $z > 0$, read:

$$z > 0\,:\, \begin{cases} 0.14\,T_1 < T_2 \leq 0.16\,T_1\,, & \frac{4.44\,T_1\,T_2}{3.74\,T_1 - 0.93\,T_2} \leq T_3 \leq \frac{2.10\,T_1\,T_2}{1.78\,T_1 - 0.47\,T_2}\,; \\ 0.16\,T_1 < T_2 < 0.18\,T_1\,, & \frac{4.44\,T_1\,T_2}{3.74\,T_1 - 0.93\,T_2} \leq T_3 \leq \frac{4.10\,T_1\,T_2}{3.44\,T_1 - 0.81\,T_2}\,. \end{cases} \tag{3.21}$$

[4] The quoted solutions are valid, as can be shown, provided $M_3/\Lambda_3 < M_2/\Lambda_2 < 0.5(1+\sqrt{5})M_3/\Lambda_3$, which is fulfilled for the NMEs given in Table 2.1.

These conditions imply that given T_1, a constructive interference is possible only if T_2 lies in a relatively narrow interval and T_3 has a value in extremely narrow intervals, the interval for T_2 being determined by the value of T_1, while that for T_3 - by T_1 and the interval for T_2. The fact that both the intervals for T_2 and T_3 are so narrow is a consequence of the values of the NMEs used, more precisely, of the fact that, for each of the two mechanisms discussed, the NMEs for the three nuclei considered differ relatively little: we have $|M_i - M_j| << M_i, M_j$, $|\Lambda_i - \Lambda_j| << \Lambda_i, \Lambda_j$, $i \neq j = 1, 2, 3$, and typically $|M_i - M_j|/(0.5(M_i + M_j)) \sim 10^{-1}$, $|\Lambda_i - \Lambda_j|/(0.5(\Lambda_i + \Lambda_j)) \sim (10^{-2} - 10^{-1})$. We get similar results for the other sets of NMEs, quoted in Table 2.1 and calculated with the "large basis". In order to have a constructive interference in a much wider interval of values of T_2, i.e., to have the minimal value of T_2 much smaller than the maximal value of T_2 in case A) in eq. (3.20), for instance, the following inequality has to be satisfied: $\Lambda_1/\Lambda_2 << M_1/M_2$. An inspection of Table 2.1 shows that this inequality is not satisfied by any of the relevant sets of NMEs. Numerically, the intervals of values of T_2 and T_3 given in eq. (4.37), for which $z > 0$, are very similar to those quoted in eq. (4.12).

For the value of T(^{76}Ge)= $2.23{\cdot}10^{25}$ y, for instance, the conditions for a constructive interference are given by:

$$\begin{aligned} &3.18 \cdot 10^{24}\ \text{y} < T_2 \leq 3.55 \cdot 10^{24}\ \text{y}, \quad \frac{1.19 T_2}{1.00 - 1.12 \cdot 10^{-26}\ \text{y}^{-1} T_2} < T_3 < \frac{1.19 T_2}{1.00 - 1.18 \cdot 10^{-26} \text{y}^{-1} T_2} \\ &3.55 \cdot 10^{24}\ \text{y} < T_2 < 3.97 \cdot 10^{24}\ \text{y}, \quad \frac{1.186 T_2}{1.00 - 1.117 \cdot 10^{-26} \text{y}^{-1} T_2} < T_3 < \frac{1.189 T_2}{1.00 - 1.059 \cdot 10^{-26} \text{y}^{-1} T_2}\,. \end{aligned} \tag{3.22}$$

Given the fact that $3.18 \cdot 10^{24}$ y $< T_2 \leq 3.97 \cdot 10^{24}$ y and that T_2 enters in the denominators of the limiting values of T_3 multiplied by 10^{-26} y^{-1}, the interval of values of T_3 of interest is extremely narrow. We have $z > 0$ for, e.g., T(^{76}Ge)= $2.23{\cdot}10^{25}$ y, T(^{100}Mo)= $3.7{\cdot}10^{24}$ y and T(^{130}Te)= $4.58{\cdot}10^{24}$ y, as is also illustrated in Fig. 3.11.

There are cases in which one has $|\eta_\nu|^2 = 0$ or $|\eta_{\lambda'}|^2 = 0$. The general conditions for having $|\eta_\nu|^2 = 0$ or $|\eta_{\lambda'}|^2 = 0$ can be derived from eqs. (4.32) - (3.16) and read:

$$\begin{aligned} &|\eta_\nu|^2 = 0, |\eta_{\lambda'}|^2 \neq 0, \quad \begin{cases} T2 = \frac{\Lambda_1^2}{\Lambda_2^2} \frac{G_1}{G_2} T_1 \\ T_3 = \frac{(M_2 \Lambda_2 \Lambda_1^2 - M_1 \Lambda_1 \Lambda_2^2) \frac{G_2}{G_3} T_2}{(M_3 \Lambda_3 \Lambda_1^2 - M_1 \Lambda_1 \Lambda_3^2) + \frac{T_2 G_2}{T_1 G_1} (M_2 \Lambda_2 \Lambda_3^2 - M_3 \Lambda_3 \Lambda_2^2)}\,; \end{cases} \\ &|\eta_{\lambda'}|^2 = 0, |\eta_\nu|^2 \neq 0 \quad \begin{cases} T_2 = \frac{M_1^2}{M_2^2} \frac{G_1}{G_2} T_1\,, \\ T_3 = \frac{(M_2 \Lambda_2 M_1^2 - M_1 \Lambda_1 M_2^2) \frac{G_2}{G_3} T_2}{(M_3 \Lambda_3 M_1^2 - M_1 \Lambda_1 M_3^2) + \frac{T_2 G_2}{T_1 G_1} (M_2 \Lambda_2 M_3^2 - M_3 \Lambda_3 M_2^2)}\,. \end{cases} \end{aligned} \tag{3.23}$$

They correspond to some of the limiting values of T_2 and T_3 in eq. (3.20). We will illustrate them below numerically using the NMEs calculated with the CD-Bonn potential, the "large basis" and $g_A = 1.25$. If, for instance, one fixes $T_1 \equiv$ T(^{76}Ge)= $2.23{\cdot}10^{25}$, we have i) $|\eta_\nu|^2 = 0$ (and zero interference term) for $T_2 = 3.18 \cdot 10^{24}$ y and $T_3 = 3.91 \cdot 10^{24}$ y; ii) $|\eta_{\lambda'}|^2 = 0$ (and zero interference term) for $T_2 = 3.97 \cdot 10^{24}$ y and $T_3 = 4.93 \cdot 10^{24}$ y, where T_2 and T_3 denote the half-lives of ^{100}Mo and ^{130}Te, respectively. In general,

given T_1 we have $|\eta_\nu|^2 = 0$, $|\eta_{\lambda'}|^2 \neq 0$ if

$$T_2 = 0.14 T_1\,, \quad T_3 = \frac{2.10\, T_1\, T_2}{1.78\, T_1 - 0.47\, T_2} \cong 0.18\, T_1\,, \tag{3.24}$$

and $|\eta_{\lambda'}|^2 = 0$, $|\eta_\nu|^2 \neq 0$ provided

$$T_2 = 0.18 T_1\,, \quad T_3 = \frac{4.10\, T_1 T_2}{3.44\, T_1 - 0.81\, T_2} \cong 0.22\, T_1\,. \tag{3.25}$$

The conditions for having zero interference term, $z = 0$, but $|\eta_\nu|^2 \neq 0$ or $|\eta_{\lambda'}|^2 \neq 0$, read:

$$\begin{cases} \frac{\Lambda_1^2}{\Lambda_2^2}\,\frac{G_1}{G_2}\, T_1 < T_2 < \frac{M_1^2}{M_2^2}\,\frac{G_1}{G_2}\, T_1\,, \\ T_3 = \frac{(M_2^2\Lambda_1^2 - M_1^2\Lambda_2^2)\,\frac{G_2}{G_3}\, T_2}{(M_3^2\Lambda_1^2 - M_1^2\Lambda_3^2) + \frac{T_2 G_2}{T_1 G_1}(M_2^2\Lambda_3^2 - M_3^2\Lambda_2^2)}\,. \end{cases} \tag{3.26}$$

Given T_1, the general conditions for destructive interference, i.e. for $z < 0$, can be derived in a similar way. They read:

$$A) \quad \begin{cases} 0 < T_2 \leq \frac{\Lambda_1^2}{\Lambda_2^2}\,\frac{G_1}{G_2}\, T_1, \\ 0 < T_3 < \frac{(M_2\Lambda_2\Lambda_1^2 - M_1\Lambda_1\Lambda_2^2)\,\frac{G_2}{G_3}\, T_2}{(M_3\Lambda_3\Lambda_1^2 - M_1\Lambda_1\Lambda_3^2) + \frac{T_2 G_2}{T_1 G_1}(M_2\Lambda_2\Lambda_3^2 - M_3\Lambda_3\Lambda_2^2)}\,; \end{cases} \tag{3.27}$$

$$B) \quad \begin{cases} \frac{\Lambda_1^2}{\Lambda_2^2}\,\frac{G_1}{G_2}\, T_1 < T_2 \leq \frac{M_1^2}{M_2^2}\,\frac{G_1}{G_2}\, T_1\,, \\ 0 < T_3 < \frac{(M_2^2\Lambda_1^2 - M_1^2\Lambda_2^2)\,\frac{G_2}{G_3}\, T_2}{(M_3^2\Lambda_1^2 - M_1^2\Lambda_3^2) + \frac{T_2 G_2}{T_1 G_1}(M_2^2\Lambda_3^2 - M_3^2\Lambda_2^2)}\,; \end{cases} \tag{3.28}$$

$$C) \quad \begin{cases} \frac{M_1^2}{M_2^2}\,\frac{G_1}{G_2}\, T_1 < T_2 < \frac{M_1\Lambda_1 M_3 - \Lambda_3 M_1^2}{M_2\Lambda_2 M_3 - \Lambda_3 M_2^2}\,\frac{G_1}{G_2}\, T_1\,, \\ 0 < T_3 < \frac{(M_2\Lambda_2 M_1^2 - M_1\Lambda_1 M_2^2)\,\frac{G_2}{G_3}\, T_2}{(M_3\Lambda_3 M_1^2 - M_1\Lambda_1 M_3^2) + \frac{T_2 G_2}{T_1 G_1}(M_2\Lambda_2 M_3^2 - M_3\Lambda_3 M_2^2)}\,; \end{cases} \tag{3.29}$$

$$D) \quad \begin{cases} T_2 \geq \frac{M_1\Lambda_1 M_3 - \Lambda_3 M_1^2}{M_2\Lambda_2 M_3 - \Lambda_3 M_2^2}\,\frac{G_1}{G_2}\, T_1\,, \\ T_3 > 0. \end{cases} \tag{3.30}$$

Obviously, one has to take into account the existing experimental lower limits on T_2 and T_3 in eqs. (3.27) - (3.30). We will give next the "numerical" equivalent of the conditions (3.27) - (3.30), obtained with NMEs calculated with the CD-Bonn potential, the "large basis" and $g_A = 1.25$:

$$z < 0 : \begin{cases} T_2 \leq 0.14\, T_1\,, & T_3 \leq \frac{2.10\, T_1\, T_2}{1.78 T_1 - 0.47 T_2}\,; \\ 0.14\, T_1 < T_2 \leq 0.18\, T_1\,, & T_3 \leq \frac{4.44\, T_1\, T_2}{3.74\, T_1 - 0.93\, T_2}\,; \\ 0.18\, T_1 < T_2 < 4.23\, T_1\,, & T_3 \leq \frac{4.10\, T_1\, T_2}{3.44\, T_1 - 0.81\, T_2}\,; \\ T_2 \geq 4.23\, T_1 & T_3 > 0\,. \end{cases} \tag{3.31}$$

The intervals of values of T_2 and T_3 in eqs. (3.27) - (3.31) are very different from those corresponding to the case of two "non-interfering" $(\beta\beta)_{0\nu}$-decay mechanisms given in eq. (4.12), the only exception being the second set of intervals in eq. (3.31), which partially overlap with those in eq. (4.12). This difference can allow to discriminate experimentally between the two possibilities of $(\beta\beta)_{0\nu}$-decay being triggered by two "non-interfering" mechanisms or by two "destructively interfering" mechanisms. We have check how the intervals of values of the half-life T_3 given in Table 3.2, corresponding to NMEs derived with the CD-Bonn potential, $g_A = 1.25$ and the "large basis", change when one uses the NMEs obtained with the same potential and basis, but using $g_A = 1.0$, as well as the NMEs found with the Argonne potential for $g_A = 1.25;\ 1.0$ and the "large basis". The results are shown in Tables 3.3 - 3.5. We see that for certain values of the hypothetical half-lives of the two nuclei, the interval of allowed values of the half-life of the third nucleus becomes noticeably larger when calculated with NMEs, corresponding to $g_A = 1.0$ or to the Argonne potential. This is due to a relatively deep compensation between the three terms in the $(\beta\beta)_{0\nu}$-decay rate of the third nucleus in the case of a negative interference term (destructive interference).

Similar analysis can be performed for any other pair of "interfering" mechanisms assumed to be operative in $(\beta\beta)_{0\nu}$-decay. We note also that the extension of the analysis to more than two mechanisms generating the $(\beta\beta)_{0\nu}$-decay is rather straightforward.

Table 3.3: CD-Bonn potential and $g_A = 1$

$T^{0\nu}_{1/2}$[y](fixed)	$T^{0\nu}_{1/2}$[y](fixed)	Allowed
$T(Ge) = 2.23 \cdot 10^{25}$	$T(Mo) = 5.8 \cdot 10^{24}$	$3 \cdot 10^{24} \leq T(Te) \leq 8.62 \cdot 10^{24}$
$T(Ge) = 2.23 \cdot 10^{25}$	$T(Te) = 3 \cdot 10^{24}$	$2.55 \cdot 10^{24} \leq T(Mo) \leq 6.18 \cdot 10^{24}$
$T(Ge) = 2.23 \cdot 10^{25}$	$T(Te) = 3 \cdot 10^{25}$	$1.33 \cdot 10^{25} \leq T(Mo) \leq 3.88 \cdot 10^{26}$
$T(Ge) = 10^{26}$	$T(Mo) = 5.8 \cdot 10^{24}$	$3.62 \cdot 10^{24} \leq T(Te) \leq 6.04 \cdot 10^{24}$
$T(Ge) = 10^{26}$	$T(Te) = 3 \cdot 10^{24}$	$3.11 \cdot 10^{24} \leq T(Mo) \leq 4.70 \cdot 10^{24}$
$T(Ge) = 10^{26}$	$T(Te) = 3 \cdot 10^{25}$	$2.15 \cdot 10^{25} \leq T(Mo) \leq 8.29 \cdot 10^{25}$

Table 3.4: Argonne potential and $g_A = 1.25$

$T^{0\nu}_{1/2}$[y](fixed)	$T^{0\nu}_{1/2}$[y](fixed)	Allowed
$T(Ge) = 2.23 \cdot 10^{25}$	$T(Mo) = 5.8 \cdot 10^{24}$	$3 \cdot 10^{24} \leq T(Te) \leq 9.22 \cdot 10^{24}$
$T(Ge) = 2.23 \cdot 10^{25}$	$T(Te) = 3 \cdot 10^{24}$	$2.55 \cdot 10^{24} \leq T(Mo) \leq 7.92 \cdot 10^{24}$
$T(Ge) = 2.23 \cdot 10^{25}$	$T(Te) = 3 \cdot 10^{25}$	$1.19 \cdot 10^{25} \leq T(Mo) \leq 2.55 \cdot 10^{27}$
$T(Ge) = 10^{26}$	$T(Mo) = 5.8 \cdot 10^{24}$	$3.15 \cdot 10^{24} \leq T(Te) \leq 5.85 \cdot 10^{24}$
$T(Ge) = 10^{26}$	$T(Te) = 3 \cdot 10^{24}$	$3.25 \cdot 10^{24} \leq T(Mo) \leq 5.49 \cdot 10^{24}$
$T(Ge) = 10^{26}$	$T(Te) = 3 \cdot 10^{25}$	$2.08 \cdot 10^{25} \leq T(Mo) \leq 1.20 \cdot 10^{26}$

Table 3.5: Argonne Potential and $g_A = 1$

$T^{0\nu}_{1/2}$[y](fixed)	$T^{0\nu}_{1/2}$[y](fixed)	Allowed
$T(Ge) = 2.23 \cdot 10^{25}$	$T(Mo) = 5.8 \cdot 10^{24}$	$3 \cdot 10^{24} \leq T(Te) \leq 1.11 \cdot 10^{25}$
$T(Ge) = 2.23 \cdot 10^{25}$	$T(Te) = 3 \cdot 10^{24}$	$2.63 \cdot 10^{24} \leq T(Mo) \leq 2.04 \cdot 10^{25}$
$T(Ge) = 2.23 \cdot 10^{25}$	$T(Te) = 3 \cdot 10^{25}$	$9.19 \cdot 10^{24} \leq T(Mo) \leq 2.36 \cdot 10^{26}$
$T(Ge) = 10^{26}$	$T(Mo) = 5.8 \cdot 10^{24}$	$3 \cdot 10^{24} \leq T(Te) \leq 5.07 \cdot 10^{24}$
$T(Ge) = 10^{26}$	$T(Te) = 3 \cdot 10^{24}$	$3.82 \cdot 10^{24} \leq T(Mo) \leq 9.44 \cdot 10^{24}$
$T(Ge) = 10^{26}$	$T(Te) = 3 \cdot 10^{25}$	$1.96 \cdot 10^{25} \leq T(Mo) \leq 6.54 \cdot 10^{26}$

Finally, we would like to point out to one additional consequence of the "positivity" conditions and the condition the interference term should satisfy when two "interfering" mechanisms are responsible for the $(\beta\beta)_{0\nu}$-decay. Let us denote the two fundamental parameters characterizing the two mechanisms by η_β and η_κ. Then, given the half-life of one isotope, say of ^{76}Ge (T_1), and an experimental lower bound on the half-life of a second isotope, e.g., of ^{130}Te(T_3), the conditions $|\eta_\beta|^2 > 0$, $|\eta_\kappa|^2 > 0$ and $-|\eta_\beta||\eta_\kappa| \leq |\eta_\beta||\eta_\kappa| \cos\alpha_{\beta\kappa} \leq |\eta_\beta||\eta_\kappa|$, imply a constraint on the half-life of any third isotope, say of ^{100}Mo (T_2). This latter constraint depends noticeably on the type of the two "interfering" mechanisms generating the $(\beta\beta)_{0\nu}$-decay and can be used, in principle, to discriminate between the different possible pairs of "interfering" mechanisms. Below we illustrate this result by deriving the constraint one obtains on the half-life of ^{100}Mo, T_2, assuming that the half-life of ^{76}Ge is $T_1 = 2.23 \times 10^{25}$ y and taking into account the current experimental lower bound on the half-life of ^{130}Te, $T_3 > 3.0 \times 10^{24}$ y. Using these "data" as input, the NMEs calculated with the CD-Bonn and Argonne potentials, the "large basis" and $g_A = 1.25$, we get the following constraint on T_2 for the different pairs of "interfering" mechanisms discussed by us (the numbers in brackets are obtained with the NMEs corresponding to the Argonne potential, unless otherwise indicated).

Light Neutrino and gluino exchange mechanisms:

$$T_2 \equiv T^{0\nu}_{1/2}(^{100}Mo) > 2.46\ (2.47) \times 10^{24}\ \text{y}. \tag{3.32}$$

Increasing the value of $T^{0\nu}_{1/2}(^{76}Ge)$ leads to the increasing of the value of the lower limit.

Light Neutrino and LH Heavy neutrino exchange mechanisms:

$$T^{0\nu}_{1/2}(^{100}Mo) > 2.78\ (2.68) \times 10^{24}\ \text{y}. \tag{3.33}$$

The value of the lower limit increases with the increasing of the value of the half-life of ^{76}Ge.

LH Heavy neutrino and gluino exchange mechanisms:

$$1.36 \times 10^{24}\ \text{y} < T^{0\nu}_{1/2}(^{100}Mo) < 3.42 \times 10^{24}\ \text{y}\,. \tag{3.34}$$

Increasing the value of $T^{0\nu}_{1/2}(^{76}Ge)$ leads to a shift of the interval to larger values, and for a sufficiently large $T^{0\nu}_{1/2}(^{76}Ge) > 10^{26}$ y - even just to a lower bound on $T^{0\nu}_{1/2}(^{100}Mo)$. For $T_1 = 10^{26}$ y, for instance, we find 4.19×10^{24} y $< T^{0\nu}_{1/2}(^{100}Mo) < 3.39 \times 10^{25}$ y.

Using the NMEs derived with the Argonne potential we find a very different result - only a lower bound: $T^{0\nu}_{1/2}(^{100}Mo) > 5.97 \times 10^{23}$ y. The difference between the results obtained with the two sets of NMEs can be traced to fact that the determinant D in eqs. (4.32) and (3.15), calculated with the second set of NMEs, has opposite sign to that, calculated with the first set of NMEs. As a consequence, the dependence of the physical solutions for $|\eta^L_N|^2$ and $|\eta_{\lambda'}|^2$ on T_1, T_2 and T_3 in the two cases of NMEs is very different.

Squarks-neutrino and gluino exchange mechanisms:

$$T^{0\nu}_{1/2}(^{100}Mo) > 7.92\ (22.1) \times 10^{23}\ \text{y}. \tag{3.35}$$

For larger values of $T^{0\nu}_{1/2}(^{76}Ge)$, this lower bound assumes larger values.

We see that the two sets of NMEs lead to quite different results in the cases of the LH heavy neutrino and gluino exchange and squarks-neutrino and gluino exchange mechanisms. Nevertheless, the constraints thus obtained can be used, e.g., to exclude some of the possible cases of two "interfering" mechanisms inducing the $(\beta\beta)_{0\nu}$-decay. Indeed, if, for instance, it is confirmed that $T^{0\nu}_{1/2}(^{76}Ge) = 2.23\times10^{25}$ y, and in addition it is established, taking all relevant uncertainties into account, that $T^{0\nu}_{1/2}(^{100}Mo) \leq 10^{24}$ y, that combined with the experimental lower limit on $T^{0\nu}_{1/2}(^{130}Te)$ would rule out i) the light neutrino and gluino exchanges, and ii) the light neutrino and LH heavy neutrino exchanges, as possible mechanisms generating the $(\beta\beta)_{0\nu}$-decay.

III Final Remarks

In the present chapter we have considered the possibility of several different mechanisms contributing to the $(\beta\beta)_{0\nu}$-decay amplitude in the general case of CP nonconservation. The mechanisms discussed are light Majorana neutrino exchange, exchange of heavy Majorana neutrinos coupled to (V-A) currents, exchange of heavy Majorana neutrinos coupled to (V+A) currents, lepton charge non-conserving couplings in SUSY theories with R-parity breaking. Of the latter we have concentrated on the so-called "dominant gluino exchange" mechanism. Each of these mechanisms, described in chapter 2, is characterized by a specific fundamental LNV parameter. We have investigated in detail the cases of two "non-interfering" and two "interfering" mechanisms, generating the $(\beta\beta)_{0\nu}$-decay. In the analysis we have performed, we have used hypothetical $(\beta\beta)_{0\nu}$-decay half-lives of the following three isotopes: ^{76}Ge, ^{100}Mo and ^{130}Te. They are denoted as T_1, T_2 and T_3, respectively. Four sets of NMEs of the decays of these three nuclei were utilized: they were obtained with two different nucleon-nucleon potentials (CD-Bonn and Argonne) and two different values of the axial coupling constant $g_A = 1.25;\ 1.0$ (see Table 2.1).

If the $(\beta\beta)_{0\nu}$-decay is induced by two "non-interfering" mechanisms, which for concreteness we have considered to be the light LH Majorana neutrino exchange and the heavy RH Majorana neutrino exchange with $(V + A)$ currents, one can determine the squares of the absolute values of the two LNV parameters, characterizing these mechanisms, $|\eta_\nu|^2$ and $|\eta_R|^2$, from data on the half-lives of two nuclear isotopes. We have done that using as input all three possible pairs of half-lives of ^{76}Ge, ^{100}Mo and ^{130}Te, chosen from the intervals given in eq. (4.2) and satisfying the existing experimental lower limits, as well as the half-life of the $(\beta\beta)_{0\nu}$-decay of ^{76}Ge, claimed to be observed in [47]: $T^{0\nu}_{1/2}(^{76}Ge) = 2.23^{+0.44}_{-0.31} \times 10^{25}$ y. We find that if the half-life of one of the three nuclei is measured, the requirement that $|\eta_\nu|^2 \geq 0$ and $|\eta_R|^2 \geq 0$ ("positivity condition") constrains the other two half-lives (and the $(\beta\beta)_{0\nu}$-decay half-life of any other $(\beta\beta)_{0\nu}$-decaying isotope for that matter) to lie in specific intervals, determined by the measured half-life and the relevant NMEs (see eqs. (4.6) - (3.11)). This feature is common to all cases of two "non-interfering" mechanisms generating the $(\beta\beta)_{0\nu}$-decay. The indicated specific half-life intervals for the various isotopes, are stable with respect to the change of the NMEs (within the sets of NMEs considered by us) used to derive them. The intervals depend, in general, on the type of the two "non-interfering" mechanisms. However, these differences in the cases of the $(\beta\beta)_{0\nu}$-decay triggered by the exchange of heavy Majorana neutrinos coupled to (V+A) currents and i) the light

Majorana neutrino exchange, or ii) the gluino exchange mechanism, or i ii) the squark-neutrino exchange mechanism, are extremely small. One of the consequences of this feature of the different pairs of "non-interfering" mechanisms considered by us is that if it will be possible to rule out one of them as the cause of $(\beta\beta)_{0\nu}$-decay, most likely one will be able to rule out all three of them. Using the indicated difference to get information about the specific pair of "non-interfering" mechanisms possibly operative in $(\beta\beta)_{0\nu}$-decay requires, in the cases considered by us, an extremely high precision in the measurement of the $(\beta\beta)_{0\nu}$-decay half-lives of the isotopes considered. The levels of precision required seem impossible to achieve in the foreseeable future. If it is experimentally established that any of the indicated intervals of half-lives lies outside the interval of physical solutions of $|\eta_\nu|^2$ and $|\eta_R|^2$, obtained taking into account all relevant uncertainties, one would be led to conclude that the $(\beta\beta)_{0\nu}$-decay is not generated by the two mechanisms considered. The constraints under discussion will not be valid, in general, if the $(\beta\beta)_{0\nu}$-decay is triggered by two "interfering" mechanisms with a non-negligible (destructive) interference term, or by more than two mechanisms none of which plays a subdominant role in $(\beta\beta)_{0\nu}$-decay.

We have studied also the dependence of the physical solutions for $|\eta_\nu|^2$ and $|\eta_R|^2$ obtained on the NMEs used. Some of the results of this study are presented graphically in Figs. 3.6 and 4.6. We found that the solutions can exhibit a significant variation with the NMEs used. Given the half-life T_1, the interval of allowed values of the half-life of the second nucleus T_2, determined from the "positivity conditions", $|\eta_\nu|^2 \geq 0$, $|\eta_R|^2 \geq 0$, changes somewhat with the change of the NMEs. The solution values of the parameters $|\eta_\nu|^2$ and $|\eta_R|^2$, obtained with the two different sets of the NMEs, can differ drastically in the vicinity of the maximum and minimum values of T_2 (Figs. 3.6 and 4.6). If a given extreme value of T_2, say $\max(T_2)$, obtained with one set of NMEs, belongs to the interval of allowed values of T_2, found with a second set of NMEs, one of the fundamental parameters, calculated at $\max(T_2)$ with the first set of NMEs can be zero, and can have a relatively large nonzero value when calculated with the second set of NMEs. Moreover, there are narrow intervals of values of T_2 for which there exist physical solutions for $|\eta_\nu|^2$ and $|\eta_R|^2$ if one uses the NMEs obtained with the CD-Bonn potential and there are no physical solutions for the NMEs derived with the Argonne potential. If the measured value of T_2 falls in such an interval, this can imply that either the two mechanisms considered are not at work in $(\beta\beta)_{0\nu}$-decay, or one of the two sets of NMEs does not describe correctly the nuclear transitions.

Neutrinoless double beta decay can be generated by two competitive mechanisms whose interference contribution to the $(\beta\beta)_{0\nu}$-decay rates is non-negligible. In the case when two "interfering" mechanisms are responsible for the $(\beta\beta)_{0\nu}$-decay, the squares of the absolute values of the two relevant parameters and the interference term parameter, which involves the cosine of an unknown relative phase of the two fundamental parameters, can be uniquely determined, in principle, from data on the half-lives of three nuclei. We have analyzed in detail the case of light Majorana neutrino exchange and gluino exchange. In this case the parameters which are determined from data on the half-lives are $|\eta_\nu|^2$, $|\eta_{\lambda'}|^2$ and $z = 2\cos\alpha\,|\eta_\nu||\eta_{\lambda'}|$. The physical solutions for these parameters have to satisfy the conditions $|\eta_\nu|^2 \geq 0$, $|\eta_{\lambda'}|^2 \geq 0$ and $-2|\eta_\nu||\eta_{\lambda'}| \leq z \leq 2|\eta_\nu||\eta_{\lambda'}|$. The latter condition implies that given the half-lives of two isotopes, T_1 and T_2, the half-life of any third isotope T_3 is constrained to lie is a specific interval, if the mechanisms considered are indeed generating the $(\beta\beta)_{0\nu}$-decay. If further the half-life of one isotope T_1 is known, for the interference to be constructive (destructive) the half-lives of any other

pair of isotopes T_2 and T_3, should belong to specific intervals. These intervals depend on whether the interference between the two contributions in the $(\beta\beta)_{0\nu}$-decay rate is constructive or destructive. We have derived in analytic form the general conditions for i) constructive interference ($z > 0$), ii) destructive interference ($z < 0$), iii) $|\eta_\nu|^2 = 0$, $|\eta_{\lambda'}|^2 \neq 0$, iv) $|\eta_\nu|^2 \neq 0$, $|\eta_{\lambda'}|^2 = 0$ and v) $z = 0$, $|\eta_\nu|^2 \neq 0$, $|\eta_{\lambda'}|^2 \neq 0$.

We have found that, given T_1, a constructive interference is possible only if T_2 lies in a relatively narrow interval and T_3 has a value in extremely narrow intervals, the interval for T_2 being determined by the value of T_1, while that for T_3 - by T_1 and the interval for T_2. The fact that both the intervals for T_2 and T_3 are so narrow is a consequence of the fact that, for each of the two mechanisms discussed, the NMEs for the three nuclei considered differ relatively little: the relative difference between the NMEs of any two nuclei does not exceed 10%.

The intervals of values of T_2 and T_3 corresponding to destructive interference (eqs. (3.27) - (3.31)) are very different from those corresponding to the cases of constructive interference and of the two "non-interfering" $(\beta\beta)_{0\nu}$-decay mechanisms we have considered (eq.(4.12)). Within the set of $(\beta\beta)_{0\nu}$-decay mechanisms studied by us, this difference can allow to discriminate experimentally between the possibilities of the $(\beta\beta)_{0\nu}$-decay being triggered by two " destructively interfering" mechanisms or by two "constructively interfering" or by two "non- interfering" mechanisms.

We have shown also that further significant constraints on the physical solutions for the fundamental parameter $|\eta_\nu|^2$ in the case of the light Majorana neutrino exchange mechanism and the gluino exchange (or any other "interfering") mechanism can be obtained by using the current and the prospective upper bounds on the absolute scale of neutrino masses from the past [31, 48] and the upcoming KATRIN [48] ^3H β-decay experiments of 2.3 eV and 0.2 eV, respectively. Our results show that the KATRIN prospective upper bound of 0.2 eV, if reached, could imply particularly stringent constraints in the cases of "destructively interfering" mechanisms one of which is the light neutrino exchange, to the point of strongly disfavoring (or even excluding) some of them. The KATRIN prospective upper bound could be used to constrain also the fundamental parameters of two "non-interfering" mechanisms, one of which is the light Majorana neutrino exchange. This bound could eliminate, in particular, some parts of the half-life solution intervals where there is a significant dependence of the values of $|\eta_\nu|^2$ obtained on the set of NMEs used.

The measurements of the half-lives with rather high precision and the knowledge of the relevant NMEs with relatively small uncertainties is crucial for establishing whether more than one mechanisms are operative in $(\beta\beta)_{0\nu}$-decay. The method considered by us can be generalized to the case of more than two $(\beta\beta)_{0\nu}$-decay mechanisms. It allows to treat the cases of CP conserving and CP nonconserving couplings generating the $(\beta\beta)_{0\nu}$-decay in a unique way.

Chapter 4

Largely Different Nuclear Matrix Elements and $(\beta\beta)_{0\nu}$-Decay

The observation of $(\beta\beta)_{0\nu}$-decay of several different isotopes is crucial for obtaining information about the mechanism or mechanisms that induce the decay. In this chapter we investigate the possibility to discriminate between different pairs of CP non-conserving mechanisms inducing the $(\beta\beta)_{0\nu}$-decay by using data on $(\beta\beta)_{0\nu}$-decay half-lives of nuclei with largely different NMEs. The mechanisms studied are, as in the previous chapter, the light Majorana neutrino exchange, heavy left-handed (LH) and heavy right-handed (RH) Majorana neutrino exchanges, lepton charge non-conserving couplings in SUSY theories with R-parity breaking giving rise to the "dominant gluino exchange" and the "squark-neutrino" mechanisms. In addition to the nuclei considered in the previous chapter, ^{76}Ge, ^{82}Se, ^{100}Mo, ^{130}Te we will employ also the isotope ^{136}Xe. Four sets of nuclear matrix elements (NMEs) of the decays of these five nuclei, derived within the Self-consistent Renormalized Quasiparticle Random Phase Approximation (SRQRPA), will be employed in our analysis. The analysis we are going to present is based on the fact that for each of the five single mechanisms discussed, the NMEs for ^{76}Ge, ^{82}Se, ^{100}Mo and ^{130}Te differ relatively little —being the relative difference between the NMEs of any two nuclei not exceeding 10%. The NMEs for ^{136}Xe instead differ significantly from those of ^{76}Ge, ^{82}Se, ^{100}Mo and ^{130}Te, being by a factor $\sim (1.3 - 2.5)$ smaller. This allows, in principle, to draw conclusions about the pair of non-interfering (interfering) mechanisms possibly inducing the $(\beta\beta)_{0\nu}$-decay from data on the half-lives of ^{136}Xe and of at least one (two) more isotope(s) which can be, e.g., any of the four, ^{76}Ge, ^{82}Se, ^{100}Mo and ^{130}Te.

In the analysis we are going to perform we will employ the lower bound obtained by the EXO collaboration on the $(\beta\beta)_{0\nu}$-decay half-life of ^{136}Xe [54]:

$$T^{0\nu}_{1/2}(^{136}Xe) > 1.6 \times 10^{25}\text{y} \quad (90\,\%\,\text{CL}). \tag{4.1}$$

We use also the lower limits on the $(\beta\beta)_{0\nu}$-decay half-lives of ^{76}Ge, ^{82}Se and ^{100}Mo, and of ^{130}Te reported by the Heidelberg-Moscow [101], NEMO3 [102] and CUORICINO [99] experiments, respectively, as well as the ^{76}Ge half-life reported in [103] (see also [47]):

$$T^{0\nu}_{1/2}(^{76}Ge) > 1.9\times10^{25} y \text{ y } [101] \quad T^{0\nu}_{1/2}(^{82}Se) > 3.6\times10^{23} \text{ y } [102],$$
$$T^{0\nu}_{1/2}(^{100}Mo) > 1.1\times10^{24} \text{ y } [102], \quad T^{0\nu}_{1/2}(^{130}Te) > 3.0\times10^{24} \text{ y } [99]\,. \tag{4.2}$$
$$T^{0\nu}_{1/2}(^{76}Ge) = 2.23^{+0.44}_{-0.31}\times10^{25} \text{ y } [103]\,.$$

Following the analysis in the previous chapter, we will consider two cases:

1. $(\beta\beta)_{0\nu}$-decay induced by two mechanisms whose interference term in the $(\beta\beta)_{0\nu}$-decay rate is negligible [1] [77];

2. $(\beta\beta)_{0\nu}$-decay triggered by two CP non-conserving mechanisms whose interference term cannot be neglected.

Let us recall that in the case 1, given the two mechanisms A and B, the inverse of the $(\beta\beta)_{0\nu}$-decay half-life for a given isotope (A_i, Z_i) reads:

$$\frac{1}{T_i G_i} = |\eta_A|^2 |M'^{0\nu}_{i,A}|^2 + |\eta_B|^2 |M'^{0\nu}_{i,B}|^2\,, \tag{4.3}$$

where the index i denotes the isotope. The values of the phase space factor $G^{0\nu}_i(E,Z)$, and of the NMEs $M'^{0\nu}_{i,A}$ and $M'^{0\nu}_{i,B}$ for the mechanisms we will consider and for the isotopes ^{76}Ge, ^{82}Se, ^{100}Mo, ^{130}Te and ^{136}Xe of interest, are listed in Table 2.1. The LNV parameters are defined in chapter 2. If the two mechanisms A and B inducing the decay are interfering and CP non-conserving (case 2), the inverse of the $(\beta\beta)_{0\nu}$-decay half-life of the isotope (A_i, Z_i) can be written as:

$$\frac{1}{T^{0\nu}_{1/2,i} G^{0\nu}_i(E,Z)} = |\eta_A|^2 |M'^{0\nu}_{i,A}|^2 + |\eta_B|^2 |M'^{0\nu}_{i,B}|^2 + 2\cos\alpha |M'^{0\nu}_{i,A}||M'^{0\nu}_{i,B}||\eta_A||\eta_B|\,. \tag{4.4}$$

Here α is the relative phase of η_A and η_B.

We have seen in the previous chapter that if the $(\beta\beta)_{0\nu}$-decay is caused by two non-interfering mechanisms, the LNV parameters $|\eta_A|^2$ and $|\eta_B|^2$ characterizing the mechanisms, can be determined, in principle, from data on the $(\beta\beta)_{0\nu}$-decay half-lives of two isotopes, i.e., by solving a system of two linear equations. In the case of two interfering CP non-conserving mechanisms, the values of the two parameters $|\eta_A|^2$ and $|\eta_B|^2$ and of the cosine of the relative phase α of η_A and η_B can be obtained from data on the $(\beta\beta)_{0\nu}$-decay half-lives of three isotopes, i.e., by solving a system of three linear equations.

As was noticed and discussed in detail in the previous chapter, a very important role in identifying the physical solutions for $|\eta_A|^2$ and $|\eta_B|^2$ of the corresponding systems of two or three equations is played by the "positivity conditions" $|\eta_A|^2 \geq 0$ and $|\eta_B|^2 \geq 0$. The NMEs $M'^{0\nu}_{\nu}$, $M'^{0\nu}_{N}$, $M'^{0\nu}_{\lambda'}$ and $M'^{0\nu}_{\tilde{q}}$ used in this chapter are listed in Table 2.1. We note that these NMEs are significantly smaller (by a factor 1.3 - 2.5) when compared with those for ^{76}Ge, ^{82}Se and ^{100}Mo. The reduction of the $0\nu\beta\beta$-decay NMEs of the ^{136}Xe is explained by the closed neutron shell for this nucleus. A sharper Fermi surface leads to a reduction of this transition. This effect is clearly seen also in the case of $M'^{0\nu}_{\nu}$ of double magic nucleus ^{48}Ca [104].

[1] This possibility is realized when, e.g., the electron currents (responsible for the emission of the two electrons in the final state), associated with the two mechanisms considered, have opposite chiralities.

By glancing the Table 2.1 we see that a significant source of uncertainty is the value of the axial-vector coupling constant g_A and especially in the case of matrix elements $M'^{0\nu}_{\lambda'}$ and $M'^{0\nu}_{\tilde{q}}$. Further, the NMEs associated with heavy neutrino exchange are sensitive also to the choice of the NN interaction, the CD-Bonn or Argonne potential. These types of realistic NN interaction differ mostly by the description of the short-range interactions. Although in Table 2.1 we present results for NMEs of the nuclei of interest, calculated using both medium and large size single particle spaces within the SRQRPA method, in the numerical examples we are going to present further we will use the NMEs for a given nucleus, with the large size single particle space in both cases of Argonne and CD-Bonn potentials and for $g_A = 1.25;\ 1.00$ (i.e., altogether four NMEs).

In this work we will derive numerical results using the NMEs calculated with the large size single particle basis ("large basis") and the Argonne potential ("Argonne NMEs"). We report also results obtained with NMEs calculated with the Charge Dependent Bonn (CD-Bonn) potential ("CD-Bonn NMEs") and compared them with those derived with the Argonne NMEs.

I Two Non-interfering Mechanisms

In this case the solutions for the corresponding two LNV parameters $|\eta_A|^2$ and $|\eta_B|^2$ obtained from data on the $(\beta\beta)_{0\nu}$-decay half-lives of the two isotopes (A_i, Z_i) and (A_j, Z_j), are given by:

$$|\eta_A|^2 = \frac{|M'^{0\nu}_{j,B}|^2/T_iG_i - |M'^{0\nu}_{i,B}|^2/T_jG_j}{|M'^{0\nu}_{i,A}|^2|M'^{0\nu}_{j,B}|^2 - |M'^{0\nu}_{i,B}|^2|M'^{0\nu}_{j,A}|^2}, \quad |\eta_B|^2 = \frac{|M'^{0\nu}_{i,A}|^2/T_jG_j - |M'^{0\nu}_{j,A}|^2/T_iG_i}{|M'^{0\nu}_{i,A}|^2|M'^{0\nu}_{j,B}|^2 - |M'^{0\nu}_{i,B}|^2|M'^{0\nu}_{j,A}|^2}. \tag{4.5}$$

It follows from eq. (4.5) that if one of the two half-lives, say T_i, is fixed, the positivity conditions $|\eta_A|^2 \geq 0$ and $|\eta_B|^2 \geq 0$ can be satisfied only if T_j lies in a specific "positivity interval". Choosing for convenience always $A_j < A_i$ we get for the positivity interval:

$$\frac{G_i}{G_j}\frac{|M'^{0\nu}_{i,B}|^2}{|M'^{0\nu}_{j,B}|^2}T_i \leq T_j \leq \frac{G_i}{G_j}\frac{|M'^{0\nu}_{i,A}|^2}{|M'^{0\nu}_{j,A}|^2}T_i\,, \tag{4.6}$$

where we have used $|M'^{0\nu}_{i,A}|^2/|M'^{0\nu}_{j,A}|^2 > |M'^{0\nu}_{i,B}|^2/|M'^{0\nu}_{j,B}|^2$. In the case of $|M'^{0\nu}_{1,A}|^2/|M'^{0\nu}_{2,A}|^2 < |M'^{0\nu}_{1,B}|^2/|M'^{0\nu}_{2,B}|^2$, the interval of values of T_j under discussion is given by:

$$\frac{G_i}{G_j}\frac{|M'^{0\nu}_{i,A}|^2}{|M'^{0\nu}_{j,A}|^2}T_i \leq T_j \leq \frac{G_i}{G_j}\frac{|M'^{0\nu}_{i,B}|^2}{|M'^{0\nu}_{j,B}|^2}T_i\,. \tag{4.7}$$

Condition (4.6) is fulfilled, for instance, if A is the heavy right-handed (RH) Majorana neutrino exchange and B is the light Majorana neutrino exchange in the case of Argonne NMEs (see Table 2.1). The inequality in eq. (4.6) (or (4.7)) has to be combined with the experimental lower bounds on the half-lives of the considered nuclei, $T^{exp}_{i\ min}$. If, e.g., $T^{exp}_{i\ min}$ is the lower bound of interest for the isotope (A_i, Z_i), i.e., if $T_i \geq T^{exp}_{i\ min}$, we get from eq. (4.6):

$$T_j \geq \frac{G_i}{G_j}\frac{|M'^{0\nu}_{i,B}|^2}{|M'^{0\nu}_{j,B}|^2}T^{exp}_{i\ min}\,. \tag{4.8}$$

The lower limit in eq. (4.8) can be larger than the existing experimental lower bound on T_j. Indeed, suppose that $T_i \equiv T^{0\nu}_{1/2}(^{136}Xe)$, $T_j \equiv T^{0\nu}_{1/2}(^{76}Ge)$ and that the $(\beta\beta)_{0\nu}$-decay is due by the standard light neutrino exchange and the heavy RH Majorana neutrino exchange. In this case the positivity conditions for $|\eta_\nu|^2$ and $|\eta_R|^2$ imply for the Argonne and CD-Bonn NMEs corresponding to $g_A = 1.25\,(1.0)$:

$$1.90\,(1.85) \leq \frac{T^{0\nu}_{1/2}(^{76}Ge)}{T^{0\nu}_{1/2}(^{136}Xe)} \leq 2.70\,(2.64), \qquad \text{(Argonne NMEs)}\,; \tag{4.9}$$

$$1.30\,(1.16) \leq \frac{T^{0\nu}_{1/2}(^{76}Ge)}{T^{0\nu}_{1/2}(^{136}Xe)} \leq 2.47\,(2.30), \qquad \text{(CD-Bonn NMEs)}\,. \tag{4.10}$$

Using the EXO result, eq. (4.1), and the Argonne NMEs we get the lower bound on $T^{0\nu}_{1/2}(^{76}Ge)$:

$$T^{0\nu}_{1/2}(^{76}Ge) \geq 3.03\,(2.95) \times 10^{25}\,\text{y}. \tag{4.11}$$

This lower bound is significantly bigger that the experimental lower bound on $T^{0\nu}_{1/2}(^{76}Ge)$ quoted in eq. (4.2). If we use instead the CD-Bonn NMEs, the limit we obtain is close to the experimental lower bound on $T^{0\nu}_{1/2}(^{76}Ge)$:

$$T^{0\nu}_{1/2}(^{76}Ge) \geq 2.08\,(1.85) \times 10^{25}\,\text{y}. \tag{4.12}$$

For illustrative purposes we show in Fig. 4.1 the solutions of equation (4.5) for $|\eta_\nu|^2$ and $|\eta_R|^2$ derived by fixing $T^{0\nu}_{1/2}(^{76}Ge)$ to the best fit value claimed in [103], $T^{0\nu}_{1/2}(^{76}Ge) = 2.23 \times 10^{25}$ (see eq. (4.2)). As Fig. 4.1 shows, the positive (physical) solutions obtained using the Argonne NMEs are incompatible with the EXO result, eq. (4.1), and under the assumptions made and according to our oversimplified analysis, are ruled out. At the same time, the physical solutions obtained using the CD-Bonn NMEs are compatible with the EXO limit for values of $|\eta_\nu|^2$ and $|\eta_R|^2$ lying in a relatively narrow interval.

We consider next a second example of two non-interfering $(\beta\beta)_{0\nu}$-decay mechanisms, i.e., $(\beta\beta)_{0\nu}$-decay induced by the heavy RH Majorana neutrino exchange and the gluino exchange. Setting, as above, $T_i \equiv T^{0\nu}_{1/2}(^{136}Xe)$ and $T_j \equiv T^{0\nu}_{1/2}(^{76}Ge)$, we get for the positivity intervals using the Argonne or CD-Bonn NMEs corresponding to $g_A = 1.25\,(1.0)$:

$$2.70\,(2.64) \leq \frac{T^{0\nu}_{1/2}(^{76}Ge)}{T^{0\nu}_{1/2}(^{136}Xe)} \leq 2.78\,(2.67), \qquad \text{(Argonne NMEs)}\,; \tag{4.13}$$

$$1.30\,(1.16) \leq \frac{T^{0\nu}_{1/2}(^{76}Ge)}{T^{0\nu}_{1/2}(^{136}Xe)} \leq 4.43\,(4.25), \qquad \text{(CD-Bonn NMEs)}\,, \tag{4.14}$$

The lower bound on $T^{0\nu}_{1/2}(^{76}Ge)$ following from the EXO limit in the case of the Argonne NMEs obtained with $g_A = 1.25\,(1.0)$ reads:

$$T^{0\nu}_{1/2}(^{76}Ge) \geq 4.31\,(4.22) \times 10^{25}\,\text{y}. \tag{4.15}$$

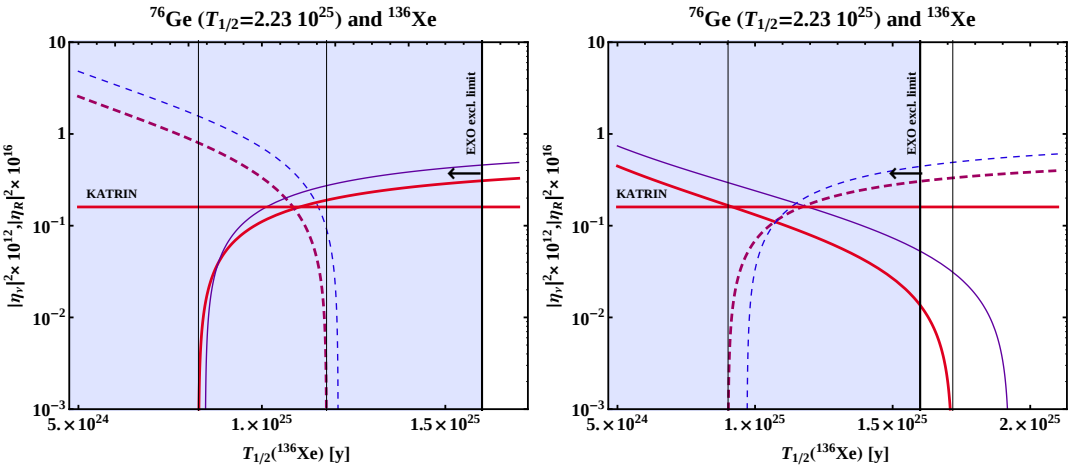

Figure 4.1: The values of $|\eta_\nu|^2$ (solid lines) and $|\eta_R|^2$ (dashed lines) obtained for $T^{0\nu}_{1/2}(^{76}Ge) = 2.23\times 10^{25}$ y [103] as a function of $T^{0\nu}_{1/2}(^{136}Xe)$, using the Argonne (left panel) and CD-Bonn (right panel) NMEs corresponding to $g_A = 1.25$ (thick lines) and $g_A = 1$ (thin lines). The region of physical (positive) solutions for $g_A = 1.25$ are delimited by the two vertical lines. The solid horizontal line corresponds to the prospective upper limit from the KATRIN experiment [48], while the thick solid vertical line indicates the EXO lower bound [54]. The gray areas correspond to excluded values of $|\eta_\nu|^2$ and $|\eta_R|^2$.

This lower limit is by a factor of 2.27 bigger than the experimental lower limit quoted in eq. (4.2). It is also incompatible with the 4σ range of values of $T^{0\nu}_{1/2}(^{76}Ge)$ found in [103]. The lower bound obtained using the CD-Bonn NMEs is less stringent:

$$T^{0\nu}_{1/2}(^{76}Ge) \geq 2.08\,(1.85)\times 10^{25}\,\mathrm{y}. \tag{4.16}$$

In Fig. 4.2 we show that if $T^{0\nu}_{1/2}(^{76}Ge) = 2.23\times 10^{25}$, the recent EXO lower limit allows positive (physical) solutions for the corresponding two LNV parameters $|\eta_{\lambda'}|^2$ and $|\eta_R|^2$ only for the CD-Bonn NMEs and for values of $|\eta_{\lambda'}|^2$ and $|\eta_R|^2$ lying in a very narrow interval.

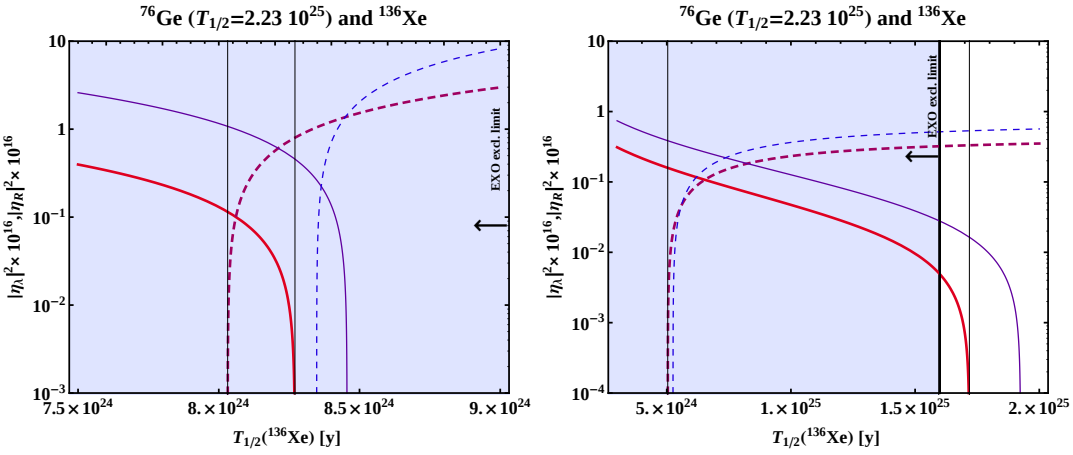

Figure 4.2: The same as in Fig. 4.1 but for the values of the rescaled parameters $|\eta_{\lambda'}|^2$ (solid lines) and $|\eta_R|^2$ (dashed lines).

We get similar results for the third pair of non-interfering mechanisms - the squark-neutrino exchange and the heavy RH neutrino exchange. Indeed, using the Argonne NMEs corresponding to $g_A = 1.25\,(1.0)$ we find for the positivity interval:

$$2.52\,(2.40) \leq \frac{T^{0\nu}_{1/2}(^{76}Ge)}{T^{0\nu}_{1/2}(^{136}Xe)} \leq 2.70\,(2.64)\,, \tag{4.17}$$

The EXO lower bound in this case implies:

$$T^{0\nu}_{1/2}(^{76}Ge) \geq 4.03\,(3.84) \times 10^{25}\,\mathrm{y}. \tag{4.18}$$

From the NMEs computed with the CD-Bonn potential we get

$$1.30\,(1.16) \leq \frac{T^{0\nu}_{1/2}(^{76}Ge)}{T^{0\nu}_{1/2}(^{136}Xe)} \leq 2.95\,(2.81)\,, \tag{4.19}$$

and

$$T^{0\nu}_{1/2}(^{76}Ge) \geq 2.08\,(1.85) \times 10^{25}\,\mathrm{y}. \tag{4.20}$$

In the case the non-interfering LH and RH heavy Majorana neutrino exchanges, the NMEs for the two mechanisms coincide and the system of equation in (4.5) reduces to a relation between the half-lives of the two considered isotopes:

$$T_j = T_i \frac{G_i |M'^{0\nu}_{i,N}|^2}{G_j |M'^{0\nu}_{j,N}|^2}\,. \tag{4.21}$$

In this case the EXO lower bound implies the following lower limits on $T_j \equiv T^{0\nu}_{1/2}(^{76}Ge)$ for the sets of NMEs we are considering for $g_A = 1.25\ (1.0)$:

$$T^{0\nu}_{1/2}(^{76}Ge) \geq 4.31\,(4.22) \times 10^{25}\,\mathrm{y} \qquad \text{(Argonne NMEs)}\,, \tag{4.22}$$

$$T^{0\nu}_{1/2}(^{76}Ge) \geq 2.08\,(1.85) \times 10^{25}\,\mathrm{y} \qquad \text{(CD-Bonn NMEs)}. \tag{4.23}$$

The range of positive solutions for the LNV parameters in equation (4.6) shifts towards larger values if T_i is increased. As we noticed in [64], if the experimentally determined interval of allowed values of the ratio T_j/T_i of the half-lives of the two isotopes considered, including all relevant uncertainties, lies outside the range of positive solutions for $|\eta_A|^2$ and $|\eta_B|^2$, one would be led to conclude that the $(\beta\beta)_{0\nu}$-decay is not generated by the two mechanisms under discussion.

Assuming the half-lives of two isotopes, say, of ^{76}Ge and ^{136}Xe, $T^{0\nu}_{1/2}(^{76}\mathrm{Ge}) \equiv T_1$ and $T^{0\nu}_{1/2}(^{136}\mathrm{Xe}) \equiv T_2$, to be known, and $(\beta\beta)_{0\nu}$-decay triggered by a pair of non-interfering mechanisms A and B, one can always use the physical solutions for $|\eta^{LFV}_{A,B}|^2(T_1, T_2)$, obtained using the two half-lives $T_{1,2}$ (in eq. (4.5)), to find the range of the half-life of a third isotope:

$$\frac{1}{T_3} = G_3(|\eta_A(T_1, T_2)|^2 |M'^{0\nu}_{3,A}|^2 + |\eta_B(T_1, T_2)|^2 |M'^{0\nu}_{3,B}|^2)\,, \tag{4.24}$$

In Tables 4.1 and 4.2 we give numerical predictions based on this observation. Fixing the half-life of ^{76}Ge to $T_1 = 10^{26}$ y and assuming the ^{136}Xe half-life T_2 lies in an interval compatible with the existing constraints, the system of two equations is solved and the

Table 4.1: Predictions using Argonne and CD-Bonn NMEs corresponding to g_A=1.25 (g_A=1 in parenthesis) in the case of two non-interfering mechanism: light and heavy RH Majorana neutrino exchanges. The physical solutions for $|\eta_\nu|^2$ and $|\eta_R|^2$ derived for given half-lives of ^{76}Ge and ^{136}Xe, are used to obtain predictions for the half-lives of ^{82}Se, ^{100}Mo and ^{130}Te. The ^{76}Ge half-life was set to T(^{76}Ge) = 10^{26} yr, while the interval of values of the ^{136}Xe half-life was determine from the positivity conditions.

Argonne NMEs	
Positive solutions	Predictions
$3.71(3.79)\cdot 10^{25} < T(^{136}Xe) < 5.27(5.42)\cdot 10^{25}$	$2.30(2.34)\cdot 10^{25} < T(^{82}Se) < 2.39(2.49)\cdot 10^{25}$
	$1.45(1.46)\cdot 10^{25} < T(^{100}Mo) < 1.80(1.76)\cdot 10^{25}$
	$1.76(1.78)\cdot 10^{25} < T(^{130}Te) < 2.44(2.49)\cdot 10^{25}$
CD-Bonn NMEs	
Positive solutions	Predictions
$4.04(4.35)\cdot 10^{25} < T(^{136}Xe) < 7.71(8.63)\cdot 10^{25}$	$2.30(2.33)\cdot 10^{25} < T(^{82}Se) < 2.39(2.48)\cdot 10^{25}$
	$1.44(1.45)\cdot 10^{25} < T(^{100}Mo) < 1.78(1.74)\cdot 10^{25}$
	$1.65(1.68)\cdot 10^{25} < T(^{130}Te) < 2.21(2.27)\cdot 10^{25}$

Table 4.2: The same as in Table 4.1 but for the gluino and RH heavy Majorana neutrino exchange mechanisms.

Argonne NMEs	
Positive solutions	Predictions
$3.60(3.74)\cdot 10^{25} < T(^{136}Xe) < 3.71(3.79)\cdot 10^{25}$	$2.27(2.32)\cdot 10^{25} < T(^{82}Se) < 2.30(2.34)\cdot 10^{25}$
	$1.43(1.459)\cdot 10^{25} < T(^{100}Mo) < 1.45(1.460)\cdot 10^{25}$
	$1.76(1.78)\cdot 10^{25} < T(^{130}Te) < 1.80(1.86)\cdot 10^{25}$
CD-Bonn NMEs	
Positive solutions	Predictions
$2.26(2.35)\cdot 10^{25} < T(^{136}Xe) < 7.71(8.63)\cdot 10^{25}$	$2.27(2.32)\cdot 10^{25} < T(^{82}Se) < 2.30(2.33)\cdot 10^{25}$
	$1.43(1.4542)\cdot 10^{25} < T(^{100}Mo) < 1.44(1.4543)\cdot 10^{25}$
	$1.65(1.68)\cdot 10^{25} < T(^{130}Te) < 1.75(1.81)\cdot 10^{25}$

values of $|\eta_A|^2 > 0$ and $|\eta_B|^2 > 0$ thus obtained are used to get predictions for the half-life of a third isotope, in this case ^{82}Se, ^{100}Mo and ^{130}Te. The mechanisms considered are a) light and heavy RH Majorana neutrino exchanges (Table 4.1) and b) gluino and heavy RH Majorana neutrino exchanges (Table 4.2). It follows from the results shown in Tables 4.1 and 4.2 that the intervals of allowed values of the half-lives of ^{82}Se, ^{100}Mo and ^{130}Te thus obtained i) are rather narrow [2], and ii) exhibit weak dependence on the NMEs used to derive them (within the sets of NMEs considered).

One can use eq. (4.24) and the lower bound, e.g., on $T^{0\nu}_{1/2}(^{136}Xe)$ reported by the EXO experiment, to derive a lower bound on one of the half-lives involved in the study of two non-interfering mechanisms, say T_1. Indeed, we can set $T_3 = T^{0\nu}_{1/2}(^{136}Xe)$, in eq. (4.24), use the explicit form of the solutions for $|\eta^{LFV}_{A,B}|^2(T_1, T_2)$ and apply the existing

[2] We note that the experimental lower bounds quoted in eq. (4.2) have to be taken into account since, in principle, they can further constrain the range of allowed values of $|\eta_A|^2$ and $|\eta_B|^2$ and of the half-life of the third isotope of interest.

EXO lower bound. We get:

$$\frac{1}{T_3} = \frac{D_1}{NT_1} + \frac{D_2}{NT_2} < \frac{1}{1.6 \times 10^{25}\,\mathrm{y}}, \tag{4.25}$$

where

$$D_1 = \frac{G_3}{G_1}\left(|M'^{0\nu}_{2,A}|^2|M'^{0\nu}_{3,B}|^2 - |M'^{0\nu}_{3,A}|^2|M'^{0\nu}_{2,B}|^2\right), \quad D_2 = \frac{G_3}{G_2}\left(|M'^{0\nu}_{3,A}|^2|M'^{0\nu}_{1,B}|^2 - |M'^{0\nu}_{1,A}|^2|M'^{0\nu}_{3,B}|^2\right),$$

and

$$N = |M'^{0\nu}_{2,A}|^2|M'^{0\nu}_{1,B}|^2 - |M'^{0\nu}_{1,A}|^2|M'^{0\nu}_{2,B}|^2\,. \tag{4.26}$$

Using further the positivity constraint given in eq. (4.6),

$$a\,T_1 \leq T_2 \leq b\,T_1\,, \tag{4.27}$$

where $b \equiv |M'^{0\nu}_{1,A}|^2/|M'^{0\nu}_{2,A}|^2 > a \equiv |M'^{0\nu}_{1,B}|^2/|M'^{0\nu}_{2,B}|^2$, we get [3] the following lower limit on T_1 from eq. (4.25):

$$T_1 \geq T_3\left(\frac{D_1}{N} + \frac{D_2}{b\,N}\right) > 1.6 \times 10^{25}\,\mathrm{y}\left(\frac{\mathrm{D_1}}{\mathrm{N}} + \frac{\mathrm{D_2}}{\mathrm{b\,N}}\right). \tag{4.28}$$

This lower bound on T_1 depends only on T_3 and on the NMEs $|M'^{0\nu}_{i,A}|^2$ and $|M'^{0\nu}_{j,B}|^2$, $i,j = 1,2,3$. We give examples of predictions based on the eq. (4.28) in Tables 4.3 and 4.4. We notice that, for the NMEs used in the present study, the EXO lower limit on $T^{0\nu}_{1/2}(^{136}Xe)$ sets a lower bound on the half-lives of the other isotopes considered by us that usually exceed their respective current experimental lower bounds.

Table 4.3: Lower bound on T_1 from eq. (4.28) using the EXO limit on $T^{0\nu}_{1/2}(^{136}Xe)$, eq. (4.1), and the Argonne and CD-Bonn NMEs corresponding to g_A=1.25 (g_A=1), in the case of two non-interfering mechanisms - light and heavy RH Majorana neutrino exchanges. See text for details.

(T_1,T_2)	Argonne g_A=1.25 (1.0)	CD-Bonn g_A=1.25 (1.0)
^{130}Te - ^{76}Ge	T(^{130}Te)¿ 7.40 (7.35)· 10^{24}	T(^{130}Te)¿ 3.43 (3.11) · 10^{24}
^{100}Mo - ^{76}Ge	T(^{100}Mo)¿ 5.45 (5.19)· 10^{24}	T(^{130}Te)¿ 3.00 (2.70) · 10^{24}
^{82}Se - ^{76}Ge	T(^{82}Se)¿ 7.25 (7.37)· 10^{24}	T(^{82}Se)¿ 4.76 (4.32) · 10^{24}

II Discriminating between Different Pairs of Non-interfering Mechanisms

The first thing to notice is that, as it follows from Table 1, for each of the four different mechanisms of $(\beta\beta)_{0\nu}$-decay considered, the relative difference between NMEs of the decays of ^{76}Ge, ^{82}Se, ^{100}Mo and ^{130}Te does not exceed approximately 10%: $(M'^{0\nu}_{j,X} - M'^{0\nu}_{i,X})/(0.5(M'^{0\nu}_{j,X} + M'^{0\nu}_{i,X})) \lesssim 0.1$, where $i \neq j = {}^{76}$Ge,^{82}Se,^{100}Mo,^{130}Te, and X

[3] The inequality in eq. (4.27) was derived assuming that $D_2/N > 0$. In the case of $D_2/N < 0$ one has to interchange a and b in it.

Table 4.4: The same as in Table 4.3 for the gluino and heavy RH Majorana neutrino exchange mechanisms. See text for details.

(T_1,T_2)	Argonne g_A=1.25 (1.0)	CD-Bonn g_A=1.25 (1.0)
^{130}Te - ^{76}Ge	$T(^{130}Te) > 7.59\,(7.53) \cdot 10^{24}$	$T(^{130}Te) > 3.43\,(3.11) \cdot 10^{24}$
^{100}Mo - ^{76}Ge	$T(^{100}Mo) > 6.25\,(6.16) \cdot 10^{24}$	$T(^{130}Te) > 3.00\,(2.70) \cdot 10^{24}$
^{82}Se - ^{76}Ge	$T(^{82}Se) > 9.90\,(9.87) \cdot 10^{24}$	$T(^{82}Se) > 4.76\,(4.32) \cdot 10^{24}$

denotes any one of the four mechanisms discussed. As was shown in the previous chapter, this leads to degeneracies between the positivity intervals of values of the ratio of the half-lives of any two given of the indicated four isotopes, corresponding to the different pairs of mechanisms inducing the $(\beta\beta)_{0\nu}$-decay. The degeneracies in question make it practically impossible to distinguish between the different pairs of $(\beta\beta)_{0\nu}$-decay mechanisms, considered in the previous chapter and in the present chapter, using data on the half-lives of two or more of the four nuclei ^{76}Ge, ^{82}Se, ^{100}Mo and ^{130}Te. At the same time, it is possible, in principle, to exclude them all using data on the half-lives of at least two of the indicated four nuclei.

In contrast, the NMEs for the $(\beta\beta)_{0\nu}$-decay of ^{136}Xe, corresponding to each of the four different mechanisms we are considering are by a factor of $\sim (1.3 - 2.5)$ smaller than the $(\beta\beta)_{0\nu}$-decay NMEs of the other four isotopes listed above: $(M'^{0\nu}_{j,X} - M'^{0\nu}_{i,X})/M'^{0\nu}_{i,X}) \cong (0.3 - 1.5)$, where $i = {}^{136}Xe$ and $j = {}^{76}$Ge,^{82}Se,^{100}Mo,^{130}Te (see Figs. 4.3 and 4.4). As a consequence, using data on the half-life of ^{136}Xe as input in determining the positivity interval of values of the half-life of any second isotope lifts to a certain degree the degeneracy of the positivity intervals corresponding to different pairs of non-interfering mechanisms. This allows, in principle, to draw conclusions about the pair of mechanisms possibly inducing the $(\beta\beta)_{0\nu}$-decay from data on the half-lives of ^{136}Xe and a second isotope which can be, e.g., any of the four considered above, ^{76}Ge, ^{82}Se, ^{100}Mo and ^{130}Te.

To be more specific, it follows from eqs. (4.9), (4.13), (4.17), (4.21) and Table 2.1 that if the Argonne (CD-Bonn) NMEs derived for $g_A = 1.25\,(1.0)$ are correct, all four pairs of mechanisms of $(\beta\beta)_{0\nu}$-decay discussed by us will be disfavored, or ruled out, if it is established experimentally that $R(^{76}Ge,^{136}Xe) > 2.8$ (4.5) or that $R(^{76}Ge,^{136}Xe) < 1.8$ (1.1), where $R(^{76}Ge,^{136}Xe) \equiv T^{0\nu}_{1/2}(^{76}Ge)/T^{0\nu}_{1/2}(^{136}Xe)$. Further, assuming the validity of the Argonne NMEs, one would conclude that the light and heavy RH Majorana neutrino exchanges are the only possible pair of mechanisms operative in $(\beta\beta)_{0\nu}$-decay if it is found experimentally that $1.9 \leq R(^{76}Ge,^{136}Xe) < 2.4$. For $1.9 \leq R(^{76}Ge,^{136}Xe) < 2.6$, i) the gluino and RH Majorana neutrino exchanges, and ii) the LH and RH heavy Majorana neutrino exchanges, will be disfavored or ruled out. One finds similar results using the CD-Bonn NMEs. The numbers we quote in this paragraph should be considered as illustrative only. In a realistic analysis one has to take into account the various relevant experimental and theoretical uncertainties.

We analyze next the possibility to discriminate between two pairs of non-interfering mechanisms triggering the $(\beta\beta)_{0\nu}$-decay when the pairs share one mechanism. Given three different non-interfering mechanisms A, B and C, we can test the hypothesis of the $(\beta\beta)_{0\nu}$-decay induced by the pairs i) $A + B$ or ii) $C + B$, using the half-lives of the same two isotopes. As a consequence of the fact that B is common to both pairs of

mechanisms, the numerators of the expressions for $|\eta_A|^2$ and $|\eta_C|^2$, as it follows from eq. (4.5), coincide. Correspondingly, using the half-lives of the same two isotopes would allow us to distinguish, in principle, between the cases i) and ii) if the denominators in the expressions for the solutions for $|\eta_A|^2$ and $|\eta_C|^2$ have opposite signs. Indeed, in this case the physical solutions for $|\eta_A|^2$ in the case i) and $|\eta_C|^2$ in the case ii) will lie either in the positivity intervals (4.6) and (4.7), respectively, or in the intervals (4.7) and (4.6). Thus, the positivity solution intervals for $|\eta_A|^2$ and $|\eta_C|^2$ would not overlap, except for the point corresponding to a value of the second isotope half-life where $\eta_A = \eta_C = 0$. This would allow, in principle, to discriminate between the two considered pairs of mechanisms.

It follows from the preceding discussion that in order to be possible to discriminate between the pairs $A+B$ and $C+B$ of non-interfering mechanisms of $(\beta\beta)_{0\nu}$-decay, the following condition has to be fulfilled:

$$\frac{Det\begin{pmatrix} |M'^{0\nu}_{i,A}|^2 & |M'^{0\nu}_{i,B}|^2 \\ |M'^{0\nu}_{j,A}|^2 & |M'^{0\nu}_{j,B}|^2 \end{pmatrix}}{Det\begin{pmatrix} |M'^{0\nu}_{i,C}|^2 & |M'^{0\nu}_{i,B}|^2 \\ |M'^{0\nu}_{j,C}|^2 & |M'^{0\nu}_{j,B}|^2 \end{pmatrix}} = \frac{|M'^{0\nu}_{i,A}|^2|M'^{0\nu}_{j,B}|^2 - |M'^{0\nu}_{i,B}|^2|M'^{0\nu}_{j,A}|^2}{|M'^{0\nu}_{i,C}|^2|M'^{0\nu}_{j,B}|^2 - |M'^{0\nu}_{i,B}|^2|M'^{0\nu}_{j,C}|^2} < 0\,. \tag{4.29}$$

This condition is satisfied if one of the following two sets of inequalities holds:

$$I) \qquad \frac{M'^{0\nu}_{j,C} - M'^{0\nu}_{i,C}}{M'^{0\nu}_{i,C}} < \frac{M'^{0\nu}_{j,B} - M'^{0\nu}_{i,B}}{M'^{0\nu}_{i,B}} < \frac{M'^{0\nu}_{j,A} - M'^{0\nu}_{i,A}}{M'^{0\nu}_{i,A}}, \tag{4.30}$$

$$II) \qquad \frac{M'^{0\nu}_{j,A} - M'^{0\nu}_{i,A}}{M'^{0\nu}_{i,A}} < \frac{M'^{0\nu}_{j,B} - M'^{0\nu}_{i,B}}{M'^{0\nu}_{i,B}} < \frac{M'^{0\nu}_{j,C} - M'^{0\nu}_{i,C}}{M'^{0\nu}_{i,C}}. \tag{4.31}$$

One example of a possible application of the preceding results is provided by the mechanisms of light Majorana neutrino exchange (A), RH heavy Majorana neutrino exchange (B) and gluino exchange (C) and the Argonne NMEs. We are interested in studying cases involving ^{136}Xe since, as it was already discussed earlier, the NMEs of ^{136}Xe differ significantly from those of the lighter isotopes such as ^{76}Ge (see Table 2.1). Indeed, as can be shown, it is possible, in principle, to discriminate between the two pairs $A+B$ and $C+B$ of the three mechanisms indicated above if we combine data on the half-life of ^{136}Xe with those on the half-life of one of the four isotopes ^{76}Ge, ^{82}Se, ^{100}Mo and ^{130}Te, and use the Argonne NMEs in the analysis. In this case the inequalities (4.30) are realized, as can be seen in Fig. 4.3, where we plot the relative differences $(M'^{0\nu}_j - M'^{0\nu}_i)/M'^{0\nu}_i$ for the Argonne NMEs where the indices i and j refer respectively to ^{136}Xe and to one of the four isotopes ^{76}Ge, ^{82}Se, ^{100}Mo and ^{130}Te. In the case of the CD-Bonn NMEs (Fig. 4.4), the inequalities (4.30) or (4.31) do not hold for the pairs of mechanisms considered. The inequalities given in eq. (4.30) hold, as it follows from Fig. 4.4, if, e.g., the mechanisms A, B and C are respectively the heavy RH Majorana neutrino exchange, the light Majorana neutrino exchange and the gluino exchange.

The preceding considerations are illustrated graphically in Figs. 4.5 and 4.6. In Fig. 4.5 we use $T_i \equiv T^{0\nu}_{1/2}(^{76}Ge)$ and $T_j \equiv T^{0\nu}_{1/2}(^{136}Xe)$ and the Argonne (left panel) and CD-Bonn (right panel) NMEs for the decays of ^{76}Ge and ^{136}Xe to show the possibility of discriminating between the two pairs of non-interfering mechanisms considered earlier:

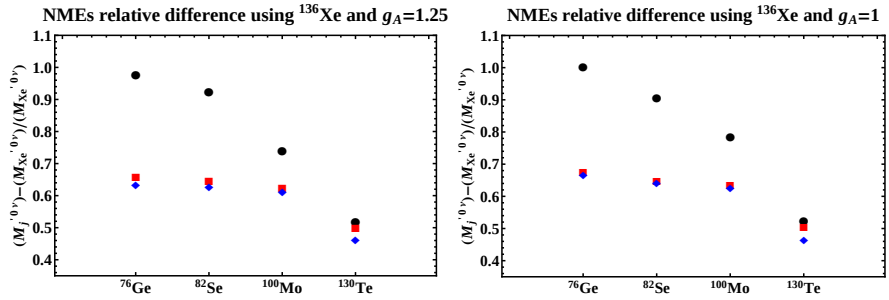

Figure 4.3: The relative differences between the Argonne NMEs $(M'^{0\nu}_j - M'^{0\nu}_i)/M'^{0\nu}_i$, where i=^{136}Xe and j =^{76}Ge,^{82}Se,^{100}Mo,^{130}Te, for $g_A = 1.25$ (left panel) and $g_A = 1$ (right panel) and for three different non-interfering mechanisms: light Majorana neutrino exchange (circles), RH heavy Majorana neutrino exchange (squares) and gluino exchange (diamonds). See text for details.

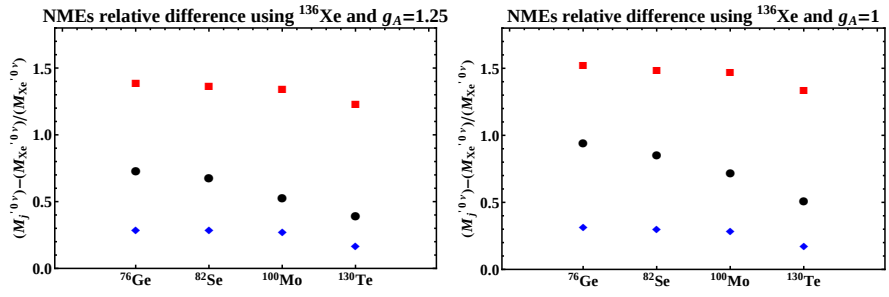

Figure 4.4: The same as in Fig. 4.3 for the CD-Bonn NMEs. See text for details.

i) light Majorana neutrino exchange and heavy RH Majorana neutrino exchange (RHN) and ii) heavy RH Majorana neutrino exchange and gluino exchange. The ^{76}Ge half-life is set to $T_i = 5 \times 10^{25}$ y, while that of ^{136}Xe, T_j, is allowed to vary in a certain interval. The solutions for the three LNV parameters corresponding to the three mechanisms considered, $|\eta_\nu|^2$, $|\eta_R|^2$ and $|\eta_{\lambda'}|^2$, obtained for the chosen value of T_i and interval of values of T_j, are shown as functions of T_j. As is clearly seen in the left panel of Fig. 4.5, if $|\eta_\nu|^2$, $|\eta_R|^2$ and $|\eta_{\lambda'}|^2$ are obtained using the Argonne NMEs, the intervals of values of T_j for which one obtains the physical positive solutions for $|\eta_\nu|^2$ and $|\eta_{\lambda'}|^2$, do not overlap. This makes it possible, in principle, to determine which of the two pairs of mechanisms considered (if any) is inducing the $(\beta\beta)_{0\nu}$-decay. The same result does not hold if one uses the CD-Bonn NMEs in the analysis, as is illustrated in the right panel of Fig. 4.5. In this case none of the inequalities (4.30) and (4.31) is fulfilled, the intervals of values of T_j for which one obtains physical solutions for $|\eta_\nu|^2$ and $|\eta_\lambda|^2$ overlap and the discrimination between the two pairs of mechanisms is problematic.

We show in Fig. 4.6 that the features of the solutions for $|\eta_\nu|^2$ and $|\eta_\lambda|^2$ we have discussed above, which are related to the values of the relevant NMEs, do not change if one uses in the analysis the half-lives and NMEs of ^{136}Xe and of another lighter isotope instead of ^{76}Ge, namely, of ^{100}Mo.

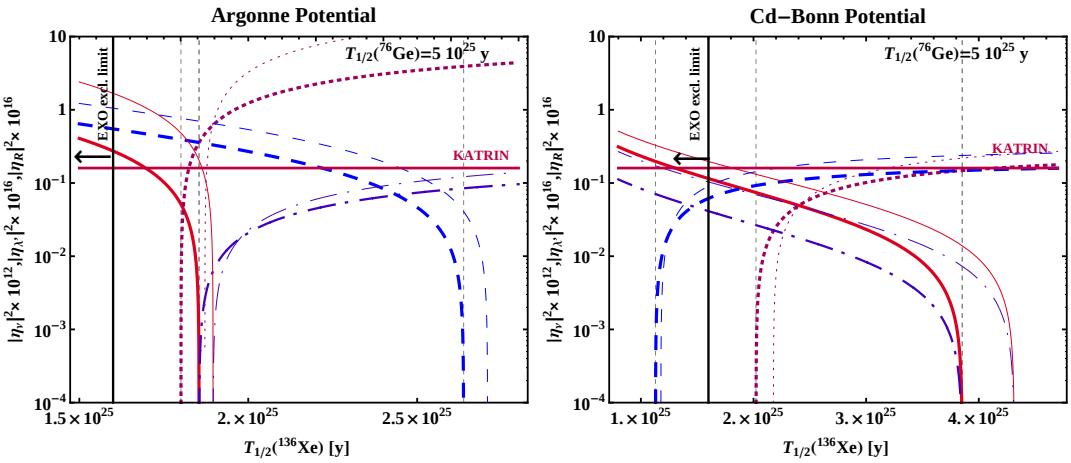

Figure 4.5: Solutions for the LNV parameters corresponding to two pairs of non-interfering mechanisms: i) $|\eta_\nu|^2$ and $|\eta_R|^2$ (dot-dashed and dashed lines) and ii) $|\eta_{\lambda'}|^2$ and $|\eta_R|^2$ (solid and dotted lines). The solutions are obtained by fixing $T_i = T^{0\nu}_{1/2}(^{76}Ge) = 5 \times 10^{25}$ y and letting free $T_j = T^{0\nu}_{1/2}(^{136}Xe)$ and using the sets of Argonne (left panel) and CD-Bonn (right panel) NMEs calculated for $g_A = 1.25$ (thick lines) and $g_A = 1$ (thin lines). The range of positive solutions in the case of Argonne NMEs and $g_A = 1.25$ is delimited by the two vertical dashed lines. The horizontal solid line corresponds to the prospective upper limit $|\langle m\rangle| < 0.2$ eV [48]. The thick solid vertical line indicates the EXO lower limit on $T^{0\nu}_{1/2}(^{136}Xe)$ [54]. See text for details.

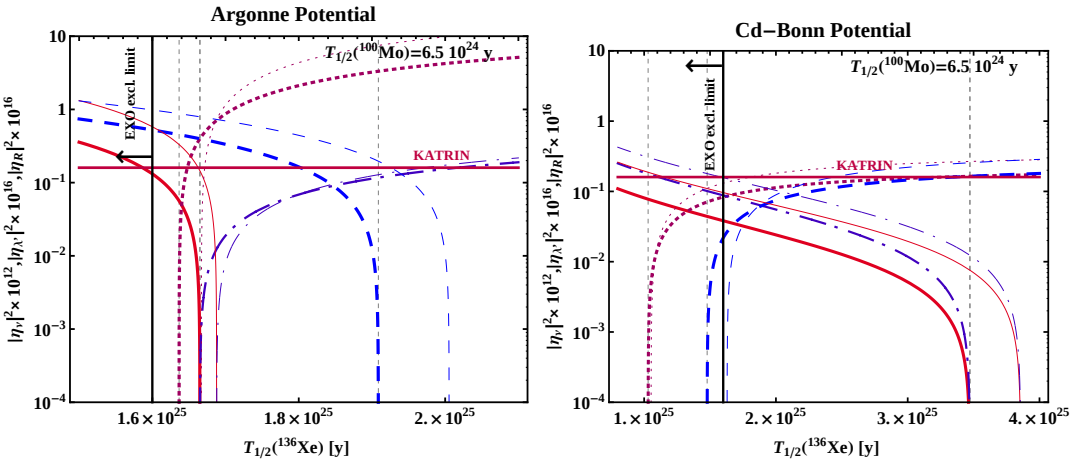

Figure 4.6: Solutions for the LNV parameters of two pairs of non-interfering $(\beta\beta)_{0\nu}$-decay mechanisms i) $|\eta_\nu|^2$ and $|\eta_R|^2$ (dot-dashed and dashed lines) and ii) $|\eta_{\lambda'}|^2$ and $|\eta_R|^2$ (solid and dotted lines) obtained by fixing $T_i = T^{0\nu}_{1/2}(^{100}Mo) = 6.5 \times 10^{24}$ yr and letting free $T_j = T^{0\nu}_{1/2}(^{136}Xe)$. The other notations are the same as in Fig. 4.5. See text for details.

III Two Interfering Mechanisms

We analyze in the present Section the possibility of $(\beta\beta)_{0\nu}$-decay induced by two interfering CP-non-conserving mechanisms. As we have seen in the previous chapter this case is characterized by three parameters: the absolute values and the relative phase of the two LNV parameters associated with the two mechanisms. They can be determined, in principle, from data on the half-lives of three isotopes, T_i, $i = 1, 2, 3$. Given $T_{1,2,3}$ and denoting by A and B the two mechanisms, one can set a system of three linear equations in three unknowns, the solution of which reads:

$$|\eta_A|^2 = \frac{D_i}{D}\,, \quad |\eta_B|^2 = \frac{D_j}{D}\,, \quad z \equiv 2\cos\alpha|\eta_A||\eta_B| = \frac{D_k}{D}\,, \tag{4.32}$$

where D, D_i, D_j and D_k are the following determinants:

$$D = \begin{vmatrix} (M'^{0\nu}_{i,A})^2 & (M'^{0\nu}_{i,B})^2 & M'^{0\nu}_{i,B}M'^{0\nu}_{i,A} \\ (M'^{0\nu}_{j,A})^2 & (M'^{0\nu}_{j,B})^2 & M'^{0\nu}_{j,B}M'^{0\nu}_{j,A} \\ (M'^{0\nu}_{k,A})^2 & (M'^{0\nu}_{k,B})^2 & M'^{0\nu}_{k,B}M'^{0\nu}_{k,A} \end{vmatrix}\,, \quad D_i = \begin{vmatrix} i/T_iG_i & (M'^{0\nu}_{i,B})^2 & M'^{0\nu}_{i,B}M'^{0\nu}_{i,A} \\ i/T_jG_j & (M'^{0\nu}_{j,B})^2 & M'^{0\nu}_{j,B}M'^{0\nu}_{j,A} \\ i/T_kG_k & (M'^{0\nu}_{k,B})^2 & M'^{0\nu}_{k,B}M'^{0\nu}_{k,A} \end{vmatrix}\,, \tag{4.33}$$

$$D_j = \begin{vmatrix} (M'^{0\nu}_{i,A})^2 & i/T_iG_i & M'^{0\nu}_{i,B}M'^{0\nu}_{i,A} \\ (M'^{0\nu}_{j,A})^2 & i/T_jG_j & M'^{0\nu}_{j,B}M'^{0\nu}_{j,A} \\ (M'^{0\nu}_{k,A})^2 & i/T_kG_k & M'^{0\nu}_{k,B}M'^{0\nu}_{k,A} \end{vmatrix}\,, \quad D_k = \begin{vmatrix} (M'^{0\nu}_{i,A})^2 & (M'^{0\nu}_{i,B})^2 & i/T_iG_i \\ (M'^{0\nu}_{j,A})^2 & (M'^{0\nu}_{j,B})^2 & i/T_jG_j \\ (M'^{0\nu}_{k,A})^2 & (M'^{0\nu}_{k,B})^2 & i/T_kG_k \end{vmatrix}\,. \tag{4.34}$$

As in the case of two non-interfering mechanisms, the LNV parameters must be non-negative $|\eta_A|^2 \geq 0$ and $|\eta_B|^2 \geq 0$, and in addition the interference term must satisfy the following condition:

$$-2|\eta_A||\eta_B| \leq 2\cos\alpha|\eta_A||\eta_B| \leq 2|\eta_A||\eta_B|\,. \tag{4.35}$$

These conditions will be called from here on "positivity conditions".

Using the positivity conditions it is possible to determine the interval of positive solutions for one of the three half-life, e.g., T_k, if the values of the other two half-lives in the equations have been measured and are known. The condition on the interference term in equation (4.6) can considerably reduce the interval of values of T_k where $|\eta_A|^2 \geq 0$ and $|\eta_B|^2 \geq 0$. In Table 4.5 we give examples of the constraints on T_k following from the positivity conditions for three different pairs of interfering mechanisms: light Majorana neutrino and supersymmetric gluino exchange; light Majorana neutrino exchange and heavy LH Majorana neutrino exchange; gluino exchange and heavy LH Majorana neutrino exchange. It follows from the results shown in Table 4.5, in particular, that when $\mathrm{T}(^{76}Ge)$ is set to $\mathrm{T}(^{76}Ge) = 2.23 \times 10^{25}; 10^{26}$ y, but $\mathrm{T}(^{130}Te)$ is close to the current experimental lower limit, the positivity constraint intervals of values of $\mathrm{T}(^{136}Xe)$ for the each of the three pairs of interfering mechanisms considered are incompatible with the EXO lower bound on $\mathrm{T}(^{136}Xe)$, eq. (4.1).

Table 4.5: Ranges of the half-live of ^{136}Xe for different fixed values of the half-lives of ^{76}Ge and ^{130}Te in the case of three pairs of interfering mechanisms: light Majorana neutrino exchange and gluino exchange (upper table); light Majorana and heavy LH Majorana neutrino exchanges (middle table); gluino exchange and heavy LH Majorana neutrino exchange (lower table). The results shown are obtained with the "large basis" $g_A = 1.25$ Argonne NMEs. One star (two stars) indicate that the EXO bound constrains further (rules out) the corresponding solution.

$\mathrm{T}^{0\nu}_{1/2}$[y](fixed)	$\mathrm{T}^{0\nu}_{1/2}$[y](fixed)	Allowed Range
$\mathrm{T}(Ge) = 2.23 \cdot 10^{25}$**	$\mathrm{T}(Te) = 3 \cdot 10^{24}$	$2.95 \cdot 10^{24} \leq T(Xe) \leq 5.65 \cdot 10^{24}$
$\mathrm{T}(Ge) = 10^{26}$**	$\mathrm{T}(Te) = 3 \cdot 10^{24}$	$3.43 \cdot 10^{24} \leq T(Xe) \leq 4.66 \cdot 10^{24}$
$\mathrm{T}(Ge) = 2.23 \cdot 10^{25}$	$\mathrm{T}(Te) = 3 \cdot 10^{25}$	$1.74 \cdot 10^{25} \leq T(Xe) \leq 1.66 \cdot 10^{26}$
$\mathrm{T}(Ge) = 10^{26}$	$\mathrm{T}(Te) = 3 \cdot 10^{25}$	$2.58 \cdot 10^{25} \leq T(Xe) \leq 6.90 \cdot 10^{25}$

$\mathrm{T}^{0\nu}_{1/2}$[y](fixed)	$\mathrm{T}^{0\nu}_{1/2}$[y](fixed)	Allowed Range
$\mathrm{T}(Ge) = 2.23 \cdot 10^{25}$**	$\mathrm{T}(Te) = 3 \cdot 10^{24}$	$4.93 \cdot 10^{24} \leq T(Xe) \leq 6.21 \cdot 10^{24}$
$\mathrm{T}(Ge) = 10^{26}$**	$\mathrm{T}(Te) = 3 \cdot 10^{24}$	$5.23 \cdot 10^{24} \leq T(Xe) \leq 5.83 \cdot 10^{24}$
$\mathrm{T}(Ge) = 2.23 \cdot 10^{25}$	$\mathrm{T}(Te) = 3 \cdot 10^{25}$	$3.95 \cdot 10^{25} \leq T(Xe) \leq 8.25 \cdot 10^{25}$
$\mathrm{T}(Ge) = 10^{26}$	$\mathrm{T}(Te) = 3 \cdot 10^{25}$	$4.68 \cdot 10^{25} \leq T(Xe) \leq 6.61 \cdot 10^{25}$

$\mathrm{T}^{0\nu}_{1/2}$[y](fixed)	$\mathrm{T}^{0\nu}_{1/2}$[y](fixed)	Allowed Range
$\mathrm{T}(Ge) = 2.23 \cdot 10^{25}$**	$\mathrm{T}(Te) = 3 \cdot 10^{24}$	$5.59 \cdot 10^{23} \leq T(Xe) \leq 1.26 \cdot 10^{25}$
$\mathrm{T}(Ge) = 10^{26}$*	$\mathrm{T}(Te) = 3 \cdot 10^{24}$	$1.21 \cdot 10^{24} \leq T(Xe) \leq 4.71 \cdot 10^{25}$
$\mathrm{T}(Ge) = 2.23 \cdot 10^{25}$**	$\mathrm{T}(Te) = 3 \cdot 10^{25}$	$1.05 \cdot 10^{24} \leq T(Xe) \leq 2.42 \cdot 10^{24}$
$\mathrm{T}(Ge) = 10^{26}$*	$\mathrm{T}(Te) = 3 \cdot 10^{25}$	$3.32 \cdot 10^{24} \leq T(Xe) \leq 2.16 \cdot 10^{25}$

We consider next a case in which the half-life of ^{136}Xe is one of the two half-lives assumed to have been experimentally determined. The $(\beta\beta)_{0\nu}$-decay is supposed to be triggered by light Majorana neutrino and gluino exchange mechanisms with LFV parameters $|\eta_\nu|^2$ and $|\eta_{\lambda'}|^2$. We use in the analysis the half-lives of ^{76}Ge, ^{136}Xe and

^{130}Te, which will be denoted for simplicity respectively as T_1, T_2 and T_3. Once the experimental bounds on T_i, $i = 1, 2, 3$, given in eq. (4.2), are taken into account, the conditions for destructive interference, i.e., for $\cos\alpha < 0$, are given by:

$$z < 0 \; : \begin{cases} 1.9 \times 10^{25} < T_1 \leq 1.90 T_2, & T_3 \geq \dfrac{9.64 T_1 T_2}{16.32 T_1 + 8.59 T_2}; \\ 1.90 T_2 < T_1 \leq 2.78 T_2, & T_3 > \dfrac{3.82 T_1 T_2}{6.33 T_1 + 3.66 T_2}; \\ T_1 > 2.78 T_2, & T_3 \geq \dfrac{7.33 T_1 T_2}{11.94 T_1 + 7.61 T_2}\,, \end{cases} \tag{4.36}$$

where we have used the "large basis" $g_A = 1.25$ Argonne NMEs (see Table 2.1). The conditions for constructive interference read:

$$z > 0 \; : \begin{cases} 1.90 T_2 < T_1 \leq 2.29 T_2, & \dfrac{9.64 T_1 T_2}{16.32 T_1 + 8.59 T_2} \leq T_3 \leq \dfrac{3.82 T_1 T_2}{6.33 T_1 + 3.66 T_2}; \\ 2.29 T_2 < T_1 < 2.78 T_2, & \dfrac{7.33 T_1 T_2}{11.94 T_1 + 7.61 T_2} \leq T_3 \leq \dfrac{3.82 T_1 T_2}{6.33 T_1 + 3.66 T_2}. \end{cases} \tag{4.37}$$

If we set, e.g., the ^{76}Ge half-life to the value claimed in [103] $T_1 = 2.23 \times 10^{25}$ y, we find that only destructive interference between the contributions of the two mechanisms considered in the $(\beta\beta)_{0\nu}$-decay rate, is possible. Numerically we get in this case

$$T_3 > \frac{3.44 T_2}{5.82 + 1.37 \times 10^{-25} T_2}\,. \tag{4.38}$$

For $1.37 \times 10^{-25} T_2 \ll 5.82$ one finds:

$$T(^{130}Te) \gtrsim 0.59\, T(^{136}Xe) \gtrsim 9.46 \times 10^{24} \text{ y}\,, \tag{4.39}$$

where the last inequality has been obtained using the EXO lower bound on $T(^{136}Xe)$. Constructive interference is possible for the pair of interfering mechanisms under discussion only if $T(^{76}Ge) \gtrsim 3.033 \times 10^{25}$ y.

The possibilities of destructive and constructive interference are illustrated in Figs. 4.7 and 4.8, respectively. In these figures the physical allowed regions, determined through the positivity conditions, correspond to the areas within the two vertical lines (the solutions must be compatible also with the existing lower limits given in eq (4.2)). For instance, using the Argonne "large basis" NMEs corresponding to $g_A = 1.25$ and setting $T(^{76}Ge) = 2.23 \times 10^{25}$ y and $T(^{130}Te) = 10^{25}$ y, positive solutions are allowed only in the interval $1.60 \times 10^{25} \leq T(^{136}Xe) \leq 2.66 \times 10^{25}$ y (Fig. 4.7). As can be seen in Figs. 4.7 and 4.8, a constructive interference is possible only if $T_2 \equiv T(^{136}Xe)$ lies in a relatively narrow interval and $T_3 \equiv T(^{130}Te)$ is determined through the conditions in eq. (4.37).

Next, we would like to illustrate the possibility to distinguish between two pairs of interfering mechanisms i) A+B and ii) B+C, which share one mechanism, namely B, from the data on the half-lives of three isotopes. In this case we can set two systems of three equations, each one in three unknowns. We will denote the corresponding LNV parameters as i) $|\eta_A|^2$, $|\eta_B|^2$ and ii) $|\eta_B|^2$ and $|\eta_C|^2$, while the interference parameters will be denoted as i) z and ii) z'. Fixing two of the three half-lives, say T_i and T_j, the possibility to discriminate between the mechanisms A and C relies on the dependence of $|\eta_A|^2$ and $|\eta_C|^2$ on the third half-life, T_k. Given T_i and T_j, it will be possible to

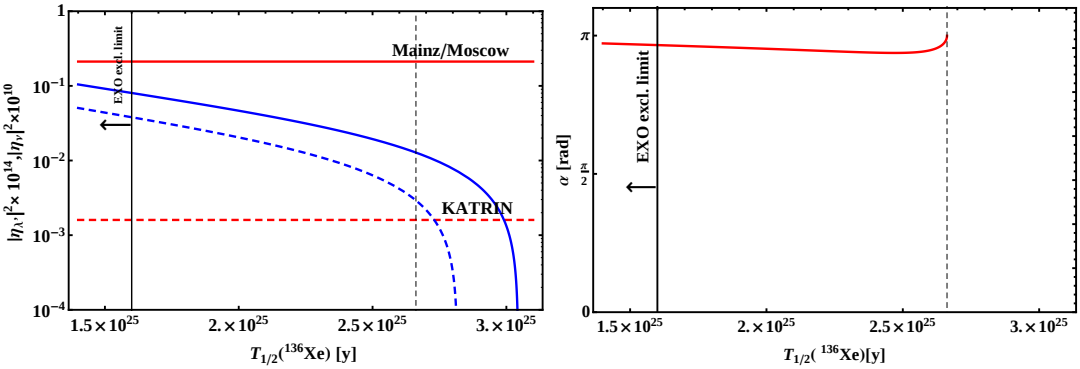

Figure 4.7: Left panel: the values of $|\eta_\nu|^2 \times 10^{10}$ (thick solid line) and $|\eta_{\lambda'}|^2 \times 10^{14}$ (dotted line), obtained as solutions of the system of equations (4.4) for fixed values of $T(^{76}Ge) = 2.23 \times 10^{25}$ y and $T(^{130}Te) = 10^{25}$ y, and letting $T^{0\nu}_{1/2}(^{136}Xe)$ free. The physical allowed regions correspond to the areas within the two vertical lines. Right panel: the values of the phase α in the allowed interval of values of $T^{0\nu}_{1/2}(^{136}Xe)$, corresponding to physical solutions for $|\eta_\nu|^2$ and $|\eta_{\lambda'}|^2$. In this case $\cos\alpha < 0$ and the interference is destructive. See text for details.

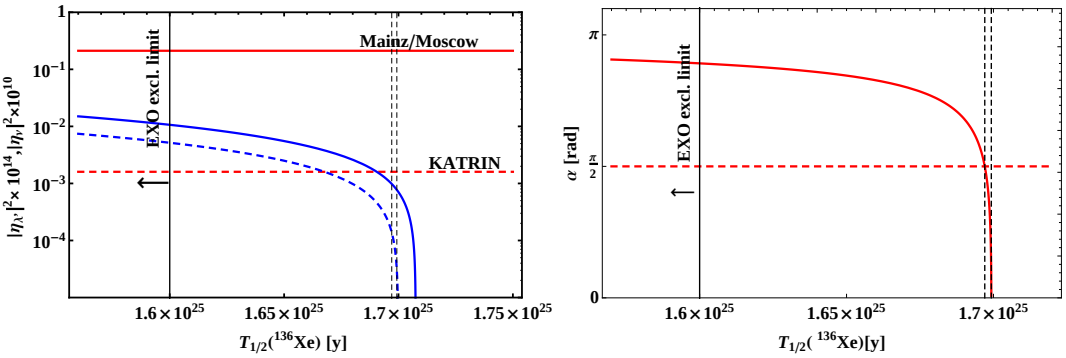

Figure 4.8: Left panel: the same as in Fig. 4.7 but for $T(^{76}Ge) = 3.5 \times 10^{25}$ y and $T(^{130}Te) = 8.0 \times 10^{25}$ y. The interval of values of $T^{0\nu}_{1/2}(^{130}Xe)$ between i) the vertical solid and right dashed lines ii) the two vertical dashed lines, and iii) the vertical solid and left dashed lines, correspond respectively to i) physical (non-negative) solutions for $|\eta_\nu|^2$ and $|\eta_{\lambda'}|^2$, ii) constructive interference ($z > 0$), and iii) destructive interference ($z < 0$). Right panel: the corresponding values of the phase α as a function of $T^{0\nu}_{1/2}(^{130}Xe)$. Constructive interference is possible only for values of $T^{0\nu}_{1/2}(^{130}Xe)$ between the two vertical dashed lines. See text for details.

discriminate between the mechanisms A and C if the two intervals of values of T_k where $|\eta_A|^2 > 0$ and $|\eta_C|^2 > 0$, do not overlap. If, instead, the two intervals partially overlap, complete discrimination would be impossible, but there would be a large interval of values of T_k (or equivalently, positive solutions values of the LNV parameters) that can be excluded using present or future experimental data. In order to have non-overlapping positive solution intervals of T_K, corresponding to $|\eta_A|^2 > 0$ and $|\eta_C|^2 > 0$, the following inequality must hold:

$$\frac{(M'^{0\nu}_{k,A}M'^{0\nu}_{i,B} - M'^{0\nu}_{i,A}M'^{0\nu}_{k,B})(M'^{0\nu}_{k,A}M'^{0\nu}_{j,B} - M'^{0\nu}_{j,A}M'^{0\nu}_{k,B})}{(M'^{0\nu}_{k,B}M'^{0\nu}_{i,C} - M'^{0\nu}_{i,B}M'^{0\nu}_{k,C})(M'^{0\nu}_{k,B}M'^{0\nu}_{j,C} - M'^{0\nu}_{j,B}M'^{0\nu}_{k,C})} < 0. \qquad (4.40)$$

The above condition can be satisfied only for certain sets of isotopes. Obviously, whether it is fulfilled or not depends on the values of the relevant NMEs. We will illustrate this on the example of an oversimplified analysis involving the light Majorana neutrino exchange, the heavy LH Majorana neutrino exchange and the gluino exchange as mechanisms A, B and C, respectively, and the half-lives of ^{76}Ge, ^{130}Te and ^{136}Xe: $T_1 \equiv T(^{76}Ge)$, $T_2 \equiv T(^{130}Te)$ and $T_3 \equiv T(^{136}Xe)$. Fixing $T_1 = 2.23 \times 10^{25}$ y and $T_3 = 1.6 \times 10^{25}$ y (the EXO 90% C.L. lower limit), we obtain the results shown in Fig. 4.9. As it follows from Fig. 4.9, in the case of the Argonne NMEs (left panel), it is possible to discriminate between the standard light neutrino exchange and the gluino exchange mechanisms: the intervals of values of T_2, where the positive solutions for the LNV parameters of the two pairs of interfering mechanisms considered occur, do not overlap. Further, the physical solutions for the two LNV parameters related to the gluino mechanism are excluded by the CUORICINO limit on $T(^{130}Te)$ [99]. This result does not change with the increasing of T_3. Thus, we are lead to conclude that for $T_3 > 1.6 \times 10^{25}$ y and T_1 given by the value claimed in [103], of the two considered pairs of possible interfering $(\beta\beta)_{0\nu}$-decay mechanisms, only the light and heavy LH Majorana neutrino exchanges can be generating the decay. The solution for $|\eta_\nu|^2$ must be compatible with the upper limit $|\langle m \rangle| < 2.3$ eV [31, 48], indicated with a solid horizontal line in Fig. 4.9. In the right panel of Fig. 4.9 we plot also the solutions obtained with the CD-Bonn NMEs. In this case is not possible to discriminate between the two considered pair of mechanisms since the condition in eq. (4.40) is not satisfied.

Another interesting example is the case in which A is the light Majorana neutrino exchange, B is the gluino exchange and C the heavy LH Majorana neutrino exchange, i.e., we try to discriminate between i) the light neutrino plus gluino exchange mechanisms, and ii) the heavy LH Majorana neutrino plus gluino exchange mechanisms. We fix, like in the previous case, the values for $T_1 = 2.23 \times 10^{25}$y and $T_3 = 1.6 \times 10^{25}$y. The results of this analysis are plotted in Fig. 4.10. Since the condition in eq. (4.40) is now satisfied for NMEs obtained either with the Argonne potential or with the CD-Bonn potential, in this case it is possible, in principle, to discriminate between the two pair of mechanisms independently of the set of NMEs used (within the sets considered by us). This result does not change with the increasing of T_3. Hence, as far as T_1 is fixed to the value claimed in [103] and the limits in eq. (4.2) are satisfied, the two intervals of values of T_2, in which the "positivity conditions" for i) $|\eta_\nu|^2$, $|\eta_{\lambda'}|^2$ and z, and for ii) $|\eta_{\lambda'}|^2$, $|\eta_N|^2$ and z', are satisfied, are not overlapping (Fig. 4.10).

IV Final Remarks

In this chapter we have investigated the possibility to discriminate between different pairs of CP non-conserving mechanisms inducing the neutrinoless double beta $(\beta\beta)_{0\nu}$-decay by using data on $(\beta\beta)_{0\nu}$-decay half-lives of nuclei with largely different NMEs. The mechanisms studied are: light Majorana neutrino exchange, heavy left-handed (LH) and heavy right-handed (RH) Majorana neutrino exchanges, lepton charge non-conserving couplings in SUSY theories with R-parity breaking giving rise to the "dominant gluino exchange" and the "squark-neutrino" mechanisms. Each of these mechanisms is characterized by a specific lepton number violating (LNV) parameter η_κ, where the index κ labels the mechanism. For the five mechanisms listed above we use the notations $\kappa = \nu, L, R, \lambda', \tilde{q}$, respectively. The parameter η_κ will be complex, in general, if

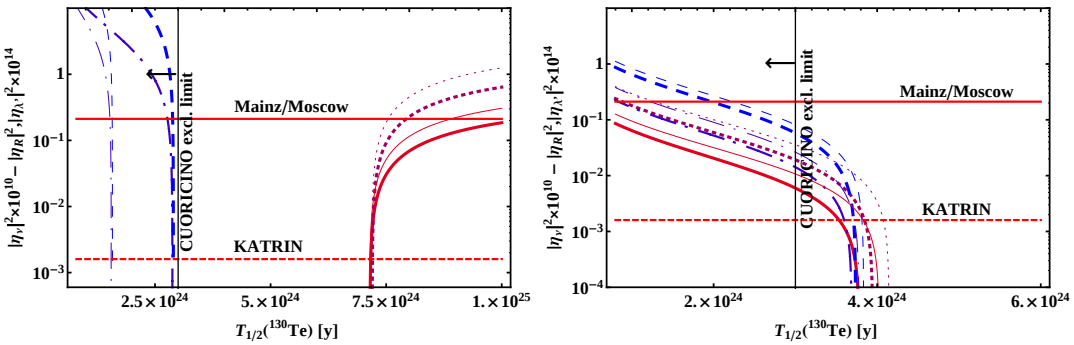

Figure 4.9: The parameters $|\eta_\nu|^2 \times 10^{10}$ (solid line) and $|\eta_L|^2 \times 10^{14}$ (dotted line) of the light and heavy LH Majorana neutrino exchange mechanisms, and $|\eta_{\lambda'}|^2 \times 10^{14}$ (dashed-dotted line) and $|\eta_L|^2 \times 10^{14}$ (dashed line) of the gluino and heavy LH Majorana neutrino exchange mechanisms, obtained from eq. (4.32) using the Argonne NMEs (left panel) and CD-Bonn NMEs (right panel), corresponding to $g_A = 1.25$ (thick lines) and $g_A = 1$ (thin lines), for $T^{0\nu}_{1/2}(^{76}Ge) = 2.23 \times 10^{25}$y, $T^{0\nu}_{1/2}(^{136}Xe) = 1.60 \times 10^{25}$y and letting $T^{0\nu}_{1/2}(^{130}Te)$ free. See text for details.

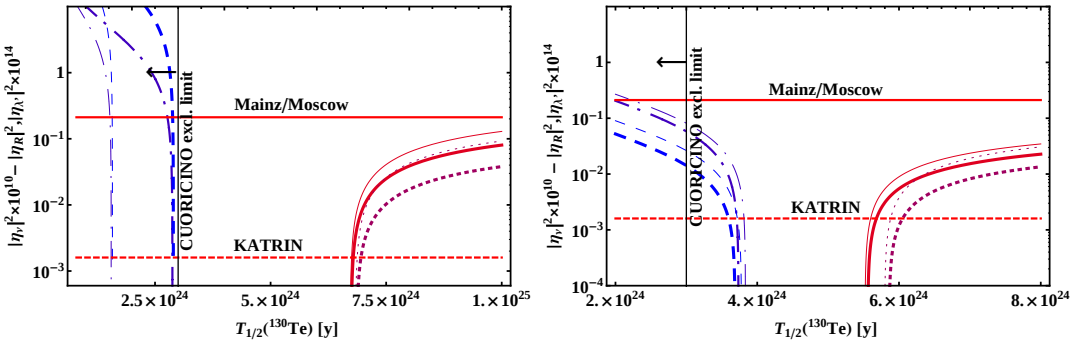

Figure 4.10: The same as in Fig. 4.9, but for i) $|\eta_\nu|^2 \times 10^{10}$ (thick solid line) and $|\eta_{\lambda'}|^2 \times 10^{14}$ (thick dotted line) of the light neutrino and gluino exchange mechanisms, and ii) $|\eta_L|^2 \times 10^{14}$ (thick dashed-dotted line) and $|\eta_{\lambda'}|^2 \times 10^{14}$ (thick dashed line) of the heavy LH Majorana neutrino and gluino exchange mechanisms, and using $T^{0\nu}_{1/2}(^{76}Ge) = 2.23 \times 10^{25}$ y and $T^{0\nu}_{1/2}(^{136}Xe) = 1.60 \times 10^{25}$ y. See text for details.

the mechanism κ does not conserve the CP symmetry. The nuclei considered are ^{76}Ge, ^{82}Se, ^{100}Mo, ^{130}Te and ^{136}Xe. Four sets of NMEs of the $(\beta\beta)_{0\nu}$-decays of these five nuclei, derived within the Self-consistent Renormalized Quasiparticle Random Phase Approximation (SRQRPA), were employed in our analysis. They correspond to two types of nucleon-nucleon potentials - Argonne ("Argonne NMEs") and CD-Bonn ("CD-Bonn NMEs"), and two values of the axial coupling constant $g_A = 1.25; 1.00$. Given the NMEs and the phase space factors of the decays, the half-life of a given nucleus depends on the parameters $|\eta_\kappa|^2$ of the mechanisms triggering the decay (eq. (4.5)).

In the present chapter we have considered in detail the cases of two non-interfering and two interfering mechanisms inducing the $(\beta\beta)_{0\nu}$-decay. If two non-interfering mechanisms A and B cause the decay, the parameters $|\eta_A|^2$ and $|\eta_B|^2$ can be determined from data on the half-lives of two isotopes, T_1 and T_2 as solutions of a system of two linear equations. If the half-life of one isotope is known, say T_1, the positivity condition which the solutions $|\eta_A|^2$ and $|\eta_B|^2$ must satisfy, $|\eta_A|^2 \geq 0$ and $|\eta_B|^2 \geq 0$, constrain the half-life of the second isotope T_2 (and the half-life of any other isotope for that matter) to lie in a specific interval. If A and B are interfering mechanisms, $|\eta_A|^2$ and $|\eta_B|^2$ and the interference term parameter, $z_{AB} \equiv 2\cos\alpha_{AB}|\eta_A\eta_B|$ which involves the cosine of an unknown relative phase α_{AB} of η_A and η_B, can be uniquely determined, in principle, from data on the half-lives of three nuclei, $T_{1,2,3}$. In this case, given the half-life of one isotope, say T_1, the "positivity conditions" $|\eta_A|^2 \geq 0$, $|\eta_B|^2 \geq 0$ and $-1 \leq \cos\alpha_{AB} \leq 1$ constrain the half-life of a second isotope, say T_2, to lie in a specific interval, and the half-life of a third one, T_3, to lie in an interval which is determined by the value of T_1 and the interval of allowed values of T_2.

For all possible pairs of non-interfering mechanisms we have considered (light, or heavy LH Majorana neutrino, and heavy RH Majorana neutrino exchanges; gluino, or squark-neutrino, and RH Majorana neutrino mechanisms), these "positivity condition" intervals of values of T_2 were shown to be essentially degenerate if T_1 and T_2 correspond to the half-lives of any pair of the four nuclei ^{76}Ge, ^{82}Se, ^{100}Mo and ^{130}Te. This is a consequence of the fact that for each of the five single mechanisms discussed, the NMEs for ^{76}Ge, ^{82}Se, ^{100}Mo and ^{130}Te differ relatively little [64,76,105]: the relative difference between the NMEs of any two nuclei does not exceed 10%. One has similar degeneracy of "positivity condition" intervals T_2 and T_3 in the cases of two constructively interfering mechanisms (within the set considered). These degeneracies might irreparably plague the interpretation of the $(\beta\beta)_{0\nu}$-decay data if the process will be observed.

The NMEs for ^{136}Xe, results of calculations of which using the SRQRPA method are presented in the present chapter, differ significantly from those of ^{76}Ge, ^{82}Se, ^{100}Mo and ^{130}Te, being by a factor $\sim (1.3 - 2.5)$ smaller. As we have shown in the present chapter, this allows to lift to a certain degree the indicated degeneracies and to draw conclusions about the pair of non-interfering (interfering) mechanisms possibly inducing the $(\beta\beta)_{0\nu}$-decay from data on the half-lives of ^{136}Xe and of at least one (two) more isotope(s) which can be, e.g., any of the four, ^{76}Ge, ^{82}Se, ^{100}Mo and ^{130}Te considered.

We have analyzed also the possibility to discriminate between two pairs of non-interfering (or interfering) $(\beta\beta)_{0\nu}$-decay mechanisms when the pairs have one mechanism in common, i.e., between the mechanisms i) $A + B$ and ii) $C + B$, using the half-lives of the same two isotopes. We have derived the general conditions under which it would be possible, in principle, to identify which pair of mechanisms is inducing the decay (if any). We have shown that the conditions of interest are fulfilled, e.g., for the following two pairs of non-interfering mechanisms i) light neutrino exchange (A) and

heavy RH Majorana neutrino exchange (B) and ii) gluino exchange (C) and heavy RH Majorana neutrino exchange (B), and for the following two pairs of interfering mechanisms i) light neutrino exchange (A) and heavy LH Majorana neutrino exchange (B) and ii) gluino exchange (C) and heavy LH Majorana neutrino exchange (B), if one uses the Argonne NMEs in the analysis. They are fulfilled for both the Argonne NMEs and CD-Bonn NMEs, e.g., for the following two pairs of interfering mechanisms i) light neutrino exchange (A) and gluino exchange (B), and ii) heavy LH Majorana neutrino exchange (C) and gluino exchange (B).

We have also exploited the implications of the EXO lower bound on the half-life of ^{136}Xe for the problem studied. We have shown, in particular, that for all four pairs of non-interfering mechanisms considered and the Argonne NMEs, the half-life of ^{76}Ge claimed in [103] is incompatible with the EXO lower bound on the half-life of ^{136}Xe [54]. If we use the CD-Bonn NMEs instead, we find that the result half-life of ^{76}Ge claimed in [103] is compatible with the EXO lower bound on the half-life of ^{136}Xe for values of the corresponding LNV parameters lying in extremely narrow intervals.

To summarize, the results obtained in the present chapter show that using the $(\beta\beta)_{0\nu}$-decay half-lives of nuclei with largely different NMEs would help resolving the problem of identifying the mechanisms triggering the decay.

Part II

On Models of Neutrino Masses and Mixing

Chapter 5

Overview

Understanding the origin of the patterns of neutrino masses and mixing, emerging from neutrino oscillations, ^3H $\beta-$decay and cosmological data is one of the most challenging problems in neutrino physics. It is part of the more general fundamental problem in particle physics of understanding the origin of flavour, i.e., of the patterns of the quark, charged lepton and neutrino masses and of the quark and lepton mixing. Albeit the impressive experimental progresses of the last years, one has to admit that we are still completely ignorant about the underlying symmetries, if any, in the lepton sector related to the mixing in the case of three generations and about the mechanism of generation of neutrino masses and its relative mass scale. Indeed it is a long-standing question whether and how we can explain the form of the lepton mixing matrix, the Pontecorvo-Maki-Nakagawa-Sakata (PMNS) mixing matrix, $U_{\rm PMNS}$.

The PMNS mixing matrix, with two large angles and one small, is quite peculiar and differs considerably from the one observed in the quark sector in which the mixing angles are hierarchical with the largest one being the Cabibbo angle $\sin\theta^C \approx 0.22$ [6].

For convenience we recall here in Table 5.1 two of the most up to date global fits analysis of the neutrino data which combine results from several experiments [29, 30].

In modern theories the generation of the mass terms for fermions, and thus the mixing, appears in the Lagrangian of particle interaction as a result of the breaking of underlying symmetries. In spite of the great success of continuous gauge symmetries, widely used in particle physics and in particular in the Glashow-Weinberg-Salam Model describing electroweak interactions, there is still no clue how to solve the flavour puzzle, both in the quark and lepton sectors. Moreover we do not have any indication about an eventual connection between non zero neutrino masses and eventual symmetries that could predict the lepton mixing. Nevertheless the lepton mixing matrix can well be due to the existence of an approximate symmetry, which can be continuous (corresponding, e.g., to the conservation of the non-standard lepton charge $L' = L_e - L_\mu - L_\tau$ [18]), or discrete (see, e.g., [8, 19, 20]).

Following the symmetry approach, one would be led to ask whether the origin of the different masses and mixing patterns of quarks and leptons can arise from a symmetry which acts "horizontally" among the three generations. Along this line, the first authors who considered a "family symmetry" were Froggatt and Nielsen [106]. In that case, using a continuous symmetry $U(1)_{FN}$, one could explain the hierarchies of quark and charged lepton masses and mixings assigning appropriate charges to the quark and lepton fields. However, Abelian groups, like $U(1)$, suffer from the limit of

Parameter	Fogli et al. [29]	Gonzalez-Garcia et al. [30]
$\Delta m^2_{21}[10^{-5}\text{eV}^2]$	$7.54^{+0.26}_{-0.22}$	7.50 ± 0.185
$\Delta m^2_{31}[10^{-3}\text{eV}^2]$	$2.43^{+0.06}_{-0.10}$ $-2.42^{+0.11}_{-0.07}$	$2.47^{+0.069}_{-0.067}$ $-2.43^{+0.042}_{-0.065}$
$\sin^2\theta_{12}$	$0.307^{+0.018}_{-0.016}$	0.30 ± 0.013
$\sin^2\theta_{23}$	$0.386^{+0.024}_{-0.021}$ $0.392^{+0.039}_{-0.022}$	$0.41^{+0.037}_{-0.025}$ $0.41^{+0.037}_{-0.025} \oplus 0.59^{+0.021}_{-0.022}$
$\sin^2\theta_{13}$	0.0241 ± 0.0025 $0.0244^{+0.0023}_{-0.0025}$	0.023 ± 0.0023

Table 5.1: The table summarizes two recent global fit analysis to the available experimental data for the neutrino oscillation parameters corresponding to 1σ uncertainty. For Δm^2_{31}, $\sin^2\theta_{23}$ and $\sin^2\theta_{13}$ the upper (lower) row corresponds to normal (inverted) neutrino mass ordering. These values and the methods to extract them from experimental data are discussed in respectively in [29] and [30].

having only one-dimensional representations therefore there would be no explanation for the number of generations. On the contrary, non-Abelian family symmetry can explain the existence of three generations since we can accommodate them in a three dimensional irreducible representations (i.e. triplets) therefore it is straightforward to consider $U(3)$ and its subgroups.

In the last decade there has been remarkable interest in investigating the connection of discrete finite non-Abelian symmetries with the symmetry properties of the mixing matrix both in the quark and lepton sector, and, more interestingly, in connection with the possible neutrino mass terms and the nature of massive neutrinos thus generated, Dirac or Majorana.

In the last years [107, 108] the approach to impose a discrete finite non-Abelian group as flavor symmetry in the lepton sector, namely G_l, (for reviews see [8, 19, 20] and [109]) which is broken to different (Abelian) subgroups G_e and G_ν in the charged lepton and neutrino sector respectively, has been considered interesting because this approach allows to fix the entries of the U_{PMNS}, up to possible permutations of rows and columns and phases, in such a way that the mixing angles and the Dirac phase δ can be predicted[1]. The breaking of G_l, that generates a non-trivial Yukawa structure, is obtained through the existence of scalar fields —the so-called "flavons"— which are singlets under the Standard Model (SM) gauge group but they are charged under the symmetry G_l in such a way that their vacuum expectation values (vevs) spontaneously break the symmetry.

The recent experimental results concerning the measurement of the angle θ_{13} had a strong impact on the community studying neutrino flavour physics since for long time this angle was supposed to be small or even zero. A large variety of models proposed in the literature based on non-Abelian discrete symmetries and featuring a vanishing or very small θ_{13}, like Bi-Maximal mixing (BM) ($\theta_{23} = \theta_{12} = \pi/4$ and $\theta_{13} = 0$) or

[1]Indeed there are a set of possibilities depending on the residual subgroups

Tri-BiMaximal mixing (TBM) [110–113], ($\theta_{23} = \pi/4$, $\sin\theta_{12} = 1/\sqrt{3}$ and $\theta_{13} = 0$) are now disfavored by the experimental data. Their mixing matrices respectively read:

$$U_{BM} = \begin{pmatrix} \frac{1}{\sqrt{2}} & \frac{1}{\sqrt{2}} & 0 \\ -\frac{1}{2} & \frac{1}{2} & \frac{1}{\sqrt{2}} \\ \frac{1}{2} & -\frac{1}{2} & \frac{1}{\sqrt{2}} \end{pmatrix}, \quad U_{TBM} = \begin{pmatrix} \sqrt{\frac{2}{3}} & \sqrt{\frac{1}{3}} & 0 \\ -\sqrt{\frac{1}{6}} & \sqrt{\frac{1}{3}} & -\sqrt{\frac{1}{2}} \\ -\sqrt{\frac{1}{6}} & \sqrt{\frac{1}{3}} & \sqrt{\frac{1}{2}} \end{pmatrix}. \tag{5.1}$$

Despite of the fact that these textures for the PMNS mixing matrix are now ruled out as exact by the experimental results, they still play an important role from the model building point of view.

Given the experimental data, and especially the unexpected "large" value of θ_{13}, one might think that the origin of the observed pattern in the lepton sector does not emerge from an underlying principle or symmetry. This interpretation has been adopted by some authors who have labeled the neutrino mass matrix as "anarchical" [114]. Nevertheless there exist alternative choices with respect to this approach.

One of these consists in generating a non zero value of the angle θ_{13} by the BM/TBM mixing patterns and then add perturbative corrections coming from the diagonalization of the charged lepton mass matrix. Being the PMNS the matrix that accounts for the basis mismatch in the charged lepton and neutrino sectors i.e. $U_{PMNS} = U_\ell^\dagger U_\nu$ one could think that the "large" value of $\theta_{13} \backsimeq 0.16$ arises from contributions due to the charged lepton sector only.

This option is particularly tantalizing in the context of grand unified theories and this approach has been pursued recently by a number of authors using a minimal supersymmetric unification model based on $SU(5)$ or the Pati-Salam models based on $SU(4) \times SU(2)_L \times SU(2)_R$ [115–117]. In these frameworks θ_{13} can be "large" because it can be related to the Cabibbo mixing angle, θ^C, via the unification assumptions. In fact grand unified symmetries, as those mentioned, usually permit to relate the down-type quark and the charged lepton Yukawa couplings, Y_d, and Y_e, since both down-type quarks and charged leptons are unified in the same representation of the group.

More concretely the down-quark and transposed charged lepton mass matrices coincide in the minimal $SU(5)$ models leading to wrong predictions for the fermion mass ratios like m_b/m_τ and m_s/m_μ. In Table 5.2 we report the available data taken from [6].

Parameter	Value
m_e	0.511 ± 10^{-8} MeV
m_μ	$105.658 \pm 3.5 \times 10^{-6}$ MeV
m_s (2 GeV)	95 ± 5 MeV
m_d (2 GeV)	$4.8^{+0.5}_{-0.3}$ MeV
m_s/m_d (2 GeV)	$17 - 22$
$\lvert V_{us}\rvert$	0.2252 ± 0.0009

Table 5.2: Available data on fermion masses taken from [6].

However this relation can be modified by the Clebsch-Gordan coefficients (CGs), namely α_{ij}, appearing in the renormalizable or non-renormalizable operators of the model under study i.e. $(Y_d)_{ij} = \alpha_{ij}(Y_e)^T_{ij}$. These coefficients can be constrained to be in a finite set of rational numbers given by the specific contraction of gauge indexes in

the operator used in the model under study. For example, if we consider a minimal $SU(5)$ model there exist only two renormalizable operators giving rise to the Y_d and Y_e Yukawa couplings and therefore two possible CGs depending on whether the Higgs is accommodated in a $\bar{\mathbf{5}}$, then $\alpha_{ij} = 1$, or in a $\bar{\mathbf{45}}$, then $\alpha_{ij} = -3$. This is due to the fact that the $\bar{\mathbf{45}}$ is a representation, that can be written as an antisymmetric tensor, $H_c^{ab} = -H_c^{ba}$ with $a, b, c, = 1, \ldots, 5$. The fact that $H_c^{ab} = -H_c^{ba}$ implies that the tensor must be traceless, $H_a^{ab} = 0$. If the $\bar{\mathbf{45}}$ takes a vev, than the three contributions coming form the colored quarks must cancel in the lepton sector and this is possible only if $\alpha_{ij} = -3$. Specifically one finds that the vev can be written as $\langle (H_j^{i5}) \rangle = v_{45}(\delta_j^i - 4\delta_{j4}^{i4})$ with $i, j = 1, \ldots, 4$. Other possibilities arise if one uses in the Higgs sector other representations such as the adjoint representation **24**. In this case the vev can be written as $\langle (H_a^a) \rangle = v_{24}(2\delta_{\alpha a} - 3\delta_{\beta a})$ with $a = 1, \ldots, 5$, $\alpha = 1, 2, 3$ and $\beta = 4, 5$ (details for different GUT predictions can be found in [118]).

More importantly in this scenarios the relative position of the CGs in the Yukawa matrices plays a fundamental role in the determination of θ_{13}. In chapter 6 we will describe an attempt to construct a unified model of flavour elaborated in [65], which describes correctly the quark and charged lepton masses, the mixing and CP violation in the quark sector, the mixing in the lepton sector, including the relatively large value of the angle θ_{13}, providing predictions for the light neutrino masses compatible with the existing relevant data and constraints. The unified model of flavour we are proposing is supersymmetric and is based on $SU(5)$ as gauge group and T' as discrete family symmetry.

The group T' is the double covering of the group A_4 and has 24 elements[2]. More importantly, it is the smallest group that allows 1-, 2-, and 3-dimensional representations and for which the three representations can be related by the multiplication rule $\mathbf{2} \otimes \mathbf{2} = \mathbf{3} \oplus \mathbf{1}$. The description of the group T' is provided in Appendix III. In the model that will be discussed in chapter 6 a type I see-saw mechanism of neutrino mass generation is implemented, which predicts the reactor neutrino angle to be $\theta_{13} \approx 0.14$ close to the recent results from the Daya Bay and RENO experiments. The model predicts also values of the solar and atmospheric neutrino mixing angles, which are compatible with the existing data. The T' breaking leads to TBM mixing in the neutrino sector[3], which is perturbed by sizeable corrections from the charged lepton sector. In the model all complex phases have their origin from the complex CGs of T'. The values of the Dirac and Majorana CP violating phases are predicted. For the Dirac phase in the standard parametrization of the neutrino mixing matrix we get a value close to 90°: $\delta \cong \pi/2 - 0.45\theta^C \cong 84.3°$. The neutrino mass spectrum can be with normal ordering (2 cases) or inverted ordering. In each case the values of the three light neutrino masses are predicted with relatively small uncertainties, which allows to get also unambiguous predictions for the $(\beta\beta)_{0\nu}$-decay effective Majorana mass.

An alternative approach to explain the lepton mixing pattern is the direct search for non-Abelian discrete groups which can give rise to mixing patterns with values of θ_{12}, θ_{23} and θ_{13} compatible with the experimental data. One can in fact fix G_l as a family symmetry in the lepton sector and then break the group, spontaneously

[2] The only other 24-element group that has representation of the same dimensions is the octahedral group O (which is isomorphic to S_4). In this case, however, the product of two doublet reps does not contain a triplet [119].

[3] The breaking is realized in a basis where both the lepton and neutrino mass matrix are not diagonal

or explicitly, to two different Abelian subgroups G_e and G_ν in the charged lepton and neutrino sector [107,108,120]. We assign the three generations of left-handed leptons to an irreducible three-dimensional representation, because we want to discuss patterns with at least two non-vanishing lepton mixing angles. We furthermore choose the representation to be faithful in the group G_l so that we (mostly) study mixing patterns which originate from the group itself and not from one of its proper subgroups.[4] For fixing the mixing angles we also have to assume that the three generations of left-handed leptons transform as three inequivalent one-dimensional representations under the residual symmetries G_e and G_ν.

Therefore as regards the symmetries, G_e can be any Abelian group which is capable of distinguishing among the three generations, while the nature of the neutrinos — Dirac or Majorana— determines G_ν. For Dirac neutrinos G_ν is subject to the same constraints as G_e, while if neutrinos are Majorana particles, G_ν is constrained to be specifically a (subgroup of) Klein group[5].

After the indication of T2K of a non-zero θ_{13}, among the first groups which have been discussed in the literature to apply this strategy there are $\Delta(96)$ and $\Delta(384)$ which both belong (like the group $S_4 \simeq \Delta(24)$) to the series of groups $\Delta(6n^2)$ [120,121] which is a well-known series of finite discrete non-Abelian subgroups of $SU(3)$. For example two models which employ the group $\Delta(96)$ as flavor group can be found in [122].

Another possibility which has been considered by several authors (for example see [123–126]) is that G_ν is only partly contained in the group G_l. One of the best known examples are models with the flavor symmetry A_4 in which an accidental symmetry Z_2 is present in the neutrino sector. In this way a free parameter in the PMNS pattern appears and can be used to accommodate the experimental data. On the contrary if one uses an additional Z_2 symmetry, the whole PMNS can be predicted at leading order (LO). [127–129]. Recently, also models with flavor and CP symmetries have been discussed in [130] (with emphasis on the prediction of the lepton mixing parameters) and in [131] (emphasizing mathematical properties of the CP transformation). The latter two approaches have in common that a free parameter, not determined by the choice of the groups G_e, G_ν and G_l, is present in the PMNS matrix which allows to accommodate a non-vanishing reactor mixing angle. At the same time, the approach involving CP symmetry allows to constrain not only the Dirac phase, but also the Majorana phases if one sets $G_\nu = Z_2 \times CP$.

We follow the approach to search for new discrete groups and focus in chapter 7 on the so-called "exceptional" finite groups $\Sigma(n\varphi)$: $\Sigma(36\varphi)$, $\Sigma(72\varphi)$, $\Sigma(216\varphi)$, $\Sigma(360\varphi)$ with $\varphi = 1, 3$, which are subgroups of $SU(3)$ ($\varphi = 3$) or of $SU(3)/C$ ($\varphi = 1$) with C being the center of $SU(3)$[6] [132]. Groups with $\varphi = 1$ are not suitable for our purposes,[7]

[4] The requirement of faithfulness of the three-dimensional representation also excludes the possibility to choose G_e or G_ν to be non-Abelian, since a faithful representation of G_l usually decomposes into an irreducible representation of dimension larger than one in G_e or G_ν so that a distinction among the three lepton generations becomes impossible. Indeed if a non-Abelian residual symmetry for the charged leptons is chosen then a complete or partial degeneracy of the mass spectrum is obtained and this is clearly not in accordance with the hierarchy among the charged lepton masses. This is not valid for G_ν for which one can admit a degeneracy in the mass spectrum.

[5] The Klein symmetry, $Z_2 \otimes Z_2$, is defined for the four elements e, g_1, g_2, g_3 where e is the identity element and $\{e, g_1, g_2 | g_1^2 = g_2^2 = g_3^2 = e \wedge g_3 = g_1 g_2 = g_2 g_1\}$. We will comment about this statement in chapter 7.

[6] The center of SU(3) is a Z_3 i.e. the three roots of unity $e^{\mathrm{i}n\frac{2\pi}{3}}$ with $n = 0, 1, 2$.

[7] The group $\Sigma(36)$ is among the finite groups which can appear as symmetry group of the scalar

since they do not possess an irreducible faithful three-dimensional representation, while the groups with $\varphi = 3$, i.e. $\Sigma(36 \times 3)$, $\Sigma(72 \times 3)$, $\Sigma(216 \times 3)$, $\Sigma(360 \times 3)$, do have such representations.

Apart from $\Sigma(360 \times 3)$ none of these has Klein subgroups, so that $\Sigma(36 \times 3)$, $\Sigma(72 \times 3)$ and $\Sigma(216 \times 3)$ are only appropriate as flavor group G_l, if neutrinos are Dirac particles or G_ν is only partly contained in G_l.

We find only a few patterns compatible with the experimental data on lepton mixing and predict the reactor mixing angle θ_{13} to be $0.1 \lesssim \theta_{13} \lesssim 0.2$. All these patterns lead to a CP conserving Dirac phase. Patterns which instead reveal CP violation tend to be not in agreement with the experimental data. This analysis will be described in chapter 7 and it is part of the work performed in [66].

sector of a three Higgs doublet model without leading to a potential with a continuous symmetry [133].

Chapter 6

A Viable and Testable Unified Model of Flavour

Stimulated by the fact that all three angles in the PMNS matrix are determined with a relatively high precision, we describe here an attempt to construct a unified model of flavour, which describes correctly the quark and charged lepton masses, the mixing and CP violation in the quark sector, the mixing in the lepton sector, including the relatively large value of the angle θ_{13}, and provides predictions for the light neutrino masses compatible with the existing relevant data and constraints. The unified model of flavour we are proposing is supersymmetric and is based on $SU(5)$ as gauge group and T' as discrete family symmetry. It includes three right-handed (RH) neutrino fields N_{lR}, $l = e, \mu, \tau$, which possess a Majorana mass term. The light neutrino masses are generated by the type I see-saw mechanism [10–13, 39] and are naturally small. The corresponding Majorana mass term of the left-handed flavour neutrino fields $\nu_{lL}(x)$, $l = e, \mu, \tau$, is diagonalized by a unitary matrix which, up to a diagonal phase matrix, is of the TBM form [111–113] (see also [110]).

In order to account for the current data on the neutrino mixing, and more specifically, for the fact that $\theta_{13} \neq 0$, $U_{\rm TBM}$ has to be "corrected". The requisite correction is provided by the unitary matrix originating from the signalization of the charged lepton mass matrix M_e (for a general discussion of such corrections see, e.g., [115, 134–136]). Since the model is based on the $SU(5)$ GUT symmetry, the charged lepton mass matrix M_e is related to the down-quark mass matrix M_d. As a consequence, in particular, of the connection between M_e and M_d, the smallest angle in the neutrino mixing matrix θ_{13}, is related to the Cabibbo angle θ^C: $\sin^2\theta_{13} \cong C^2(\sin^2\theta^C)/2 \cong (\sin^2\theta^C)/2.5$, where $C \cong 0.9$ is a constant determined from the fit.

The down-quark mass matrix M_d, and the charged lepton mass matrix M_e, by construction are neither diagonal nor CP conserving. The matrix M_e is the only source of CP violation in the lepton sector. Actually, the CP violation predicted by the model in the quark and lepton sectors is entirely geometrical in origin i.e. the CP phases appearing in the Yukawa couplings are determined by the geometry of the group, or in other words by the tensor products allowed by the groups. This aspect of the $SU(5)\times T'$ model we propose is a consequence, in particular, of one of the special properties of the group T' [1], namely, that its group theoretical Clebsch-Gordan (CG) coefficients are intrinsically complex [140]. The idea to use the complexity of the Clebsch-Gordan

[1] There have been also T' models without a GUT embedding, e.g. [137–139].

coefficients (CGs) of T' to generate the requisite CP violation in the quark sector and a related CP violation in the lepton sector was pioneered in [141]. For the class of models where the CP violation is geometrical in origin, it is essential to provide a solution to the vacuum alignment problem for which all the flavon vevs are real. In this chapter we present a solution of this problem for the models based on the $SU(5) \times T'$ symmetry.

Let us note finally that a model of flavour based on the symmetry group $SU(5) \times T'$ was proposed, to our knowledge, first in [142] and its properties were further elaborated in [141] and [143]. Although some generic features, as like the connection between the reactor mixing angle θ_{13} and the Cabibbo angle θ^C, which are based on the underlying $SU(5)$ symmetry, are present both in the model constructed in [141, 142] and in the model presented here, the detailed structure and the quantitative predictions of the two models are very different. The quark, charged lepton, RH neutrino mass matrices and the matrix of the neutrino Yukawa couplings have different forms in the two models. This leads to considerable differences in the predictions for various observables. In the quark sector, for instance, the value of the CKM phase we find is in much better agreement with experimental data. More importantly, in the model proposed in [141, 142], the reactor mixing angle θ_{13} is predicted to have the value $\sin\theta_{13} \cong \sin\theta^c/(3\sqrt{2}) \cong 0.016$, which is ruled out by the current data on θ_{13}. In contrast, due to non-standard $SU(5)$ Clebsch–Gordan relations between the down-type quark and the charged lepton Yukawa couplings [115, 118], we get a realistic value for this angle. Moreover, in the model we propose both neutrino mass spectra with normal and inverted ordering are possible, while the model developed in [141, 142] admits only neutrino mass spectrum with normal ordering [143].

This chapter is organized as follows. We first present a brief overview of the considered model in section I. In section II we discuss the quark and charged lepton sector including a χ^2 fit to the experimental data. The section III is completely devoted to the neutrino sector. There we describe in detail the predictions for the mixing parameters (including CP violating phases), the mass spectra and observables such as the sum of the neutrino masses, the neutrinoless double beta ($(\beta\beta)_{0\nu}$-) decay effective Majorana mass and the rephasing invariant related to the Dirac phase in the PMNS matrix, $J_{\rm CP}$. We give as well the UV construction of the model and a solution for the flavon vacuum alignment in sections IV and V. We summarize and conclude in section VI. In the Appendix III we discuss the properties of the discrete group T'. We would like to add that in this part of the thesis a different parametrization of the Majorana phases is used, namely $Q' = \mathrm{Diag}(e^{-\mathrm{i}\,\beta_1/2}, e^{-\mathrm{i}\,\beta_2/2}, 1)$. Obviously, $Q = e^{\mathrm{i}\,\beta_1/2} Q'$, with $\alpha_{21} = \beta_1 - \beta_2$ and $\alpha_{31} = \beta_1$ [2].

I Matter, Higgs and Flavon Field Content of the Model

In this section we describe the matter, the Higgs and the flavon content of our $SU(5) \times T'$ unified model of flavour. A rather large "shaping" symmetry, $Z_{12} \times Z_8^3 \times Z_6^2 \times Z_4$, is needed to solve the vacuum alignment issue and forbids unwanted terms and couplings in the superpotential (specifically in the renormalisable one as described in section IV, as well as in the effective one after integrating out heavy messenger fields). We further impose an additional $U(1)_R$ symmetry, the continuous generalization of the usual R-

[2] For "technical" reasons related to the fitting code we will employ, we will use in what follows quite often the parametrization given by Q'.

	T_3	T_a	$\bar{F}$	N	$H_5^{(1)}$	$H_5^{(2)}$	$H_5^{(3)}$	$\bar{H}_5^{(1)}$	$\bar{H}_5^{(2)}$	$\bar{H}_5^{(3)}$	$\bar{H}_5''$	H_{24}''	$\tilde{H}_{24}''$
$SU(5)$	**10**	**10**	$\bar{\mathbf{5}}$	**1**	**5**	**5**	**5**	$\bar{\mathbf{5}}$	$\bar{\mathbf{5}}$	$\bar{\mathbf{5}}$	$\bar{\mathbf{5}}$	**24**	**24**
T'	**1**	**2**	**3**	**3**	**1**	**1**	**1**	**1**	**1**	**1**	**1″**	**1″**	**1″**
$U(1)_R$	1	1	1	1	0	0	0	0	0	0	0	0	0
Z_{12}^u	2	11	1	9	8	8	2	9	3	6	3	0	3
Z_8^d	4	0	2	6	0	4	0	1	4	7	7	4	2
Z_8^ν	7	6	2	0	2	6	4	1	1	5	7	4	0
Z_8	0	5	2	2	0	0	6	0	0	6	6	4	2
Z_6	5	0	1	0	2	5	2	2	0	2	2	0	0
Z_6'	2	3	1	0	2	5	2	5	0	2	2	0	0
Z_4	3	3	0	0	2	0	2	0	1	1	0	0	1

Table 6.1: Matter and Higgs field content of the model including quantum numbers.

parity[3]. The messenger fields and auxiliary flavons used for the flavon superpotential are discussed in the section IV.

The model includes the three generations of matter fields in the usual $\bar{\mathbf{5}}$ and **10**, representations of $SU(5)$, $\bar{F} = (d^c, L)_L$ and $T = (q, u^c, e^c)_L$ and three heavy right-handed Majorana neutrino fields N, singlets under $SU(5)$. The light active neutrino masses are generated through the type I seesaw mechanism [10–13,39]. Furthermore we introduce a number of copies of Higgs fields in the **5** and $\bar{\mathbf{5}}$ representation of $SU(5)$ which contain as linear combinations the two Higgs doublets of the MSSM. To get realistic mass ratios between down-type quarks and charged leptons [118] and to get a large reactor mixing angle [115] we have introduced Higgs fields in the adjoint representation of $SU(5)$, the **24**, which are as well responsible for breaking the GUT group.

The matter and Higgs fields including their transformation properties under all imposed symmetries are summarized in Tab. 6.1. Note that the right-handed neutrinos N and the five-dimensional matter representations are organized in T' triplets, while the ten-plets are organized in a doublet and a singlet i.e. $(T_1, T_2) \sim \mathbf{2}$ and $T_3 \sim \mathbf{3}$. This assignment has been known to give realistic quark mixing matrix and mass hierarchy [144]. Specifically this is used to generate the masses of the heaviest matter fields through tree level interactions with the Higgs fields while the masses of lighter matter fields arise by higher dimensional interactions involving, in addition to the regular Higgs fields, the so-called flavons (flavor Higgs fields). After integrating out the superheavy ($\sim M$) mediators, the mass terms of the light matter fields get suppressed by a factor of $\langle\phi\rangle/M$, where $\langle\phi\rangle$ is the vev of a flavon of the theory and M is the UV-cutoff of the effective theory above which the flavor symmetry is exact. In this case M can be assumed lighter than M_{GUT}.

On the one hand the assignment of $N \sim \mathbf{3}$ will give us tri-bimaximal mixing (TBM) in the neutrino sector before considering corrections from the charged lepton sector and on the other hand the complex Clebsch–Gordan coefficients for the doublets will give us CP violation in the quark and in the lepton sector finally.

[3] The requirement of a continuous symmetry like $U(1)_R$ is due to the need of eliminating the operators that can mediate proton decay, which are severely constrained. A simple additional symmetry, called R parity, under which all the SM particles have charge +1, while all superparticles have charge 1 is widely used in supersymmetric scenarios. In the model we are going to present in this chapter this symmetry is extended to a continuous one, called $U(1)_R$ symmetry.

There are 13 flavons, which will give us the desired structure for the Yukawa couplings that will be discussed in the next section. First of all we have three triplets which will develop vevs into two different directions in flavour space,

$$\langle\phi\rangle = \begin{pmatrix}0\\0\\1\end{pmatrix}\phi_0\ , \quad \langle\tilde{\phi}\rangle = \begin{pmatrix}0\\0\\1\end{pmatrix}\tilde{\phi}_0\ , \quad \langle\xi\rangle = \begin{pmatrix}1\\1\\1\end{pmatrix}\xi_0\ . \tag{6.1}$$

The first two flavons will be relevant for the quark and the charged lepton sector and the third one couples only to the neutrino sector.

Then we have introduced four complex T' doublets. Notice that this spinorial representations of the T' group are essential since, having complex CGs (see Appendix III), it is responsible of the CP violation in both quark and charged lepton sector. We assume that CP is conserved on the fundamental level (all couplings are real) and all flavon vevs are real. In section V we give a superpotential that has the desired flavon vev directions as a solution and also fixes the phases of the vevs up to a few discrete choices. For the doublets we find the vev alignments

$$\begin{aligned}\langle\psi'\rangle &= \begin{pmatrix}1\\0\end{pmatrix}\psi'_0\ , \quad \langle\psi''\rangle = \begin{pmatrix}0\\1\end{pmatrix}\psi''_0\ ,\\ \langle\tilde{\psi}'\rangle &= \begin{pmatrix}1\\0\end{pmatrix}\tilde{\psi}'_0\ , \quad \langle\tilde{\psi}''\rangle = \begin{pmatrix}0\\1\end{pmatrix}\tilde{\psi}''_0\end{aligned} \tag{6.2}$$

Furthermore we have introduced six flavons in one-dimensional representations of T' which receive all non-vanishing (and real) vev(the prime or double prime indicate if they are $\mathbf{1'}$ or $\mathbf{1''}$ singlets:

$$\langle\zeta'\rangle = \zeta'_0\ , \quad \langle\zeta''\rangle = \zeta''_0\ , \quad \langle\tilde{\zeta}'\rangle = \tilde{\zeta}'_0\ , \quad \langle\tilde{\zeta}''\rangle = \tilde{\zeta}''_0\ , \quad \langle\rho\rangle = \rho_0\ , \quad \langle\tilde{\rho}\rangle = \tilde{\rho}_0\ . \tag{6.3}$$

All flavons including their quantum numbers are summarized in Tab. 6.2. As we will see soon the flavon field ζ' does not directly couple to the matter sector. Nevertheless, we mention it here because it behaves differently than the auxiliary ϵ flavons which we have introduced to get the desired alignment and make all vevs real, see section V.

II The Quark and Charged Lepton Sector

In this section we describe the superpotential of the quark and charged lepton content of the chiral superfields of the model under study. We will consider the three generations of matter fields in the usual $\bar{\mathbf{5}}$ and $\mathbf{10}$, five and ten- dimensional, representations of $SU(5)$, $\bar{F} = (d^c, L)_L$ and $T = (q, u^c, e^c)_L$. The elements of the Yukawa coupling matrices are generated dynamically through a number of effective operators whose structure is tightly related to the matter fields assignment under the T' discrete symmetry. Indeed the Yukawa coupling matrices can be written only after the breaking of the T' discrete symmetry. As will be clear soon, in this description CP violation in the quark and charged lepton sector is entirely due to geometrical origin, specifically from the use of the spinorial representation of the T' group. Finally, in this section we will present a χ^2 fit analysis that has been performed by us to get the low energy masses and mixing parameters in the quark and charged lepton sector. The RGE running of the parameters of the model has been considered as well fixing the SUSY scale at 750 GeV and the GUT scale at 2×10^{26} GeV. We show as well that the simple CKM phase sum rule from [145] can be applied here.

	$\tilde{\phi}$	$\tilde{\psi}''$	$\tilde{\psi}'$	$\tilde{\zeta}''$	$\tilde{\zeta}'$	ϕ	ψ''	ψ'	ζ''	ζ'	ξ	ρ	$\tilde{\rho}$
$SU(5)$	**1**	**1**	**1**	**1**	**1**	**1**	**1**	**1**	**1**	**1**	**1**	**1**	**1**
T'	**3**	**2″**	**2′**	**1″**	**1′**	**3**	**2″**	**2′**	**1″**	**1′**	**3**	**1**	**1**
$U(1)_R$	0	0	0	0	0	0	0	0	0	0	0	0	0
Z_{12}^u	0	3	9	0	0	6	3	9	6	0	6	6	6
Z_8^d	0	0	0	0	0	2	1	7	6	4	4	4	4
Z_8^ν	4	1	7	0	0	2	7	1	6	4	0	0	0
Z_8	4	7	5	4	0	2	5	3	6	4	4	4	4
Z_6	4	4	2	4	2	0	3	3	0	0	0	0	0
Z_6'	4	4	2	4	2	3	0	0	0	0	0	0	0
Z_4	0	2	2	0	0	0	3	1	2	0	0	0	0

Table 6.2: Flavon fields coupling to the matter sector including their quantum numbers. In fact, ζ' does not couple directly to the matter fields, but it behaves very similar like the other flavons and not like the auxiliary flavons ϵ which will be introduced in section V.

II.I Effective Operators and Yukawa Matrices

Before we come to the effective operators which will give us the Yukawa couplings we first fix the conventions used for the Yukawa matrices. Throughout this chapter we will use the RL convention, i.e.,

$$-\mathcal{L} = Y_{ij}\overline{f_R^i} f_L^j H + \text{H.c.} \tag{6.4}$$

or in other words we have to diagonalize the combination $Y^\dagger Y$. Keep also in mind that $\bar{F} = (d^c, L)_L$ and $T = (q, u^c, e^c)_L$.

We restrict ourselves to effective operators up to mass dimension seven. These operators generate Yukawa couplings of the order of 10^{-5} or smaller (see our fit results in Tab. 6.4). Higher dimensional operators hence can be expected to give only negligible corrections.

After integrating out the heavy messenger fields, see section IV, we obtain the effective operators

$$\begin{aligned}\mathcal{W}_{Y_u} = {} & y_{33}^{(u)} H_5^{(1)} T_3 T_3 + \frac{y_{23}^{(u)}}{\Lambda_u^2}(T_a\tilde{\phi})_{2'} H_5^{(2)} (T_3\tilde{\psi}'')_{2''} + \frac{y_{22}^{(u)}}{\Lambda_u^3}(T_a\tilde{\psi}'')_3 (H_5^{(1)}\tilde{\zeta}')_{1'}(T_a\tilde{\psi}'')_3 \\ & + \frac{y_{21}^{(u)}}{\Lambda_u^4}(T_a\tilde{\phi})_{2'}(H_5^{(1)}\tilde{\zeta}')_{1'}(\tilde{\psi}'(T_a\tilde{\psi}')_3)_{2'} + \frac{y_{11}^{(u)}}{\Lambda_u^4}((T_a\tilde{\phi})_2\tilde{\zeta}'')_{2''} H_5^{(3)}(\tilde{\zeta}''(T_a\tilde{\phi})_{2''})_{2'} \,,\end{aligned} \tag{6.5}$$

which give the up-type quark Yukawa matrices after the flavons developed their vevs. Here Λ_u stands for the messenger scale suppressing the non-renormalisable operators in the up-sector and in the down-sector we will introduce Λ_d correspondingly. We have also given the T' contractions as indices on the round brackets. Note that in general there are many different contractions possible (for T' and to a less degree for $SU(5)$) which give different results. Nevertheless, we have specified in section IV the fields mediating the non-renormalisable operators which transform in a specific way under T' such that we pick up only the contractions which we want.

Multiplying the T' and $SU(5)$ indices out we obtain for the up-type quark Yukawa matrix at the GUT scale (which is roughly equal to the scale of T' breaking)

$$Y_u = \begin{pmatrix} \bar{\omega} a_u & \mathrm{i}\, b_u & 0 \\ \mathrm{i}\, b_u & c_u & \omega d_u \\ 0 & \omega d_u & e_u \end{pmatrix} , \tag{6.6}$$

where $\omega = (1+\mathrm{i})/\sqrt{2}$ and $\bar{\omega} = (1-\mathrm{i})/\sqrt{2}$. The parameters a_u, b_u, c_u, d_u and e_u are (real) functions of the underlying parameters. Note at this point, that the phases of the flavon vevs have to be fixed. Otherwise the coefficients in the Yukawa matrix are complex parameters and we would not be able to make definite predictions anymore.

For the down-type quarks and charged leptons (remember that those two sectors are closely related in $SU(5)$) we find for the superpotential

$$\begin{aligned} \mathcal{W}_{Y_{d,\ell}} = & \frac{y^{(d)}_{33}}{\Lambda_d^2}((\bar{H}^{(2)}_5 \bar{F})_3 \phi)_{1'} (H''_{24} T_3)_{1''} + \frac{y^{(d)}_{22}}{\Lambda_d^3}((\phi T_a)_{2'} H''_{24})_2 (\psi' (\bar{H}^{(1)}_5 \bar{F})_3)_2 \\ & + \frac{y^{(d)}_{12}}{\Lambda_d^4}(((T_a \tilde{H}''_{24})_{2''} (\bar{F}\psi')_{2''})_3 \psi')_{2''} (\bar{H}^{(3)}_5 \psi')_{2'} + \frac{y^{(d)}_{21}}{\Lambda_d^4}((\bar{F}\psi')_{2''} (\zeta'' \bar{H}^{(1)}_5)_{1''} \zeta'')_2 (T_a \phi)_2 \\ & + \frac{y^{(d)}_{11}}{\Lambda_d^4}((\bar{F}\psi'')_{2'} (H''_{24}\psi'')_{2'} \bar{H}''_5)_{1'} (T_a \psi'')_{1''} , \end{aligned} \tag{6.7}$$

where we have again specified the T' contractions. From this superpotential and considering the correct $SU(5)$ contractions, which we could not display here for the sake of readability, we get the down-type quark and charged lepton Yukawa matrices

$$Y_d = \begin{pmatrix} \omega\, a_d & \mathrm{i}\, b'_d & 0 \\ \bar{\omega}\, b_d & c_d & 0 \\ 0 & 0 & d_d \end{pmatrix} \quad \text{and} \quad Y_e = \begin{pmatrix} -\frac{3}{2}\,\omega\, a_d & \bar{\omega}\, b_d & 0 \\ 6\ \mathrm{i}\ b'_d & 6\, c_d & 0 \\ 0 & 0 & -\frac{3}{2}\, d_d \end{pmatrix} , \tag{6.8}$$

where a_d, b_d, b'_d, c_d and d_d are (real) functions of the underlying parameters.

Note that the prediction from the minimal $SU(5)$ model $Y_d = Y_e^T$ does not hold. Indeed it has to be broken to get realistic fermion masses. For the second generation this is known for a long time [146]. In some recent work [118] some new relations to fix this issue were proposed. From those we will use here $y_\tau/y_b = -3/2$ and $y_\mu/y_s \approx 6$ where y_τ, y_μ, y_b and y_s stand for the eigenvalues of the Yukawa matrices associated to the masses of the τ, the μ, the b and the s quark respectively. Furthermore it was shown in [115] (see also [116]) that those new $SU(5)$ Clebsch–Gordan coefficients might also give a large reactor neutrino mixing angle θ_{13}. For the current chapter we have chosen one of the possible combinations given in [115] but we remark that in principle also other combinations are still possible which might be realized in another unified flavour model with a similar good fit to the fermion masses and mixing angles.

II.II Fit Results and the CKM Phase Sum Rule

In the last section we have discussed the structure of the Yukawa matrices in the quark and the charged lepton sector. These matrices have five free parameters, which in principle can be fitted to the low-energy mass and mixing parameters using the

renormalization group. But doing so one has to take into account SUSY threshold corrections [147–150] which modify the masses and mixing angles significantly. For example without including them, the GUT scale Yukawa coupling ratio, y_τ/y_b, would be roughly 1.3 which is not close to the usual GUT prediction of 1. There is a large amount of literature on how to use SUSY threshold corrections to get $b-\tau$ Yukawa unification, for recent papers see, for instance, [118, 151, 152]. From these studies it is known that in order to get $b-\tau$ Yukawa unification, it is necessary to either consider a negative μ-term or to have a very high - $\mathcal{O}(10$ TeV), SUSY scale. Nevertheless, we will not use unification but instead we use the recently proposed GUT scale relation $y_\tau/y_b = 3/2$ induced by the vev of an adjoint of $SU(5)$ [118], which is viable in a large region of the parameter space even in constrained MSSM scenarios.

Due to the importance of the threshold corrections for our fit we briefly revise the most important formulas which also defines our parametrization. In [153] the approximate matching conditions at the SUSY scale, M_{SUSY},

$$y_{e,\mu,\tau}^{\text{SM}} = (1+\epsilon_l \tan\beta)\; y_{e,\mu,\tau}^{\text{MSSM}} \cos\beta \;, \tag{6.9}$$

$$y_{d,s}^{\text{SM}} = (1+\epsilon_q \tan\beta)\; y_{d,s}^{\text{MSSM}} \cos\beta \;, \tag{6.10}$$

$$y_{b}^{\text{SM}} = (1+(\epsilon_q+\epsilon_A) \tan\beta)\; y_{b}^{\text{MSSM}} \cos\beta \;, \tag{6.11}$$

for the Yukawa couplings and

$$\theta_{i3}^{\text{SM}} = \frac{1+\epsilon_q \tan\beta}{1+(\epsilon_q+\epsilon_A)\tan\beta}\; \theta_{i3}^{\text{MSSM}} \;, \tag{6.12}$$

$$\theta_{12}^{\text{SM}} = \theta_{12}^{\text{MSSM}} \;, \tag{6.13}$$

$$\delta_{\text{CKM}}^{\text{SM}} = \delta_{\text{CKM}}^{\text{MSSM}} \;, \tag{6.14}$$

for the quark mixing parameters were given, where the SUSY threshold corrections are parametrized in terms of the three parameters ϵ_l, ϵ_q and ϵ_A. We will adopt this parametrization neglecting ϵ_l, which is usually one order smaller than ϵ_q [151]. Furthermore we want to assume, that SUSY is broken similar to the constrained MSSM scenario with a positive μ parameter and hence we adopt the recently proposed GUT relation $y_\tau/y_b = 3/2$ for the third generation, as mentioned earlier. For the second generation we use $y_\mu/y_s \approx 6$ [118].

We have fixed the SUSY scale to 750 GeV, the GUT scale to 2×10^{16} GeV and $\tan\beta$ to 35. Therefore we have to fit the ten parameters in the Yukawa matrices and the two parameters from the SUSY threshold corrections to the thirteen low energy observables in the quark and the charged lepton sector (nine masses, three mixing angles and one phase), so that we have one prediction (degree of freedom).

The RGE running and parametrization of the matrices was done using the `REAP` package [156]. Performing a χ^2 fit we have found as minimum the results listed in Tab. 6.3 for the parameters and in Tab. 6.4 and in Fig. 6.1 we have presented the results of the fit for the low energy observables compared to the experimental results. Note that we have assumed an uncertainty of 3% on the Yukawa couplings for the charged leptons. Their experimental uncertainty is much smaller, so that their theoretical uncertainty (Accuracy of RGEs, neglecting SUSY threshold corrections for the leptons, NLO effects, ...) is much bigger, which we estimate to be 3%.

We find good agreement between our model and experimental data with a minimal χ^2 per degree of freedom of 2.76. In fact this agreement is not accidental. We have

Parameter	Value
a_u	$5.81 \cdot 10^{-6}$
b_u	$-9.96 \cdot 10^{-5}$
c_u	$-8.55 \cdot 10^{-4}$
d_u	$1.99 \cdot 10^{-2}$
e_u	0.525
a_d	$-2.82 \cdot 10^{-5}$
b_d	$-5.73 \cdot 10^{-4}$
b'_d	$-5.09 \cdot 10^{-4}$
c_d	$2.50 \cdot 10^{-3}$
d_d	$1.82 \cdot 10^{-1}$
$\epsilon_q \tan\beta$	0.1788
$\epsilon_A \tan\beta$	-0.0001

Table 6.3: Values of the effective parameters of the quark and charged lepton Yukawa matrices for $\tan\beta = 35$ and $M_{\text{SUSY}} = 750$ GeV. The two parameters ϵ_q and ϵ_A parametrize the SUSY threshold corrections. The numerical values are determined from a χ^2-fit to experimental data with a lowest χ^2 per degree of freedom of 2.76.

Quantity (at $m_t(m_t)$)	Experiment	Model	Deviation
y_τ in 10^{-2}	1.00	0.99	-0.388
y_μ in 10^{-4}	5.89	5.90	0.044
y_e in 10^{-6}	2.79	2.79	-0.003
y_b in 10^{-2}	1.58 ± 0.05	1.57	-0.157
y_s in 10^{-4}	2.99 ± 0.86	2.57	-0.484
y_s/y_d	18.9 ± 0.8	18.9	-0.012
y_t	0.936 ± 0.016	0.936	0.0001
y_c in 10^{-3}	3.39 ± 0.46	2.79	-1.317
y_u in 10^{-6}	$7.01^{+2.76}_{-2.30}$	7.01	-0.0003,
θ_{12}^{CKM}	$0.2257^{+0.0009}_{-0.0010}$	0.2257	-0.0107
θ_{23}^{CKM}	$0.0415^{+0.0011}_{-0.0012}$	0.0416	0.1268
θ_{13}^{CKM}	0.0036 ± 0.0002	0.0036	0.2043
δ_{CKM}	$1.2023^{+0.0786}_{-0.0431}$	1.2610	0.7465

Table 6.4: Fit results for the quark Yukawa couplings and mixing and the charged lepton Yukawa couplings at low energy compared to experimental data. The values for the Yukawa couplings are extracted from [154], the ratio y_s/y_d is taken from [155] and the CKM parameters from [6]. Note that the experimental uncertainty on the charged lepton Yukawa couplings are negligible small and we have assumed a relative uncertainty of 3 % for them. The χ^2 per degree of freedom is 2.76. A pictorial representation of the agreement between our fit and experiment can be found as well in Fig. 6.1.

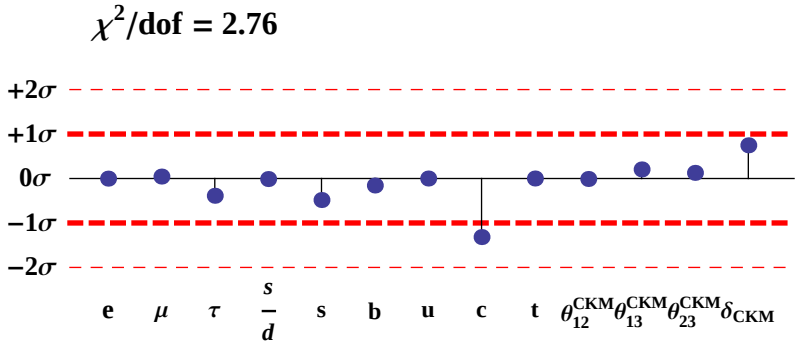

Figure 6.1: Pictorial representation of the deviation of our fit from low energy experimental data for the charged lepton Yukawa couplings and quark Yukawa couplings and mixing parameters. The deviations of the charged lepton masses are given in 3% while all other deviations are given in units of standard deviations σ.

chosen the $SU(5)$ coefficients such that, we expect good agreement and we have also enough free parameters to fix the mixing angles. In other words one could determine the eigenvalues and mixing angles from the data and then the CKM phase would be a prediction. But as we will demonstrate now, the choice for our phases in the Yukawa matrices was done in such a way, that we can expect a good prediction for the CKM phase as well.

We will show in the following that the sum rule given in [145] can be used here. To apply the sum rule we have to find approximate expressions for the complex mixing angles (see [145]). For the rest of the subsection we will use the notation of [145] which we just briefly summarize here for convenience. The CKM matrix $U_{\rm CKM}$ can be written as

$$U_{\rm CKM} = U_{u_L} U_{d_L}^\dagger = (U_{23}^{u_L} U_{13}^{u_L} U_{12}^{u_L})^\dagger U_{23}^{d_L} U_{13}^{d_L} U_{12}^{d_L} \,, \tag{6.15}$$

where the matrices U_{u_L} and U_{d_L} diagonalize the up- and down-type quark mass matrices and the unitary matrix

$$U_{12} = \begin{pmatrix} \cos\theta_{12} & \sin\theta_{12}\, \mathrm{e}^{-\mathrm{i}\,\delta_{12}} & 0 \\ -\sin\theta_{12}\, \mathrm{e}^{\mathrm{i}\,\delta_{12}} & \cos\theta_{12} & 0 \\ 0 & 0 & \end{pmatrix} . \tag{6.16}$$

The matrices U_{13} and U_{23} are given by analogous expressions.

We find at leading order for the respective mixing angles and phases

$$\theta_{12}^d\, \mathrm{e}^{-\mathrm{i}\,\delta_{12}^d} = \left|\frac{b_d}{c_d}\right| \mathrm{e}^{-\mathrm{i}\,\frac{7\pi}{4}} \,, \quad \theta_{13}^d = \theta_{23}^d = 0 \,, \tag{6.17}$$

$$\theta_{12}^u\, \mathrm{e}^{-\mathrm{i}\,\delta_{12}^u} \approx \left|\frac{b_u}{\sqrt{2} c_u}\right| \mathrm{e}^{-\mathrm{i}\,\frac{5\pi}{4}} \,, \quad \theta_{23}^u\, \mathrm{e}^{-\mathrm{i}\,\delta_{23}^u} = \left|\frac{d_u}{e_u}\right| \mathrm{e}^{-\mathrm{i}\,\frac{5\pi}{4}} \,, \quad \theta_{13}^u\, \mathrm{e}^{-i\delta_{13}^u} = \left|\frac{b_u d_u}{e_u^2}\right| \mathrm{e}^{-\mathrm{i}\,\frac{\pi}{4}} \,, \tag{6.18}$$

where we have used for θ_{12}^u that $d_u^2 \approx -1/2 c_u$ and $e_u \approx 0.5$ from our fit. So we see that δ_{12}^u is not simply $\pi/2$ as one would expect from a quick first inspection. Note also that the phase sum rule was derived for $\theta_{13}^u = \theta_{13}^d = 0$, which is not exactly true in our case for θ_{13}^u. But in fact it is sufficient, that $\theta_{13}^u \ll \theta_{12}^u \theta_{23}$ which is fulfilled here.

The angle α in the CKM unitarity triangle is experimentally measured to be $\alpha = (90.7^{+4.5}_{-2.9})^\circ$ [157, 158] for which the sum rule

$$\alpha \approx \delta^d_{12} - \delta^u_{12} \,, \tag{6.19}$$

was given in [145]. Plugging in our approximate analytical expressions for $\delta^{d/u}_{12}$, eqs. (6.17) and (6.18), we find that $\alpha \approx \pi/2$ and our model is in good agreement with experimental data as we have also seen it before from our numerical fit.

III Neutrino Sector

The model includes three heavy right-handed Majorana neutrino fields N which are singlets under $SU(5)$ and a triplet under T'. Through the type I seesaw mechanism [10–13, 39] we generate light neutrino masses. The neutrino sector is described by the following terms in the superpotential

$$\mathcal{W}_\nu = \lambda_1 N N \xi + N N(\lambda_2 \rho + \lambda_3 \tilde{\rho}) + \frac{y_\nu}{\Lambda}(N\bar{F})_1 (H^{(2)}_5 \rho)_1 + \frac{\tilde{y}_\nu}{\Lambda}(N\bar{F})_1 (H^{(2)}_5 \tilde{\rho})_1 \,, \tag{6.20}$$

where we have given the T' contractions as indices at the brackets for non-renormalisable terms and from now on Λ labels a generic messenger scale. Note that the contraction of three triplets in general is not unique, see also Tab. A.3, because the product of two triplets contains a symmetric and an antisymmetric triplet. But since we multiply here two N with each other only the symmetric combination gives a non-vanishing contribution. In the following we will discuss the phenomenological implications of this superpotential (including corrections from the charged lepton sector).

III.I The Neutrino Mass Spectrum

From eq. (6.20) we obtain for the mass matrix for the right-handed neutrinos and the Dirac neutrino mass matrix

$$M_R = \begin{pmatrix} 2Z+X & -Z & -Z \\ -Z & 2Z & -Z+X \\ -Z & -Z+X & 2Z \end{pmatrix} \,, \quad M_D = \begin{pmatrix} 1 & 0 & 0 \\ 0 & 0 & 1 \\ 0 & 1 & 0 \end{pmatrix} \frac{\rho'}{\Lambda} \,, \tag{6.21}$$

where X, Z and ρ' are real parameters depending on the couplings and the vevs in eq. (6.20). The right-handed neutrino mass matrix M_R is diagonalised by the tri-bimaximal mixing (TBM) matrix [110–113]

$$U_{\text{TBM}} = \begin{pmatrix} \sqrt{2/3} & \sqrt{1/3} & 0 \\ -\sqrt{1/6} & \sqrt{1/3} & -\sqrt{1/2} \\ -\sqrt{1/6} & \sqrt{1/3} & \sqrt{1/2} \end{pmatrix} \,, \tag{6.22}$$

such that the heavy RH neutrino masses read:

$$U^T_{\text{TBM}} M_R U_{\text{TBM}} = D_N = \text{Diag}(3Z+X, X, 3Z-X) = \text{Diag}(M_1 e^{\mathrm{i}\,\phi_1}, M_2 e^{\mathrm{i}\,\phi_2}, M_3 e^{\mathrm{i}\,\phi_3}) \,,\; M_{1,2,3} > 0 \,, \tag{6.23}$$

where

$$M_1 = |X+3Z| \equiv |X|\,|1+\alpha e^{\mathrm{i}\,\phi}|, \;\; \phi_1 = \arg(X+3Z) \tag{6.24}$$

$$M_2 = |X|, \quad \phi_2 = \arg(X) \tag{6.25}$$

$$M_3 = |X-3Z| \equiv |X|\,|1-\alpha e^{\mathrm{i}\,\phi}|, \quad \phi_3 = \arg(3Z-X) \,. \tag{6.26}$$

Here $\alpha \equiv |3Z/X| > 0$ and $\phi \equiv \arg(Z) - \arg(X)$. Since X and Z are real parameters, the phases ϕ_1, ϕ_2, ϕ_3 and ϕ take values 0 or π. A light neutrino Majorana mass term is generated after electroweak symmetry breaking via the type I see-saw mechanism:

$$M_\nu \;=\; -M_D^T\, M_R^{-1}\, M_D = U_\nu^*\, \mathrm{Diag}\,(m_1, m_2, m_3)\, U_\nu^\dagger\,, \tag{6.27}$$

where

$$U_\nu = \mathrm{i}\; U_{\rm TBM}\; \mathrm{Diag}\left(e^{\mathrm{i}\,\phi_1/2}, e^{\mathrm{i}\,\phi_2/2}, e^{\mathrm{i}\,\phi_3/2}\right) \equiv \mathrm{i}\; U_{\rm TBM}\, \tilde{Q}\,,\;\; \tilde{Q} \equiv \mathrm{Diag}\left(e^{\mathrm{i}\,\phi_1/2}, e^{\mathrm{i}\,\phi_2/2}, e^{\mathrm{i}\,\phi_3/2}\right)\,, \tag{6.28}$$

and $m_{1,2,3} > 0$ are the light neutrino masses,

$$m_i = \left(\frac{\rho'}{\Lambda}\right)^2\; \frac{1}{M_i}\,,\;\; i = 1, 2, 3\,. \tag{6.29}$$

The phase factor i in eq. (6.28) corresponds to an unphysical phase and we will drop it in what follows. Note also that one of the phases ϕ_k, say ϕ_1, is physically irrelevant since it can be considered as a common phase of the neutrino mixing matrix. In the following we always set $\phi_1 = 0$. This corresponds to the choice $(X + 3Z) > 0$.

The type of the neutrino mass spectrum in the model is determined [4] by the value of the phase ϕ. Indeed, as it is not difficult to show, we have:

$$\Delta m^2_{31} \equiv \Delta m^2_A = \frac{1}{|X|^2}\, \left(\frac{\rho'}{\Lambda}\right)^4\; \frac{4\alpha\, \cos\phi}{|1 + \alpha\, e^{\mathrm{i}\,\phi}|^2\, |1 - \alpha\, e^{\mathrm{i}\,\phi}|^2}\,. \tag{6.30}$$

Thus, for $\cos\phi = +1$, we get $\Delta m^2_{31} > 0$, i.e., a neutrino mass spectrum with normal ordering (NO), while for $\cos\phi = -1$ one has $\Delta m^2_{31} < 0$, i.e., neutrino mass spectrum with inverted ordering (IO). We have also:

$$\Delta m^2_{21} \equiv \Delta m^2_\odot = \frac{1}{|X|^2}\, \left(\frac{\rho'}{\Lambda}\right)^4\; \frac{\alpha\,(\alpha + 2\cos\phi)}{|1 + \alpha\, e^{\mathrm{i}\,\phi}|^2}\,. \tag{6.31}$$

For a given type of neutrino mass spectrum, i.e., for a fixed $\phi = 0$ or π, a constraint on the parameter α can be obtained from the requirement that $\Delta m^2_{21} > 0$ and from the data on the ratio:

$$r = \frac{\Delta m^2_\odot}{|\Delta m^2_A|} = \frac{1}{4}\; (\alpha + 2\cos\phi)\left(1 - 2\alpha\cos\phi + \alpha^2\right) = 0.032 \pm 0.006\,. \tag{6.32}$$

Using the values of α thus found and the value of, e.g., Δm^2_{21}, one can get (for a given type of the spectrum) the value of the factor in eq. (6.31), $|X|^{-2}(\rho'/\Lambda)^4$. Knowing this factor and α, one can obtain the value of the lightest neutrino mass, which together with the data on Δm^2_{21} and $\Delta m^2_{31(32)}$ allows to obtain the values of the other two light neutrino masses. Knowing the latter one can find also the two ratios of the heavy Majorana neutrino masses.

In the case of NO neutrino mass spectrum ($\phi = 0$), there are two values of α which satisfy equation (6.32) for $r = 0.032$: $\alpha \cong 1.20$ (solution A), and $\alpha \cong 0.79$ (solution B). In the case of solution A, as it is not difficult to show, the phases

$$\phi_2 = 0\,,\quad \phi_3 = 0\,,\;\; \text{solution A (NO)}\,, \tag{6.33}$$

[4] We are following in this part the similar analysis performed in [159].

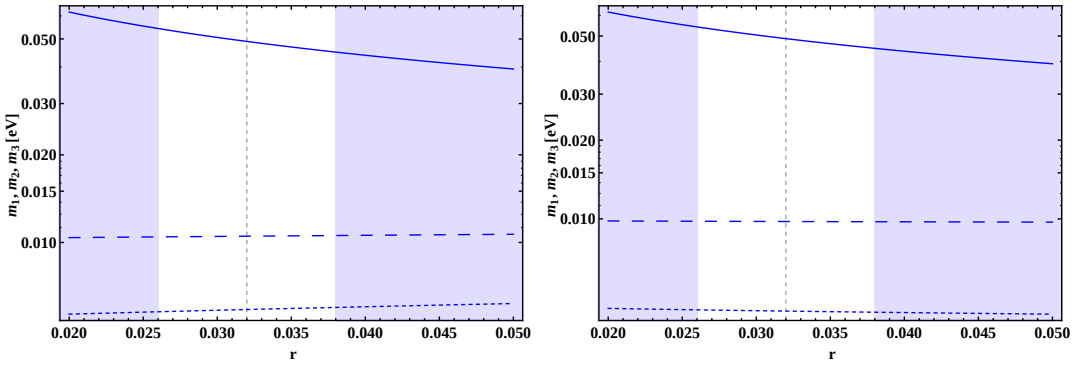

Figure 6.2: The values of the three light neutrino masses corresponding to the solutions A (left panel) and B (right panel) in the case of NO spectrum, versus r. The dotted, dashed and solid lines correspond to the three light neutrino masses m_1, m_2, m_3. The gray region is excluded by present oscillation data. The vertical dashed line corresponds to the best fit value for $r = 0.032$. See text for further details.

and the three neutrino masses have the values:

$$m_1 \cong 4.44 \times 10^{-3}\ \text{eV}\,, m_2 \cong 9.77 \times 10^{-3}\ \text{eV}\,, m_3 \cong 4.89 \times 10^{-2}\ \text{eV}\,,\ \text{solution A (NO)}\,. \tag{6.34}$$

Evidently, the spectrum is mildly hierarchical. The ratios of the heavy Majorana neutrino masses read: $M_1/M_3 \cong 11.0$ and $M_2/M_3 \cong 5.0$. Thus, we have $M_3 < M_2 < M_1$.

For solution B we find

$$\phi_2 = 0\,, \quad \phi_3 = \pi\,, \quad \text{solution B (NO)}\,, \tag{6.35}$$

while for the values of the three neutrino masses we get:

$$m_1 \cong 5.89 \times 10^{-3}\ \text{eV}\,, m_2 \cong 1.05 \times 10^{-2}\ \text{eV}\,, m_3 \cong 4.90 \times 10^{-2}\ \text{eV}\,,\ \text{solution B (NO)}\,. \tag{6.36}$$

The heavy Majorana neutrino mass ratios are given by: $M_1/M_3 \cong 8.33$ and $M_2/M_3 \cong 4.67$. Therefore also in this case we have $M_3 < M_2 < M_1$.

For the IO spectrum ($\phi = \pi$), we find only one value of α which satisfies eq. (6.32) with $r = 0.032$: $\alpha \cong 2.014$. The phases ϕ_2 and ϕ_3 take the values: $\phi_2 = \pi$, $\phi_3 = 0$. The light neutrino masses read:

$$m_1 \cong 5.17 \times 10^{-2}\ \text{eV}\,, m_2 \cong 5.24 \times 10^{-2}\ \text{eV}\,, m_3 \cong 1.74 \times 10^{-2}\ \text{eV}\,,\ \text{(IO)}\,, \tag{6.37}$$

i.e., the light neutrino mass spectrum is not hierarchical exhibiting only partial hierarchy. For the heavy Majorana neutrino mass ratios we obtain: $M_1/M_2 \cong 1.014$ and $M_3/M_2 \cong 3.01$. Thus, in this case N_1 and N_2 are quasi-degenerate in mass: $M_1 \cong M_2 < M_3$.

In the Figs. 6.2 and 6.3 we present the dependence of the neutrino masses with respect to r for normal and inverted ordering respectively.

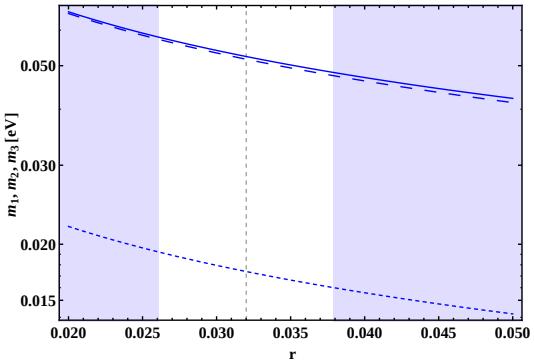

Figure 6.3: The values of the three light neutrino masses in the case of the solution corresponding to IO spectrum, versus r. The dotted, dashed and solid lines correspond to the three light neutrino masses m_3, m_1, m_2. The gray region is excluded by present oscillation data. The vertical dashed line corresponds to the best fit value for $r = 0.032$.

III.II The Mixing Angles and the Dirac and Majorana CP Violation Phase

The PMNS neutrino mixing matrix received contributions from the diagonalisation of the neutrino Majorana mass matrix M_ν and of the charged lepton mass matrix $M_e = v_d Y_e$: $U_{\rm PMNS} = U_{eL}^\dagger U_\nu$, where U_ν is given in eq. (6.28) with $\tilde{Q} = {\rm Diag}(1, e^{{\rm i}\,\phi_2/2}, e^{{\rm i}\,\phi_3/2})$ and the values of the phases ϕ_2 and ϕ_3 in the cases of NO and IO spectra were specified in the preceding subsection. The matrix of charged lepton Yukawa couplings Y_e, eq. (6.8), and thus M_e, has a block-diagonal form. The unitary matrix U_{eL} diagonalizes the Hermitian matrix $M_e^\dagger M_e$: $M_e^\dagger M_e = U_{eL}(M_e^d)^2 U_{eL}^\dagger$, where $M_e^d = {\rm diag}(m_e, m_\mu, m_\tau)$, m_l being the mass of the charged lepton l. As a consequence of the block-diagonal form of M_e, the matrix U_{eL} can be parametrized in terms of one mixing angle (θ_{12}^e) and one phase (φ): $U_{eL} = \Phi\, R_{12}(\theta_{12}^e)$, where $\Phi = {\rm diag}(1, {\rm e}^{{\rm i}\,\varphi}, 1)$ and

$$R_{12}(\theta_{12}^e) = \begin{pmatrix} \cos\theta_{12}^e & \sin\theta_{12}^e & 0 \\ -\sin\theta_{12}^e & \cos\theta_{12}^e & 0 \\ 0 & 0 & 1 \end{pmatrix} . \tag{6.38}$$

Due to the $SU(5)$ symmetry of the model, Y_d and Y_e (and therefore the corresponding down quark and charged lepton mass matrices) are expressed in terms of the same parameters. As a consequence, the angle θ_{12}^e in the model considered is related to the Cabibbo angle $\theta^C \cong 0.226$. Using, for example, the approximate formulas from [115], we find that

$$\theta_{12}^e \cong \left|\frac{b'_d}{b_d}\right| \theta^C \cong 0.9\,\theta^C , \tag{6.39}$$

where we have used the values of b'_d and b_d from Table 6.3.

Comparing next the expressions on the two sides of the equation $M_e^\dagger M_e = U_{eL}(M_e^d)^2 U_{eL}^\dagger$ we get, in particular:

$${\rm e}^{-{\rm i}(\varphi+\frac{\pi}{2})}\,(m_\mu^2 - m_e^2)\,\cos\theta_{12}^e \sin\theta_{12}^e = v_d^2 \left(\frac{3}{2} b_d a_d - 36 c_d b'_d\right) . \tag{6.40}$$

Using the fit results in Table 6.3 one can check that the right hand side of the last equation is real and positive. Comparing the phases of the two expressions one concludes that

$$\varphi = \frac{3}{2}\pi\,. \tag{6.41}$$

In the approximation we are using the PMNS matrix is given by:

$$\tilde{U}_{\rm PMNS} = \begin{pmatrix} \sqrt{2/3}c^e_{12} + \sqrt{1/6}s^e_{12}e^{-\,{\rm i}\,\varphi} & \sqrt{1/3}c^e_{12} - \sqrt{1/3}s^e_{12}e^{-\,{\rm i}\,\varphi} & \sqrt{1/2}s^e_{12}e^{-\,{\rm i}\,\varphi} \\ \sqrt{2/3}s^e_{12} - \sqrt{1/6}c^e_{12}{\rm e}^{-\,{\rm i}\,\varphi} & \sqrt{1/3}s^e_{12} + \sqrt{1/3}c^e_{12}{\rm e}^{-\,{\rm i}\,\varphi} & -\sqrt{1/2}c^e_{12}{\rm e}^{-\,{\rm i}\,\varphi} \\ -\sqrt{1/6} & \sqrt{1/3} & \sqrt{1/2} \end{pmatrix} \tilde{Q}\,, \tag{6.42}$$

where $c^e_{12} = \cos\theta^e_{12}$, $s^e_{12} = \sin\theta^e_{12}$ and $\tilde{Q}$ is the diagonal phase matrix defined in eq. (6.28). It follows from the above expression for the PMNS matrix that the angle θ_{13} is given approximately by

$$\sin^2\theta_{13} \cong \frac{1}{2}C^2\,\sin^2\theta^C \cong \frac{\sin^2\theta^C}{2.5} \cong 0.02\;,\; C \cong 0.9 \tag{6.43}$$

where we took into account the relation in eq. (6.39) and the value of $C \equiv |b'_d/b_d|$.

As was shown in, e.g., [115], the phase φ and the Dirac phase δ, appearing in the standard parametrization of the PMNS mixing matrix, are related (at leading order) as follows:

$$\delta = \varphi + \pi\,. \tag{6.44}$$

Thus, for the Dirac phase we get from (6.41):

$$\delta = \frac{\pi}{2}\,. \tag{6.45}$$

Numerically, for $\varphi = 3\pi/2$ and $s^e_{12} = 0.203$ (see eq. (6.39)), the PMNS matrix, eq. (6.42), reads:

$$U_{\rm PMNS} \cong \begin{pmatrix} 0.804e^{{\rm i}\,5.81^\circ} & 0.577e^{-\,{\rm i}\,11.50^\circ} & 0.144e^{-\,{\rm i}\,270.000^\circ} \\ 0.433e^{-\,{\rm i}\,67.85^\circ} & 0.577e^{{\rm i}\,78.50^\circ} & -\,0.692e^{-\,{\rm i}\,270.000^\circ} \\ -0.408 & 0.577 & 0.707 \end{pmatrix} \tilde{Q}\,. \tag{6.46}$$

Thus, comparing the absolute values of the elements U_{e1}, U_{e2}, $U_{\mu 3}$ and $U_{\tau 3}$ of the PMNS matrix in the standard parametrization , and in eq. (6.46), we have: $c_{12}c_{13} = 0.804$, $s_{12}c_{13} = 0.577$, $s_{23}c_{13} = 0.692$ and $c_{23}c_{13} = 0.707$. Using the predicted value of θ_{13}, eq. (6.43), these relations allow us to obtain the values of θ_{12} and θ_{23}. We note that the tri-bimaximal mixing value of the solar neutrino mixing angle θ_{12}, which corresponds to $\sin^2\theta_{12} = 1/3$, is corrected by a quantity which, as it follows from the general form of such corrections [115, 134, 136], is determined by the angle θ_{13} and the Dirac phase δ:

$$\sin^2\theta_{12} \cong \frac{1}{3} + \frac{2\sqrt{2}}{3}\,\sin\theta_{13}\,\cos\delta \tag{6.47}$$

where δ is the Dirac phase in the standard parametrization of the PMNS matrix. As we have seen, to leading order $\delta = \pi/2$. The Majorana phases β_1, β_2 (or α_{21} and α_{31}) are determined, as it follows from the standard parametrization and (6.42) (or (6.46)), by the diagonal matrix $\tilde{Q}$ and take CP conserving values. Note, however, that the parametrisation of the PMNS matrix in eq. (6.46) differs from the standard one: it

Quantity	Experiment (2σ ranges)	Model
$\sin^2\theta_{12}$	0.275 – 0.342	0.340
$\sin^2\theta_{23}$	0.36 – 0.60	0.490
$\sin^2\theta_{13}$	0.015 – 0.032	0.020
δ	-	84.3°

Table 6.5: Numerical results for the neutrino sector. The experimental results are taken from [25] apart from the value for θ_{13} which is the DayaBay result [26].

corresponds to one of the several possible parametrisations of the PMNS matrix [136]. Thus, in order to get the values of the Dirac and Majorana phases δ and β_1, β_2 (or α_{21}, α_{31}), of the standard parametrisation of the PMNS matrix, one has to bring the expressions (6.46) in a form which corresponds to the "standard" one. This can be done by using the freedom of multiplying the rows of the PMNS matrix with arbitrary phases and by shifting some of the common phases of the columns to a diagonal phase matrix P. The results for the numerical matrix in eq. (6.46) is:

$$U_{\rm PMNS} \cong \begin{pmatrix} 0.804 & 0.577 & 0.144 e^{-\,{\rm i}\,84.25^\circ} \\ -\,0.433 e^{{\rm i}\,10.59^\circ} & 0.577 e^{-\,{\rm i}\,5.75^\circ} & 0.692 \\ 0.408 e^{-\,{\rm i}\,11.56^\circ} & -\,0.577 e^{{\rm i}\,5.75^\circ} & 0.707 \end{pmatrix} P\,\tilde{Q}\,, \tag{6.48}$$

where $\tilde{Q} = {\rm Diag}(1, e^{{\rm i}\,\phi_2/2}, e^{{\rm i}\,\phi_3/2}) = e^{{\rm i}\,\phi_3/2}\,{\rm Diag}(e^{-\,{\rm i}\,\phi_3/2}, e^{-\,{\rm i}(\phi_3-\phi_2)/2}, 1)$ and the new 2phase matrix $P = {\rm Diag}(e^{{\rm i}\,11.50^\circ}, e^{-\,{\rm i}\,5.81^\circ}, -1)$. Now comparing eq. (6.48) with with the standard parametrization, we can obtain the values of the Dirac and the two Majorana phases of the standard parametrisation of the PMNS matrix, predicted by the model. For the Dirac phase we find $\delta \cong 84.3^\circ$. Note that the Majorana phases $\beta_1/2$ and $\beta_2/2$ (or $\alpha_{21}/2$ and $\alpha_{31}/2$) in the standard parametrisation are not CP conserving [143]: due to the matrix P they get CP violating corrections to the CP conserving values 0 and $\pi/2$ or $3\pi/2$.

As we have seen, the value of the Dirac phase δ predicted by the model is close to $\pi/2$. This implies that the magnitude of the CP violation effects in neutrino oscillations, is also predicted to be relatively large. Indeed, the rephasing invariant associated with the Dirac phase [160, 161], $J_{\rm CP} = {\rm Im}(U^*_{e1} U_{\mu 1} U_{e3} U^*_{\mu 3})$, which determines the magnitude of CP violation effects in neutrino oscillations [162], has the following value:

$$J_{\rm CP} = 0.0324\,. \tag{6.49}$$

The values we have obtained for both $\sin\theta_{13}$ and δ are in very good agreement with the numerical results in Table 6.5 derived using the `REAP` package [156].

It is possible to derive simple analytic expressions which explain the numerical results obtained above and quoted in Table 6.5. Indeed, up to corrections of order

$(\theta_{12}^e)^2$ we have:

$$\theta_{12} = \arcsin\frac{1}{\sqrt{3}} + \frac{\sqrt{2}}{8}(\theta_{12}^e)^2 \,, \tag{6.50}$$

$$\theta_{13} = \frac{1}{\sqrt{2}}\theta_{12}^e \,, \tag{6.51}$$

$$\theta_{23} = \frac{\pi}{4} - \frac{1}{4}(\theta_{12}^e)^2 \,, \tag{6.52}$$

$$\delta = \frac{\pi}{2} - \frac{1}{2}\theta_{12}^e \,, \tag{6.53}$$

$$\beta_1 = 2\pi - 2\theta_{12}^e + \phi_3 \,, \tag{6.54}$$

$$\beta_2 = 2\pi + \theta_{12}^e + \phi_3 - \phi_2 \,, \tag{6.55}$$

where $\theta_{12}^e \cong 0.888\theta^C$. Note that the expression for δ is correct up to $\mathcal{O}(\theta_{12}^e)$ only because it appears always with θ_{13} which is of order θ_{12}^e itself. Numerically, these approximations give for $\theta_{12}^e = 0.2$:

$$\sin^2\theta_{12} = 0.340 \,, \tag{6.56}$$

$$\sin^2\theta_{13} = 0.020 \,, \tag{6.57}$$

$$\sin^2\theta_{23} = 0.490 \,, \tag{6.58}$$

$$\delta = 84.3^\circ \,, \tag{6.59}$$

$$\beta_1 = 337.1^\circ + \phi_3 \,, \tag{6.60}$$

$$\beta_2 = 11.5^\circ + \phi_3 - \phi_2 \,. \tag{6.61}$$

As we see, the results obtained using the approximate analytic expressions are in very good agreement with those derived in the numerical analysis.

Note that all these relations were derived neglecting RGE corrections. Indeed they are under control. For the inverted ordering the RGE corrections can be expected to be largest, because there m_1 and m_2 are almost equal [163]. We have found numerically with the REAP package [156] that the biggest deviation is in δ which goes down to 81.2°. The Majorana phases run less than one degree and also the mixing angles stay well within their two sigma ranges.

III.III Predictions for Other Observables in the Neutrino Sector

We derive in this section the predictions for the sum of the neutrino masses and the effective Majorana mass $|\langle m\rangle|$ in neutrinoless double beta decay (see, e.g., [9, 46, 67]) using the standard parametrization of the PMNS mixing matrix and the results on the neutrino masses, mixing angles and CPV phases obtained in preceding subsections of this Section.

In the case of solution A for the NO neutrino mass spectrum we get for the sum of the neutrino masses:

$$\sum_{k=1}^{3} m_k = 6.31 \times 10^{-2} \text{ eV} \,, \quad \text{solution A (NO)} \,. \tag{6.62}$$

In this case we have $\phi_2 = \phi_3 = 0$ (see subsection 4.1) and for the effective Majorana

mass we obtain using eqs. (6.34) and (6.48):

$$|\langle m\rangle| \ = |\sum_{k=1}^{3}(U_{\rm PMNS})_{ek}^2 m_k| = 4.90\times 10^{-3}\ \text{eV}\ , \quad \text{solution A (NO)}\,. \tag{6.63}$$

The same quantities for solution B of the NO spectrum have the values:

$$\sum_{k=1}^{3} m_k = 6.54\times 10^{-2}\ \text{eV}\ , \quad \text{solution B (NO)}\,, \tag{6.64}$$

and

$$|\langle m\rangle| \ = 7.95\times 10^{-3}\ \text{eV}\ , \quad \text{solution B (NO)}\,, \tag{6.65}$$

where we have used the fact that for solution B we have $\phi_2 = 0$ and $\phi_3 = \pi$. As a consequence, in particular, of the values of $\phi_{2,3}$, the three terms in the expression for $|\langle m\rangle|$ essentially add.

Finally, in the case of IO spectrum we obtain:

$$\sum_{k=1}^{3} m_k = 12.1\times 10^{-2}\ \text{eV}\ , \quad \text{(IO)}\,, \tag{6.66}$$

and

$$|\langle m\rangle| \ = 2.17\times 10^{-2}\ \text{eV}\ , \quad \text{(IO)}\,, \tag{6.67}$$

We recall that for the IO spectrum we have $\phi_2 = \pi$ and $\phi_3 = 0$ and there is a partial compensation in $|\langle m\rangle|$ between the dominant contributions due to the terms $\propto m_1$ and $\propto m_2$.

IV UV Completion of the model: the Messenger Sector

In our model we consider non-renormalisable operators. In general the contraction of the $SU(5)$ and T' indices may not be unique which is nevertheless essential for our model. Our predictions are based on the fact, that only a certain contraction is allowed as we have, for example, indicated in eq. 6.5 for the T' indices. For the connection between the so-called UV completion and predictivity of a model see also [164]. Hence we have to specify the so-called messenger fields which generate only the desired contractions in the operators after being integrated out in a specific order.

The full list of messenger fields of our model is given in Tab. 6.6. Every messenger pair in every line receives a mass term in the superpotential, like, for example, $M_{\Sigma_1^a}\Sigma_1^a\bar{\Sigma}_1^a$. For the sake of brevity we do not write down all mass terms, but it is important to note, that there are no mass terms between messengers in different lines allowed. We assume all the messenger masses to be above the scale of T' and $SU(5)$ breaking, which are closely related in our model as we will see in the next section. Many messengers carry $SU(5)$ quantum numbers so that above the messenger scale, which we denote by Λ the gauge coupling becomes quickly non-perturbative, so that we are not predictive above this scale.

After this general remarks we now turn to the superpotential which describes the couplings of the various fields to the messengers. We start with the messengers coupling to the matter, Higgs and flavon fields. The supergraphs showing these couplings are

Messenger Fields	$SU(5)$	T'	$U(1)_R$	Z_{12}^u	Z_8^d	Z_8^ν	Z_8	Z_6	Z_6'	Z_4
Σ_1^a, $\bar{\Sigma}_1^a$	**1**, **1**	**1**, **1**	0, 2	4, 8	0, 0	0, 0	0, 0	2, 4	2, 4	0, 0
Σ_1^b, $\bar{\Sigma}_1^b$	**1**, **1**	**1**, **1**	0, 2	4, 8	0, 0	0, 0	0, 0	0, 0	0, 0	0, 0
$\Sigma_{1'}^a$, $\bar{\Sigma}_{1''}^a$	**1**, **1**	**1′**, **1″**	0, 2	6, 6	4, 4,	4, 4	4, 4	0, 0	0, 0	2, 2
$\Sigma_{1'}^b$, $\bar{\Sigma}_{1''}^b$	**1**, **1**	**1′**, **1″**	0, 2	8, 4	4, 4,	4, 4	4, 4	4, 2	4, 2	0, 0
$\Sigma_{1'}^c$, $\bar{\Sigma}_{1''}^c$	**1**, **1**	**1′**, **1″**	0, 2	8, 4	0, 0	0, 0	0, 0	2, 4	2, 4	0, 0
$\Sigma_{1''}^a$, $\bar{\Sigma}_{1'}^a$	**1**, **1**	**1″**, **1′**	0, 2	6, 6	4, 4	0, 0	4, 4	1, 5	1, 5	0, 0
$\Sigma_{1''}^b$, $\bar{\Sigma}_{1'}^b$	**1**, **1**	**1″**, **1′**	0, 2	0, 0	6, 2	2, 6	6, 2	3, 3	3, 3	0, 0
$\Sigma_{1''}^c$, $\bar{\Sigma}_{1'}^c$	**24**, **24**	**1″**, **1′**	0, 2	3, 9	2, 6	0, 0	6, 2	0, 0	3, 3	1, 3
$\Sigma_{2''}^a$, $\bar{\Sigma}_{2'}^a$	**1**, **1**	**2″**, **2′**	0, 2	9, 3	5, 3	7, 1	1, 7	3, 3	3, 3	3, 1
$\Sigma_{2''}^b$, $\bar{\Sigma}_{2'}^b$	**1**, **1**	**2″**, **2′**	0, 2	9, 3	4, 4	5, 3	3, 5	4, 2	1, 5	2, 2
Σ_3^a, $\bar{\Sigma}_3^a$	**1**, **1**	**3**, **3**	0, 2	6, 6	4, 4	0, 0	4, 4	1, 5	1, 5	0, 0
Σ_3^b, $\bar{\Sigma}_3^b$	**1**, **1**	**3**, **3**	0, 2	0, 0	6, 2	2, 6	6, 2	3, 3	3, 3	0, 0
Σ_3^c, $\bar{\Sigma}_3^c$	**1**, **1**	**3**, **3**	0, 2	0, 0	0, 0	4, 4	0, 0	3, 3	3, 3	2, 2
Σ_3^d, $\bar{\Sigma}_3^d$	**1**, **1**	**3**, **3**	0, 2	0, 0	0, 0	0, 0	4, 4	0, 0	3, 3	2, 2
$\Xi_{1'}^a$, $\bar{\Xi}_{1''}^a$	**5**, $\bar{\mathbf{5}}$	**1′**, **1″**	1, 1	5, 7	0, 0	4, 4	0, 0	5, 1	5, 1	2, 2
$\Xi_{2'}^a$, $\bar{\Xi}_{2''}^a$	**5**, $\bar{\mathbf{5}}$	**2′**, **2″**	1, 1	2, 10	7, 1	5, 3	3, 5	2, 4	5, 1	3, 1
$\Xi_{2''}^a$, $\bar{\Xi}_{2'}^a$	**5**, $\bar{\mathbf{5}}$	**2″**, **2′**	1, 1	8, 4	5, 3	7, 1	1, 7	2, 4	5, 1	1, 3
Ω_1^a, $\bar{\Omega}_1^a$	**5**, $\bar{\mathbf{5}}$	**1**, **1**	0, 2	2, 10	0, 0	2, 10	4, 4	5, 1	5, 1	0,0
$\Omega_{1'}^a$, $\bar{\Omega}_{1''}^a$	**5**, $\bar{\mathbf{5}}$	**1′**, **1″**	2, 0	8, 4	0, 0	8, 4	0, 0	4, 2	4, 2	2, 2
$\Omega_{1'}^b$, $\bar{\Omega}_{1''}^b$	**5**, $\bar{\mathbf{5}}$	**1′**, **1″**	2, 0	9, 3	1, 7	9, 3	2, 6	4, 2	1, 5	2, 2
$\Omega_{2''}^a$, $\bar{\Omega}_{2'}^a$	**5**, $\bar{\mathbf{5}}$	**2″**, **2′**	2, 0	9, 3	2, 6	9, 3	7, 1	1, 5	4, 2	2, 2
Ω_3^a, $\bar{\Omega}_3^a$	**5**, $\bar{\mathbf{5}}$	**1**, **1**	0, 2	0, 0	3, 5	0, 0	4, 4	4, 2	4, 2	1, 3
$\Upsilon_{1''}^a$, $\bar{\Upsilon}_{1'}^a$	**10**, $\bar{\mathbf{10}}$	**1″**, **1′**	1, 1	2, 10	1, 7	5, 3	2, 6	3, 3	3, 3	2, 2
$\Upsilon_{1''}^b$, $\bar{\Upsilon}_{1'}^b$	**10**, $\bar{\mathbf{10}}$	**1″**, **1′**	1, 1	2, 10	0, 0	3, 5	4, 4	5, 1	2, 4	3, 1
Υ_2^a, $\bar{\Upsilon}_2^a$	**10**, $\bar{\mathbf{10}}$	**2**, **2**	1, 1	11, 1	0, 0	2, 6	1, 7	4, 2	1, 5	3, 1
Υ_2^b, $\bar{\Upsilon}_2^b$	**10**, $\bar{\mathbf{10}}$	**2**, **2**	1, 1	5, 7	2, 6	0, 0	7, 1	0, 0	0, 0	3, 1
Υ_2^c, $\bar{\Upsilon}_2^c$	**10**, $\bar{\mathbf{10}}$	**2**, **2**	1, 1	5, 7	6, 2	4, 4	3, 5	0, 0	0, 0	3, 1
$\Upsilon_{2'}^a$, $\bar{\Upsilon}_{2''}^a$	**10**, $\bar{\mathbf{10}}$	**2′**, **2″**	1, 1	11, 1	0, 0	2, 6	1, 7	4, 2	1, 5	3, 1
$\Upsilon_{2'}^b$, $\bar{\Upsilon}_{2''}^b$	**10**, $\bar{\mathbf{10}}$	**2′**, **2″**	1, 1	5, 7	0, 0	4, 4	7, 1	4, 2	1, 5	3, 1
$\Upsilon_{2'}^c$, $\bar{\Upsilon}_{2''}^c$	**10**, $\bar{\mathbf{10}}$	**2′**, **2″**	1, 1	5, 7	2, 6	0, 0	7, 1	0, 0	0, 0	3, 1
$\Upsilon_{2'}^d$, $\bar{\Upsilon}_{2''}^d$	**10**, $\bar{\mathbf{10}}$	**2′**, **2″**	1, 1	11, 1	0, 0	2, 6	5, 3	2, 4	5, 1	3, 1
$\Upsilon_{2''}^a$, $\bar{\Upsilon}_{2'}^a$	**10**, $\bar{\mathbf{10}}$	**2″**, **2′**	1, 1	5, 7	4, 4	0, 0	7, 1	3, 3	0, 0	1, 3
$\Upsilon_{2''}^b$, $\bar{\Upsilon}_{2'}^b$	**10**, $\bar{\mathbf{10}}$	**2″**, **2′**	1, 1	11, 1	0, 0	2, 6	1, 7	4, 2	1, 5	3, 1
$\Upsilon_{2''}^c$, $\bar{\Upsilon}_{2'}^c$	**10**, $\bar{\mathbf{10}}$	**2″**, **2′**	1, 1	2, 10	2, 6	6, 2	7, 1	0, 0	3, 3	0, 0
$\Upsilon_{2''}^d$, $\bar{\Upsilon}_{2'}^d$	**10**, $\bar{\mathbf{10}}$	**2″**, **2′**	1, 1	11, 1	0, 0	2, 6	5, 3	2, 4	5, 1	3, 1
$\Upsilon_{2''}^e$, $\bar{\Upsilon}_{2'}^e$	**10**, $\bar{\mathbf{10}}$	**2″**, **2′**	1, 1	11, 1	0, 0	6, 2	5, 3	0, 0	0, 0	1, 3
Υ_3^a, $\bar{\Upsilon}_3^a$	**10**, $\bar{\mathbf{10}}$	**3**, **3**	1, 1	2, 10	0, 0	7, 1	4, 4	4, 2	1, 5	1, 3
Υ_3^b, $\bar{\Upsilon}_3^b$	**10**, $\bar{\mathbf{10}}$	**3**, **3**	1, 1	8, 4	0, 0	5, 3	2, 6	2, 4	5, 1	1, 3
Υ_3^c, $\bar{\Upsilon}_3^c$	**10**, $\bar{\mathbf{10}}$	**3**, **3**	1, 1	8, 4	2, 6	5, 3	6, 2	5, 1	5, 1	3, 1
Υ_3^d, $\bar{\Upsilon}_3^d$	**10**, $\bar{\mathbf{10}}$	**3**, **3**	1, 1	2, 10	5, 3	5, 3	6, 2	3, 3	0, 0	0, 0
$\Gamma_{2''}^a$, $\bar{\Gamma}_{2'}^a$	**24**, **24**	**2″**, **2′**	2, 0	9, 3	3, 5	5, 3	7, 1	3, 3	0, 0	1, 3

Table 6.6: Messenger fields used in our model. After integrating out these fields we end up with the desired effective operators. For the sake of brevity we do not list all mass terms in the text. The messenger pair in every line has a mass term and there are no cross terms allowed.

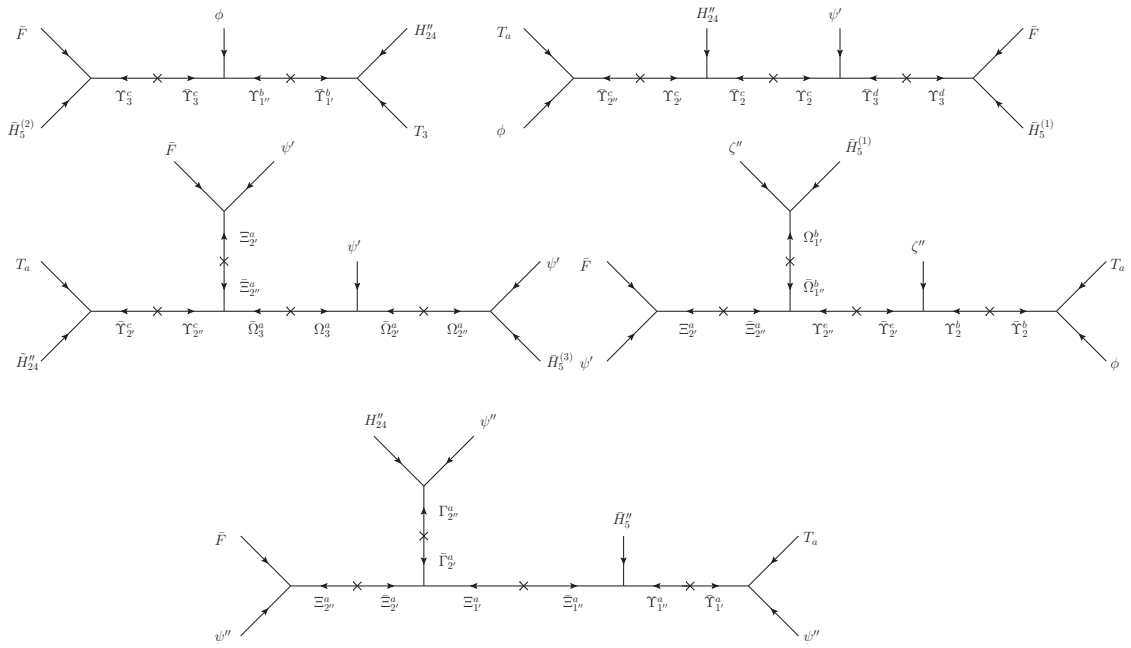

Figure 6.4: The supergraphs before integrating out the messengers for the down-type quark and charged lepton sector.

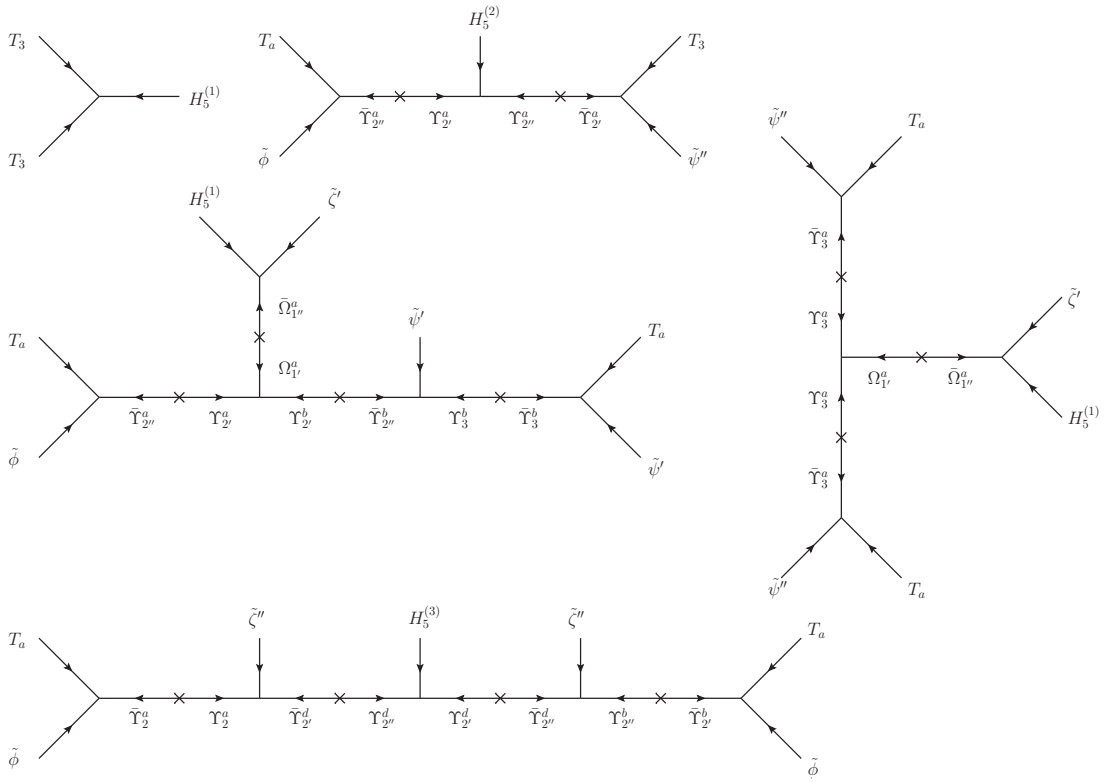

Figure 6.5: The supergraphs before integrating out the messengers for the up-type quark sector.

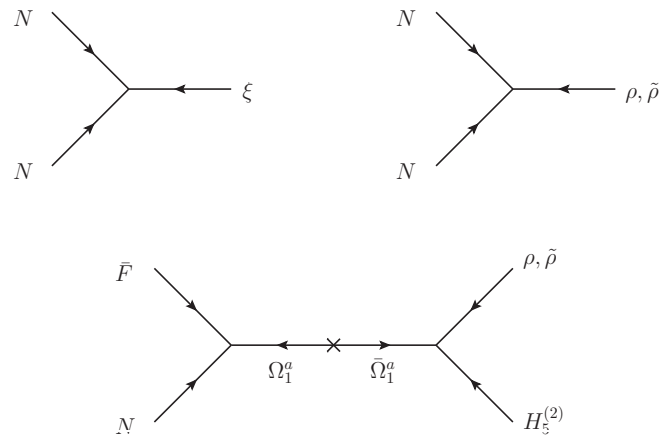

Figure 6.6: The supergraphs before integrating out the messengers for the neutrino sector.

given in Figs. 6.4-6.6. From these diagrams one can read off all the relevant contractions and couplings. Nevertheless, we give now the renormalisable superpotential containing the messenger fields.

Apart from the messenger mass terms (which we do not write down explicitly) there are no terms with one or two fields involving matter, Higgs and flavon fields. For the down-type quark diagrams we find (here and in this whole section we do not write down the couplings)

$$\mathcal{W}_d^{\text{ren}} = \bar{F}\bar{H}_5^{(2)}\Upsilon_3^c + \phi\bar{\Upsilon}_3^c\Upsilon_{1''}^b + H_{24}''T_3\bar{\Upsilon}_{1'}^b \tag{6.68}$$
$$+ T_a\phi\bar{\Upsilon}_{2''}^c + H_{24}''\bar{\Upsilon}_2^c\Upsilon_{2'}^c + \psi'\Upsilon_2^c\bar{\Upsilon}_3^d + \bar{F}\bar{H}_5^{(1)}\Upsilon_3^d \tag{6.69}$$
$$+ T_a\tilde{H}_{24}''\bar{\Upsilon}_{2'}^c + \bar{H}_5^{(3)}\psi'\Omega_{2''}^a + \bar{\Omega}_{2'}^a\psi'\Omega_3^a + \bar{\Omega}_3^a\Upsilon_{2''}^c\Xi_{2''}^a \tag{6.70}$$
$$+ \bar{F}\psi'\Xi_{2'}^a + \bar{\Xi}_{2''}^a\Upsilon_{2''}^e\bar{\Omega}_{1''}^b + \zeta''\bar{H}_5^{(1)}\Omega_{1'}^b + \zeta''\bar{\Upsilon}_{2'}^e\Upsilon_2^b + T_a\phi\bar{\Upsilon}_2^b \tag{6.71}$$
$$+ \bar{F}\psi''\Xi_{2''}^a + \bar{\Xi}_{2'}^a\Xi_{1'}^a\bar{\Gamma}_{2'}^a + H_{24}''\psi''\Gamma_{2''}^a + \bar{H}_5''\bar{\Xi}_{1''}^a\Upsilon_{1''}^a + \bar{\Upsilon}_{1'}^aT_a\psi'' \,, \tag{6.72}$$

for the up-type quarks

$$\mathcal{W}_u^{\text{ren}} = H_5^{(1)}T_3^2 + T_a\tilde{\phi}\bar{\Upsilon}_{2''}^a + H_5^{(2)}\Upsilon_{2'}^a\Upsilon_{2''}^a + T_3\tilde{\psi}''\bar{\Upsilon}_{2'}^a \tag{6.73}$$
$$+ T_a\tilde{\psi}''\bar{\Upsilon}_3^a + \tilde{\zeta}'H_5^{(1)}\bar{\Omega}_{1''}^a + \Omega_{1'}^a\Upsilon_3^a\Upsilon_3^a \tag{6.74}$$
$$+ T_a\tilde{\phi}\bar{\Upsilon}_{2''}^a + \Upsilon_{2'}^a\Omega_{1'}^a\Upsilon_{2'}^b + H_5^{(1)}\tilde{\zeta}'\bar{\Omega}_{1''}^a + \tilde{\psi}'\bar{\Upsilon}_{2''}^b\Upsilon_3^b + \bar{\Upsilon}_3^bT_a\tilde{\psi}' \tag{6.75}$$
$$+ T_a\tilde{\phi}\bar{\Upsilon}_2^a + \Upsilon_2^a\tilde{\zeta}''\bar{\Upsilon}_{2'}^d + H_5^{(3)}\Upsilon_{2''}^d\Upsilon_{2'}^d + \tilde{\zeta}''\bar{\Upsilon}_{2''}^d\Upsilon_{2''}^b + T_a\tilde{\phi}\bar{\Upsilon}_{2'}^b \,, \tag{6.76}$$

and for the neutrino sector

$$\mathcal{W}_\nu^{\text{ren}} = N^2\xi + N^2\rho + N^2\tilde{\rho} + \bar{F}N\Omega_1^a + H_5^{(2)}\rho\bar{\Omega}_1^a + H_5^{(2)}\tilde{\rho}\bar{\Omega}_1^a \,. \tag{6.77}$$

There are five additional operators which generate dimension eight or more operators in the matter sector, which we neglect. For completeness we give them as well

$$\mathcal{W}_{d\geq 8}^{\text{ren, matter}} = \zeta'\Upsilon_2^c\bar{\Upsilon}_{2''}^c + \bar{\Upsilon}_2^c\Upsilon_3^d\psi'' + \psi''\Omega_{2''}^a\bar{\Omega}_3^a + \bar{\Gamma}_{2'}^a\bar{\Upsilon}_{2''}^c\Upsilon_3^d + \bar{\Gamma}_{2'}^a\bar{\Upsilon}_2^b\Upsilon_3^d \,. \tag{6.78}$$

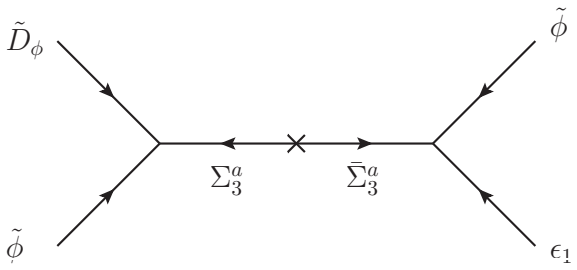

Figure 6.7: One typical diagram for the messengers in the flavon sector. We consider only effective operators up to dimension four. For the sake of brevity we only show one diagram. The other ones are quite similar with the driving field on one side and the auxiliary ϵ fields on the other side.

We turn now to the messengers, which give the non-renormalisable terms in the flavon alignment superpotential which we denote collectively with Σ. In this sector all the supergraphs have the structure as given in Fig. 6.7. (The role of the auxiliary ϵ fields is described in the next section and their quantum numbers are given in Tab. 6.8.) For the sake of brevity we do not give all the diagrams for the flavon sector, but all diagrams can easily be derived from the renormalisable flavon superpotential. We give here only the terms, where a messenger is involved. The terms, where no messenger is involved will be discussed in the next section, when we discuss the superpotential responsible for the flavon alignment. The superpotential involving the Σ fields reads

$$\mathcal{W}_\Sigma^{\text{ren}} = D_\xi \xi \Sigma_3^c + D_\xi \rho \Sigma_3^c + D_\xi \tilde{\rho} \Sigma_3^c + \bar{\Sigma}_3^c \xi \epsilon_9 + \tilde{D}_\phi \tilde{\phi} \Sigma_3^a + \bar{\Sigma}_3^a \tilde{\phi} \epsilon_1 \tag{6.79}$$

$$+ \tilde{D}_\phi \tilde{\phi} \Sigma_{1''}^a + \bar{\Sigma}_{1'}^a \tilde{\zeta}'' \epsilon_2 + D_\phi \phi \Sigma_3^b + \bar{\Sigma}_3^b \phi \epsilon_4 + D_\phi \phi \Sigma_{1''}^b + \bar{\Sigma}_{1'}^b \zeta'' \epsilon_5 \tag{6.80}$$

$$+ D_\psi \psi'' \Sigma_{2''}^a + \bar{\Sigma}_{2'}^a \psi'' \epsilon_6 + D_\psi \phi \Sigma_{1'}^a + S_\zeta'' \epsilon_7 \Sigma_{1'}^a + \bar{\Sigma}_{1''}^a \zeta' \epsilon_7 + S_1 \psi' \Sigma_{2''}^b + \bar{\Sigma}_{2'}^b \tilde{\psi}'' \epsilon_8 \tag{6.81}$$

$$+ S_2' \zeta' \Sigma_{1'}^b + \bar{\Sigma}_{1''}^b \zeta' \epsilon_{12} + S_2' \tilde{\zeta}' \Sigma_{1'}^c + \bar{\Sigma}_{1''}^c \tilde{\zeta}' \epsilon_{13} + S_{\epsilon_{12}} \epsilon_{12} \Sigma_1^a + \bar{\Sigma}_1^a \epsilon_{12}^2 \tag{6.82}$$

$$+ S_{\epsilon_{13}} \epsilon_{13} \Sigma_1^b + \bar{\Sigma}_1^b \epsilon_{13}^2 + \tilde{S}_{24}'' \tilde{H}_{24}'' \Sigma_{1''}^c + \bar{\Sigma}_{1'}^c \epsilon_{10} \tilde{H}_{24}'' + \tilde{S}_{24}'' \xi \Sigma_3^d + \bar{\Sigma}_3^d \epsilon_{11} \xi \, . \tag{6.83}$$

Apart from these there are as well operators which give dimension five operators in the flavon alignment superpotential after integrating out the messenger fields, which we will neglect. These operators are

$$\mathcal{W}_{d\geq 5}^{\text{ren, flavon}} = S_\zeta'' \Sigma_1^a \Sigma_{1'}^b + S_{\tilde{\zeta}}'' \Sigma_1^b \Sigma_{1'}^c + S_{\tilde{\zeta}}'' \Sigma_{1''}^a \Sigma_{1''}^a + S_\zeta'' \Sigma_{1''}^b \Sigma_{1''}^b + S_{\tilde{\zeta}}'' \Sigma_3^a \Sigma_3^a + S_\zeta'' \Sigma_3^b \Sigma_3^b \tag{6.84}$$

$$+ S_{24}'' \Sigma_3^c \Sigma_3^c + S_{24}'' \Sigma_3^d \Sigma_3^d + (S_{\epsilon_i} + S_\xi + S_\rho) \Sigma_3^c \Sigma_3^c + (S_{\epsilon_i} + S_\xi + S_\rho) \Sigma_3^d \Sigma_3^d \, . \tag{6.85}$$

Now we have discussed the messenger sector. After integrating out the messengers from the renormalisable superpotential we end up with the effective operators which give us the desired flavon vev alignments and structures of the Yukawa matrices.

V Flavon Vacuum Alignment

In this part we present the solution for our flavon vacuum alignment. In the present model all the discussed results crucially depend on the vev structure and on the fact

	$\tilde{D}_\phi$	$\tilde{S}_\psi$	$\tilde{S}''_\zeta$	$\tilde{S}_\zeta$	D_ϕ	D_ψ	S''_ζ	D_ξ	S_ξ	S_ρ	S''_{24}	$\tilde{S}''_{24}$	S_1	S'_2	S_{ϵ_i}
T'	**3**	**1**	**1″**	**1**	**3**	**3**	**1″**	**3**	**1**	**1**	**1″**	**1″**	**1**	**1′**	**1**
Z_{12}^u	6	0	0	0	6	0	0	6	0	0	0	6	6	4	0
Z_8^d	4	0	0	0	0	2	4	4	0	0	0	4	5	0	0
Z_8^ν	4	0	0	0	4	2	4	4	0	0	0	0	2	0	0
Z_8	0	4	0	4	0	2	4	4	0	0	0	0	2	0	0
Z_6	1	0	4	0	3	0	0	3	0	0	0	0	5	2	0
Z'_6	1	0	4	0	0	3	0	3	0	0	0	3	5	2	0
Z_4	0	0	0	0	0	2	0	2	0	0	0	2	1	0	0

Table 6.7: List of the driving fields from the superpotential which give the desired vacuum alignment. All driving fields are $SU(5)$ gauge singlets and charged under $U(1)_R$ with charge +2.

	ϵ_1	ϵ_2	ϵ_3	ϵ_4	ϵ_5	ϵ_6	ϵ_7	ϵ_8	ϵ_9	ϵ_{10}	ϵ_{11}	ϵ_{12}	ϵ_{13}
Z_{12}^u	6	6	0	6	6	6	6	6	6	0	6	8	8
Z_8^d	4	4	0	4	0	4	0	4	4	0	0	0	4
Z_8^ν	4	0	0	0	4	0	0	4	4	0	0	0	0
Z_8	0	0	4	4	0	4	0	4	4	4	0	0	0
Z_6	3	3	0	3	3	0	0	0	3	0	0	4	0
Z'_6	3	3	0	3	3	0	0	0	3	0	0	4	0
Z_4	0	0	0	0	2	0	2	0	2	0	2	0	0

Table 6.8: List of the auxiliary flavon fields that do not couple to the matter sector. The ϵ_i fields are all $SU(5) \times T'$ singlets and carry no $U(1)_R$ charge.

that all flavon vevs are real.

In the flavon potential two new kinds of fields are introduced. First we have to add driving fields which are gauge singlets but transform in a non trivial way under the family and shaping symmetries and have a $U(1)_R$ charge of two. Minimizing the F-term equations of this fields will give us the correct alignment (including phases) as one possible solution. Second we introduce auxiliary fields ϵ_i, $i = 1, \ldots, 13$, which are singlets under $SU(5)$ and T', but they transform in a non trivial way under the additional shaping symmetries. They appear only in the flavon superpotential. Indeed, these fields are introduced to compensate the charges of different operators, so that they are related to each other in the F-term equations. Note that we have to include for our alignment non-renormalisable operators, where we restrict ourselves to operators with mass dimension not higher than four in the superpotential. The driving fields are listed in Table 6.7 and the auxiliary fields are listed in Table 6.8.

Before going into the more complicated details of the flavon vacuum alignment we briefly discuss the "alignment" of the auxiliary flavons, which is simply the question how to give them a real vev. For this purpose we used the simple idea advocated in [165], which we can directly illustrate at the alignment for the ϵ fields itself. The superpotential for their alignment reads

$$\mathcal{W}_\epsilon = S_{\epsilon_i}\left(\epsilon_i^2 - M_{\epsilon_i}^2\right) + S_{\epsilon_j}\left(\frac{1}{\Lambda}\,\epsilon_j^3 - M_{\epsilon_j}^2\right) , \tag{6.86}$$

where $i = 1, \ldots, 11$ and $j = 12, 13$. Note that for the sake of readability we do not include any couplings. The driving fields S_{ϵ_i} and S_{ϵ_j} are total singlets so that terms like $S_\epsilon M_\epsilon^2$ are allowed. The F-Term equations for the driving fields give, e.g.

$$F_{S_{\epsilon_1}} = \epsilon_1^2 - M_{\epsilon_1}^2 = 0 \, . \tag{6.87}$$

And since we assume that our fundamental theory is CP conserving the mass M_{ϵ_1} is real (like the coupling parameters which are not shown) and hence the vev of ϵ_1 is real and non-vanishing. For ϵ_{12} and ϵ_{13} this has to be slightly modified. For them we find three possible solutions, two of them complex and only one real. But we assume that the real solution is picked up, which could be preferred by higher order corrections, supergravity corrections or some low-energy soft terms in the scalar potential. To discuss this corrections in detail is beyond the scope of this work.

Note also that all the S_{ϵ_i} driving fields have the same quantum numbers and hence can mix with each other. In other words each of these driving fields could couple to each ϵ field. We have chosen here the basis in which the superpotential has the above structure, which makes the alignment clear (see also the appendix of [165]).

The same method can be applied to the real triplet and singlet flavons of our model, after we have fixed their alignment by some different kind of operators. But for the complex doublets ($\mathbf{2'}$, $\mathbf{2''}$) and singlets ($\mathbf{1'}$, $\mathbf{1''}$) we have to use other relations, because the representation squared cannot form a total singlet.

Before we come to this complex representations we discuss the alignment for the flavons appearing in the neutrino sector (ξ, ρ, $\tilde{\rho}$) where this complication is absent [5]. The superpotential for these flavons reads

$$\mathcal{W}_{\xi,\rho,\tilde{\rho}} = \frac{D_\xi}{\Lambda} \left(\xi^2 \epsilon_9 + \xi \rho \epsilon_9 + \xi \tilde{\rho} \epsilon_9 \right) + S_\xi \left(\xi^2 - M_\xi^2 \right) + S_\rho \left(\rho^2 + \tilde{\rho}^2 - M_\rho^2 \right) \, . \tag{6.88}$$

The first thing to note here, is that we used the auxiliary flavon ϵ_9 in the first set of operators involving the triplet driving field D_ξ. Since ϵ_9 appears in all three operators, it drops out in the F-term conditions, but nevertheless it is real and hence would just modify the value of the vev without introducing any phase. The F-term conditions are

$$\frac{\partial \mathcal{W}_{\xi,\rho,\tilde{\rho}}}{\partial D_{\xi_1}} = 2\xi_1^2 - 2\xi_2\xi_3 + \xi_1(\rho + \tilde{\rho}) = 0 \, , \tag{6.89}$$

$$\frac{\partial \mathcal{W}_{\xi,\rho,\tilde{\rho}}}{\partial D_{\xi_2}} = 2\xi_2^2 - 2\xi_1\xi_3 + \xi_3(\rho + \tilde{\rho}) = 0 \, , \tag{6.90}$$

$$\frac{\partial \mathcal{W}_{\xi,\rho,\tilde{\rho}}}{\partial D_{\xi_3}} = 2\xi_3^2 - 2\xi_2\xi_1 + \xi_2(\rho + \tilde{\rho}) = 0 \, , \tag{6.91}$$

$$\frac{\partial \mathcal{W}_{\xi,\rho,\tilde{\rho}}}{\partial S_\xi} = \xi_1^2 + 2\xi_2\xi_3 - M_\xi^2 = 0 \, , \tag{6.92}$$

$$\frac{\partial \mathcal{W}_{\xi,\rho,\tilde{\rho}}}{\partial S_\rho} = \rho^2 + \tilde{\rho}^2 - M_\rho^2 = 0 \, . \tag{6.93}$$

Besides the trivial solution $\xi_i = 0$, $i = 1, 2, 3$, we find for the first three of these equations by cyclic permutations in ξ_i the desired solution for which $\xi_i = \xi_0 \neq 0$ if $\rho_0 = -\tilde{\rho}_0$. The fact that the vevs are non-vanishing and real can then be read off from the last two equations for which we used the method from [165] discussed above.

[5] The alignment for the triplets follows the discussion in the seminal paper [127].

Now we come to the most complicated part of the flavon alignment sector, the flavons present in the quark and charged lepton sectors. Although we have two different set of flavons, one for the up-quark sector at the one hand and one for the down-type quark and charged lepton sector at the other hand, we cannot separate their alignments completely. In fact, we found that the alignment is itself independent from each other but the simplest solution which we found to make all vevs real involves cross couplings between the two sectors. The flavon superpotential reads

$$\mathcal{W}_f = \frac{\tilde{D}_\phi}{\Lambda}\left(\tilde{\phi}\tilde{\phi}\,\epsilon_1 + \tilde{\phi}\tilde{\zeta}''\epsilon_2\right) + \tilde{S}''_\zeta(\tilde{\zeta}''\tilde{\zeta}'' + \tilde{\phi}\tilde{\phi} - M_{\tilde{\zeta}'}\tilde{\zeta}') + \tilde{S}_\zeta\left(\tilde{\zeta}'\tilde{\zeta}'' - M_{\tilde{\zeta}}\,\epsilon_3\right) \tag{6.94}$$

$$+ \tilde{S}_\psi\left(\tilde{\psi}'\tilde{\psi}'' - \tilde{\zeta}'\tilde{\zeta}''\right) + \frac{D_\phi}{\Lambda}\left(\phi\phi\,\epsilon_4 + \phi\,\zeta''\,\epsilon_5\right) + \frac{D_\psi}{\Lambda}\left(\left(\psi''\right)^2\epsilon_6 + \phi\zeta'\epsilon_7\right) \tag{6.95}$$

$$+ S_\psi\left(\psi'\psi'' - M_\psi^2\right) + S''_\zeta\left(\zeta''\zeta'' + \phi\phi - M_{\zeta'}\zeta' + \frac{\epsilon_7^2}{\Lambda}\zeta'\right) \tag{6.96}$$

$$+ S_1\left(\psi'\,\tilde{\psi}''\,\frac{\epsilon_8}{\Lambda} - M_{S_1}^2\right) + S'_2\left((\zeta')^2\epsilon_{12} - (\tilde{\zeta}')^2\epsilon_{13}\right)\,, \tag{6.97}$$

where in the last equations the cross couplings between the two sectors are written. We do not want to discuss here all the details of the alignment in detail, instead we will only discuss the phases of the vevs of the complex fields in a bit more detail. Nevertheless, we quote all the F-term conditions, in which it is then quite easy to plug in the flavon vevs from eqs. (6.1)-(6.3) and see that they form a viable solution. The F-term conditions read for the up sector

$$\frac{\partial\mathcal{W}_f}{\partial\tilde{D}_{\phi_1}} = \epsilon_1(2\tilde{\phi}_1^2 - 2\tilde{\phi}_2\tilde{\phi}_3) + \epsilon_2\tilde{\phi}_2\tilde{\zeta}'' = 0\,, \tag{6.98}$$

$$\frac{\partial\mathcal{W}_f}{\partial\tilde{D}_{\phi_2}} = \epsilon_1(2\tilde{\phi}_2^2 - 2\tilde{\phi}_1\tilde{\phi}_3) + \epsilon_2\tilde{\phi}_1\tilde{\zeta}'' = 0\,, \tag{6.99}$$

$$\frac{\partial\mathcal{W}_f}{\partial\tilde{D}_{\phi_3}} = \epsilon_1(2\tilde{\phi}_3^2 - 2\tilde{\phi}_1\tilde{\phi}_2) + \epsilon_2\tilde{\phi}_3\tilde{\zeta}'' = 0\,, \tag{6.100}$$

$$\frac{\partial\mathcal{W}_f}{\partial\tilde{S}''_\zeta} = (\tilde{\zeta}'')^2 - M_{\tilde{\zeta}'}\tilde{\zeta}' + \tilde{\phi}_3^2 + 2\tilde{\phi}_1\tilde{\phi}_2 = 0\,, \tag{6.101}$$

$$\frac{\partial\mathcal{W}_f}{\partial\tilde{S}_\zeta} = \tilde{\zeta}'\tilde{\zeta}'' - M_{\tilde{\zeta}}\epsilon_3 = 0\,, \tag{6.102}$$

$$\frac{\partial\mathcal{W}_f}{\partial\tilde{S}_\psi} = \tilde{\psi}'_1\tilde{\psi}''_2 - \tilde{\psi}'_2\tilde{\psi}''_1 - \tilde{\zeta}'\tilde{\zeta}'' = 0\,, \tag{6.103}$$

for the down sector

$$\frac{\partial \mathcal{W}_f}{\partial D_{\phi_1}} = \epsilon_4(2\phi_1^2 - 2\phi_2\phi_3) + \epsilon_5\phi_2\zeta'' = 0 \,, \tag{6.104}$$

$$\frac{\partial \mathcal{W}_f}{\partial D_{\phi_2}} = \epsilon_4(2\phi_2^2 - 2\phi_1\phi_3) + \epsilon_5\phi_1\zeta'' = 0 \,, \tag{6.105}$$

$$\frac{\partial \mathcal{W}_f}{\partial D_{\phi_3}} = \epsilon_4(2\phi_3^2 - 2\phi_1\phi_2) + \epsilon_5\phi_3\zeta'' = 0 \,, \tag{6.106}$$

$$\frac{\partial \mathcal{W}_f}{\partial D_{\psi_1}} = \epsilon_6((\psi_2'')^2 + \epsilon_7\phi_3\zeta' = 0 \,, \tag{6.107}$$

$$\frac{\partial \mathcal{W}_f}{\partial D_{\psi_2}} = \mathrm{i}\,\epsilon_6((\psi_1'')^2 + \epsilon_7\phi_2\zeta' = 0 \,, \tag{6.108}$$

$$\frac{\partial \mathcal{W}_f}{\partial D_{\psi_3}} = (1-\mathrm{i})\epsilon_6\psi_1''\psi_2'' + \epsilon_7\phi_1\zeta' = 0 \,, \tag{6.109}$$

$$\frac{\partial \mathcal{W}_f}{\partial S_\psi} = \psi_1'\psi_2'' - \psi_2'\psi_1'' - M_\psi^2 = 0 \,, \tag{6.110}$$

$$\frac{\partial \mathcal{W}_f}{\partial S_\zeta''} = (\zeta'')^2 - \left(M_{\zeta'} + \frac{\epsilon_7^2}{\Lambda}\right)\zeta' = 0 \,, \tag{6.111}$$

and for the cross couplings between the two sectors

$$\frac{\partial \mathcal{W}_f}{\partial S_1} = \left(\psi_1'\tilde{\psi}_2'' - \psi_2'\tilde{\psi}_1''\right)\frac{\epsilon_8}{\Lambda} - M_{S_1}^2 = 0 \,, \tag{6.112}$$

$$\frac{\partial \mathcal{W}_f}{\partial S_2'} = (\zeta')^2\epsilon_{12} - (\tilde{\zeta}')^2\epsilon_{13} = 0 \,. \tag{6.113}$$

So how do we make the vevs of the complex representations real? Exemplary we discuss the complex singlets $\tilde{\zeta}''$, $\tilde{\zeta}'$, ζ'' and ζ'. From eqs. (6.101) and (6.102) we find a polynomial in $\tilde{\zeta}''$

$$(\tilde{\zeta}'')^3 + \tilde{\zeta}''(\tilde{\phi}_3^2 + 2\tilde{\phi}_1\tilde{\phi}_2) - M_{\tilde{\zeta}'}M_{\tilde{\zeta}}\epsilon_3 = 0 \,, \tag{6.114}$$

which has a real solution (at least for a certain choice of parameters and plugging in the real vev of $\tilde{\phi}$) which we pick here. Then we know that $(\tilde{\zeta}'')^3$ is real, while $\tilde{\zeta}'$ has the opposite phase of $\tilde{\zeta}''$ so it is real as well. From eq. (6.113) we then find ζ' to be real and from eq. (6.111) we obtain ζ'' to be real and all the singlet vevs are real. For the doublets a similar mechanism applies.

The last alignment we want to discuss here is strictly speaking not an alignment. But since we have used adjoints of $SU(5)$ in our operators to get the desired Yukawa coupling relations between the charged leptons and the down-type quarks we add here a mechanism which generates the vev of these adjoints and also show explicitly that they are real. For the fields H_{24}'' and $\tilde{H}_{24}''$ we can write down the following superpotential using the two driving fields S_{24}'' and $\tilde{S}_{24}''$

$$\mathcal{W}_{24} = S_{24}''\left(H_{24}''H_{24}'' - \xi^2\right) + \frac{\tilde{S}_{24}''}{\Lambda}\left(\tilde{H}_{24}''\tilde{H}_{24}''\epsilon_{10} - \xi^2\epsilon_{11}\right) \,. \tag{6.115}$$

We see that the vev of ξ triggers a vev for the two adjoint fields and even more these two vevs are directly related to the T' symmetry breaking scale. That means that in our model the GUT scale and the scale of T' coincide (up to some order one coefficients).

In principle, we can again choose here between two different vevs for the adjoints. One pointing into the SM direction and the other one pointing into the $SU(4) \times U(1)$ direction and we assume the first option to be realized. We also note here, that the solution of the Doublet-Triplet-Splitting problem and hence the construction of the whole Higgs sector is clearly beyond the scope of this work.

VI Final Remarks

In this chapter we have presented a $SU(5) \times T'$ unified model of flavour, which predicts the reactor neutrino mixing angle θ_{13} to be in the range determined by DayaBay [26] and RENO [27] experiments, and all other mixing angles are predicted to have values within the experimental uncertainties. It implements a type I seesaw mechanism and from the breaking of the discrete family symmetry T' we obtain tri-bimaximal mixing in the neutrino sector. The relatively large value of θ_{13} is then generated entirely by corrections coming from the charged lepton sector. This is a generic effect in GUTs where Yukawa couplings are related to each other. Here we have used recently proposed $SU(5)$ GUT relations [118] between the down-type quark Yukawa matrix and the charged lepton Yukawa matrix to get the relatively large prediction for the reactor mixing angle θ_{13} along the lines proposed in [115, 116].

The corrections to the solar and the atmospheric neutrino mixing angle are under control due to the structure of the charged lepton Yukawa matrix and the pattern of the complex CP violation phases. The model exhibits a special kind of CP violation, the so-called "geometrical" CP violation. All parameters and vevs are real and all non-trivial phases are coming from the complex Clebsch–Gordan coefficients of T' and are integer multiples of $\pi/4$. We have given the renormalisable superpotential which generates effectively the Yukawa matrices after integrating out heavy messenger fields and plugging in the family symmetry breaking flavon vevs. The flavon vevs point in special directions in flavour space and are all real. These results come out as solutions to the flavon alignment superpotential we have presented in section V.

We have shown, in particular, that the phase pattern in the Yukawa matrices actually gives a very good fit of the quark and charged lepton masses and the CKM parameters at low energies. This fit fixes the charged lepton Yukawa matrix completely and since we find tri-bimaximal mixing in the neutrino sector itself, we can make predictions for the neutrino masses and all PMNS parameters. The angle θ_{13} is predicted to have a value corresponding to $\sin^2\theta_{13} \cong 0.8 \sin^2\theta^C/2 = 0.02$. For the Dirac phase δ we obtain in the standard parametrisation of the PMNS matrix $\delta = 84.3°$. Our model also predicts $\sin^2\theta_{12} = 0.340$ and $\sin^2\theta_{23} = 0.490$. There are three different possible solutions for the neutrino masses, two with normal ordering (NO, solutions A and B) and one with inverted ordering (IO). All three cases can be tested in experiments determining the absolute neutrino mass scale (or the sum of the three neutrino masses), in experiments which can measure the solar and atmospheric neutrino mixing angles with a high precision, in experiments searching for CP violation in neutrino oscillations and in neutrinoless double beta decay experiments. For the sum of three neutrino masses we get (with relatively small uncertainties, see Figs. (2) and (3)): $\sum_{k=1}^{3} m_k = 6.31 \times 10^{-2}$ eV (NO, A); 6.54×10^{-2} eV (NO, B) and 12.1×10^{-2} eV (IO). The $(\beta\beta)_{0\nu}$-decay effective Majorana mass for the three solutions is also unambiguously predicted: $|\langle m \rangle| = 4.90 \times 10^{-3}$ eV (NO, A); 7.95×10^{-3} eV (NO, B); 2.17×10^{-2} eV

(IO). The three solutions differ only in the values of the three neutrino masses and of the Majorana phases, so that we make one single prediction for the rephasing invariant which determines the magnitude of CP violation effects in neutrino oscillations: $J_{\mathrm{CP}} = 0.0324$. This value of J_{CP} is relatively large and can be tested in the experiments on CP violation in neutrino oscillations.

Chapter 7

Mixing Patterns from the Groups $\Sigma(n\varphi)$

As announced in the introduction of this part of the thesis an alternative approach to explain the lepton mixing pattern is the direct investigation of non-Abelian discrete groups which can give rise to mixing patterns with values of θ_{12}, θ_{23} and θ_{13} compatible with the experimental data. In this section of the thesis we want to show, as an illustrative example, the analysis we have performed using the so called "exceptional" groups $\Sigma(n\,\varphi)$.[1] A tantalizing approach is based on the assumption that a (lepton) flavor symmetry G_l is broken to two Abelian subgroups G_e and G_ν in the charged lepton and neutrino sector, respectively. The mismatch of the embedding of these two subgroups into the group G_l determines the lepton mixing encoded in the Pontecorvo-Maki-Nakagawa-Sakata (PMNS) mixing matrix. More precisely, the PMNS matrix is determined up to possible permutations of rows and columns (and phases).

We follow the approach to search for new discrete groups and focus in the present chapter on the so-called "exceptional" finite groups $\Sigma(n\varphi)$: $\Sigma(36\varphi)$, $\Sigma(72\varphi)$, $\Sigma(216\varphi)$, $\Sigma(360\varphi)$ with $\varphi = 1, 3$, which are subgroups of $SU(3)$ ($\varphi = 3$) or of $SU(3)/C$ ($\varphi = 1$) with C being the center of $SU(3)$ [132]. Since groups with $\varphi = 1$ do not possess irreducible faithful three-dimensional representations,[2], we will focus on groups with $\varphi = 3$ which do have such representations. We compute all mixing patterns related to these groups, assuming neutrinos to be either Dirac or Majorana particles. Among these four groups we recall that if neutrinos are assumed to be Majorana particles only $\Sigma(360 \times 3)$ has Klein subgroups and is thus suitable as G_l. $\Sigma(36 \times 3)$, $\Sigma(72 \times 3)$ and $\Sigma(216 \times 3)$ instead are only appropriate as G_l, if neutrinos are Dirac particles or only one of the Z_2 symmetries of the neutrino mass matrix is contained in G_l. In the latter case only one of the columns of the PMNS matrix is determined through the breaking of the flavor symmetry G_l to G_e and G_ν. One can generalize this idea and consider as G_e or G_ν subgroups of G_l which are generated by elements that are represented by matrices with two degenerate eigenvalues. Then only one of the rows or columns of the PMNS matrix is fixed. This row/column is called "mixing vector" [166]. The authors of [167] have shown that the groups $\Sigma(72 \times 3)$, $\Sigma(216 \times 3)$ and $\Sigma(360 \times 3)$ are

[1] Throughout this chapter we use the values given in the right column of the table 5.1, taken from [30], which are obtained by performing a global fit in which the reactor fluxes have been left free and short baseline reactor data with $L \lesssim 100$ m are included, called "Free Fluxes + RSBL".

[2] The group $\Sigma(36)$ is among the finite groups which can appear as symmetry group of the scalar sector of a three Higgs doublet model without leading to a potential with a continuous symmetry [133].

suitable for realizing a version of minimal flavor violation in the quark sector with a discrete group, since the products of (faithful) three-dimensional representations with their complex conjugates decompose in the same way as in $SU(3)$, i.e. $\mathbf{3} \times \mathbf{3}^\star = \mathbf{1} + \mathbf{8}$ with $\mathbf{8}$ being irreducible in G_l.

We find that the two smaller groups $\Sigma(36 \times 3)$ and $\Sigma(72 \times 3)$ only give rise to a few new mixing patterns, while the larger groups lead to several new patterns, since they have a richer structure of subgroups. Generically one sees (as already suggested by the scans of groups making use of the computer program GAP [166, 168, 169]) that only a very few patterns are well-compatible with the experimental data of all three different mixing angles [30], i.e. for each group one to two. Thus, in explicit models in which one of the other patterns is realized one either has to invoke large corrections to the leading order results in order to reconcile them with the data or one needs to consider modifications of the breaking pattern, such as the one involving a CP symmetry [130, 131]. It is interesting to note that patterns which fit the experimental data better usually do not lead to a non-trivial Dirac phase (although all mixing angles are different from 0 and $\pi/2$).[3] On the other hand, among the patterns associated with the group $\Sigma(216 \times 3)$ we find several ones which give rise to non-vanishing CP violation and at the same time accommodate the solar and atmospheric mixing angles at the 3σ level or better. Only the reactor mixing angle turns out to be too large, see table 7.2. Furthermore, we apply outer automorphisms of the groups $\Sigma(n\varphi)$, $\varphi = 3$, in order to relate their irreducible faithful three-dimensional representations among each other.

This chapter is structured as follows: in section I we review the approach used in order to relate the mixing pattern with the group G_l and its breaking to the subgroups G_e and G_ν in the charged lepton and neutrino sectors. In section II we discuss the mathematical properties of the different groups $\Sigma(n\varphi)$, the representations to which the three generations of left-handed leptons can be assigned to, the relevant Abelian subgroups and the resulting mixing patterns and predictions for mixing angles θ_{ij} and the Jarlskog invariant J_{CP}. We use as figure of merit χ^2 assuming the best fit values and errors of the mixing angles as given in Table (5.1). We also comment on the mixing vectors for each group. We summarize in section III.

I Approach

We briefly review how lepton mixing can be predicted with a non-Abelian discrete flavor symmetry G_l which is, spontaneously or explicitly, broken to two different Abelian subgroups G_e and G_ν in the charged lepton and neutrino sector [107, 108, 120]. We assign the three generations of left-handed leptons to an irreducible three-dimensional representation, because we want to discuss patterns with at least two non-vanishing lepton mixing angles. We furthermore choose the representation to be faithful in the group G_l so that we (mostly) study mixing patterns which originate from this group itself and not from one of its proper subgroups.[4] For fixing the mixing angles we also have to assume that the three generations of left-handed leptons transform as three inequivalent one-dimensional representations under the residual symmetries G_e and G_ν.

[3] Similar observations can also be made in the analyses found in [168–170].

[4] The requirement of faithfulness of the three-dimensional representation also excludes the possibility to choose G_e or G_ν to be non-Abelian, since a faithful representation of G_l usually decomposes into an irreducible representation of dimension larger than one in G_e or G_ν so that a distinction among the three lepton generations becomes impossible.

A possible set of generators of G_e and G_ν is called $g_{e,i}$, $i = 1, 2, ...$ and $g_{\nu,j}$, $j = 1, 2, ...$, respectively.[5] Clearly, these are also elements of the group G_l. The requirement that a subgroup G_e is conserved entails that the combination $m_e m_e^\dagger$ (with the convention $\overline{\Psi}_L m_e \Psi_R$) has to be invariant under the symmetry G_e, i.e.

$$g_{e,i}^\dagger m_e m_e^\dagger g_{e,i} = m_e m_e^\dagger \quad , \quad i = 1, 2, \dots , \tag{7.1}$$

while requiring that G_ν is a symmetry of the neutrino mass matrix m_ν entails that $m_\nu m_\nu^\dagger$ (m_ν itself) is invariant under G_ν for Dirac (Majorana) neutrinos

$$g_{\nu,j}^\dagger m_\nu m_\nu^\dagger g_{\nu,j} = m_\nu m_\nu^\dagger \quad , \quad j = 1, 2, ... \quad \text{or} \quad g_{\nu,j}^T m_\nu g_{\nu,j} = m_\nu \quad , \quad j = 1, 2, \dots . \tag{7.2}$$

For Majorana neutrinos G_ν is strongly constrained, since it has to be (a subgroup of) a Klein symmetry for three generations of neutrinos.

This comes from the fact that, in the case we are considering three generations, the Majorana mass term $M_\nu = (M_\nu)^T$ is invariant under a Klein symmetry [6]. This can simply be explained considering that, in the mass eigenstates basis, the diagonal Majorana mass matrix M_ν^d is left invariant under a transformation S_{ij} such that:

$$S_{ij}^T M_\nu^d S_{ij} = M_\nu^d, \quad \text{with} \quad S_{ij} = \begin{pmatrix} (-1)^i & 0 & 0 \\ 0 & (-1)^j & 0 \\ 0 & 0 & (-1)^{i+j} \end{pmatrix}, \tag{7.3}$$

where i and j can take the values 0 or 1. Obviously there exist three possible matrices S_{10}, S_{01}, S_{11} beside the trivial fourth one, $S_{00} = e$. These four matrices form a Klein group defined as $\{e, S_{10}, S_{01}, S_{11} | e = S_{10}^2 = S_{01}^2 = (S_{10}S_{01})^2 \wedge S_{11} = S_{10}S_{01}\}$. One can also find the explicit form of the symmetry S_{ij} in the basis in which the Majorana neutrino mass matrix is non-diagonal. Since $U_\nu^T M_\nu U_\nu = M_\nu^d$ the one can write:

$$U_\nu^* S_{ij}^T U_\nu^T M_\nu U_\nu S_{ij} U_\nu^T = M_\nu \tag{7.4}$$

thus we can define $\tilde{S}_{ij} = U_\nu S_{ij} U_\nu^T$ as the expression of the matrix that determines the Klein symmetry of the Majorana mass matrix in the basis where the Majorana neutrino mass matrix is non-diagonal. Obviously $\tilde{S}_{ij}$ corresponds to an element belonging to the residual subgroup G_ν and S_{ij} is related to $\tilde{S}_{ij}$ through a unitary transformation.

If neutrinos are Dirac particles, G_ν is subject the same constraint as G_e of the charged lepton sector, i.e. it can be any Abelian group, capable of distinguishing the three generations. In our actual analysis we follow a minimality principle when choosing G_e and G_ν, since we consider all minimal (Abelian) subgroups of the group G_l which allow the distinction of three generations.[7] Furthermore, we wish to focus on those mixing patterns which are associated with the group G_l and not only with one of its subgroups and thus we require that the generators of the subgroups G_e and G_ν give rise to the entire group G_l. We can change basis via the unitary transformations U_e and U_ν so that $g_{e,i}$ and $g_{\nu,j}$ are diagonalized ($g^d_{e\,(\nu),i\,(j)}$ are diagonal matrices), respectively,

[5] In abuse of notation we denote in the following the abstract elements of the groups G_e, G_ν and G_l with the same symbol as their matrix representatives.

[6] We recall also that in the simple case of one generation the Majorana mass term $\bar{\chi}_L m (\chi_L)^c$ is invariant under a change of sign i.e. $\chi \to \chi' = -\chi$.

[7] For example, if a subgroup $G_e = G_1$ is sufficient in order to distinguish among the generations, we do not discuss the case in which $G_e = G_1 \times G_2 \subset G_l$, since the presence of the group $G_2 \subset G_e$ would not add any information as far as lepton mixing is concerned.

$$U_e^\dagger g_{e,i} U_e = g_{e,i}^d \quad , \quad i = 1, 2, ... \quad \text{and} \quad U_\nu^\dagger g_{\nu,j} U_\nu = g_{\nu,j}^d \quad , \quad j = 1, 2, ... \,. \tag{7.5}$$

One can show that also $m_e m_e^\dagger$ and $m_\nu m_\nu^\dagger$ for Dirac (or m_ν for Majorana) neutrinos are diagonalized by U_e and U_ν, respectively. In order to prove this, let us use the expression in eq. (7.5) into the eq. (7.1). We get:

$$(U_e g_{e,i}^d U_e^\dagger)^\dagger m_e m_e^\dagger U_e g_{e,i}^d U_e^\dagger = m_e m_e^\dagger \tag{7.6}$$

therefore we find that $[g_{e,i}^d, U_e^\dagger (m_e m_e^\dagger) U_e] = 0$. This implies that $U_e^\dagger (m_e m_e^\dagger) U_e$ has to be diagonal and that U_e is the matrix that diagonalizes both $m_e m_e^\dagger$ and the element $g_{e,i}$. So, since $m_e m_e^\dagger$ and $m_\nu m_\nu^\dagger$ for Dirac (or m_ν for Majorana) neutrinos are diagonalized by U_e and U_ν, respectively, the PMNS mixing matrix can be derived diagonalizing two elements of the group, namely $g_{e,i}$ and $g_{\nu,i}$ and clearly one obtains:

$$U_{PMNS} = U_e^\dagger U_\nu \,. \tag{7.7}$$

The matrices U_e and U_ν are uniquely determined up to permutations and phases of their column vectors, since we consider a scenario in which the three generations of left-handed leptons are distinguished, but no further assumption or prediction is made about the lepton masses. As a consequence, the PMNS mixing matrix is fixed up to permutations of rows and columns and the multiplication with phase matrices from the left- and the right-hand side. In turn, the mixing angles θ_{ij} can be found considering the absolute values of the elements of the PMNS matrix $|U_{PMNS}|$ (for the notation see the introductory chapter of this thesis). We also determined the value of the Jarlskog invariant J_{CP}, once the octants of the angles are defined. An exchange of the roles of the subgroups G_e and G_ν transforms the PMNS matrix into its hermitian conjugate. Two pairs of subgroups, $\{G_e, G_\nu\}$ and $\{G'_e, G'_\nu\}$, lead to the same result for the PMNS matrix, if their generators $g_{e,i}$, $g_{\nu,j}$ and $g'_{e,i}$, $g'_{\nu,j}$ are related by a similarity transformation [8].

We also consider the case in which the generators of G_e or G_ν are represented by matrices with two degenerate eigenvalues. In this case only one generation can be distinguished from the other two ones and thus only one row or column can be fixed through the choice of G_e, G_ν and G_l. Such a row or column is called "mixing vector" [166].

Up to this point we have not fully specified the three-dimensional representation under which the three generations of left-handed leptons transform, apart from requesting that it should be irreducible and faithful in G_l (definitions can be found in the appendix). However, in general, a group G_l possesses several representations which meet these requirements. If so, we have to analyze whether the results for the mixing patterns do also depend on the choice of the three-dimensional representation and not only on the choice of the groups G_e, G_ν and G_l. One can prove that in all groups $\Sigma(n\varphi)$ the mixing patterns are independent of the actual choice of the representation and that it is thus sufficient to study the mixing patterns for only one of them [66].

[8] In this case in fact if $g'_{e,i} = a_0 g_{e,i} a_0^{-1}$ and $g'_{\nu,j} = a_0 g_{\nu,i} a_0^{-1}$ then using eq. (7.5) we find that the matrices that diagonalize $g'_{e,i}$ and $g'_{\nu,i}$ are respectively $U'_e = a_0 U_e$ and $U'_\nu = a_0 U_\nu$ so $U_{PMNS} = U_e'^\dagger U'_\nu = U_e^\dagger a_0^{-1} a_0 U_\nu = U_e^\dagger U_\nu$.

II Groups $\Sigma(n\varphi)$ and mixing patterns

The four groups we discuss in the following are $\Sigma(36 \times 3)$, $\Sigma(72 \times 3)$, $\Sigma(216 \times 3)$ and $\Sigma(360 \times 3)$. As we show, only the latter group has Klein subgroups, while the three other ones not. Thus, if G_ν is required to be a subgroup of G_l and neutrinos are Majorana particles, only $\Sigma(360 \times 3)$ can be chosen as G_l. In the other cases neutrinos are either Dirac particles or G_ν is only partly contained in G_l (i.e. one of the two Z_2 factors of the Klein group is accidental).

We first present a set of generators for each group together with the relations they have to satisfy. We then focus on the irreducible three-dimensional representations and discuss in some detail why it is sufficient for each of the four groups to only consider one of the representations when deriving the lepton mixing patterns. We detail the different Abelian subgroups of the different $\Sigma(n\varphi)$ with $\varphi = 3$ and comment on those which are admissible as G_e and G_ν, because they are capable of distinguishing the three lepton generations (in our chosen three-dimensional representation), and on those which can only be employed in order to predict a mixing vector. As we will see, the groups $\Sigma(36 \times 3)$, $\Sigma(72 \times 3)$ and $\Sigma(360 \times 3)$ contain Z_2 and Z_6 generating elements which are represented by matrices with partly degenerate eigenvalues, while $\Sigma(216 \times 3)$ also comprises Z_9 generating elements with this property.

We show all patterns which can arise from a certain choice of G_l, G_e and G_ν, following our minimality principle for G_e and G_ν as well as imposing the requirement that the generators of these two groups give rise to the whole group G_l. As explained, the ordering of rows and columns is not fixed by the choice of the subgroups G_e and G_ν. We choose it in the presentation of our results in such a way that the of χ^2 is minimized. The latter is computed using the experimental results for the mixing angles found in [30] and listed in the Introduction:

$$\chi^2 = \sum \left(\frac{\sin^2\theta_{ij}^{num} - \sin^2\theta_{ij}^{bf}}{\sigma_{\theta ij}^{bf}} \right)^2 , \tag{7.8}$$

where we used the numerical values $\sin^2\theta_{ij}^{num}$ obtained using $\tan\theta_{12} = |U_{e2}|/|U_{e1}|$, $\tan\theta_{23} = |U_{\mu 3}|/|U_{\tau 3}|$ and $\sin^2\theta_{13} = |U_{e3}|^2$ (with U denoting the PMNS mixing matrix).

In several occasions we do not only show the pattern with rows and columns permuted in a way that χ^2 is minimized, but we also mention further patterns with a slightly larger χ^2. The exact notion of "slightly larger" depends on the minimal value of the χ^2: for the latter being smaller than 100 we consider patterns with values of χ^2 up to 5% larger than the minimal one, while for a minimal value of χ^2 between 100 and 1000 we only mention patterns with values of χ^2 up to $1\% \div 2\%$ larger than the minimal one. In all cases we additionally require that at least one mixing angle agrees within $3\,\sigma$ with the experimental results [30]. If the minimal value of χ^2 is larger than 1000 we only show the pattern belonging to this value, unless there are two mixing angles which are in accordance with the experimental data within 3σ. If there are two permutations of a pattern leading to a similar χ^2 and we display both, we denote them with the same Roman numeral, but a different letter, e.g. pattern Ia and Ib, as in table 7.1 for the group $\Sigma(216 \times 3)$. It turns out that in all cases the two permutations of a certain pattern are related through the exchange of the second and third rows of the PMNS matrix. Thus, they generally lead to the same reactor and solar mixing angles, while the atmospheric one changes from θ_{23} to $\pi/2 - \theta_{23}$, i.e. $\sin^2\theta_{23}$ is replaced

by $1-\sin^2\theta_{23}$. The tables 7.1, 7.2 and 7.4-7.6 summarize our results for the mixing patterns derived with the groups $\Sigma(216\times 3)$ and $\Sigma(360\times 3)$. We mark mixing angles that are accordance with the experimental data at the 3σ level or better in these tables with a star ($\star$).

II.I Group $\Sigma(36\times 3)$

The group $\Sigma(36\times 3)$ (identification number [[108,15]] in the computer program GAP [171]) has 108 elements and can be represented in terms of three generators a, v and z which fulfill the following relations [172, 173]

$$a^3=e\ ,\ \ v^4=e\ ,\ \ z^3=e\ ,\ \ av^{-1}zv=e\ ,\ \ avz^{-1}v^{-1}=e\ ,\ \ (az)^3=e\ . \tag{7.9}$$

Here and in the following, we denote the neutral element of the group with e. For one of the irreducible faithful three-dimensional representations, identified with $\mathbf{3^{(0)}}$ of [172, 173], the generators are given by the matrices

$$a=\begin{pmatrix}0&1&0\\0&0&1\\1&0&0\end{pmatrix}\ ,\quad v=\frac{1}{\sqrt{3}i}\begin{pmatrix}1&1&1\\1&\omega&\omega^2\\1&\omega^2&\omega\end{pmatrix}\ ,\quad z=\begin{pmatrix}1&0&0\\0&\omega&0\\0&0&\omega^2\end{pmatrix} \tag{7.10}$$

with $\omega=e^{2\pi i/3}$. Note that all generators have determinant $+1$. The group $\Sigma(36\times 3)$ possesses in total eight faithful irreducible three-dimensional representations which form four complex conjugated pairs. The representation matrices of the generators a, v and z in the three other faithful three-dimensional representations $\mathbf{3^{(p)}}$, $\mathrm{p}=1,2,3$, are closely related to a, v and z of $\mathbf{3^{(0)}}$

$$a\ ,\ \ i^{\mathrm{p}}v\ ,\ \ z\quad\text{with}\quad p=1,2,3 \tag{7.11}$$

and those of (the complex conjugated representations) $(\mathbf{3^{(p)}})^\star$, $\mathrm{p}=0,1,2,3$, are obtained through complex conjugation. Apart from these, the irreducible representations of the group are: four one-dimensional representations, two real and two complex ones, and two real four-dimensional representations. Notice that they are all unfaithful in $\Sigma(36\times 3)$. The character table of the group can be found, for example, in [172, 173].

Clearly, the mixing patterns which can be derived by assuming that the three generations of leptons are assigned to any of the representations $\mathbf{3^{(p)}}$ have to coincide with those derived from assigning them to $\mathbf{3^{(0)}}$, since the additional factor i^{p} in the generator v cannot change the eigenvectors. Similarly, all mixing matrices originating from one of the complex conjugated representations $(\mathbf{3^{(p)}})^\star$ are the same as those derived from $\mathbf{3^{(p)}}$, up to complex conjugation[9]. The products of two irreducible three-dimensional representations are of the following type

$$\mathbf{3^{(p_1)}}\times\mathbf{3^{(p_2)}}=(\mathbf{3^{(p_3)}})^\star+(\mathbf{3^{(p_4)}})^\star+(\mathbf{3^{(p_5)}})^\star\quad\text{and}\quad(\mathbf{3^{(p_1)}})\times(\mathbf{3^{(p_2)}})^\star=\mathbf{1^{(q)}}+\mathbf{4}+\mathbf{4'}\ , \tag{7.12}$$

with $\mathrm{p}_i,\mathrm{q}=0,1,2,3$, $i=1,...,5$, especially

$$\mathbf{3^{(0)}}\times\mathbf{3^{(0)}}=(\mathbf{3^{(0)}})^\star+(\mathbf{3^{(1)}})^\star+(\mathbf{3^{(3)}})^\star\quad\text{and}\quad(\mathbf{3^{(0)}})\times(\mathbf{3^{(0)}})^\star=\mathbf{1^{(0)}}+\mathbf{4}+\mathbf{4'}\ . \tag{7.13}$$

[9] This is proven specifically in appendix of [66] where we comment on the outer automorphism group of $\Sigma(36\times 3)$ and the possibility to understand relations among the three-dimensional representations using the latter

Thus, this group does not belong to those singled out in the analysis of [167] as being a suitable candidate for the implementation of a version of minimal flavor violation with a discrete group. Nevertheless, we discuss the mixing patterns which can be derived from $\Sigma(36\times 3)$, since its order is still rather small.

For analyzing all Abelian subgroups of $\Sigma(36\times 3)$ it is convenient to make use of the fact that all elements g of the group $\Sigma(36\times 3)$ can be written, in the three-dimensional representations, in the form

$$g = \omega^o z^\zeta a^\alpha v^\chi \quad \text{with} \quad o,\, \zeta,\, \alpha = 0,1,2\,, \chi = 0,1,2,3 \tag{7.14}$$

and that a representative (again in the three-dimensional representations) for each of the fourteen classes $c_1\,\mathcal{C}_{c_2}$ (with c_1 denoting the number of elements of the class $\mathcal{C}_{c_2}$ and c_2 their order) can be found [172,173]

$$\begin{aligned} &1\,\mathcal{C}_1 \,:\, e \;,\quad 9\,\mathcal{C}_2 \,:\, v^2 \;,\quad 1\,\mathcal{C}_3 \,:\, aza^2z^2 = \omega\, e \;,\quad 1\,\mathcal{C}_3 \,:\, a^2zaz^2 = \omega^2\, e \;, \\ &12\,\mathcal{C}_3 \,:\, z \;,\quad 12\,\mathcal{C}_3 \,:\, za \;,\quad 9\,\mathcal{C}_4 \,:\, v \;,\quad 9\,\mathcal{C}_4 \,:\, v^3 \;,\quad 9\,\mathcal{C}_6 \,:\, \omega\, v^2 \;, \\ &9\,\mathcal{C}_6 \,:\, \omega^2\, v^2 \;,\quad 9\,\mathcal{C}_{12} \,:\, \omega\, v \;,\quad 9\,\mathcal{C}_{12} \,:\, \omega^2\, v \;,\quad 9\,\mathcal{C}_{12} \,:\, \omega\, v^3 \;,\quad 9\,\mathcal{C}_{12} \,:\, \omega^2\, v^3 \;. \end{aligned} \tag{7.15}$$

The Abelian subgroups of $\Sigma(36\times 3)$ are nine Z_2 symmetries, 13 Z_3 symmetries (including C, the center of $SU(3)$), nine Z_4 and nine Z_6 symmetries, as well as nine Z_{12} groups. Furthermore, there are four groups $Z_3\times Z_3$ where, however, one of the two Z_3 groups is the center of $SU(3)$. We have checked that all Z_2 symmetries, all Z_4, all Z_6 and also all Z_{12} symmetries are conjugate to each other. The Z_3 symmetries fall instead into three categories: two with six such symmetries which are conjugated among each other and a third one which comprises only the center of $SU(3)$. Since $\Sigma(36\times 3)$ does not contain a Klein group, neutrinos have to be either Dirac particles or the symmetry of the neutrino sector is only partly contained in G_l. Using the representation matrices in eq.(7.10) we see that 30 elements of $\Sigma(36\times 3)$ are represented by matrices with (at least) two degenerate eigenvalues: the ones belonging to the center of $SU(3)$, the ones generating Z_2 groups as well as the ones generating Z_6 symmetries. Therefore these elements cannot be used as generators of the subgroups G_e and G_ν alone, if we wish to fix all three mixing angles through the breaking of G_l to G_e and G_ν.

With this classification of subgroups of $\Sigma(36\times 3)$ at hand we can distinguish the following cases in which the breaking of the group $\Sigma(36\times 3)$ to G_e and G_ν fixes the mixing pattern: $G_e = Z_3$ and $G_\nu = Z_3$, $G_e = Z_3$ and $G_\nu = Z_4$ or $G_\nu = Z_{12}$, $G_e = Z_4$ or $G_e = Z_{12}$ and $G_\nu = Z_4$ or $G_\nu = Z_{12}$. Out of these possibilities only two categories are interesting and can pass our constraint of generating the entire group $\Sigma(36\times 3)$ with the generators of G_e and G_ν. The first interesting case arises for $G_e = Z_3$ and $G_\nu = Z_4$ or $G_\nu = Z_{12}$. In all admissible cases we find as mixing pattern

$$|U_{PMNS}| = \frac{1}{\sqrt{2(3+\sqrt{3})}} \begin{pmatrix} 1+\sqrt{3} & \sqrt{2} & 0 \\ 1 & \sqrt{2+\sqrt{3}} & \sqrt{3+\sqrt{3}} \\ 1 & \sqrt{2+\sqrt{3}} & \sqrt{3+\sqrt{3}} \end{pmatrix} \approx \begin{pmatrix} 0.888 & 0.460 & 0 \\ 0.325 & 0.628 & 0.707 \\ 0.325 & 0.628 & 0.707 \end{pmatrix} . \tag{7.16}$$

The mixing angles read $\sin^2\theta_{12} \approx 0.211$, $\sin^2\theta_{23} = 0.5$ and $\theta_{13} = 0$. Since the reactor mixing angle vanishes, also the Jarlskog invariant J_{CP} vanishes. The value of χ^2 is $\chi^2 \approx 151.5$ in this case and only the atmospheric mixing angle is in agreement with the experimental results within 3σ. Examples of generators of G_e and G_ν are $g_e = \omega^2 za^2$ and $g_\nu = za^2v$ and $g_\nu = \omega z^2a^2v^3$, respectively. The pattern in eq.(7.16) has been

recently found in a study in which the flavor group $\Delta(27)$ and is combined with a CP symmetry [174].

If G_e and G_ν are instead both Z_4 or Z_{12} subgroups of $\Sigma(36\times3)$ (excluding, obviously, the cases in which G_e and G_ν are the same or one is a subgroup of the other one), we always obtain the pattern

$$|U_{PMNS}| = \frac{1}{2\sqrt{2}} \begin{pmatrix} \sqrt{3+\sqrt{3}} & \sqrt{3} & \sqrt{2-\sqrt{3}} \\ \sqrt{2} & \sqrt{3-\sqrt{3}} & \sqrt{3+\sqrt{3}} \\ \sqrt{3-\sqrt{3}} & \sqrt{2+\sqrt{3}} & \sqrt{3} \end{pmatrix} \approx \begin{pmatrix} 0.769 & 0.612 & 0.183 \\ 0.500 & 0.398 & 0.769 \\ 0.398 & 0.683 & 0.612 \end{pmatrix} \quad (7.17)$$

leading to the mixing angles $\sin^2\theta_{12} \approx 0.388$, $\sin^2\theta_{23} \approx 0.612$ and $\sin^2\theta_{13} \approx 0.033$. Again, J_{CP} vanishes. The value of χ^2 is 69.1. If the second and third rows of the PMNS matrix in eq.(7.17) are exchanged, the atmospheric mixing angle reads $\sin^2\theta_{23} \approx 0.388$ like the solar one and the value of χ^2 slightly increases, $\chi^2 \approx 69.4$. For both patterns only the atmospheric mixing angle agrees within 3σ with the experimental data. Examples for the generators of the groups G_e and G_ν are: if both are Z_4 subgroups, we can take $g_e = za^2v$ and $g_\nu = \omega^2 z^2 a v^3$; if G_e is a Z_4 and G_ν a Z_{12} subgroup, we can use $g_e = za^2v$ and $g_\nu = \omega z^2 a^2 v^3$ (we might also switch the roles of G_e and G_ν and still obtain the same mixing pattern); and for G_e and G_ν being both Z_{12} subgroups, we can choose for example the generators $g_e = \omega z^2 a^2 v^3$ and $g_\nu = \omega^2 z v$. As one can see, all results which can be achieved with a Z_4 symmetry can also be obtained with an appropriate Z_{12} group. This happens, because all Z_{12} generating elements have a matrix representation which can be written as product of a matrix giving rise to a Z_4 generating element and a matrix representing a non-trivial element of the center of $SU(3)$.

Furthermore, we can consider the case in which one of the subgroups G_e or G_ν is generated by an element of $\Sigma(36\times3)$ which has two degenerate eigenvalues, i.e. G_e or G_ν is a Z_2 or Z_6 symmetry. The resulting mixing vectors can take only three possible forms (in absolute values), namely a vector with only one non-vanishing entry, a vector with two equal entries and one vanishing one or a vector equal to the first column of the PMNS matrix shown in eq.(7.17). It is not by chance that the set of mixing vectors arising from Z_2 and Z_6 generating elements is the same, since one check that all Z_6 generating elements are represented by matrices which are products of a matrix representing the generator of a Z_2 and a matrix which represents a non-trivial element of the center of $SU(3)$.

II.II Group $\Sigma(72\times3)$

In order to generate the group $\Sigma(72\times3)$ which has the identification number [[216,88]] in the computer program GAP we add one generator x to the set of generating elements a, v and z of the group $\Sigma(36\times3)$. This additional generator fulfills the relations [172,173]

$$x^2 = z^2v^2 \quad \text{and} \quad x^4 = e\,. \quad (7.18)$$

In the three-dimensional representation, called $\mathbf{3^{(0,0)}}$ in [172,173], the matrices of the generators can be chosen as a, v, z in eq.(7.10) together with

$$x = \frac{1}{\sqrt{3}i} \begin{pmatrix} 1 & 1 & \omega^2 \\ 1 & \omega & \omega \\ \omega & 1 & \omega \end{pmatrix}\,. \quad (7.19)$$

Notice also the matrix representative of the element x has determinant $+1$. This representation is one of the eight faithful irreducible three-dimensional representations of $\Sigma(72\times 3)$ which form four complex conjugated pairs $\mathbf{3^{(p_1,p_2)}}$ and $(\mathbf{3^{(p_1,p_2)}})^\star$ with $\mathrm{p}_{1,2}=0,1$. The representation matrices of the generators a, v, z and x in the three-dimensional representations $\mathbf{3^{(p_1,p_2)}}$ are given by

$$a\ ,\ \ (-1)^{\mathrm{p}_1}v\ ,\ \ (-1)^{\mathrm{p}_2}x\ ,\ \ z\quad\text{with}\quad \mathrm{p}_{1,2}=0,1 \tag{7.20}$$

and those of $(\mathbf{3^{(p_1,p_2)}})^\star$ by the complex conjugated representation matrices. Like in the case of the three-dimensional representations of the group $\Sigma(36\times 3)$ this shows that $\mathbf{3^{(p_1,p_2)}}$ and $(\mathbf{3^{(p_1,p_2)}})^\star$, $\mathrm{p}_{1,2}=0,1$, all must lead to the same results for the mixing patterns. Apart from $\mathbf{3^{(p_1,p_2)}}$ and $(\mathbf{3^{(p_1,p_2)}})^\star$ the group contains four one-dimensional, one two-dimensional, one eight-dimensional and two six-dimensional irreducible representations. The latter two are complex conjugated and faithful, while the former ones are all real and unfaithful. The character table of $\Sigma(72\times 3)$ can be found in [172,173].

The generic form of the products among two three-dimensional representations is like in $SU(3)$, i.e.

$$\mathbf{3^{(p_{1,1},p_{2,1})}}\times\mathbf{3^{(p_{1,2},p_{2,2})}}=(\mathbf{3^{(q_1,q_2)}})^\star+\mathbf{6}^\star\quad\text{and}\quad \mathbf{3^{(p_{1,1},p_{2,1})}}\times(\mathbf{3^{(p_{1,2},p_{2,2})}})^\star=\mathbf{1^{(q_1,q_2)}}+\mathbf{8}\ , \tag{7.21}$$

with $\mathrm{q}_1=\mathrm{p}_{1,1}+\mathrm{p}_{1,2}\bmod 2$ and $\mathrm{q}_2=\mathrm{p}_{2,1}+\mathrm{p}_{2,2}\bmod 2$, $\mathrm{p}_{i,j}=0,1$, especially we have

$$\mathbf{3^{(0,0)}}\times\mathbf{3^{(0,0)}}=(\mathbf{3^{(0,0)}})^\star+\mathbf{6}^\star\quad\text{and}\quad \mathbf{3^{(0,0)}}\times(\mathbf{3^{(0,0)}})^\star=\mathbf{1^{(0,0)}}+\mathbf{8}\ . \tag{7.22}$$

All elements g, in the three-dimensional representations, can be uniquely written in the form

$$g=\omega^o z^\zeta a^\alpha v^\chi x^\xi\quad\text{with}\quad o,\,\zeta,\,\alpha=0,1,2\ ,\ \chi=0,1,2,3\ ,\ \xi=0,1\ . \tag{7.23}$$

Also here we display, for convenience, a representative (again in the three-dimensional representations) of each of the sixteen classes [172,173]

$$\begin{aligned}&1\,\mathcal{C}_1\ :\ e\ ,\quad 9\,\mathcal{C}_2\ :\ v^2\ ,\quad 1\,\mathcal{C}_3\ :\ aza^2z^2=\omega\,e\ ,\quad 1\,\mathcal{C}_3\ :\ a^2zaz^2=\omega^2\,e\ ,\\ &24\,\mathcal{C}_3\ :\ z\ ,\quad 18\,\mathcal{C}_4\ :\ v\ ,\quad 18\,\mathcal{C}_4\ :\ x\ ,\quad 18\,\mathcal{C}_4\ :\ \omega^2\,vx\ ,\quad 9\,\mathcal{C}_6\ :\ \omega\,v^2\ ,\\ &9\,\mathcal{C}_6\ :\ \omega^2\,v^2\ ,\quad 18\,\mathcal{C}_{12}\ :\ \omega\,v\ ,\quad 18\,\mathcal{C}_{12}\ :\ \omega^2\,v\ ,\quad 18\,\mathcal{C}_{12}\ :\ \omega\,x\ ,\quad 18\,\mathcal{C}_{12}\ :\ \omega^2\,x\ ,\\ &18\,\mathcal{C}_{12}\ :\ vx\ ,\quad 18\,\mathcal{C}_{12}\ :\ \omega\,vx\ .\end{aligned} \tag{7.24}$$

Similarly to what we have seen for the representation $\mathbf{3^{(0)}}$ of the group $\Sigma(36\times 3)$ also here 30 elements of the group are represented by matrices with at least two degenerate eigenvalues and clearly these coincide with those already found for $\Sigma(36\times 3)$. The Abelian subgroups of $\Sigma(72\times 3)$ are: nine Z_2 symmetries, 13 Z_3 symmetries, 27 Z_4 groups, nine Z_6 symmetries, 27 Z_{12} groups as well as four $Z_3\times Z_3$ groups. The Z_2 and Z_6 groups are all conjugate to each other, while the Z_3 symmetries form two categories (one with twelve members and the second one containing the center of $SU(3)$ only). The Z_4 groups and the Z_{12} groups fall into three categories with nine members each which are conjugate to each other. In the following we will not use the four $Z_3\times Z_3$ groups as G_e or G_ν, since one of the Z_3 factors is the center of $SU(3)$. As one can see, also $\Sigma(72\times 3)$ does not possess Klein subgroups.

Considering all possible admissible choices for the generators of the groups G_e and G_ν we see that they have to be either both Z_4 subgroups or Z_{12} subgroups of $\Sigma(72\times 3)$

or one is a Z_4, while the other one is a Z_{12} subgroup. In all other cases the generators of G_e and G_ν cannot give rise to the entire group $\Sigma(72\times 3)$. The mixing pattern arising from the admissible combinations is uniquely determined to be of the form

$$|U_{PMNS}| = \frac{1}{2\sqrt{2}} \begin{pmatrix} \sqrt{3+\sqrt{3}} & \sqrt{4-\sqrt{3}} & 1 \\ \sqrt{2} & \sqrt{3+\sqrt{3}} & \sqrt{3-\sqrt{3}} \\ \sqrt{3-\sqrt{3}} & 1 & \sqrt{4+\sqrt{3}} \end{pmatrix} \approx \begin{pmatrix} 0.769 & 0.532 & 0.354 \\ 0.500 & 0.769 & 0.398 \\ 0.398 & 0.354 & 0.846 \end{pmatrix} . \tag{7.25}$$

For the mixing angles follows $\sin^2\theta_{12} \approx 0.324$, $\sin^2\theta_{23} \approx 0.181$ and $\sin^2\theta_{13} = 0.125$. Consequently, the value of χ^2 is very large, $\chi^2 \approx 1984.1$, and only the solar mixing angle turns out to be within the 3σ range of the global fit [30]. Similar results are found, if the second and third rows of the PMNS matrix in eq.(7.25) are exchanged or the transpose (hermitian conjugate) of this matrix is considered as PMNS matrix. One interesting feature of this mixing matrix is that the Jarlskog invariant does not vanish: $|J_{CP}| = \sqrt{3}/32 \approx 0.0541$. Examples of generators g_e and g_ν of the subgroups G_e and G_ν are: for both G_e and G_ν being Z_4 groups, $g_e = \omega^2 z^2 a^2 x$ and $g_\nu = z a^2 v$ can be chosen; for both G_e and G_ν being Z_{12} subgroups, we can take $g_e = zvx$ and $g_\nu = z^2 a v^2 x$, while for G_e being a Z_4 and G_ν a Z_{12} subgroup one possible combination of generators is $g_e = \omega^2 z^2 a^2 x$ and $g_\nu = zvx$. If G_e or G_ν is a Z_2 or a Z_6 subgroup, we can only fix one row or column of the PMNS matrix and the resulting mixing vectors coincide, as expected, with those found for the group $\Sigma(36\times 3)$. The observations which have been made for the matrices representing Z_4 and Z_{12} and Z_2 and Z_6 generating elements, respectively, in $\Sigma(36\times 3)$ are also valid in the case of the group $\Sigma(72\times 3)$ and thus clearly the pattern in eq.(7.25) can be achieved with Z_4 or Z_{12} subgroups and the mixing vectors arising from matrices representing Z_2 or Z_6 generating elements are the same.

II.III Group $\Sigma(216\times 3)$

If we add the element w which fulfills the relations [172, 173]

$$w^9 = e \ , \quad w^{-1} a w = z a \ , \quad w^{-1} v^2 w = z v^2 \tag{7.26}$$

to the generators a, v and z of the group $\Sigma(36\times 3)$, we arrive at the group $\Sigma(216\times 3)$ (identification number [[648, 532]] in GAP). Note that $x = wvw^{-1}$, see eqs.(7.18,7.19), is also an element of this group. For one of the faithful three-dimensional representations, denoted by $\mathbf{3^{(0)}}$ in [172, 173], we choose the generators a, v, z and w to be represented by the matrices found in eq.(7.10) and

$$w = \begin{pmatrix} \epsilon & 0 & 0 \\ 0 & \epsilon & 0 \\ 0 & 0 & \epsilon\,\omega \end{pmatrix} \tag{7.27}$$

with $\epsilon = e^{4\pi i/9}$. Since $zw = wz$ holds, both generators z and w can be represented by diagonal matrices. Notice also that $w^3 = \omega^2 e$ in the three-dimensional representation $\mathbf{3^{(0)}}$. The group $\Sigma(216\times 3)$ possesses in total seven irreducible three-dimensional representations: one of them, $\mathbf{3^{(a)}}$, is unfaithful and real, while the six other ones are faithful and form three pairs of complex conjugated representations $\mathbf{3^{(p)}}$ and $(\mathbf{3^{(p)}})^\star$, p = 0, 1, 2. The representation matrices of the three faithful representations $\mathbf{3^{(p)}}$ can be chosen as

$$a \ , \quad v \ , \quad \omega^p\, w \ , \quad z \quad \text{with} \quad \mathrm{p} = 0, 1, 2 \ . \tag{7.28}$$

As is obvious from this, we can constrain ourselves to only consider the representation $\mathbf{3^{(0)}}$ in our analysis of the mixing patterns. Apart from these $\Sigma(216\times 3)$ contains three one-, three two- and three eight-dimensional representations, which are organized as one real representation and one complex conjugated pair. All these representations are unfaithful, while the three complex conjugated pairs of six-dimensional and the pair of nine-dimensional representations are faithful in $\Sigma(216\times 3)$.

The structure of the products of the faithful three-dimensional representations is similar to the ones of the fundamental representation of $SU(3)$

$$\mathbf{3^{(p_1)}}\times\mathbf{3^{(p_2)}}=(\mathbf{3^{(q_1)}})^\star+(\mathbf{6^{(q_1)}})^\star \quad\text{and}\quad \mathbf{3^{(p_1)}}\times(\mathbf{3^{(p_2)}})^\star=\mathbf{1^{(q_2)}}+\mathbf{8^{(q_2)}} \tag{7.29}$$

with $\mathrm{q_1}=-\mathrm{p_1}-\mathrm{p_2}\bmod 3$, $\mathrm{q_2}=\mathrm{p_1}-\mathrm{p_2}\bmod 3$ and $\mathrm{p_{1,2}}=0,1,2$. Especially, we have

$$\mathbf{3^{(0)}}\times\mathbf{3^{(0)}}=(\mathbf{3^{(0)}})^\star+(\mathbf{6^{(0)}})^\star \quad\text{and}\quad \mathbf{3^{(0)}}\times(\mathbf{3^{(0)}})^\star=\mathbf{1^{(0)}}+\mathbf{8^{(0)}}\,. \tag{7.30}$$

All elements g of the group $\Sigma(216\times 3)$ can be written, at least in the faithful three-dimensional representations, as

$$g=\omega^o z^\zeta a^\alpha v^\chi x^\xi w^\kappa \quad\text{with}\quad o,\,\zeta,\,\alpha,\,\kappa=0,1,2\,,\ \chi=0,1,2,3\,,\ \xi=0,1 \tag{7.31}$$

We mention one representative (in the faithful three-dimensional representations) for each of the 24 classes of this group [172, 173]

$$\begin{aligned}
&1\,\mathcal{C}_1\ :\ e\ ,\quad 9\,\mathcal{C}_2\ :\ v^2\ ,\quad 1\,\mathcal{C}_3\ :\ aza^2z^2=\omega\,e\ ,\quad 1\,\mathcal{C}_3\ :\ a^2zaz^2=\omega^2\,e\ ,\\
&24\,\mathcal{C}_3\ :\ z\ ,\quad 72\,\mathcal{C}_3\ :\ aw\ ,\quad 72\,\mathcal{C}_3\ :\ aw^2\ ,\quad 54\,\mathcal{C}_4\ :\ v\ ,\quad 9\,\mathcal{C}_6\ :\ \omega\,v^2\ ,\\
&9\,\mathcal{C}_6\ :\ \omega^2\,v^2\ ,\quad 12\,\mathcal{C}_9\ :\ w\ ,\quad 12\,\mathcal{C}_9\ :\ \omega\,w\ ,\quad 12\,\mathcal{C}_9\ :\ \omega^2\,w\ ,\\
&12\,\mathcal{C}_9\ :\ w^2\ ,\quad 12\,\mathcal{C}_9\ :\ \omega\,w^2\ ,\quad 12\,\mathcal{C}_9\ :\ \omega^2\,w^2\ ,\quad 54\,\mathcal{C}_{12}\ :\ \omega\,v\ ,\\
&54\,\mathcal{C}_{12}\ :\ \omega^2\,v\ ,\quad 36\,\mathcal{C}_{18}\ :\ v^2w\ ,\quad 36\,\mathcal{C}_{18}\ :\ \omega\,v^2w\ ,\quad 36\,\mathcal{C}_{18}\ :\ \omega^2\,v^2w\ ,\\
&36\,\mathcal{C}_{18}\ :\ vw^2\ ,\quad 36\,\mathcal{C}_{18}\ :\ \omega\,vw^2\ ,\quad 36\,\mathcal{C}_{18}\ :\ \omega^2\,vw^2\ .
\end{aligned} \tag{7.32}$$

Most of the Abelian subgroups of $\Sigma(216\times 3)$ form one category in which all members are conjugate to each other: the nine Z_2 subgroups, the 27 Z_4 groups, the nine Z_6 groups, the twelve Z_9 symmetries, the 27 Z_{12} groups as well as the 36 Z_{18} symmetries. Only the 85 Z_3 groups instead form three categories of conjugated groups: one which only contains the center of $SU(3)$, one with twelve members and the third one which comprises 72 Z_3 groups. Apart from these there are further Abelian subgroups, $Z_3\times Z_3$ and $Z_3\times Z_9$, in which however one/the Z_3 factor is always given by the center of $SU(3)$ so that these groups are not relevant for our discussion. Notice also the group $\Sigma(216\times 3)$ does not possess Klein subgroups and as consequence, neutrinos have to be either Dirac particles or G_ν can only be partly contained in $G_l=\Sigma(216\times 3)$. 102 elements of this group are represented by matrices with at least two degenerate eigenvalues in the representation $\mathbf{3^{(0)}}$: these are the elements of the center of $SU(3)$, all Z_2 generating, all Z_6 as well as all Z_9 generating elements. All these cannot function as generators of the groups G_e and G_ν; at least not alone, since the three generations of left-handed leptons cannot be distinguished in this way.

In table 7.1 and 7.2 on the next two pages we show the permutations of the mixing patterns with the smallest values of χ^2 for all combinations of subgroups G_e and G_ν which pass our constraints (i.e. their generators give rise to the entire group $\Sigma(216\times 3)$ and they allow to distinguish the three generations). As one can see, only two patterns

Ia and Ib agree well with the experimental results for all mixing angles so that they can be considered as a good leading order form which only requires modest corrections in order to achieve full accordance with the experimental data. Three of the patterns lead to atmospheric and solar mixing angles which agree within 3σ with the experimental data (i.e. both these angles carry a star ($\star$)), while for the reactor mixing angle there is only one such pattern, pattern V. Patterns with smaller values of χ^2, e.g. $\chi^2 \lesssim 200$, do not lead to a non-trivial Dirac phase, although all mixing angles are non-zero in the majority of the cases. On the other hand, patterns with larger χ^2 in general give rise to non-vanishing J_{CP} and thus CP violation. Interestingly, almost all patterns VIIa through Xb accommodate both, solar and atmospheric, mixing angles well; however, the value of $\sin^2\theta_{13}$ is too large (in all cases this one is still at least a factor of two smaller than the other two $\sin^2\theta_{ij}$). However, the pattern with the smallest value of χ^2 ($\chi^2 \approx 10.6$) is obtained for $G_e = Z_3$ and $G_\nu = Z_{18}$. We do not list this case in tables 7.1 and 7.2, since the generators of G_e and G_ν do not give rise to the whole group $\Sigma(216 \times 3)$, but only a group of order 162 with the mathematical structure $((Z_9 \times Z_3) \rtimes Z_3) \rtimes Z_2$. It is denoted by [[162, 14]] in the computer program GAP. The mixing pattern reads

$$|U_{PMNS}| = \frac{1}{\sqrt{6}} \begin{pmatrix} 2c_{18} & \sqrt{2} & 2s_{18} \\ c_{18} - \sqrt{3}s_{18} & \sqrt{2} & \sqrt{3}c_{18} + s_{18} \\ c_{18} + \sqrt{3}s_{18} & \sqrt{2} & \sqrt{3}c_{18} - s_{18} \end{pmatrix} \approx \begin{pmatrix} 0.804 & 0.577 & 0.142 \\ 0.279 & 0.577 & 0.767 \\ 0.525 & 0.577 & 0.625 \end{pmatrix} \quad (7.33)$$

where we have defined $s_{18} = \sin\pi/18 \approx 0.174$ and $c_{18} = \cos\pi/18 \approx 0.985$. The resulting mixing angles are: $\sin^2\theta_{12} \approx 0.340$, $\sin^2\theta_{23} \approx 0.601$ and $\sin^2\theta_{13} \approx 0.020$ so that only the value of the solar mixing angle is marginally outside the 3σ range [30]. The Jarlskog invariant vanishes and thus the Dirac phase is trivial. A fit with a value of χ^2 only slightly larger than the optimal one, $\chi^2 \approx 10.8$, can be achieved, if the second and third rows are exchanged in the PMNS matrix in eq.(7.33). Then the atmospheric mixing angle is determined to be $\sin^2\theta_{23} \approx 0.399$ which is well within the 3σ range of [30]. Note that the PMNS matrix in eq.(7.33) can be written as the product of the TBM mixing matrix and a rotation in the (13)-plane by the angle $\theta = -\pi/18$: $|U_{PMNS}| = |U_{TBM}R_{13}(-\pi/18)|$. If we exchange the second and third rows in eq.(7.33), θ has to change sign, $\theta = \pi/18$.[10] Such type of pattern has already been found [120, 121, 168, 170], when studying groups belonging to the series $\Delta(6n^2)$, $n \in \mathbb{N}$.

In [120, 121] it has been suggested that there might be a general rule, namely for $G_e = Z_3$, $G_\nu = Z_{2n}$ and $G_l = \Delta(6n^2)$ the angle θ reads $\theta = \pm\pi/(2n)$. In our case one would have to choose $n = 9$ and indeed the group [[162,14]] is a subgroup of $\Delta(6n^2)$ for $n = 9$. As example for the generators g_e and g_ν of G_e and G_ν, respectively, we can take $g_e = \omega^2 z^2 a v^3 x w$ and $g_\nu = a^2 v x w$. We note that the first column of the matrix in eq.(7.33) has been considered as mixing vector in [166], while the authors of [168] found the same mixing pattern in their scan for the group $(Z_{18} \times Z_6) \rtimes S_3$ (which has the identification number [[648,259]] in GAP), assuming that neutrinos are Majorana particles and G_e is a Z_3 symmetry. Very recently, the same authors have performed a scan of smaller groups allowing neutrinos to be Dirac particles [169]. They also find the pattern in eq.(7.33) for the group with the identification number [[162,14]] in GAP.

Assuming that one of the groups G_e or G_ν is generated by an element with order 2 or 6 which is represented by a matrix with two degenerate eigenvalues in the representation $\mathbf{3^{(0)}}$, we find as mixing vectors those which have already been found for the group

[10] We use here the same conventions as used in [120, 121] for the signs in the TBM mixing matrix U_{TBM} and for the definition of the angle θ.

$\Sigma(36 \times 3)$ and three additional ones that are: a vector which coincides (in absolute values) with the second column of pattern Ia found in the tables 7.1 and 7.2, a vector whose form is the one of the first row of pattern II and a vector with a form equal to the one of the second column of pattern III. The last mixing vector has also been considered in [166] and found for the groups with identification numbers [[162,14]] and [[486,61]] in GAP, respectively. If we choose G_e or G_ν to be generated by an element of order 9, we find instead eight possible mixing vectors: a vector with only one non-vanishing entry and a vector with two equal entries (as regards the absolute value) and one vanishing one (these two are in common with the mixing vectors derived from $\Sigma(36 \times 3)$), a tri-maximal mixing vector, a vector with the same absolute values as the second and third rows of the TBM mixing matrix, a vector which coincides (in absolute values) with the third row of pattern Ia, a vector equal to the third column of pattern II, a vector of the same form as the first column of pattern III and a vector equal to the third column in pattern IV. The vector coinciding with the first column of pattern III equals the columns, up to permutations, of a pattern mentioned in [174], which comprises an analysis of the mixing matrices arising from the flavor group $\Delta(27)$ and a CP symmetry.

As expected, we also find in our analysis of the patterns and mixing vectors of the group $\Sigma(216 \times 3)$ that Z_4 and Z_{12} subgroups lead to the same patterns, if chosen as subgroups, and the representation matrices of Z_2 and Z_6 generating elements are related via the matrices representing the non-trivial elements of the center of $SU(3)$.

Table 7.1: Mixing patterns associated with $\Sigma(216\times 3)$. We mention the patterns, the subgroups G_e and G_ν, an example of their generators, the absolute value of J_{CP}, the sine squares of the mixing angles as well as the value of χ^2. In all cases g_e and g_ν generate $\Sigma(216\times 3)$. Note that we only give one example of g_e and g_ν. Analytic expressions of the patterns are given if sufficiently simple. We use as figure of merit χ^2, computed with the results of the global fit in [30] in table 1 in which the reactor fluxes have been left free and short baseline reactor data are included (called "Free Fluxes + RSBL"). We always display the permutation of the pattern with the minimum value of χ^2. We show more than one permutation, if the χ^2 value of the further pattern(s) is very close to the minimum one. A star ($\star$) next to a result for a mixing angle $\sin^2\theta_{ij}$ indicates that its contribution to the χ^2 value is less than 9 which is equivalent to being within in the experimental 3σ interval. See the text for more details.

#	Pattern	(G_e, G_ν)	Example of (g_e, g_ν)	$\lvert J_{CP}\rvert$	$(\sin^2\theta_{12}, \sin^2\theta_{23}, \sin^2\theta_{13})$	χ^2
Ia	$\frac{1}{2\sqrt{2(3+\sqrt{3})}}\begin{pmatrix}\sqrt{2}(2+\sqrt{3}) & \sqrt{2(3+\sqrt{3})} & -1+\sqrt{3}\\ \sqrt{6} & \sqrt{2(3+\sqrt{3})} & 3+\sqrt{3}\\ 2 & 2\sqrt{3+\sqrt{3}} & 2\sqrt{2+\sqrt{3}}\end{pmatrix} \approx \begin{pmatrix}0.858 & 0.500 & 0.119\\ 0.398 & 0.500 & 0.769\\ 0.325 & 0.707 & 0.628\end{pmatrix}$	(Z_{18}, Z_4) (Z_{18}, Z_{12})	$(\omega^2 zavxw,\, v)$	0	$\sin^2\theta_{12}\approx 0.254$ $\sin^2\theta_{23} = 0.600\star$ $\sin^2\theta_{13}\approx 0.014$	28.3
Ib	$\frac{1}{2\sqrt{2(3+\sqrt{3})}}\begin{pmatrix}\sqrt{2}(2+\sqrt{3}) & \sqrt{2(3+\sqrt{3})} & -1+\sqrt{3}\\ 2 & 2\sqrt{3+\sqrt{3}} & 2\sqrt{2+\sqrt{3}}\\ \sqrt{6} & \sqrt{2(3+\sqrt{3})} & 3+\sqrt{3}\end{pmatrix} \approx \begin{pmatrix}0.858 & 0.500 & 0.119\\ 0.325 & 0.707 & 0.628\\ 0.398 & 0.500 & 0.769\end{pmatrix}$	(Z_{18}, Z_4) (Z_{18}, Z_{12})	$(\omega^2 zavxw,\, v)$	0	$\sin^2\theta_{12}\approx 0.254$ $\sin^2\theta_{23} = 0.400\star$ $\sin^2\theta_{13}\approx 0.014$	28.5
II	$\frac{1}{2\sqrt{3}}\begin{pmatrix}3 & \sqrt{3} & 0\\ \sqrt{2} & \sqrt{6} & 2\\ 1 & \sqrt{3} & 2\sqrt{2}\end{pmatrix} \approx \begin{pmatrix}0.866 & 0.500 & 0\\ 0.408 & 0.707 & 0.577\\ 0.289 & 0.500 & 0.816\end{pmatrix}$	(Z_{18}, Z_{18})	(za^2v^2xw, zv^2w)	0	$\sin^2\theta_{12} = 0.250$ $\sin^2\theta_{23}\approx 0.333$ $\sin^2\theta_{13} = 0$	120.8
III	$\begin{pmatrix}0.844 & 0.525 & 0.110\\ 0.449 & 0.804 & 0.390\\ 0.293 & 0.279 & 0.914\end{pmatrix}$	(Z_3, Z_{18})	$(\omega^2 z^2 av^3xw,\, z^2v^3w)$	0	$\sin^2\theta_{12}\approx 0.279\star$ $\sin^2\theta_{23}\approx 0.154$ $\sin^2\theta_{13}\approx 0.012$	131.2
IV	$\frac{1}{2\sqrt{3+\sqrt{3}}}\begin{pmatrix}\sqrt{3(3+\sqrt{3})} & \sqrt{3+\sqrt{3}} & 0\\ \sqrt{2+\sqrt{3}} & \sqrt{3(2+\sqrt{3})} & 2\\ 1 & \sqrt{3} & 2\sqrt{2+\sqrt{3}}\end{pmatrix} \approx \begin{pmatrix}0.866 & 0.500 & 0.\\ 0.444 & 0.769 & 0.460\\ 0.230 & 0.398 & 0.888\end{pmatrix}$	(Z_4, Z_{18}) (Z_{12}, Z_{18})	$(v,\, z^2v^2w)$	0	$\sin^2\theta_{12} = 0.250$ $\sin^2\theta_{23}\approx 0.211$ $\sin^2\theta_{13} = 0$	175.7
V	$\begin{pmatrix}0.804 & 0.578 & 0.139\\ 0.525 & 0.800 & 0.290\\ 0.279 & 0.160 & 0.947\end{pmatrix}$	(Z_3, Z_4) (Z_3, Z_{12})	$(\omega^2 vw,\, v)$	0	$\sin^2\theta_{12}\approx 0.341$ $\sin^2\theta_{23}\approx 0.086$ $\sin^2\theta_{13}\approx 0.019\star$	182.7

Table 7.2: Mixing patterns associated with $\Sigma(216 \times 3)$. For further details see the caption of table 7.1 and the text.

#	Pattern	(G_e, G_ν)	Example of (g_e, g_ν)	$\lvert J_{CP}\rvert$	$(\sin^2\theta_{12}, \sin^2\theta_{23}, \sin^2\theta_{13})$	χ^2
VIa	$\begin{pmatrix} 0.874 & 0.429 & 0.228 \\ 0.429 & 0.621 & 0.657 \\ 0.228 & 0.657 & 0.719 \end{pmatrix}$	(Z_3, Z_3)	$(\omega z^2 a^2 xw, \omega^2 z^2 a v^3 xw)$	0.0321	$\sin^2\theta_{12} \approx 0.194$ $\sin^2\theta_{23} \approx 0.455\star$ $\sin^2\theta_{13} \approx 0.052$	231.7
VIb	$\begin{pmatrix} 0.874 & 0.429 & 0.228 \\ 0.228 & 0.657 & 0.719 \\ 0.429 & 0.621 & 0.657 \end{pmatrix}$	(Z_3, Z_3)	$(\omega z^2 a^2 xw, \omega^2 z^2 a v^3 xw)$	0.0321	$\sin^2\theta_{12} \approx 0.194$ $\sin^2\theta_{23} \approx 0.545\star$ $\sin^2\theta_{13} \approx 0.052$	235.5
VIIa	$\begin{pmatrix} 0.804 & 0.525 & 0.279 \\ 0.483 & 0.445 & 0.754 \\ 0.346 & 0.726 & 0.595 \end{pmatrix}$	(Z_4, Z_3) (Z_{12}, Z_3)	$(v,\ \omega z^2 a^2 xw)$	$\frac{1}{24} \approx 0.0417$	$\sin^2\theta_{12} \approx 0.299\star$ $\sin^2\theta_{23} \approx 0.616\star$ $\sin^2\theta_{13} \approx 0.078$	554.6
VIIb	$\begin{pmatrix} 0.804 & 0.525 & 0.279 \\ 0.346 & 0.726 & 0.595 \\ 0.483 & 0.445 & 0.754 \end{pmatrix}$	(Z_4, Z_3) (Z_{12}, Z_3)	$(v,\ \omega z^2 a^2 xw)$	$\frac{1}{24} \approx 0.0417$	$\sin^2\theta_{12} \approx 0.299\star$ $\sin^2\theta_{23} \approx 0.384\star$ $\sin^2\theta_{13} \approx 0.078$	554.9
VIII	$\begin{pmatrix} 0.804 & 0.525 & 0.279 \\ 0.517 & 0.723 & 0.458 \\ 0.293 & 0.449 & 0.844 \end{pmatrix}$	(Z_{18}, Z_3)	$(za^2 v^2 xw,\ \omega^2 z^2 a v^3 xw)$	$\frac{1}{12\sqrt{3}} \approx 0.0481$	$\sin^2\theta_{12} \approx 0.299\star$ $\sin^2\theta_{23} \approx 0.227$ $\sin^2\theta_{13} \approx 0.078$	608.7
IXa	$\frac{1}{2\sqrt{6}} \begin{pmatrix} \sqrt{3(3+\sqrt{3})} & \sqrt{9-\sqrt{3}} & \sqrt{2(3-\sqrt{3})} \\ \sqrt{3(3-\sqrt{3})} & \sqrt{9+\sqrt{3}} & \sqrt{2(3+\sqrt{3})} \\ \sqrt{6} & \sqrt{6} & 2\sqrt{3} \end{pmatrix} \approx \begin{pmatrix} 0.769 & 0.550 & 0.325 \\ 0.398 & 0.669 & 0.628 \\ 0.500 & 0.500 & 0.707 \end{pmatrix}$	(Z_4, Z_{18}) (Z_{12}, Z_{18})	$(v,\ za^2 v^2 xw)$	$\frac{1}{16} = 0.0625$	$\sin^2\theta_{12} \approx 0.339\star$ $\sin^2\theta_{23} \approx 0.441\star$ $\sin^2\theta_{13} \approx 0.106$	1255.5
IXb	$\frac{1}{2\sqrt{6}} \begin{pmatrix} \sqrt{3(3+\sqrt{3})} & \sqrt{9-\sqrt{3}} & \sqrt{2(3-\sqrt{3})} \\ \sqrt{6} & \sqrt{6} & 2\sqrt{3} \\ \sqrt{3(3-\sqrt{3})} & \sqrt{9+\sqrt{3}} & \sqrt{2(3+\sqrt{3})} \end{pmatrix} \approx \begin{pmatrix} 0.769 & 0.550 & 0.325 \\ 0.5 & 0.5 & 0.707 \\ 0.398 & 0.669 & 0.628 \end{pmatrix}$	(Z_4, Z_{18}) (Z_{12}, Z_{18})	$(v,\ za^2 v^2 xw)$	$\frac{1}{16} = 0.0625$	$\sin^2\theta_{12} \approx 0.339\star$ $\sin^2\theta_{23} \approx 0.559\star$ $\sin^2\theta_{13} \approx 0.106$	1257.5
Xa	$\frac{1}{2\sqrt{3}} \begin{pmatrix} \sqrt{7} & \sqrt{3} & \sqrt{2} \\ \sqrt{3} & \sqrt{3} & \sqrt{6} \\ \sqrt{2} & \sqrt{6} & 2 \end{pmatrix} \approx \begin{pmatrix} 0.764 & 0.500 & 0.408 \\ 0.500 & 0.500 & 0.707 \\ 0.408 & 0.707 & 0.577 \end{pmatrix}$	(Z_{18}, Z_{18})	$(za^2 v^2 xw,\ za^2 v^3 w)$	$\frac{1}{8\sqrt{3}} \approx 0.0722$	$\sin^2\theta_{12} = 0.300\star$ $\sin^2\theta_{23} = 0.600\star$ $\sin^2\theta_{13} \approx 0.167$	3753.2
Xb	$\frac{1}{2\sqrt{3}} \begin{pmatrix} \sqrt{7} & \sqrt{3} & \sqrt{2} \\ \sqrt{2} & \sqrt{6} & 2 \\ \sqrt{3} & \sqrt{3} & \sqrt{6} \end{pmatrix} \approx \begin{pmatrix} 0.764 & 0.500 & 0.408 \\ 0.408 & 0.707 & 0.577 \\ 0.500 & 0.500 & 0.707 \end{pmatrix}$	(Z_{18}, Z_{18})	$(za^2 v^2 xw,\ za^2 v^3 w)$	$\frac{1}{8\sqrt{3}} \approx 0.0722$	$\sin^2\theta_{12} = 0.300\star$ $\sin^2\theta_{23} = 0.400\star$ $\sin^2\theta_{13} \approx 0.167$	3753.4

II.IV Group $\Sigma(360 \times 3)$

The last group we discuss is $\Sigma(360 \times 3)$ which has 1080 elements. Its identification number in the computer program GAP is [[1080,260]]. We can define it in terms of four generators a, f, h and q. The relations they fulfill can be found in [132]

$$\begin{aligned} &a^3 = e\ ,\ \ f^2 = e\ ,\ \ h^2 = e\ ,\ \ q^2 = e\ , \\ &(fq)^2 = e\ ,\ \ (ah)^2 = e\ ,\ \ (af)^3 = e\ ,\ \ (fh)^3 = e\ ,\ \ (hq)^3 = e\ ,\ \ (aq)^6 = e \end{aligned} \tag{7.34}$$

For an alternative set of generators (fulfilling a different set of relations) see also [132]. We mention its character table in table 7.3. This table is adapted from [175]. This group has four irreducible faithful three-dimensional representations which form two complex conjugated pairs. Apart from the three-dimensional representations $\Sigma(360\times 3)$ has also a pair of complex conjugated six- and fifteen-dimensional representations which are faithful. Out of the three nine-dimensional representations only two are faithful which are complex, while the unfaithful one is real. The other six unfaithful representations have dimension one, five (two representations), eight (two representations) and ten and are all real. The form of the product of $\mathbf{3^{(1)}}$ with itself and with its complex conjugated representation is like in $SU(3)$ [11]

$$\mathbf{3^{(1)}} \times \mathbf{3^{(1)}} = (\mathbf{3^{(1)}})^\star + \mathbf{6}^\star \quad \text{and} \quad \mathbf{3^{(1)}} \times (\mathbf{3^{(1)}})^\star = \mathbf{1} + \mathbf{8^{(1)}}\ . \tag{7.35}$$

The generators of the group can be represented by the following matrices in the representation $\mathbf{3^{(1)}}$: a is as in eq.(7.10) and

$$f = \begin{pmatrix} 1 & 0 & 0 \\ 0 & -1 & 0 \\ 0 & 0 & -1 \end{pmatrix}\ ,\quad h = \frac{1}{2}\begin{pmatrix} -1 & \mu_- & \mu_+ \\ \mu_- & \mu_+ & -1 \\ \mu_+ & -1 & \mu_- \end{pmatrix}\ ,\quad q = \begin{pmatrix} -1 & 0 & 0 \\ 0 & 0 & -\omega \\ 0 & -\omega^2 & 0 \end{pmatrix} \tag{7.36}$$

with $\mu_\pm = \frac{1}{2}\left(-1 \pm \sqrt{5}\right)$. All these matrices have determinant $+1$. A set of representation matrices for the other three-dimensional representations $\mathbf{3^{(2)}}$, $(\mathbf{3^{(1)}})^\star$ and $(\mathbf{3^{(2)}})^\star$ can be constructed by using outer automorphisms of the group $\Sigma(360\times 3)$ which relate the other representations and their matrix realizations to $\mathbf{3^{(1)}}$ and a, f, h and q, see eqs. (7.10,7.36),

$$\begin{aligned} \mathbf{3^{(1)}} \to \mathbf{3^{(2)}} \ &: \quad a \to ahq\ ,\ f \to fahf\ ,\ h \to q\ ,\ q \to a^2h\ , \\ \mathbf{3^{(1)}} \to (\mathbf{3^{(1)}})^\star \ &: \quad a \to a^2hq\ ,\ f \to fa^2hf\ ,\ h \to q\ ,\ q \to ah\ , \\ \mathbf{3^{(1)}} \to (\mathbf{3^{(2)}})^\star \ &: \quad a \to a^2\ ,\ f \to f\ ,\ h \to h\ ,\ q \to q\ . \end{aligned} \tag{7.37}$$

These outer automorphisms can be nicely seen as symmetries of the character table: the first one exchanges the representations $\mathbf{3^{(1)}}$ and $\mathbf{3^{(2)}}$ as well as their complex conjugates and $\mathbf{8^{(1)}}$ with $\mathbf{8^{(2)}}$ and at the same time the classes: $\mathcal{C}_8 \leftrightarrow \mathcal{C}_9$, $\mathcal{C}_{14} \leftrightarrow \mathcal{C}_{16}$ and $\mathcal{C}_{15} \leftrightarrow \mathcal{C}_{17}$, while the second one exchanges all representations with their complex conjugate, i.e. $\mathbf{3^{(1)}}$ with $(\mathbf{3^{(1)}})^\star$, $\mathbf{3^{(2)}}$ with $(\mathbf{3^{(2)}})^\star$, $\mathbf{6}$ and $\mathbf{6}^\star$, $\mathbf{9^{(2)}}$ with $(\mathbf{9^{(2)}})^\star$ and $\mathbf{15}$ with $\mathbf{15}^\star$ and it also exchanges the classes: $\mathcal{C}_3 \leftrightarrow \mathcal{C}_4$, $\mathcal{C}_{10} \leftrightarrow \mathcal{C}_{11}$, $\mathcal{C}_{12} \leftrightarrow \mathcal{C}_{13}$, $\mathcal{C}_{14} \leftrightarrow \mathcal{C}_{17}$ and $\mathcal{C}_{15} \leftrightarrow \mathcal{C}_{16}$. The third automorphism exchanges the representations $\mathbf{3^{(1)}}$ and $(\mathbf{3^{(2)}})^\star$ as well as their complex conjugates, $\mathbf{6}$ with $\mathbf{6}^\star$, the two real eight-dimensional representations $\mathbf{8^{(1)}}$ and

[11] The form of the products is very similar for $\mathbf{3^{(2)}}$. The combinations $\mathbf{3^{(1)}} \times \mathbf{3^{(2)}}$ and $\mathbf{3^{(1)}} \times (\mathbf{3^{(2)}})^\star$ and alike instead are irreducible in $\Sigma(360 \times 3)$.

$\mathbf{8^{(2)}}$, the complex conjugated pair of nine-dimensional representations as well as the fifteen-dimensional representations; at the same time the following classes have to be exchanged: $\mathcal{C}_3 \leftrightarrow \mathcal{C}_4$, $\mathcal{C}_8 \leftrightarrow \mathcal{C}_9$, $\mathcal{C}_{10} \leftrightarrow \mathcal{C}_{11}$, $\mathcal{C}_{12} \leftrightarrow \mathcal{C}_{13}$, $\mathcal{C}_{14} \leftrightarrow \mathcal{C}_{15}$ and $\mathcal{C}_{16} \leftrightarrow \mathcal{C}_{17}$. The group of outer automorphisms is a Klein group $Z_2 \times Z_2$. Thus, the mentioned mappings have order two and commute among each other, as can be checked.

The Abelian subgroups of $\Sigma(360 \times 3)$ which are generated by a single element are 45 Z_2 groups, 121 Z_3 symmetries, 45 Z_4 symmetries, 36 Z_5 groups, 45 Z_6 symmetries, 45 Z_{12} groups as well as 36 Z_{15} symmetries. All these Z_n subgroups are conjugate among each other, apart from the Z_3 symmetries which form three categories (one of which contains only the center of $SU(3)$, a second one with 60 conjugate members as well as a third one with also 60 members). There are 30 Klein groups which form two categories comprising 15 conjugate groups each. There are also Abelian subgroups of the form $Z_3 \times Z_3$ and $Z_2 \times Z_6$ which however contain the center of $SU(3)$ and thus are not relevant for our discussion.

The patterns we find for $\Sigma(360 \times 3)$ are listed in tables 7.4-7.6. Patterns Ia through XVIII all arise from subgroups G_e and G_ν which are generated by a single element each and thus require neutrinos to be Dirac particles. The only exception are the patterns XIa and XIb which can also be achieved, if both groups G_e and G_ν are Klein symmetries. Furthermore, there are several patterns, called KI through KVII, that are generated, if one of the two residual symmetries, G_e or G_ν, is a Klein group. Indeed for all patterns apart from KI the permutation with the minimum value of χ^2 is compatible with G_ν being a Klein group. Thus, neutrinos can naturally be Majorana particles. Overall there are only a few patterns with a value of χ^2 smaller than 100: patterns Ia through IIIb. Unfortunately, all these predict vanishing CP violation. This is very similar to what we have already observed in the case of the group $\Sigma(216 \times 3)$, see tables 7.1 and 7.2. The pattern with the smallest χ^2 ($\chi^2 \approx 338.0$) and with non-vanishing J_{CP} is pattern VII which, however, does not fit any of the three mixing angles at the 3σ level or better. Only pattern XVIII turns out to lead to maximal CP violation, $|\sin\delta| = 1$, as we indicate with a circle ($\circ$) in table 7.6. Although CP violation is not maximal in the other cases, we frequently find patterns with $|\sin\delta| \gtrsim 0.9$. Almost half of the patterns Ia through XVIII fits the atmospheric mixing angle well, while none leads to a reactor mixing angle which is compatible at the 3σ level with the results found in [30]. On top of that only pattern Ia is able to accommodate two of the three mixing angles well. Among the patterns Ki, i=I, ..., VII, the smallest value of χ^2 is $\chi^2 \approx 148.1$ which is larger than those of the patterns Ia to IIIb. Although pattern KI has $\chi^2 \approx 148.1$ and only fits the solar mixing angle well, it might be interesting, since J_{CP} is non-vanishing in this case. This is at variance to what we have found for the patterns which are produced in setups with G_e and G_ν being both generated by one element each. It is likely to be a coincidence, but indeed all patterns Ki, i=I, ..., VII lead to non-zero J_{CP}. Two of these, pattern KV and KVI, have also been mentioned in [126]. Generally speaking, all patterns would require additional ingredients to be present which allow them to be compatible with the experimental data [30]. These might be suitable corrections coming from symmetry breaking terms or modifications of the breaking, e.g. by involving CP. As one can see from tables 7.4-7.6, the choice of Z_4 or Z_{12} subgroups and of Z_5 or Z_{15} subgroups, respectively, leads to the same mixing patterns. This is, like in the other groups $\Sigma(n\varphi)$ with $\varphi = 3$, due to the relation of these subgroups via the center of $SU(3)$.

As one can check there are 138 matrices among the representation matrices in $\mathbf{3^{(1)}}$

which have at least two degenerate eigenvalues: these are all Z_2 and all Z_6 generating elements as well as the elements which comprise the center of $SU(3)$. The former can be identified with the generators of G_e or G_ν and then give rise to one of fourteen mixing vectors: the three vectors which have been found in the analysis of the group $\Sigma(36\times 3)$, a vector of the same form (in absolute values) as the first column of the TBM mixing matrix, a vector which is trimaximal, a vector which equals the first row of the pattern KI see table 7.6, another one of the form of the third row of pattern KI, a vector equal to the second column of pattern KII, another one which is of the form as the third column of pattern KII, a vector which coincides with the third column of pattern KIII, vectors like the second and the third columns of pattern KIVa, a vector with the same form as the third column of pattern KV as well as a vector which coincides with the second column of pattern KVI. As regards the vector which is of the same form (in absolute values) as the second column of the pattern KIVa we notice that it has been discussed as mixing vector in [166]. There it has been associated with the group $\Sigma(60)$ which is isomorphic to A_5. Due to the relation of the representation matrices of Z_2 and Z_6 generating elements via the center of $SU(3)$ the sets of mixing vectors have to coincide.

Table 7.3: Character table of the group $\Sigma(360 \times 3)$, adapted from [175]. $c_1\,\mathcal{C}_{c_2}$ denote the classes with c_1 elements which have order c_2. G is a representative of the class $c_1\,\mathcal{C}_{c_2}$ in terms of the generators a, f, h and q. Furthermore, $\rho = e^{2\pi i/5}$ and $\zeta = e^{2\pi i/15}$.

	Classes																
	C_1 $1\,\mathcal{C}_1$	C_2 $45\,\mathcal{C}_2$	C_3 $1\,\mathcal{C}_3$	C_4 $1\,\mathcal{C}_3$	C_5 $120\,\mathcal{C}_3$	C_6 $120\,\mathcal{C}_3$	C_7 $90\,\mathcal{C}_4$	C_8 $72\,\mathcal{C}_5$	C_9 $72\,\mathcal{C}_5$	C_{10} $45\,\mathcal{C}_6$	C_{11} $45\,\mathcal{C}_6$	C_{12} $90\,\mathcal{C}_{12}$	C_{13} $90\,\mathcal{C}_{12}$	C_{14} $72\,\mathcal{C}_{15}$	C_{15} $72\,\mathcal{C}_{15}$	C_{16} $72\,\mathcal{C}_{15}$	C_{17} $72\,\mathcal{C}_{15}$
G	1	q	$(qa)^2$	$(aqa)^2$	a	hqa	fqh	$(hqafq)^3$	$(hqafq)^6$	qa	qa^2	afq	a^2fq	$hqafq$	$(hqafq)^2$	$(hqafq)^{13}$	$(hqafq)^{14}$
$\mathbf{1}$	1	1	1	1	1	1	1	1	1	1	1	1	1	1	1	1	1
$\mathbf{3^{(1)}}$	3	-1	3ω	$3\omega^2$	0	0	1	$-\rho^2-\rho^3$	$-\rho-\rho^4$	$-\omega^2$	$-\omega$	ω^2	ω	$-\zeta^2-\zeta^8$	$-\zeta-\zeta^4$	$-\zeta^{11}-\zeta^{14}$	$-\zeta^7-\zeta^{13}$
$\mathbf{3^{(2)}}$	3	-1	3ω	$3\omega^2$	0	0	1	$-\rho-\rho^4$	$-\rho^2-\rho^3$	$-\omega^2$	$-\omega$	ω^2	ω	$-\zeta^{11}-\zeta^{14}$	$-\zeta^7-\zeta^{13}$	$-\zeta^2-\zeta^8$	$-\zeta-\zeta^4$
$(\mathbf{3^{(1)}})^\star$	3	-1	$3\omega^2$	3ω	0	0	1	$-\rho^2-\rho^3$	$-\rho-\rho^4$	$-\omega$	$-\omega^2$	ω	ω^2	$-\zeta^7-\zeta^{13}$	$-\zeta^{11}-\zeta^{14}$	$-\zeta-\zeta^4$	$-\zeta^2-\zeta^8$
$(\mathbf{3^{(2)}})^\star$	3	-1	$3\omega^2$	3ω	0	0	1	$-\rho-\rho^4$	$-\rho^2-\rho^3$	$-\omega$	$-\omega^2$	ω	ω^2	$-\zeta-\zeta^4$	$-\zeta^2-\zeta^8$	$-\zeta^7-\zeta^{13}$	$-\zeta^{11}-\zeta^{14}$
$\mathbf{5^{(1)}}$	5	1	5	5	2	-1	-1	0	0	1	1	-1	-1	0	0	0	0
$\mathbf{5^{(2)}}$	5	1	5	5	-1	2	-1	0	0	1	1	-1	-1	0	0	0	0
$\mathbf{6}$	6	2	6ω	$6\omega^2$	0	0	0	1	1	$2\omega^2$	2ω	0	0	ω	ω^2	ω	ω^2
$\mathbf{6^\star}$	6	2	$6\omega^2$	6ω	0	0	0	1	1	2ω	$2\omega^2$	0	0	ω^2	ω	ω^2	ω
$\mathbf{8^{(1)}}$	8	0	8	8	-1	-1	0	$-\rho^2-\rho^3$	$-\rho-\rho^4$	0	0	0	0	$-\rho-\rho^4$	$-\rho^2-\rho^3$	$-\rho^2-\rho^3$	$-\rho-\rho^4$
$\mathbf{8^{(2)}}$	8	0	8	8	-1	-1	0	$-\rho-\rho^4$	$-\rho^2-\rho^3$	0	0	0	0	$-\rho^2-\rho^3$	$-\rho-\rho^4$	$-\rho-\rho^4$	$-\rho^2-\rho^3$
$\mathbf{9^{(1)}}$	9	1	9	9	0	0	1	-1	-1	1	1	1	1	-1	-1	-1	-1
$\mathbf{9^{(2)}}$	9	1	9ω	$9\omega^2$	0	0	1	-1	-1	ω^2	ω	ω^2	ω	$-\omega$	$-\omega^2$	$-\omega$	$-\omega^2$
$(\mathbf{9^{(2)}})^\star$	9	1	$9\omega^2$	9ω	0	0	1	-1	-1	ω	ω^2	ω	ω^2	$-\omega^2$	$-\omega$	$-\omega^2$	ω
$\mathbf{10}$	10	-2	10	10	1	1	0	0	0	-2	-2	0	0	0	0	0	0
$\mathbf{15}$	15	-1	15ω	$15\omega^2$	0	0	-1	0	0	$-\omega^2$	$-\omega$	$-\omega^2$	$-\omega$	0	0	0	0
$\mathbf{15^\star}$	15	-1	$15\omega^2$	15ω	0	0	-1	0	0	$-\omega$	$-\omega^2$	$-\omega$	$-\omega^2$	0	0	0	0

Table 7.4: Mixing patterns associated with $\Sigma(360 \times 3)$. For more details see the caption of table 7.1 and the text.

#	Pattern	(G_e, G_ν)	Example of (g_e, g_ν)	$\lvert J_{CP}\rvert$	$(\sin^2\theta_{12}, \sin^2\theta_{23}, \sin^2\theta_{13})$	χ^2
Ia	$\frac{1}{4}\begin{pmatrix} 1+\sqrt{5} & \sqrt{5-\sqrt{3}-\sqrt{5}+\sqrt{15}} & \sqrt{5+\sqrt{3}-\sqrt{5}-\sqrt{15}} \\ \sqrt{5-\sqrt{3}-\sqrt{5}+\sqrt{15}} & \sqrt{8+\sqrt{3}-\sqrt{15}} & \sqrt{3+\sqrt{5}} \\ \sqrt{5+\sqrt{3}-\sqrt{5}-\sqrt{15}} & \sqrt{3+\sqrt{5}} & \sqrt{8-\sqrt{3}+\sqrt{15}} \end{pmatrix} \approx \begin{pmatrix} 0.809 & 0.554 & 0.197 \\ 0.554 & 0.605 & 0.572 \\ 0.197 & 0.572 & 0.796 \end{pmatrix}$	(Z_4, Z_4) (Z_4, Z_{12}) (Z_{12}, Z_{12})	$(fqh,\ afhqa^2)$	0	$\sin^2\theta_{12} \approx 0.319\star$ $\sin^2\theta_{23} \approx 0.341\star$ $\sin^2\theta_{13} \approx 0.039$	58.0
Ib	$\frac{1}{4}\begin{pmatrix} 1+\sqrt{5} & \sqrt{5-\sqrt{3}-\sqrt{5}+\sqrt{15}} & \sqrt{5+\sqrt{3}-\sqrt{5}-\sqrt{15}} \\ \sqrt{5+\sqrt{3}-\sqrt{5}-\sqrt{15}} & \sqrt{3+\sqrt{5}} & \sqrt{8-\sqrt{3}+\sqrt{15}} \\ \sqrt{5-\sqrt{3}-\sqrt{5}+\sqrt{15}} & \sqrt{8+\sqrt{3}-\sqrt{15}} & \sqrt{3+\sqrt{5}} \end{pmatrix} \approx \begin{pmatrix} 0.809 & 0.554 & 0.197 \\ 0.197 & 0.572 & 0.796 \\ 0.554 & 0.605 & 0.572 \end{pmatrix}$	(Z_4, Z_4) (Z_4, Z_{12}) (Z_{12}, Z_{12})	$(fqh,\ afhqa^2)$	0	$\sin^2\theta_{12} \approx 0.319\star$ $\sin^2\theta_{23} \approx 0.659$ $\sin^2\theta_{13} \approx 0.039$	58.9
IIa	$\frac{1}{20}\begin{pmatrix} 5-\sqrt{5}+\sqrt{30(5+\sqrt{5})} & 4\sqrt{5} & 2\sqrt{5(7-\sqrt{5}-\sqrt{6(5-\sqrt{5})})} \\ 4\sqrt{5} & -5+\sqrt{5}+\sqrt{30(5+\sqrt{5})} & 2\sqrt{5(7-\sqrt{5}+\sqrt{6(5-\sqrt{5})})} \\ 2\sqrt{5(7-\sqrt{5}-\sqrt{6(5-\sqrt{5})})} & 2\sqrt{5(7-\sqrt{5}+\sqrt{6(5-\sqrt{5})})} & 2(5+\sqrt{5}) \end{pmatrix} \approx \begin{pmatrix} 0.875 & 0.447 & 0.186 \\ 0.447 & 0.598 & 0.665 \\ 0.186 & 0.665 & 0.724 \end{pmatrix}$	(Z_5, Z_5) (Z_5, Z_{15}) (Z_{15}, Z_{15})	$((hqafq)^3,\ a^2fqh)$	0	$\sin^2\theta_{12} \approx 0.207$ $\sin^2\theta_{23} \approx 0.458\star$ $\sin^2\theta_{13} \approx 0.035$	84.6
IIb	$\begin{pmatrix} 5-\sqrt{5}+\sqrt{30(5+\sqrt{5})} & 4\sqrt{5} & 2\sqrt{5(7-\sqrt{5}-\sqrt{6(5-\sqrt{5})})} \\ 2\sqrt{5(7-\sqrt{5}-\sqrt{6(5-\sqrt{5})})} & 2\sqrt{5(7-\sqrt{5}+\sqrt{6(5-\sqrt{5})})} & 2(5+\sqrt{5}) \\ 4\sqrt{5} & -5+\sqrt{5}+\sqrt{30(5+\sqrt{5})} & 2\sqrt{5(7-\sqrt{5}+\sqrt{6(5-\sqrt{5})})} \end{pmatrix} \approx \begin{pmatrix} 0.875 & 0.447 & 0.186 \\ 0.186 & 0.665 & 0.724 \\ 0.447 & 0.598 & 0.665 \end{pmatrix}$	(Z_5, Z_5) (Z_5, Z_{15}) (Z_{15}, Z_{15})	$((hqafq)^3,\ a^2fqh)$	0	$\sin^2\theta_{12} \approx 0.207$ $\sin^2\theta_{23} \approx 0.542\star$ $\sin^2\theta_{13} \approx 0.035$	88.9
IIIa	$\begin{pmatrix} 0.894 & 0.430 & 0.124 \\ 0.250 & 0.710 & 0.659 \\ 0.372 & 0.558 & 0.742 \end{pmatrix}$	(Z_5, Z_4) (Z_{15}, Z_4) (Z_5, Z_{12}) (Z_{15}, Z_{12})	$((hqafq)^3,\ a^2fhqa)$	0	$\sin^2\theta_{12} \approx 0.188$ $\sin^2\theta_{23} \approx 0.441\star$ $\sin^2\theta_{13} \approx 0.015$	93.0
IIIb	$\begin{pmatrix} 0.894 & 0.430 & 0.124 \\ 0.372 & 0.558 & 0.742 \\ 0.250 & 0.710 & 0.659 \end{pmatrix}$	(Z_5, Z_4) (Z_{15}, Z_4) (Z_5, Z_{12}) (Z_{15}, Z_{12})	$((hqafq)^3,\ a^2fhqa)$	0	$\sin^2\theta_{12} \approx 0.188$ $\sin^2\theta_{23} \approx 0.559\star$ $\sin^2\theta_{13} \approx 0.015$	95.0
IV	$\frac{1}{20}\begin{pmatrix} 2\sqrt{5(7+\sqrt{5}+\sqrt{6(5+\sqrt{5})})} & 4\sqrt{5} & -5-\sqrt{5}+\sqrt{30(5-\sqrt{5})} \\ 2\sqrt{5(7+\sqrt{5}-\sqrt{6(5+\sqrt{5})})} & 5+\sqrt{5}+\sqrt{30(5-\sqrt{5})} & 4\sqrt{5} \\ 2(5-\sqrt{5}) & 2\sqrt{5(7+\sqrt{5}-\sqrt{6(5+\sqrt{5})})} & 2\sqrt{5(7+\sqrt{5}+\sqrt{6(5+\sqrt{5})})} \end{pmatrix} \approx \begin{pmatrix} 0.890 & 0.447 & 0.093 \\ 0.364 & 0.817 & 0.447 \\ 0.276 & 0.364 & 0.890 \end{pmatrix}$	(Z_5, Z_5) (Z_5, Z_{15}) (Z_{15}, Z_{15})	$((hqafq)^3,\ qhqafh)$	0	$\sin^2\theta_{12} \approx 0.202$ $\sin^2\theta_{23} \approx 0.202$ $\sin^2\theta_{13} \approx 0.009$	171.0
V	$\begin{pmatrix} 0.795 & 0.602 & 0.076 \\ 0.590 & 0.739 & 0.324 \\ 0.139 & 0.302 & 0.943 \end{pmatrix}$	(Z_5, Z_4) (Z_{15}, Z_4) (Z_5, Z_{12}) (Z_{15}, Z_{12})	$((hqafq)^3,\ fqh)$	0	$\sin^2\theta_{12} \approx 0.364$ $\sin^2\theta_{23} \approx 0.106$ $\sin^2\theta_{13} \approx 0.006$	227.7
VI	$\frac{1}{2\sqrt{5}}\begin{pmatrix} \sqrt{2(5+\sqrt{15})} & \sqrt{2(5-\sqrt{15})} & 0 \\ \sqrt{5-\sqrt{15}} & \sqrt{5+\sqrt{15}} & \sqrt{10} \\ \sqrt{5-\sqrt{15}} & \sqrt{5+\sqrt{15}} & \sqrt{10} \end{pmatrix} \approx \begin{pmatrix} 0.942 & 0.336 & 0 \\ 0.237 & 0.666 & 0.707 \\ 0.237 & 0.666 & 0.707 \end{pmatrix}$	(Z_5, Z_4) (Z_{15}, Z_4) (Z_5, Z_{12}) (Z_{15}, Z_{12})	$((hqafq)^3,\ qafa^2)$	0	$\sin^2\theta_{12} \approx 0.113$ $\sin^2\theta_{23} = 0.500\star$ $\sin^2\theta_{13} = 0$	328.2
VII	$\frac{1}{6}\begin{pmatrix} 2\sqrt{3+\sqrt{5}} & \sqrt{2(9-\sqrt{5})} & -1+\sqrt{5} \\ -1+\sqrt{5} & -1+\sqrt{5} & 2\sqrt{6+\sqrt{5}} \\ \sqrt{2(9-\sqrt{5})} & 2\sqrt{3+\sqrt{5}} & -1+\sqrt{5} \end{pmatrix} \approx \begin{pmatrix} 0.763 & 0.613 & 0.206 \\ 0.206 & 0.206 & 0.957 \\ 0.613 & 0.763 & 0.206 \end{pmatrix}$	(Z_3, Z_3)	$(hqa,\ hf)$	$\frac{\sqrt{3-\sqrt{5}}}{18\sqrt{6}} \approx 0.0198$	$\sin^2\theta_{12} \approx 0.392$ $\sin^2\theta_{23} \approx 0.956$ $\sin^2\theta_{13} \approx 0.042$	338.0

Table 7.5: Mixing patterns associated with $\Sigma(360\times 3)$. Note that patterns XIa and XIb can also be achieved, if both G_e and G_ν are Klein subgroups of $\Sigma(360\times 3)$. For further explanation see the caption of table 7.4.

#	Pattern	(G_e, G_ν)	Example of (g_e, g_ν)	$\lvert J_{CP}\rvert$	$(\sin^2\theta_{12}, \sin^2\theta_{23}, \sin^2\theta_{13})$	χ^2
VIII	$\frac{1}{4}\begin{pmatrix} \sqrt{5+\sqrt{3}+\sqrt{5}+\sqrt{15}} & \sqrt{8-\sqrt{6(3+\sqrt{5})}} & \sqrt{3-\sqrt{5}} \\ -1+\sqrt{5} & \sqrt{5+\sqrt{3}+\sqrt{5}+\sqrt{15}} & \sqrt{5-\sqrt{3}+\sqrt{5}-\sqrt{15}} \\ \sqrt{5-\sqrt{3}+\sqrt{5}-\sqrt{15}} & \sqrt{3-\sqrt{5}} & \sqrt{8+\sqrt{6(3+\sqrt{5})}} \end{pmatrix} \approx \begin{pmatrix} 0.896 & 0.387 & 0.219 \\ 0.309 & 0.896 & 0.319 \\ 0.319 & 0.219 & 0.922 \end{pmatrix}$	(Z_4, Z_4) (Z_4, Z_{12}) (Z_{12}, Z_{12})	$(fqh,\ a^2fhqa)$	0	$\sin^2\theta_{12} \approx 0.157$ $\sin^2\theta_{23} \approx 0.107$ $\sin^2\theta_{13} \approx 0.048$	397.6
IX	$\frac{1}{2\sqrt{3(3-\sqrt{5})}}\begin{pmatrix} \sqrt{11-\sqrt{3}-\sqrt{5}(3-\sqrt{3})} & \sqrt{11+\sqrt{3}-\sqrt{5}(3+\sqrt{3})} & 3-\sqrt{5} \\ \sqrt{11+\sqrt{3}-\sqrt{5}(3+\sqrt{3})} & \sqrt{11-\sqrt{3}-\sqrt{5}(3-\sqrt{3})} & 3-\sqrt{5} \\ 3-\sqrt{5} & 3-\sqrt{5} & 2\sqrt{2} \end{pmatrix} \approx \begin{pmatrix} 0.838 & 0.484 & 0.252 \\ 0.484 & 0.838 & 0.252 \\ 0.252 & 0.252 & 0.934 \end{pmatrix}$	(Z_4, Z_3) (Z_{12}, Z_3)	$(fqh,\ qha)$	$\frac{1}{48}(\sqrt{5}-1)$ ≈ 0.0258	$\sin^2\theta_{12} \approx 0.251$ $\sin^2\theta_{23} \approx 0.068$ $\sin^2\theta_{13} \approx 0.064$	511.2
Xa	$\frac{1}{6}\begin{pmatrix} \sqrt{2(9+\sqrt{5})} & 1+\sqrt{5} & 2\sqrt{3-\sqrt{5}} \\ 1+\sqrt{5} & 2\sqrt{6-\sqrt{5}} & 1+\sqrt{5} \\ 2\sqrt{3-\sqrt{5}} & 1+\sqrt{5} & \sqrt{2(9+\sqrt{5})} \end{pmatrix} \approx \begin{pmatrix} 0.790 & 0.539 & 0.291 \\ 0.539 & 0.647 & 0.539 \\ 0.291 & 0.539 & 0.790 \end{pmatrix}$	(Z_3, Z_3)	$(hf,\ haq)$	$\frac{1}{36\sqrt{3}}(1+\sqrt{5})$ ≈ 0.0519	$\sin^2\theta_{12} \approx 0.318\star$ $\sin^2\theta_{23} \approx 0.318$ $\sin^2\theta_{13} \approx 0.085$	716.2
Xb	$\frac{1}{6}\begin{pmatrix} \sqrt{2(9+\sqrt{5})} & 1+\sqrt{5} & 2\sqrt{3-\sqrt{5}} \\ 2\sqrt{3-\sqrt{5}} & 1+\sqrt{5} & \sqrt{2(9+\sqrt{5})} \\ 1+\sqrt{5} & 2\sqrt{6-\sqrt{5}} & 1+\sqrt{5} \end{pmatrix} \approx \begin{pmatrix} 0.790 & 0.539 & 0.291 \\ 0.291 & 0.539 & 0.790 \\ 0.539 & 0.647 & 0.539 \end{pmatrix}$	(Z_3, Z_3)	$(hf,\ haq)$	$\frac{1}{36\sqrt{3}}(1+\sqrt{5})$ ≈ 0.0519	$\sin^2\theta_{12} \approx 0.318\star$ $\sin^2\theta_{23} \approx 0.682$ $\sin^2\theta_{13} \approx 0.085$	718.6
XIa	$\frac{1}{4}\begin{pmatrix} 1+\sqrt{5} & 2 & -1+\sqrt{5} \\ 2 & 2\sqrt{2} & 2 \\ -1+\sqrt{5} & 2 & 1+\sqrt{5} \end{pmatrix} \approx \begin{pmatrix} 0.809 & 0.500 & 0.309 \\ 0.500 & 0.707 & 0.500 \\ 0.309 & 0.500 & 0.809 \end{pmatrix}$	(Z_4, Z_4) (Z_4, Z_{12}) (Z_{12}, Z_{12}) $(Z_2\times Z_2, Z_2\times Z_2)$	$(fqh, qafa^2)$ $(\{fq, hfqh\}, \{afa^2, aqa^2\})$	$\frac{\sqrt{3}}{32} \approx 0.0541$	$\sin^2\theta_{12} \approx 0.276\star$ $\sin^2\theta_{23} \approx 0.276$ $\sin^2\theta_{13} \approx 0.095$	993.5
XIb	$\frac{1}{4}\begin{pmatrix} 1+\sqrt{5} & 2 & -1+\sqrt{5} \\ -1+\sqrt{5} & 2 & 1+\sqrt{5} \\ 2 & 2\sqrt{2} & 2 \end{pmatrix} \approx \begin{pmatrix} 0.809 & 0.500 & 0.309 \\ 0.309 & 0.500 & 0.809 \\ 0.500 & 0.707 & 0.500 \end{pmatrix}$	(Z_4, Z_4) (Z_4, Z_{12}) (Z_{12}, Z_{12}) $(Z_2\times Z_2, Z_2\times Z_2)$	$(fqh, qafa^2)$ $(\{fq, hfqh\}, \{afa^2, aqa^2\})$	$\frac{\sqrt{3}}{32} \approx 0.0541$	$\sin^2\theta_{12} \approx 0.276\star$ $\sin^2\theta_{23} \approx 0.724$ $\sin^2\theta_{13} \approx 0.095$	1000.0
XII	$\frac{1}{2\sqrt{15}}\begin{pmatrix} \sqrt{25+\sqrt{5}+\sqrt{30(5-\sqrt{5})}} & \sqrt{25+\sqrt{5}-\sqrt{30(5-\sqrt{5})}} & \sqrt{2(5-\sqrt{5})} \\ \sqrt{25+\sqrt{5}-\sqrt{30(5-\sqrt{5})}} & \sqrt{25+\sqrt{5}+\sqrt{30(5-\sqrt{5})}} & \sqrt{2(5-\sqrt{5})} \\ \sqrt{2(5-\sqrt{5})} & \sqrt{2(5-\sqrt{5})} & 2\sqrt{10+\sqrt{5}} \end{pmatrix} \approx \begin{pmatrix} 0.778 & 0.550 & 0.304 \\ 0.550 & 0.778 & 0.304 \\ 0.304 & 0.304 & 0.903 \end{pmatrix}$	(Z_5, Z_3) (Z_{15}, Z_3)	$((hqafq)^3,\ qh)$	$\frac{1}{60}\sqrt{2(5-\sqrt{5})}$ ≈ 0.0392	$\sin^2\theta_{12} \approx 0.333\star$ $\sin^2\theta_{23} \approx 0.101$ $\sin^2\theta_{13} \approx 0.092$	1034.3
XIII	$\frac{1}{\sqrt{12}}\begin{pmatrix} \sqrt{5+\sqrt{15}} & \sqrt{2} & \sqrt{5-\sqrt{15}} \\ \sqrt{2} & 2\sqrt{2} & \sqrt{2} \\ \sqrt{5-\sqrt{15}} & \sqrt{2} & \sqrt{5+\sqrt{15}} \end{pmatrix} \approx \begin{pmatrix} 0.860 & 0.408 & 0.306 \\ 0.408 & 0.816 & 0.408 \\ 0.306 & 0.408 & 0.860 \end{pmatrix}$	(Z_4, Z_3) (Z_{12}, Z_3)	$(fqh,\ afhfa)$	$\frac{1}{24} \approx 0.0417$	$\sin^2\theta_{12} \approx 0.184$ $\sin^2\theta_{23} \approx 0.184$ $\sin^2\theta_{13} \approx 0.094$	1091.6
XIV	$\frac{1}{\sqrt{6(3-\sqrt{5})}}\begin{pmatrix} \sqrt{2} & \sqrt{2} & 3-\sqrt{5} \\ \sqrt{8-3\sqrt{5}+\sqrt{3(9-4\sqrt{5})}} & \sqrt{8-3\sqrt{5}-\sqrt{3(9-4\sqrt{5})}} & \sqrt{2} \\ \sqrt{8-3\sqrt{5}-\sqrt{3(9-4\sqrt{5})}} & \sqrt{8-3\sqrt{5}+\sqrt{3(9-4\sqrt{5})}} & \sqrt{2} \end{pmatrix} \approx \begin{pmatrix} 0.661 & 0.661 & 0.357 \\ 0.609 & 0.439 & 0.661 \\ 0.439 & 0.609 & 0.661 \end{pmatrix}$	(Z_4, Z_3) (Z_{12}, Z_3)	$(fqh,\ hqa)$	$\frac{1}{48}(1+\sqrt{5})$ ≈ 0.0674	$\sin^2\theta_{12} = 0.500$ $\sin^2\theta_{23} = 0.500\star$ $\sin^2\theta_{13} \approx 0.127$	2238.5
XV	$\frac{1}{\sqrt{6(5+\sqrt{5})}}\begin{pmatrix} \sqrt{2(6+\sqrt{5}+\sqrt{15+6\sqrt{5}})} & 1+\sqrt{5} & \sqrt{2(6+\sqrt{5}-\sqrt{15+6\sqrt{5}})} \\ 1+\sqrt{5} & \sqrt{2(9+\sqrt{5})} & 1+\sqrt{5} \\ \sqrt{2(6+\sqrt{5}-\sqrt{15+6\sqrt{5}})} & 1+\sqrt{5} & \sqrt{2(6+\sqrt{5}+\sqrt{15+6\sqrt{5}})} \end{pmatrix} \approx \begin{pmatrix} 0.791 & 0.491 & 0.366 \\ 0.491 & 0.719 & 0.491 \\ 0.366 & 0.491 & 0.791 \end{pmatrix}$	(Z_5, Z_3) (Z_{15}, Z_3)	$((hqafq)^3,\ haq)$	$\frac{1}{60}\sqrt{2(5+\sqrt{5})}$ ≈ 0.0634	$\sin^2\theta_{12} \approx 0.278\star$ $\sin^2\theta_{23} \approx 0.278$ $\sin^2\theta_{13} \approx 0.134$	2269.1
XVI	$\frac{1}{\sqrt{2(5+\sqrt{5})}}\begin{pmatrix} \sqrt{4+\sqrt{5}+\sqrt{5+2\sqrt{5}}} & \sqrt{4+\sqrt{5}-\sqrt{5+2\sqrt{5}}} & \sqrt{2} \\ \sqrt{4+\sqrt{5}-\sqrt{5+2\sqrt{5}}} & \sqrt{4+\sqrt{5}+\sqrt{5+2\sqrt{5}}} & \sqrt{2} \\ \sqrt{2} & \sqrt{2} & 1+\sqrt{5} \end{pmatrix} \approx \begin{pmatrix} 0.802 & 0.467 & 0.372 \\ 0.467 & 0.802 & 0.372 \\ 0.372 & 0.372 & 0.851 \end{pmatrix}$	(Z_5, Z_4) (Z_{15}, Z_4) (Z_5, Z_{12}) (Z_{15}, Z_{12})	$((hqafq)^3,\ a^2fqha)$	$\frac{1}{80}\sqrt{6(5-\sqrt{5})}$ ≈ 0.0509	$\sin^2\theta_{12} \approx 0.253$ $\sin^2\theta_{23} \approx 0.160$ $\sin^2\theta_{13} \approx 0.138$	2532.8

Table 7.6: Mixing patterns associated with $\Sigma(360\times 3)$. Patterns called Ki require that one of the groups G_e or G_ν is a Klein group. Notice that only pattern KI requires G_e to be a Klein group instead of G_ν. The circle ($\circ$) next to the result of $|J_{CP}|$ for pattern XVIII indicates that this value corresponds to maximal CP violation $|\sin\delta| = 1$. For further explanation see table 7.4.

#	Pattern	(G_e, G_ν)	Example of (g_e, g_ν)	$\lvert J_{CP}\rvert$	$(\sin^2\theta_{12}, \sin^2\theta_{23}, \sin^2\theta_{13})$	χ^2
XVII	$\frac{1}{2\sqrt{5+\sqrt{5}}}\begin{pmatrix} \sqrt{7+\sqrt{5}+\sqrt{2(5+\sqrt{5})}} & 1+\sqrt{5} & \sqrt{7+\sqrt{5}-\sqrt{2(5+\sqrt{5})}} \\ 1+\sqrt{5} & 2\sqrt{2} & 1+\sqrt{5} \\ \sqrt{7+\sqrt{5}-\sqrt{2(5+\sqrt{5})}} & 1+\sqrt{5} & \sqrt{7+\sqrt{5}+\sqrt{2(5+\sqrt{5})}} \end{pmatrix} \approx \begin{pmatrix} 0.671 & 0.602 & 0.433 \\ 0.602 & 0.526 & 0.602 \\ 0.433 & 0.602 & 0.671 \end{pmatrix}$	(Z_5, Z_4) (Z_{15}, Z_4) (Z_5, Z_{12}) (Z_{15}, Z_{12})	$((hqafq)^3,\ afhqa^2)$	$\frac{1}{80}\sqrt{6(5+\sqrt{5})} \approx 0.0824$	$\sin^2\theta_{12} \approx 0.445$ $\sin^2\theta_{23} \approx 0.445\star$ $\sin^2\theta_{13} \approx 0.188$	5060.1
XVIII	$\frac{1}{\sqrt{5}}\begin{pmatrix} \sqrt{3} & 1 & 1 \\ 1 & \sqrt{2} & \sqrt{2} \\ 1 & \sqrt{2} & \sqrt{2} \end{pmatrix} \approx \begin{pmatrix} 0.775 & 0.447 & 0.447 \\ 0.447 & 0.632 & 0.632 \\ 0.447 & 0.632 & 0.632 \end{pmatrix}$	(Z_5, Z_5) (Z_5, Z_{15}) (Z_{15}, Z_{15})	$((hqafq)^3,\ qhafq)$	$\frac{\sqrt{15}}{50} \approx 0.0775\circ$	$\sin^2\theta_{12} = 0.250$ $\sin^2\theta_{23} = 0.500\star$ $\sin^2\theta_{13} = 0.200$	5715.1
KI	$\frac{1}{4}\begin{pmatrix} 1+\sqrt{5} & \sqrt{5+\sqrt{15}-\sqrt{2(4+\sqrt{15})}} & \sqrt{5+\sqrt{3}-\sqrt{5}(1+\sqrt{3})} \\ 2 & \sqrt{2(3+\sqrt{3})} & \sqrt{2(3-\sqrt{3})} \\ -1+\sqrt{5} & \sqrt{5-\sqrt{3}+\sqrt{5}(1-\sqrt{3})} & \sqrt{5+\sqrt{15}+\sqrt{2(4+\sqrt{15})}} \end{pmatrix} \approx \begin{pmatrix} 0.809 & 0.554 & 0.197 \\ 0.500 & 0.769 & 0.398 \\ 0.309 & 0.319 & 0.896 \end{pmatrix}$	$(Z_2\times Z_2, Z_4)$ $(Z_2\times Z_2, Z_{12})$	$(\{f,q\},\ afqha^2)$	$\frac{1}{32} \approx 0.0313$	$\sin^2\theta_{12} \approx 0.319\star$ $\sin^2\theta_{23} \approx 0.165$ $\sin^2\theta_{13} \approx 0.039$	148.1
KII	$\frac{1}{\sqrt{2(5+\sqrt{5})}}\begin{pmatrix} \sqrt{4+\sqrt{5}+\sqrt{15+6\sqrt{5}}} & \sqrt{2} & \sqrt{4+\sqrt{5}-\sqrt{15+6\sqrt{5}}} \\ \sqrt{2} & 1+\sqrt{5} & \sqrt{2} \\ \sqrt{4+\sqrt{5}-\sqrt{15+6\sqrt{5}}} & \sqrt{2} & \sqrt{4+\sqrt{5}+\sqrt{15+6\sqrt{5}}} \end{pmatrix} \approx \begin{pmatrix} 0.894 & 0.372 & 0.250 \\ 0.372 & 0.851 & 0.372 \\ 0.250 & 0.372 & 0.894 \end{pmatrix}$	$(Z_5, Z_2\times Z_2)$ $(Z_{15}, Z_2\times Z_2)$	$((hqafq)^3,\ \{a^2fa, a^2qa\})$	$\frac{1}{80}\sqrt{10-2\sqrt{5}} \approx 0.0294$	$\sin^2\theta_{12} \approx 0.147$ $\sin^2\theta_{23} \approx 0.147$ $\sin^2\theta_{13} \approx 0.063$	553.5
KIII	$\frac{\sqrt{2}}{\sqrt{3}(1+\sqrt{5})}\begin{pmatrix} \sqrt{7+3\sqrt{5}} & 1 & 1 \\ 1 & \sqrt{7+3\sqrt{5}} & 1 \\ 1 & 1 & \sqrt{7+3\sqrt{5}} \end{pmatrix} \approx \begin{pmatrix} 0.934 & 0.252 & 0.252 \\ 0.252 & 0.934 & 0.252 \\ 0.252 & 0.252 & 0.934 \end{pmatrix}$	$(Z_3, Z_2\times Z_2)$	$(hafa,\ \{f,q\})$	$\frac{1}{144}\sqrt{18-6\sqrt{5}} \approx 0.0149$	$\sin^2\theta_{12} \approx 0.068$ $\sin^2\theta_{23} \approx 0.068$ $\sin^2\theta_{13} \approx 0.064$	844.7
KIVa	$\frac{1}{2\sqrt{5+\sqrt{5}}}\begin{pmatrix} \sqrt{7+\sqrt{5}+\sqrt{6(5+\sqrt{5})}} & 1+\sqrt{5} & \sqrt{7+\sqrt{5}-\sqrt{6(5+\sqrt{5})}} \\ \sqrt{7+\sqrt{5}-\sqrt{6(5+\sqrt{5})}} & 1+\sqrt{5} & \sqrt{7+\sqrt{5}+\sqrt{6(5+\sqrt{5})}} \\ 1+\sqrt{5} & 2\sqrt{2} & 1+\sqrt{5} \end{pmatrix} \approx \begin{pmatrix} 0.739 & 0.602 & 0.302 \\ 0.302 & 0.602 & 0.739 \\ 0.602 & 0.526 & 0.602 \end{pmatrix}$	$(Z_5, Z_2\times Z_2)$ $(Z_{15}, Z_2\times Z_2)$	$((hqafq)^3,\ \{afa^2, aqa^2\})$	$\frac{1}{80}\sqrt{10+2\sqrt{5}} \approx 0.0476$	$\sin^2\theta_{12} \approx 0.398$ $\sin^2\theta_{23} \approx 0.602\star$ $\sin^2\theta_{13} \approx 0.091$	915.3
KIVb	$\frac{1}{2\sqrt{5+\sqrt{5}}}\begin{pmatrix} \sqrt{7+\sqrt{5}+\sqrt{6(5+\sqrt{5})}} & 1+\sqrt{5} & \sqrt{7+\sqrt{5}-\sqrt{6(5+\sqrt{5})}} \\ 1+\sqrt{5} & 2\sqrt{2} & 1+\sqrt{5} \\ \sqrt{7+\sqrt{5}-\sqrt{6(5+\sqrt{5})}} & 1+\sqrt{5} & \sqrt{7+\sqrt{5}+\sqrt{6(5+\sqrt{5})}} \end{pmatrix} \approx \begin{pmatrix} 0.739 & 0.602 & 0.302 \\ 0.602 & 0.526 & 0.602 \\ 0.302 & 0.602 & 0.739 \end{pmatrix}$	$(Z_5, Z_2\times Z_2)$ $(Z_{15}, Z_2\times Z_2)$	$(\ (hqafq)^3,\ \{afa^2, aqa^2\})$	$\frac{1}{80}\sqrt{10+2\sqrt{5}} \approx 0.0476$	$\sin^2\theta_{12} \approx 0.398$ $\sin^2\theta_{23} \approx 0.398\star$ $\sin^2\theta_{13} \approx 0.091$	915.5
KV	$\frac{1}{\sqrt{3(3-\sqrt{5})}}\begin{pmatrix} 1 & 1 & \sqrt{7-3\sqrt{5}} \\ 1 & \sqrt{7-3\sqrt{5}} & 1 \\ \sqrt{7-3\sqrt{5}} & 1 & 1 \end{pmatrix} \approx \begin{pmatrix} 0.661 & 0.661 & 0.357 \\ 0.661 & 0.357 & 0.661 \\ 0.357 & 0.661 & 0.661 \end{pmatrix}$	$(Z_3, Z_2\times Z_2)$	$(afha^2,\ \{f,q\})$	$\frac{1}{144}\sqrt{18+6\sqrt{5}} \approx 0.0389$	$\sin^2\theta_{12} = 0.500$ $\sin^2\theta_{23} = 0.500\star$ $\sin^2\theta_{13} \approx 0.127$	2238.5
KVI	$\frac{1}{2\sqrt{2}}\begin{pmatrix} \sqrt{3+\sqrt{3}} & \sqrt{2} & \sqrt{3-\sqrt{3}} \\ \sqrt{2} & 2 & \sqrt{2} \\ \sqrt{3-\sqrt{3}} & \sqrt{2} & \sqrt{3+\sqrt{3}} \end{pmatrix} \approx \begin{pmatrix} 0.769 & 0.500 & 0.398 \\ 0.500 & 0.707 & 0.500 \\ 0.398 & 0.500 & 0.769 \end{pmatrix}$	$(Z_4, Z_2\times Z_2)$ $(Z_{12}, Z_2\times Z_2)$	$(fqh,\ \{f, afa^2\})$	$\frac{\sqrt{5}}{32} \approx 0.0699$	$\sin^2\theta_{12} \approx 0.297\star$ $\sin^2\theta_{23} \approx 0.297$ $\sin^2\theta_{13} \approx 0.158$	3360.7
KVII	$\frac{1}{\sqrt{6}}\begin{pmatrix} 2 & 1 & 1 \\ 1 & 2 & 1 \\ 1 & 1 & 2 \end{pmatrix} \approx \begin{pmatrix} 0.816 & 0.408 & 0.408 \\ 0.408 & 0.816 & 0.408 \\ 0.408 & 0.408 & 0.816 \end{pmatrix}$	$(Z_3, Z_2\times Z_2)$	$(\ a,\ \{fq, hfqh\})$	$\frac{\sqrt{15}}{72} \approx 0.0538$	$\sin^2\theta_{12} = 0.200$ $\sin^2\theta_{23} = 0.200$ $\sin^2\theta_{13} \approx 0.167$	3892.3

III Final remarks

Non-Abelian discrete flavor symmetries G_l which are broken in a non-trivial way to G_e and G_ν in the charged lepton and neutrino sector, respectively, are still considered to be an interesting possibility to explain the peculiar lepton mixing pattern. The discovery of a large reactor mixing angle $\theta_{13} \approx 0.15$, however, strongly disfavors many mixing patterns such as TBM mixing, which is related to the flavor group S_4. Thus, efforts have been made to find new symmetries, usually larger than the group S_4, which could predict the experimentally observed mixing parameters. In this chapter we have pursued such an attempt and we have discussed the "exceptional" finite groups $\Sigma(n\varphi)$, $\varphi = 3$, which are subgroups of $SU(3)$. These four groups are interesting, since they all contain irreducible faithful three-dimensional representations and have several types of Abelian subgroups, suitable as G_e and G_ν. Since one of them, the group $\Sigma(360 \times 3)$, also comprises Klein subgroups, neutrinos could also be Majorana particles.

We find that only a few patterns give a good fit to the experimental data: one pattern associated with the group $\Sigma(36 \times 3)$, see eq.(7.17), which leads to $\theta_{13} \approx 0.18$, one associated with $\Sigma(216 \times 3)$ with $\theta_{13} \approx 0.12$, see table 7.1,[12] as well as two patterns associated with $\Sigma(360 \times 3)$ which give rise to $\theta_{13} \approx 0.20$ and $\theta_{13} \approx 0.19$, respectively, see table 7.4. Although they are associated with $\Sigma(360 \times 3)$, also the latter two patterns require neutrinos to be Dirac particles. Interestingly enough, all these patterns lead to vanishing J_{CP}. A non-trivial CP phase only arises from patterns that do not accommodate the data well, i.e. the minimum value of χ^2 is larger than 100, see tables 7.1, 7.2 and 7.4-7.6. Notice that among these are all patterns which can be derived for Majorana neutrinos from $G_l = \Sigma(360 \times 3)$. If they are implemented in a concrete model, large corrections to the symmetry breaking pattern have to be present so that the mixing angles agree reasonably well with the data. Another possibility could be to modify the breaking pattern, for example by reducing one of the residual symmetries G_e or G_ν or by involving CP symmetry in the breaking. In this way, all the presented patterns could function as starting point for the search for new patterns which lead to mixing parameters agreeing well with the data. For the group $\Sigma(216 \times 3)$ we find several patterns with $|J_{CP}| \neq 0$ which allow the solar and atmospheric mixing angles to be within the experimental 3σ ranges, but lead to a too large value of θ_{13}. It would be interesting to analyze whether a class of models can be constructed in which θ_{13} can be corrected appropriately, while the other two mixing angles (and the prediction of the Jarlskog invariant) only undergo small corrections.

[12] In our analysis of $\Sigma(216 \times 3)$ the pattern which fits the data best, see eq.(7.33), is not associated with $\Sigma(216 \times 3)$, but only with one of its subgroups of order 162. Also this pattern predicts a trivial Dirac phase.

Chapter 8

Conclusions and Outlook

I think nature's imagination Is so much greater than man's, she's never going to let us relax.

Richard P. Feynman

The existence of non-zero neutrino masses and neutrino mixing can be considered the first evidence for physics beyond the Standard Model (SM). Since the discovery of neutrino oscillations in 1998, gigantic advances have been made in order to understand the nature and the interactions of these minuscule particles. The neutrino oscillation data, accumulated over many years, have allowed to determine the frequencies and the amplitudes (i.e. the angles and the squared mass differences) which drive the solar and atmospheric neutrino oscillations and they can now be combined with the results from β-decay and double β-decay experiments and those obtained from cosmological measurements like the Planck Satellite. With the recent measurement in 2012 by the Daya Bay, RENO and Double Chooz Collaborations of the last unknown neutrino mixing angle, θ_{13}, neutrino physics has definitively entered a new era.

One could ask whether we could learn something completely new from studying the neutrinos that we still don't know already from the studies of other particles we have detected so far. The answer to this question is certainly positive and it is intimately connected with one of the most important unsolved issue in neutrino physics, i.e, the nature of massive neutrinos —Majorana or Dirac— which is one of the priority goals in the neutrino experimental search. The only feasible experiment that can unveil the nature of massive neutrinos is neutrinoless double beta decay ($(\beta\beta)_{0\nu}$-decay): $(A, Z) \to (A, Z+2) + e^- + e^-$ and it is allowed only for certain nuclei such as ^{48}Ca, ^{76}Ge, ^{82}Se, ^{100}Mo,^{130}Te and ^{136}Xe. If neutrinos will be proven to be Majorana particles then the assumption that the total lepton number is violated at some energy scale above the electroweak symmetry breaking scale of ~ 100 GeV, will be demonstrated. This in turn will imply a breakthrough in the theories of neutrino mass generation and in general in particle physics since it will constitute a proof of the existence of New Physics beyond that predicted by the SM.

In this Ph.D Thesis two main topics are discussed. The first is related to the nature of massive neutrinos and the possibility to infer from an observation of $(\beta\beta)_{0\nu}$-decay the existence of new $\Delta L = \pm 2$ couplings which could trigger the decay. In chapter 3 we have considered the possibility of several different mechanisms contributing to the $(\beta\beta)_{0\nu}$-decay amplitude in the general case of CP non-conservation. The lepton

number violating (LNV) mechanisms discussed are light Majorana neutrino exchange, exchange of heavy Majorana neutrinos coupled to (V-A) currents, exchange of heavy Majorana neutrinos coupled to (V+A) currents, lepton charge non-conserving couplings in SUSY theories with R-parity breaking. Of the latter we have concentrated on the so-called "dominant gluino exchange" mechanism. Each of these mechanisms, described in chapter 2, is characterized by a specific fundamental LNV parameter, η_k^{LNV}. Using a multi-isotope approach one can constrain or even determine these parameters and possibly disentangle the mechanisms that could trigger $(\beta\beta)_{0\nu}$-decay. This method is valid in the general case of CP non-conservation.

Moreover, since the observation of $(\beta\beta)_{0\nu}$-decay of several different isotopes is crucial for obtaining information about the mechanism or mechanisms that induce the decay, in chapter 4 we investigate the possibility to discriminate between different pairs of CP non-conserving mechanisms inducing the $(\beta\beta)_{0\nu}$-decay by using data on $(\beta\beta)_{0\nu}$-decay half-lives of nuclei with largely different NMEs. The analysis we have presented is based on the fact that for each of the five single mechanisms discussed, the NMEs for ^{76}Ge, ^{82}Se, ^{100}Mo and ^{130}Te differ relatively little —being the relative difference between the NMEs of any two nuclei not exceeding 10%. The NMEs for ^{136}Xe instead differ significantly from those of ^{76}Ge, ^{82}Se, ^{100}Mo and ^{130}Te, being by a factor $\sim (1.3 - 2.5)$ smaller. This allows, in principle, to draw conclusions about the pair of non-interfering (interfering) mechanisms possibly inducing the $(\beta\beta)_{0\nu}$-decay from data on the half-lives of ^{136}Xe and of at least one (two) more isotope(s) which can be, e.g., any of the four, ^{76}Ge, ^{82}Se, ^{100}Mo and ^{130}Te.

The second topic addressed in this Thesis is the flavour problem in the neutrino sector, i.e., the issue related to the origin of the patterns of neutrino masses and mixing. At present, all the angles of the leptonic mixing matrix, the PMNS mixing matrix, are determined with a rather good precision. This constrains flavour models severely. Indeed, the discovery of a large reactor mixing angle $\theta_{13} \approx 0.15$, strongly disfavors many mixing patterns such as exact Tri-BiMaximal mixing (TBM), ($\theta_{23} = \pi/4$, $\sin\theta_{12} = 1/\sqrt{3}$ and $\theta_{13} = 0$), which is related to the flavor group A_4. Non-Abelian discrete flavor symmetries G_l which are broken in a non-trivial way to G_e and G_ν in the charged lepton and neutrino sector, respectively, are still considered to be an interesting possibility to explain the peculiar lepton mixing pattern. For instance, they can be used to predict at leading order in the neutrino sector the TBM which can then be perturbed through sizeable corrections coming form the charged lepton sector (i.e. from the diagonalization of the charged lepton mass matrix).

This idea has been developed in chapter 6 where we have described a unified model of flavour for quarks and leptons based on $SU(5)$ as grand unified (GUT) symmetry and T' as a discrete family symmetry. The model predicts the reactor neutrino mixing angle θ_{13} to be in the range determined by DayaBay, RENO and Double Chooz experiments, and all other mixing angles are predicted to have values within the experimental uncertainties. It implements a type I seesaw mechanism and from the breaking of the discrete family symmetry T' we obtain TBM in the neutrino sector. The relatively large value of θ_{13} is then generated entirely by corrections coming from the charged lepton sector. This is a generic effect in GUTs where Yukawa couplings are related to each other. In this model we have used recently proposed $SU(5)$ GUT relations between the down-type quark Yukawa matrix and the charged lepton Yukawa matrix to get the relatively large prediction for the reactor mixing angle θ_{13}. Due to the GUT structure

we can fit the quark masses and mixing parameters and the charged lepton masses, and using the latter we make definite predictions for the neutrino mass spectrum, the leptonic mixing angles and the leptonic CP violating phases. Our model is therefore testable in a variety of experiments.

On the other hand one could explain the leptonic mixing pattern directly investigating new symmetries, usually larger than the group S_4, which could predict the experimentally observed mixing parameters. In chapter 7 we have pursued such an attempt and we have discussed the "exceptional" finite groups $\Sigma(n\varphi)$, with $\varphi = 3$, i.e. $\Sigma(36 \times 3)$, $\Sigma(72 \times 3)$, $\Sigma(216 \times 3)$, $\Sigma(360 \times 3)$, which are subgroups of $SU(3)$. These four groups are interesting, since they all contain irreducible faithful three-dimensional representations and have several types of Abelian subgroups, suitable as G_e and G_ν. Since one of them, the group $\Sigma(360 \times 3)$, also comprises the Klein subgroups, neutrinos could also be Majorana particles. We find only a few patterns compatible with the experimental data on lepton mixing and predict the reactor mixing angle θ_{13} to be $0.1 \lesssim \theta_{13} \lesssim 0.2$. Interestingly, all these patterns lead to a CP conserving Dirac phase. Patterns which instead reveal CP violation tend to be not in agreement with the experimental data.

Concluding, there is no doubt that a new exciting era of neutrino physics is ahead of us. An intense experimental search has been planned to determine the neutrino mass hierarchy and the magnitude of CP violation in the leptonic sector. The latter is one the most challenging measurement from an experimental point of view. However a detection of CP violation in the leptonic sector would be extremely tantalizing since it will have an impact on neutrino mass models and as well it could be fundamental to constrain frameworks explaining the baryon asymmetry of the Universe.

More importantly, an eventual observation of a Majorana field would be a fundamental headway. This would mean that Nature admits the existence of particles which are identical to their anti-particles and, more importantly, it could point to the existence of New Physics, or in other words to new lepton number violating couplings in the Lagrangian of particle interactions. The data on $(\beta\beta)_{0\nu}$-decay, which will be available from the currently running experiments GERDA, EXO-200, KamLAND-Zen and from the CUORE experiment will be of crucial importance to identify the mechanism(s) triggering the decay if the latter will be observed. This will help to identify the New Physics beyond that predicted by the Standard Model associated with lepton charge non-conservation and the $(\beta\beta)_{0\nu}$-decay. If the $(\beta\beta)_{0\nu}$-decay will not be observed, the data from the $(\beta\beta)_{0\nu}$-decay experiments will be used to constrain the theories of neutrino mass generation predicting lepton charge non-conservation and massive Majorana neutrinos.

This is the right time to use all the available data for creating a common framework to describe the neutrino sector and possibly have hints of New Physics beyond that predicted by the standard theory and the $(\beta\beta)_{0\nu}$-decay results can serve as the Ariadne's thread for achieving this goal.

Appendix A

Basics of Discrete Groups

I Representations and Characters

A representation of G is a homomorphic map of elements of G onto matrices, $\Gamma(g)$ for g $\in$ G. The representation matrices should satisfy $\Gamma(a)\Gamma(b) = \Gamma(c)$ if $ab = c$ for $a, b, c \in$ G. The vector space v_j , on which representation matrices act, is called a representation space such as $\Gamma(g)_{ij}v_j$ $(j = 1, \cdots, n)$. The dimension n of the vector space v_j $(j = 1, \ldots, n)$ is called the dimension of the representation. A subspace in the representation space is called invariant subspace if $\Gamma(g)_{ij}v_j$ for any vector v_j in the subspace and any element g∈G also corresponds to a vector in the same subspace. If a representation has an invariant subspace, such a representation is called reducible. A representation is irreducible if it has no invariant subspace. In particular, a representation is called completely reducible if $\Gamma(g)$ for g $\in$ G are written as the following block diagonal form,

$$\begin{pmatrix} \Gamma^1(g) & 0 & & \\ 0 & \Gamma^2(g) & & \\ & & \ddots & \\ & & & \Gamma^r(g) \end{pmatrix} \tag{A.1}$$

where each $\Gamma^p(g)$ for $p = 1, \ldots, r$ is irreducible. Furthermore, every representation of a fine group is equivalent to a unitary representation. This implies that a reducible representation $\Gamma(g)$ is the direct sum of $\Gamma^p(g)$. The simplest (irreducible) representation is found that $\Gamma(g) = 1$ for all elements g, that is, a trivial singlet. The matrix representations satisfy the following orthogonality relation:

$$\sum_{g \in G} \Gamma^p(g)_{ij}\Gamma^q(g^{-1})_{kl} = \frac{h}{d_p}\delta_{pq}\delta_{il}\delta_{jk} \tag{A.2}$$

where h is the number of finite elements in G e.g. the *order* of G and d_p is the dimension of the representation $\Gamma^p(g)$.

Indeed if Γ^p and Γ^q are two unitary representations (UIRs) of a finite group G, the direct product $\Gamma^p \otimes \Gamma^q$ is in general reducible in such a way that $\Gamma^p \otimes \Gamma^q$ is reducible to a direct sum of UIRs. Indeed, one can write

$$\Gamma^p \otimes \Gamma^q = \sum_r \oplus n^r_{pq}\Gamma^r \tag{A.3}$$

where n^r_{pq} is the number of times that the UIR Γ^r appears in the direct sum, that is the *multiplicity*. The direct sum is known as the *Clebsch-Gordan series*.

The character $\chi_\Gamma(g)$ of a representation $\Gamma(g)$ is the trace of the representation matrix,

$$\chi_\Gamma(g) = tr\Gamma(g) = \sum_{j=1}^{d_p} \Gamma(g)_{jj}. \tag{A.4}$$

A representation is real if it has real characters and the representation matrices can be written as real matrices. If the representation has real characters but its representation matrices cannot be written in a real form, it is called pseudo-real. If the representation has complex characters, it is called complex and then also its representation matrices are complex. In all groups the number of complex representations is even, since each complex representation Γ has its complex conjugate $\underline{\Gamma}$. The representation matrices of $\underline{\Gamma}$ are the complex conjugated ones of Γ (up to a similarity transformation).

It can be proven that the multiplicity is given by:

$$n^r_{pq} = \frac{1}{h} \sum_{g \in G} \chi_p(g)\chi_q(g)\chi_r(g)^* \tag{A.5}$$

where $\chi^p(g)$, $\chi^q(g)$, $\chi^r(g)$ are the characters of Γ^p, Γ^q and Γ^r respectively. In order to determine the character table of a finite group one can use the following statements.

1. The elements $g^{-1}tg$ for $g \in G$ are called elements conjugate to the element t. The set including all elements conjugated to an element a of G, $\{g^{-1}tg, \forall g \in G\}$, is called a *conjugacy class*. All the elements in a conjugacy class have the same order a since

$$(gtg^{-1})^a = gt(g^{-1}g)t(g^{-1}g)\cdots tg^{-1} = gt^a g^{-1} = geg^{-1} = e. \tag{A.6}$$

   The conjugacy class including the identity e consists of the single element e.

2. If there are m_n n-dimensional UIR, the elements of the group in a given UIR $\Gamma(g)$ are represented by $(n \times n)$ matrices. The identity e is always represented by the $(n \times n)$ identity matrix and the character of $\chi_{\Gamma^p}(C_1)$ for the conjugacy class $C_1 = e$ is found to be n for the n-dimensional UIR.

3. A trivial singlet, $\Gamma(g) = 1$ for any $g \in G$, must always be included. Thus, the corresponding character satisfies $\chi_1(g) = 1$ for any $g \in G$.

4. One can show that the number of UIR must be equal to the number of conjugacy classes and thus:

$$\sum_n m_n = \sharp \quad \text{conjugacy classes.} \tag{A.7}$$

5. The characters are constant in a conjugacy class. Indeed, the element conjugate to a has the same character because of the property of the trace,

$$tr\Gamma(g^{-1}ag) = tr\left(\Gamma(g^{-1})\Gamma(a)\Gamma(g)\right) = tr\Gamma(a). \tag{A.8}$$

6. The characters of different UIR are orthonormal and different from each others. Indeed the characters satisfy the following orthonormality relation:

$$\sum_{g\in G} \chi_{\Gamma^p}(g)^* \chi_{\Gamma^q}(g) = h\delta_{pq}. \tag{A.9}$$

7. Defined one UIR, the characters of different conjugacy classes are orthonormal and different from each others. Indeed, they must satisfy the following orthogonality relation:

$$\sum_{p} \chi_{\Gamma^p}(g_i)^* \chi_{\Gamma^p}(g_j) = \frac{h}{n_i}\delta_{pq}\delta_{C_iC_j}. \tag{A.10}$$

where C_i denotes the conjugacy class of g_i and n_i denotes the number of elements in the conjugacy class C_i. One can use this orthogonality relation to write the following expression:

$$\sum_{p} |\chi_{\Gamma^p}(C_1)|^2 = \sum_{n} m_n n^2 = m_1 + 4m_2 + 9m_3 + \cdots = h, \tag{A.11}$$

where n is a natural number.

II Clebsch Gordan Coefficients

We can assume that the tensor representation $\Gamma^p \otimes \Gamma^q$ has the set $\{\psi^p_m \cdot \psi^q_n\}$ as a basis if all these elements are independent one from each others with $m = 1, \cdots d_p$ and $n = 1, \cdots d_q$. We call this basis a tensorial set. In general $\Gamma^p \otimes \Gamma^q$ is not a UIR, so the tensorial set is reducible. In other words, in the Hilbert space spanned by the basis $\{\psi^p_m \cdot \psi^q_n\}$ there are subspaces that are invariant under the transformations of the group G. Hence since $\Gamma^p \otimes \Gamma^q \sim \oplus_r \Gamma^r$, then for all r such that $n^r_{pq} \neq 0$ there are n^r_{pq} basis sets among the $\{\psi^p_m \cdot \psi^q_n\}$ for Γ^r, composed of linear combinations of the products of functions $\{\psi^p_m \cdot \psi^q_n\}$. We shall denote these basis functions by $\theta^{r,\alpha}_l$ where r indicates the irrep Γ^r, l the row index of the basis function ($l = 1 \cdots d_r$) and α is an index running as $\alpha = 1 \cdots n^r_{pq}$. We can write that the two basis set are related in the following way:

$$\{\psi^p_m \cdot \psi^q_n\} = \left(\begin{array}{cc|c} p & q & r,\alpha \\ m & n & l \end{array}\right)^* \theta^{r,\alpha}_l \tag{A.12}$$

where $\left(\begin{array}{cc|c} p & q & r,\alpha \\ m & n & l \end{array}\right)$ are defined as the *Clebsch-Gordan coefficients* (CG). The CG coefficients may be defined as well as the elements of a non-singular unitary matrix U such that

$$\Gamma^p \otimes \Gamma^q = U \left(\sum_r \oplus n^r_{pq} \Gamma^r \right) U^\dagger \tag{A.13}$$

Hence, the CG are, as a matter of fact, the entries of the $d_p d_q \times d_p d_q$ matrix U that allow to pass from a tensor reducible representation to a sum of UIRs. Since in case of UIRs, the matrix of CG coefficients is unitary one can write:

$$\left(\begin{array}{cc|c} p & q & r,\alpha \\ m & n & l \end{array}\right)^* = \left(\begin{array}{c|cc} r,\alpha & p & q \\ l & m & n \end{array}\right). \tag{A.14}$$

From a practical point of view, in a tensor product (read e.g $\mathbf{1}\otimes\mathbf{3}$, $\mathbf{2}\otimes\mathbf{2}$...) the CG coefficients represent the numbers that we must put behind the components of the final state (read e.g **1**, **2**, **3**...). Technically the CGs are computed as follows (details can be found in [176]). We define a function $A(r,l,k)_{mn,ij}$ as follows:

$$A(r,l,k)_{mn,ij}=\frac{d_r}{g}\sum_{g\in G}\Gamma^p(g)_{mi}\Gamma^q(g)_{nj}\Gamma^r(g)^*_{lk} \tag{A.15}$$

where r is the index that labels the Γ^r UIR, $l=1,\cdots,d_r$, $m=1,\cdots,d_p$, $n=1,\cdots,d_q$ while i,j,k, are free indices that run respectively as m,n,l.

II.I Case for CGs when $n^r_{pq}=1$

Define r. Let (i_1,j_1,k_1) be a set such that $A(r,k_1,k_1)_{i_1j_1,i_1j_1}\neq 0$. With this set (that will correspond to a phase convention) the CGs coefficients are defined as follows:

$$n^r_{pq}=1,\qquad \left(\begin{array}{cc|c} p & q & r,1\\ m & n & l\end{array}\right)=\frac{A(r,l,k_1)_{mn,i_1j_1}}{A(r,k_1,k_1)^{1/2}_{i_1j_1,i_1j_1}} \tag{A.16}$$

II.II Case for CGs when $n^r_{pq}=2$

Define r. Let (i_1,j_1,k_1) and (i_2,j_2,k_2) be sets such that $A(r,k_1,k_1)_{i_1j_1,i_1j_1}\neq 0$ and $A(r,k_2,k_2)_{i_2j_2,i_2j_2}\neq 0$. The CGs are determined through these expressions:

$$n^r_{pq}=2,\quad \left(\begin{array}{cc|c} p & q & r,2\\ m & n & l\end{array}\right)=\rho^{-1/2}\left(A(r,l,k_2)_{mn,i_2j_2}-KA(r,k_2,k_1)_{mn,i_1j_1}\right) \tag{A.17}$$

where the functions ρ and K are:

$$K=\frac{A(r,k_1,k_2)_{i_1j_1,i_2j_2}}{A(r,k_1,k_1)_{i_1j_1,i_1j_1}} \tag{A.18}$$

$$\rho=A(r,k_2,k_2)_{i_2j_2,i_2j_2}-\frac{|A(r,k_2,k_1)_{i_2j_2,i_1j_1}|^2}{A(r,k_1,k_1)_{i_1j_1,i_1j_1}} \tag{A.19}$$

III T' group

The T' group is the double covering group of the tetrahedral group A_4. This group can be described by the following algebraic relations,

$$s^2=r,\quad r^2=t^3=(st)^3=e,\quad rt=tr. \tag{A.20}$$

The closed algebra including r, s and t is the T' group and it consists of 24 elements that is the order of this group is $h=24$. The element r commutes with t and s hence for the Shur Lemma $r=\lambda\mathbf{1}_n$ in the n-UIR. The 24 elements of this group are classified into 7 conjugacy classes C_i (where the index i define the number of elements in the class and a is the order of the elements):

$$\begin{aligned}
C_1 : &\quad \{e\}, &\quad a = 1 \\
C_{1'} : &\quad \{r\}, &\quad a = 2 \\
C_4 : &\quad \{t, rsts, st, ts\}, &\quad a = 3 \\
C_{4'} : &\quad \{t^2, rtst, rt^2s, rst^2\} &\quad a = 3 \\
C_{4''} : &\quad \{rt, sts, rst, rts\}, &\quad a = 6 \\
C_{4'''} : &\quad \{rt^2, tst, t^2s, st^2\}, &\quad a = 6 \\
C_6 : &\quad \{s, rs, tst^2, t^2st, rtst^2, rt^2st\}, &\quad a = 4
\end{aligned} \tag{A.21}$$

We will use in the following the points 4-7 to determine charcaters and representations for the fundamental UIRs of the group T'.

UIR Determination From point 4 we notice that there are 7 different UIRs. The latter may be determined through relations 4 and 7(second equation):

$$\begin{aligned}
\sum_n m_n &= m_1 + m_2 + m_3 + \cdots = 7 \\
24 &= 1^2 m_1 + 2^2 m_2 + 3^2 m_3 + \cdots
\end{aligned} \tag{A.22}$$

The solution is $(m_1, m_2, m_3) = (3, 3, 1)$. We will denote these UIRs as $\mathbf{1}$, $\mathbf{1'}$, $\mathbf{1''}$, $\mathbf{2}$, $\mathbf{2'}$, $\mathbf{2''}$, $\mathbf{3}$.

Characters In order to determine characters we notice that, according to point 3, a singlet has always to be included for each $g \in T'$, hence we chose $\chi_{\Gamma^\alpha}(g) = 1$ for $\alpha = \mathbf{1}$. However we know that in the UIRs of T' there must be three different singlets so in order to classify them we may use the relation $t^3 = e$. From this it easy to see that the singlets representations have three possible values that are the third roots of the unity i.e. $\chi_\alpha(t) = 1, \omega, \omega^2$ with $\omega = e^{i2\pi/3}$ and $\alpha = \mathbf{1}, \mathbf{1'}, \mathbf{1''}$. We chose $\chi_{\mathbf{1}}(t) = 1$, $\chi_{\mathbf{1'}}(t) = \omega$ and $\chi_{\mathbf{1''}}(t) = \omega^2$. Next, since $s^4 = e$, there are four possibilities for $\chi_{\mathbf{1},\mathbf{1'},\mathbf{1''}}(s) = (i)^n$ $(n = 0, 1, 2, 3)$. However, since t and ts belong to the same conjugacy class, C_4, the character of these two elements must be the same so this requires $\chi_{\mathbf{1},\mathbf{1'},\mathbf{1''}}(s) = 1$ for singlets. Similarly, since rs and s belongs both to C_6 this means $\chi_{\mathbf{1},\mathbf{1'},\mathbf{1''}}(r) = 1$. Obviously the characters of $\mathbf{1}$, $\mathbf{1'}$, $\mathbf{1''}$ of the other classes are straightforward.
Let us study now the three doublet representations $\mathbf{2}$, $\mathbf{2'}$ and $\mathbf{2''}$ and the triplet $\mathbf{3}$. Since $[r, s] = [r, t] = 0$ by the Shur's Lemma

$$r_{\mathbf{2},\mathbf{2'},\mathbf{2''}} = \lambda_{\mathbf{2},\mathbf{2'},\mathbf{2''}} \begin{pmatrix} 1 & 0 \\ 0 & 1 \end{pmatrix}, \tag{A.23}$$

$$r_{\mathbf{3}} = \lambda_{\mathbf{3}} \begin{pmatrix} 1 & 0 & 0 \\ 0 & 1 & 0 \\ 0 & 0 & 1 \end{pmatrix}, \tag{A.24}$$

In addition, since $r^2 = e$ the constants may be $\lambda_{\mathbf{2},\mathbf{2'},\mathbf{2''}} = \pm 1$ and $\lambda_{\mathbf{3}} = \pm 1$. From point 7 we can write the following orthogonality relation (remember that $C_1 = \{e\}$ and $C_{1'} = \{r\}$):

$$\sum_p \chi_{\Gamma^p}(C_1)^* \chi_{\Gamma^p}(C_{1'}) = 1+1+1+2\chi_{\mathbf{2}}(r)+2\chi_{\mathbf{2'}}(r)+2\chi_{\mathbf{2''}}(r)+3\chi_{\mathbf{3}}(r) = 0 \quad \text{(A.25)}$$

where $\Gamma^p = \mathbf{1}, \mathbf{1'1''}, \mathbf{2}, \mathbf{2'}, \mathbf{2''}, \mathbf{3}$. One possible solution is $\chi_{\mathbf{2},\mathbf{2'},\mathbf{2''}}(r) = -2$ and $\chi_{\mathbf{3}}(r) = 3$. Hence for doublets and triplet the class $C_{1'} = \{r\}$ will be represented as follows:

$$r_{\mathbf{2},\mathbf{2'},\mathbf{2''}} = -\begin{pmatrix} 1 & 0 \\ 0 & 1 \end{pmatrix}, \quad r_{\mathbf{3}} = \begin{pmatrix} 1 & 0 & 0 \\ 0 & 1 & 0 \\ 0 & 0 & 1 \end{pmatrix} \quad \text{(A.26)}$$

Let us move on now to the next conjugacy class, $C_4 \supset t$. We would like to construct t as a diagonal matrix.[1] Since $t^3 = e$, the diagonal entries of the matrix have to be the third roots of unity, i.e. ω^n with $n = 0, 1, 2$. The element t can be written as:

$$\begin{pmatrix} \omega^l & 0 \\ 0 & \omega^k \end{pmatrix} \quad \text{(A.27)}$$

where $l, k = 0, 1, 2$. In order to have t different from the identity matrix $l \neq k$. Since $1+\omega+\omega^2 = 0$ the character will be $\chi_2(t) = \omega^l + \omega^k = -\omega^n$ whit $l \neq k \neq n$. The three doublets can be differentiated using different combinations as follows:

$$t_{\mathbf{2}} = \begin{pmatrix} \omega^2 & 0 \\ 0 & \omega \end{pmatrix}, \quad t_{\mathbf{2'}} = \begin{pmatrix} 1 & 0 \\ 0 & \omega^2 \end{pmatrix}, \quad t_{\mathbf{2''}} = \begin{pmatrix} \omega & 0 \\ 0 & 1 \end{pmatrix} \quad \text{(A.28)}$$

The characters result $\chi_{\mathbf{2}}(C_4) = -1$, $\chi_{\mathbf{2'}}(C_4) = -\omega$ and $\chi_{\mathbf{2''}}(C_4) = -\omega^2$

At this point it is straightforward to calculate the explicit forms of the characters of the conjugacy classes, $C_{4'}, C_{4''}$ and $C_{4'''}$. We need to compute finally the character for the class $C_6 \supset s$. We may consider again the relation of point 6 for the element s.

$$\sum_{g \in G} \chi_{\mathbf{1}}(g)^* \chi_{\mathbf{2}}(g) = 2 - 2 - 4 - 4 + 4 + 4 + 6\chi_{\mathbf{2}}(C_6) = 0 \quad \text{(A.29)}$$

Hence, $\chi_{\mathbf{2}}(C_6) = 0$. In a similar way one can derive $\chi_{\mathbf{2'}}(C_6) = 0$, $\chi_{\mathbf{2''}}(C_6) = 0$. The results are summarized in table A.1.
Finally we need only to compute the characters of the triplet. Consider that now all the characters for singlets and doublets representations are determined. Using again relations in point 7, for the classes $C_4, C_{4'}, C_{4''}, C_{4'''}$ we obtain:

[1] This requirement will be clear in the following, but we can anticipate that it is related to the fact in the model-building, when T' is broken, the diagonalized lepton mass matrix is clearly invariant under transformations that are themselves diagonal, hence we need a subgroup of T' (such that T' breaks into this subgroup) generated by a diagonal matrix, like t.

$$\begin{aligned}
\sum_p \chi_{\Gamma^p}(C_1)^* \chi_{\Gamma^p}(C_4) &= 1+\omega+\omega^2-2(1+\omega+\omega^2)+3\chi_{\mathbf{3}}(C_4)=0 \\
\sum_p \chi_{\Gamma^p}(C_1)^* \chi_{\Gamma^p}(C_{4'}) &= 1+\omega^2+\omega-2(1+\omega^2+\omega)+3\chi_{\mathbf{3}}(C_{4'})=0 \\
\sum_p \chi_{\Gamma^p}(C_1)^* \chi_{\Gamma^p}(C_{4''}) &= 1+\omega+\omega^2+2(1+\omega+\omega^2)+3\chi_{\mathbf{3}}(C_{4''})=0 \\
\sum_p \chi_{\Gamma^p}(C_1)^* \chi_{\Gamma^p}(C_{4'''}) &= 1+\omega^2+\omega+2(1+\omega^2+\omega)+3\chi_{\mathbf{3}}(C_{4'''})=0
\end{aligned} \tag{A.30}$$

that gives $\chi_{\mathbf{3}}(C_4), \chi_{\mathbf{3}}(C_{4'}), \chi_{\mathbf{3}}(C_{4''}), \chi_{\mathbf{3}}(C_{4'''}) = 0$.

We can write the 3×3 form of the t matrix that will be diagonal with null trace. We choose

$$t_{\mathbf{3}} = \begin{pmatrix} 1 & 0 & 0 \\ 0 & \omega & 0 \\ 0 & 0 & \omega^2 \end{pmatrix} \tag{A.31}$$

Next and last step is computing $\chi_{\mathbf{3}}(C_6) = -1$ which results again from relation at point 6:

$$\sum_{g \in G} \chi_{\mathbf{1}}(C_1)^* \chi_{\mathbf{3}}(C_6) = 3 + 3 + 6\chi_{\mathbf{3}}(C_6) = 0. \tag{A.32}$$

Furthermore we can write also the matrix of the element s that will have trace equal -1. We can use the following choices:

$$\begin{aligned}
&\mathbf{1} : t = 1, r = 1, s = 1; \\
&\mathbf{1}' : t = \omega, r = 1, s = 1; \\
&\mathbf{1}'' : t = \omega^2, r = 1, s = 1; \\
&\mathbf{2} : t = \begin{pmatrix} \omega^2 & 0 \\ 0 & \omega \end{pmatrix}, r = \begin{pmatrix} -1 & 0 \\ 0 & -1 \end{pmatrix}, s = \begin{pmatrix} -\frac{i}{\sqrt{3}} & -\sqrt{\frac{2}{3}}p \\ \sqrt{\frac{2}{3}}\bar{p} & \frac{i}{\sqrt{3}} \end{pmatrix}; \\
&\mathbf{2}' : t = \begin{pmatrix} 1 & 0 \\ 0 & \omega^2 \end{pmatrix}, r = \begin{pmatrix} -1 & 0 \\ 0 & -1 \end{pmatrix}, s = \begin{pmatrix} -\frac{i}{\sqrt{3}} & -\sqrt{\frac{2}{3}}p \\ \sqrt{\frac{2}{3}}\bar{p} & \frac{i}{\sqrt{3}} \end{pmatrix}; \\
&\mathbf{2}'' : t = \begin{pmatrix} \omega & 0 \\ 0 & 1 \end{pmatrix}, r = \begin{pmatrix} -1 & 0 \\ 0 & -1 \end{pmatrix}, s = \begin{pmatrix} -\frac{i}{\sqrt{3}} & -\sqrt{\frac{2}{3}}p \\ \sqrt{\frac{2}{3}}\bar{p} & \frac{i}{\sqrt{3}} \end{pmatrix}; \\
&\mathbf{3} : t = \begin{pmatrix} 1 & 0 & 0 \\ 0 & \omega & 0 \\ 0 & 0 & \omega^2 \end{pmatrix}, r = \begin{pmatrix} 1 & 0 & 0 \\ 0 & 1 & 0 \\ 0 & 0 & 1 \end{pmatrix}, s = \begin{pmatrix} -\frac{1}{3} & \frac{2\omega}{3} & \frac{2\omega^2}{3} \\ \frac{2\omega^2}{3} & -\frac{1}{3} & \frac{2\omega}{3} \\ \frac{2\omega}{3} & \frac{2\omega^2}{3} & -\frac{1}{3} \end{pmatrix}.
\end{aligned} \tag{A.33}$$

We use the definition of the representation of T' given in [138] in which ω and p are fixed to be respectively $\omega = e^{\frac{2i\pi}{3}}$ and $p = e^{\frac{i\pi}{12}}$.

T'	C_1	$C_{1'}$	C_4	$C_{4'}$	$C_{4''}$	$C_{4'''}$	C_6
$(\#\ C)$	(1)	(1)	(4)	(4)	(4)	(4)	(6)
$ord(C)$	1	2	6	3	3	6	4
$\chi_{\mathbf{1}}$	1	1	1	1	1	1	1
$\chi_{\mathbf{1'}}$	1	1	ω	ω^2	ω	ω^2	1
$\chi_{\mathbf{1''}}$	1	1	ω^2	ω	ω^2	ω	1
$\chi_{\mathbf{2}}$	2	-2	-1	-1	1	1	0
$\chi_{\mathbf{2'}}$	2	-2	$-\omega$	ω^2	ω	ω^2	0
$\chi_{\mathbf{2''}}$	2	-2	$-\omega^2$	$-\omega$	ω^2	ω	0
$\chi_{\mathbf{3}}$	3	3	0	0	0	0	-1

Table A.1: The character table of T' with $\omega = \exp(2\pi i/3)$ adapted from [109].

$$\mathbf{1} \otimes \Gamma^p = \Gamma^p, \quad \mathbf{1} \otimes \mathbf{1'}(\mathbf{1''}) = \mathbf{1'}(\mathbf{1''}), \quad \mathbf{1'} \otimes \mathbf{1'}(\mathbf{1''}) = \mathbf{1''}(\mathbf{1}), \quad \mathbf{1'}(\mathbf{1''}) \otimes \mathbf{1''} = \mathbf{1}(\mathbf{1'})$$
$$\mathbf{2} \otimes \mathbf{1'}(\mathbf{1''}) = \mathbf{2'}(\mathbf{2''}), \quad \mathbf{2'} \otimes \mathbf{1'}(\mathbf{1''}) = \mathbf{2''}(\mathbf{2}), \quad \mathbf{2''} \otimes \mathbf{1'}(\mathbf{1''}) = \mathbf{2}(\mathbf{2'})$$
$$\mathbf{2}(\mathbf{2'}) \otimes \mathbf{2}(\mathbf{2''}) = \mathbf{1} \oplus \mathbf{3}, \quad \mathbf{2'}(\mathbf{2}) \otimes \mathbf{2'}(\mathbf{2''}) = \mathbf{1''} \oplus \mathbf{3}, \quad \mathbf{2''}(\mathbf{2}) \otimes \mathbf{2''}(\mathbf{2'}) = \mathbf{1'} \oplus \mathbf{3}$$
$$\mathbf{3} \otimes \mathbf{1'}(\mathbf{1''}) = \mathbf{3}, \quad \mathbf{3} \otimes \mathbf{2} = \mathbf{2} \oplus \mathbf{2'} \oplus \mathbf{2''}, \quad \mathbf{3} \otimes \mathbf{2'}(\mathbf{2''}) = \mathbf{2'}(\mathbf{2''}) \oplus \mathbf{2''}(\mathbf{2}) \oplus \mathbf{2}(\mathbf{2'})$$
$$\mathbf{3} \otimes \mathbf{3} = \mathbf{1} \oplus \mathbf{1'} \oplus \mathbf{1''} \oplus \mathbf{3}_S \oplus \mathbf{3}_A$$

Table A.2: T' group: Clebsch-Gordan series $\Gamma^p \otimes \Gamma^q = \Gamma^q \otimes \Gamma^p$. Here $\Gamma^p = \mathbf{1}, \mathbf{2}, \mathbf{3}$

The Clebsch-Gordan series are defined in Table A.3.
We will denote the UIRs by their components in the following notation:

$$\mathbf{1} \sim a, \quad \mathbf{1'} \sim a', \quad \mathbf{1''} \sim a'' \quad \mathbf{3} \sim \begin{pmatrix} u_1 \\ u_2 \\ u_3 \end{pmatrix}, \begin{pmatrix} u'_1 \\ u'_2 \\ u'_3 \end{pmatrix}$$
$$\mathbf{2} \sim \begin{pmatrix} x_1 \\ x_2 \end{pmatrix}, \begin{pmatrix} x'_1 \\ x'_2 \end{pmatrix} \quad \mathbf{2'} \sim \begin{pmatrix} y_1 \\ y_2 \end{pmatrix}, \begin{pmatrix} y'_1 \\ y'_2 \end{pmatrix} \quad \mathbf{2''} \sim \begin{pmatrix} z_1 \\ z_2 \end{pmatrix}, \begin{pmatrix} z'_1 \\ z'_2 \end{pmatrix} \tag{A.34}$$

The CG coefficients are described in the Table A.3.

$$a \otimes \Gamma^p = a\Gamma^p, \quad a \otimes a'(a'') = a'(a''), \quad a' \otimes a'(a'') = a''(a), \quad a'(a'') \otimes a'' = a(a')$$

$$\begin{pmatrix} x_1 \\ x_2 \end{pmatrix}_{\mathbf{2}} \otimes a'(a'') = \begin{pmatrix} x_1 a'(a'') \\ x_2 a'(a'') \end{pmatrix}_{\mathbf{2'(2'')}}, \quad \begin{pmatrix} y_1 \\ y_2 \end{pmatrix}_{\mathbf{2'}} \otimes a'(a'') = \begin{pmatrix} y_1 a'(a'') \\ y_2 a'(a'') \end{pmatrix}_{\mathbf{2''(2)}}, \begin{pmatrix} z_1 \\ z_2 \end{pmatrix}_{\mathbf{2''}} \otimes a'(a'') = \begin{pmatrix} z_1 a'(a'') \\ z_2 a'(a'') \end{pmatrix}_{\mathbf{2(2')}}$$

$$\begin{pmatrix} x_1 \\ x_2 \end{pmatrix}_{\mathbf{2(2')}} \otimes \begin{pmatrix} x'_1 \\ x'_2 \end{pmatrix}_{\mathbf{2(2'')}} = \left(\frac{x_1 x'_2 - x_2 x'_1}{\sqrt{2}} \right)_{\mathbf{1}} \oplus \begin{pmatrix} \frac{(1-\mathrm{i})}{2}(x_1 x'_2 + x_2 x'_1) \\ \mathrm{i}\, x_1 x'_1 \\ x_2 x'_2 \end{pmatrix}_{\mathbf{3}}$$

$$\begin{pmatrix} y_1 \\ y_2 \end{pmatrix}_{\mathbf{2'(2)}} \otimes \begin{pmatrix} y'_1 \\ y'_2 \end{pmatrix}_{\mathbf{2'(2'')}} = \left(\frac{y_1 y'_2 - y_2 y'_1}{\sqrt{2}} \right)_{\mathbf{1''}} \oplus \begin{pmatrix} \mathrm{i}\, y_1 y'_1 \\ y_2 y'_2 \\ \frac{(1-\mathrm{i})}{2}(y_1 y'_2 + y_2 y'_1) \end{pmatrix}_{\mathbf{3}}$$

$$\begin{pmatrix} z_1 \\ z_2 \end{pmatrix}_{\mathbf{2''(2)}} \otimes \begin{pmatrix} z'_1 \\ z'_2 \end{pmatrix}_{\mathbf{2''(2')}} = \left(\frac{z_1 z'_2 - z_2 z'_1}{\sqrt{2}} \right)_{\mathbf{1'}} \oplus \begin{pmatrix} z_2 z'_2 \\ \frac{(1-\mathrm{i})}{2}(z_1 z'_2 + z_2 z'_1) \\ \mathrm{i}\, z_1 z'_1 \end{pmatrix}_{\mathbf{3}}$$

$$(a')_{\mathbf{1'}} \otimes \begin{pmatrix} u_1 \\ u_2 \\ u_3 \end{pmatrix}_{\mathbf{3}} = \begin{pmatrix} u_3 a' \\ u_1 a' \\ u_2 a' \end{pmatrix}_{\mathbf{3}}, \quad (a'')_{\mathbf{1''}} \otimes \begin{pmatrix} u_1 \\ u_2 \\ u_3 \end{pmatrix}_{\mathbf{3}} = \begin{pmatrix} u_2 a'' \\ u_3 a'' \\ u_1 a'' \end{pmatrix}_{\mathbf{3}}$$

$$\begin{pmatrix} x_1 \\ x_2 \end{pmatrix}_{\mathbf{2}} \otimes \begin{pmatrix} u_1 \\ u_2 \\ u_3 \end{pmatrix}_{\mathbf{3}} = \tfrac{1}{\sqrt{3}} \left[\begin{pmatrix} (1+\mathrm{i})x_2 u_2 + x_1 u_1 \\ (1-\mathrm{i})x_1 u_3 - x_2 u_1 \end{pmatrix}_{\mathbf{2}} \oplus \begin{pmatrix} (1+\mathrm{i})x_2 u_3 + x_1 u_2 \\ (1-\mathrm{i})x_1 u_1 - x_2 u_2 \end{pmatrix}_{\mathbf{2'}} \oplus \begin{pmatrix} (1+\mathrm{i})x_2 u_1 + x_1 u_3 \\ (1-\mathrm{i})x_1 u_2 - x_2 u_3 \end{pmatrix}_{\mathbf{2''}} \right]$$

$$\begin{pmatrix} y_1 \\ y_2 \end{pmatrix}_{\mathbf{2'}} \otimes \begin{pmatrix} u_1 \\ u_2 \\ u_3 \end{pmatrix}_{\mathbf{3}} = \tfrac{1}{\sqrt{3}} \left[\begin{pmatrix} (1+\mathrm{i})y_2 u_1 + y_1 u_3 \\ (1-\mathrm{i})y_1 u_2 - y_2 u_3 \end{pmatrix}_{\mathbf{2}} \oplus \begin{pmatrix} (1+\mathrm{i})y_2 u_2 + y_1 u_1 \\ (1-\mathrm{i})y_1 u_3 - y_2 u_1 \end{pmatrix}_{\mathbf{2'}} \oplus \begin{pmatrix} (1+\mathrm{i})y_2 u_3 + y_1 u_2 \\ (1-\mathrm{i})y_1 u_1 - y_2 u_2 \end{pmatrix}_{\mathbf{2''}} \right]$$

$$\begin{pmatrix} z_1 \\ z_2 \end{pmatrix}_{\mathbf{2''}} \otimes \begin{pmatrix} u_1 \\ u_2 \\ u_3 \end{pmatrix}_{\mathbf{3}} = \tfrac{1}{\sqrt{3}} \left[\begin{pmatrix} (1+\mathrm{i})z_2 u_3 + z_1 u_2 \\ (1-\mathrm{i})z_1 u_1 - z_2 u_2 \end{pmatrix}_{\mathbf{2}} \oplus \begin{pmatrix} (1+\mathrm{i})z_2 u_1 + z_1 u_3 \\ (1-\mathrm{i})z_1 u_2 - z_2 u_3 \end{pmatrix}_{\mathbf{2'}} \oplus \begin{pmatrix} (1+\mathrm{i})z_2 u_2 + z_1 u_1 \\ (1-\mathrm{i})z_1 u_3 - z_2 u_1 \end{pmatrix}_{\mathbf{2''}} \right]$$

$$\begin{aligned} \begin{pmatrix} u_1 \\ u_2 \\ u_3 \end{pmatrix}_{\mathbf{3}} \otimes \begin{pmatrix} u'_1 \\ u'_2 \\ u'_3 \end{pmatrix}_{\mathbf{3}} = {} & \tfrac{1}{\sqrt{3}} \left[(u_1 u'_1 + u_2 u'_3 + u_3 u'_2)_{\mathbf{1}} \oplus (u_1 u'_2 + u_2 u'_1 + u_3 u'_3)_{\mathbf{1'}} \oplus (u_1 u'_3 + u_2 u'_2 + u_3 u'_1)_{\mathbf{1''}} \right] \oplus \\ & \oplus \tfrac{1}{\sqrt{6}} \begin{pmatrix} 2u_1 u'_1 - u_2 u'_3 - u_3 u'_2 \\ 2u_3 u'_3 - u_1 u'_2 - u_2 u'_1 \\ 2u_2 u'_2 - u_1 u'_3 - u_3 u'_1 \end{pmatrix}_{\mathbf{3}} \oplus \tfrac{1}{\sqrt{2}} \begin{pmatrix} u_2 u'_3 - u_3 u'_2 \\ u_1 u'_2 - u_2 u'_1 \\ u_3 u'_1 - u_1 u'_3 \end{pmatrix}_{\mathbf{3}} \end{aligned}$$

Table A.3: The Clebsch–Gordan coefficients for the tensor products of T'.

Acknowledgements

There are many people I would like to thank at the end of this Ph.D. in SISSA.

First and foremost my supervisor Serguey T. Petcov who helped me and encouraged me during these years to develop myself as a scientist and whose guidance has been inspiring and enlightening from different point of view.

I acknowledge here Martin Spinrath for his helpful comments about a part of this Ph. D. Thesis. I would like to thank him above all for the really nice collaboration of these last two years.
I would like to thank Claudia Hagedorn for valuable comments about the second part of this manuscript and for her patience of teaching me new aspects of discrete groups that I was not aware of.
I would like to thank M.-C. Chen, A. Faessler, K. T. Mahanthappa, E. Molinaro, F. Simkovic, J. Vergados for fruitful collaborations.
I want to acknowledge Jacobo L. Pavon for interesting duscussions.

Special thanks go to Ivan Girardi for the great work we have been doing in the last months. A special thought goes to my present and old officemates: Giorgio Arcadi, Dario Bettoni, Giulio D'Odorico, Hani Santosa and Maryam Tavakoli with whom I shared the bad and the good news of everyday life and much more.

I acknowledge all the people of the APP, TPP and AP Sectors with whom I had the pleasure of exchanging opinions and create a nice environment both from a scientific and human point of view. I thank all the SISSA staff who make my stay in SISSA very enjoyable (Riccardo, thanks for all the burocratic help!).

And now maybe the most difficult part. Here I will not write names (also because I fear to forget some of them!). During these years, as a Ph.D., I had the great pleasure to meet fantastic people in SISSA with whom I spent great times.

To all these people, to my family, to those who, near or far away, are by my side, to those who leave forever, THANKS.

All this would have been impossible without you.

In My Life

There are places I'll remember all my life,
though some have changed.
Some forever not for better
some have gone and some remain.
All these places have their moments
with lovers and friends I still can recall.
Some are dead and some are living,
in my life I've loved them all.
But of all these friends and lovers
there is no one compares with you.
And these memories lose their meaning
when I think of love as something new.
Though I know I'll never lose affection
for people and things that went before
I know I'll often stop and think about them
in my life I love you more.

J. Lennon

Bibliography

[1] B. Pontecorvo. Mesonium and anti-mesonium. *Sov.Phys.JETP*, 6:429, 1957.

[2] B. Pontecorvo. Inverse beta processes and nonconservation of lepton charge. *Sov.Phys.JETP*, 7:172–173, 1958.

[3] Ziro Maki, Masami Nakagawa, and Shoichi Sakata. Remarks on the unified model of elementary particles. *Prog.Theor.Phys.*, 28:870–880, 1962.

[4] B. Pontecorvo. Neutrino Experiments and the Problem of Conservation of Leptonic Charge. *Sov.Phys.JETP*, 26:984–988, 1968.

[5] Ettore Majorana. Theory of the Symmetry of Electrons and Positrons. *Nuovo Cim.*, 14:171–184, 1937.

[6] K. Nakamura and S.T. Petcov. in Review of Particle Physics (RPP), J. Beringer *et al. Phys.Rev.*, D86:010001, 2012.

[7] Werner Rodejohann. Neutrino-less Double Beta Decay and Particle Physics. *Int.J.Mod.Phys.*, E20:1833–1930, 2011.

[8] Stephen F. King and Christoph Luhn. Neutrino Mass and Mixing with Discrete Symmetry. *Rept.Prog.Phys.*, 76:056201, 2013.

[9] S. M. Bilenky and S. T. Petcov. Massive neutrinos and neutrino oscillations. *Reviews of Modern Physics*, 59:671–754, July 1987.

[10] Peter Minkowski. $\mu \to e\,\gamma$ at a Rate of One Out of 1-Billion Muon Decays? *Phys.Lett.*, B67:421, 1977.

[11] P. Ramond M. Gell-Mann and R. Slansky. Supergravity. *ed. by D. Freedman and P. Van Nieuwenhuizen, North Holland, Amsterdam, pp. 315-321*, 1979.

[12] Tsutomu Yanagida. HORIZONTAL SYMMETRY AND MASSES OF NEUTRINOS. *Conf.Proc.*, C7902131:95–99, 1979.

[13] Rabindra N. Mohapatra and Goran Senjanovic. Neutrino Mass and Spontaneous Parity Violation. *Phys.Rev.Lett.*, 44:912, 1980.

[14] M. Fukugita and T. Yanagida. Baryogenesis Without Grand Unification. *Phys.Lett.*, B174:45, 1986.

[15] V.A. Kuzmin, V.A. Rubakov, and M.E. Shaposhnikov. On the Anomalous Electroweak Baryon Number Nonconservation in the Early Universe. *Phys.Lett.*, B155:36, 1985.

[16] G.F. Giudice, A. Notari, M. Raidal, A. Riotto, and A. Strumia. Towards a complete theory of thermal leptogenesis in the SM and MSSM. *Nucl.Phys.*, B685:89–149, 2004.

[17] W. Buchmuller, P. Di Bari, and M. Plumacher. Leptogenesis for pedestrians. *Annals Phys.*, 315:305–351, 2005.

[18] S.T. Petcov. On Pseudodirac Neutrinos, Neutrino Oscillations and Neutrinoless Double beta Decay. *Phys.Lett.*, B110:245–249, 1982.

[19] Guido Altarelli and Ferruccio Feruglio. Discrete Flavor Symmetries and Models of Neutrino Mixing. *Rev.Mod.Phys.*, 82:2701–2729, 2010.

[20] Hajime Ishimori, Tatsuo Kobayashi, Hiroshi Ohki, Yusuke Shimizu, Hiroshi Okada, et al. Non-Abelian Discrete Symmetries in Particle Physics. *Prog.Theor.Phys.Suppl.*, 183:1–163, 2010.

[21] S. M. Bilenky, J. Hosek, and S.T. Petcov. On Oscillations of Neutrinos with Dirac and Majorana Masses. *Phys.Lett.*, B94:495, 1980.

[22] K. Abe et al. Indication of Electron Neutrino Appearance from an Accelerator-produced Off-axis Muon Neutrino Beam. *Phys.Rev.Lett.*, 107:041801, 2011.

[23] P. Adamson et al. Search for the disappearance of muon antineutrinos in the NuMI neutrino beam. *Phys.Rev.*, D84:071103, 2011.

[24] Y. Abe et al. Indication for the disappearance of reactor electron antineutrinos in the Double Chooz experiment. *Phys.Rev.Lett.*, 108:131801, 2012.

[25] G. L. Fogli, E. Lisi, A. Marrone, A. Palazzo, and A. M. Rotunno. Evidence of $\theta_{13} \to 0$ from global neutrino data analysis. *Phys.Rev.D*, 84(5):053007, September 2011.

[26] F. P. An, J. Z. Bai, A. B. Balantekin, H. R. Band, D. Beavis, W. Beriguete, M. Bishai, S. Blyth, K. Boddy, R. L. Brown, and et al. Observation of Electron-Antineutrino Disappearance at Daya Bay. *Physical Review Letters*, 108(17):171803, April 2012.

[27] J.K. Ahn et al. Observation of Reactor Electron Antineutrino Disappearance in the RENO Experiment. *Phys.Rev.Lett.*, 108:191802, 2012.

[28] Mauro Mezzetto and Thomas Schwetz. θ_{13}: Phenomenology, present status and prospect. *J.Phys.*, G37:103001, 2010.

[29] G.L. Fogli, E. Lisi, A. Marrone, D. Montanino, A. Palazzo, et al. Global analysis of neutrino masses, mixings and phases: entering the era of leptonic CP violation searches. *Phys.Rev.*, D86:013012, 2012.

[30] M.C. Gonzalez-Garcia, Michele Maltoni, Jordi Salvado, and Thomas Schwetz. Global fit to three neutrino mixing: critical look at present precision. *JHEP*, 1212:123, 2012.

[31] V. M. Lobashev. The search for the neutrino mass by direct method in the tritium beta-decay and perspectives of study it in the project KATRIN. *Nuclear Physics A*, 719:153, May 2003.

[32] KATRIN: an experiment to determine the neutrino mass from the beta decay of tritium. 2013.

[33] The Scientific programme of Planck. 2006.

[34] P.A.R. Ade et al. Planck 2013 results. XVI. Cosmological parameters. 2013.

[35] Z. Hou, C.L. Reichardt, K.T. Story, B. Follin, R. Keisler, et al. Constraints on Cosmology from the Cosmic Microwave Background Power Spectrum of the 2500-square degree SPT-SZ Survey. 2012.

[36] R. Laureijs et al. Euclid Definition Study Report. 2011.

[37] Jan Hamann, Steen Hannestad, and Yvonne Y.Y. Wong. Measuring neutrino masses with a future galaxy survey. *JCAP*, 1211:052, 2012.

[38] Steven Weinberg. Varieties of Baryon and Lepton Nonconservation. *Phys.Rev.*, D22:1694, 1980.

[39] S.L. Glashow. THE FUTURE OF ELEMENTARY PARTICLE PHYSICS. *NATO Adv.Study Inst.Ser.B Phys.*, 59:687, 1980.

[40] M. Magg and C. Wetterich. NEUTRINO MASS PROBLEM AND GAUGE HIERARCHY. *Phys.Lett.*, B94:61, 1980.

[41] J. Schechter and J.W.F. Valle. Neutrino Masses in SU(2) x U(1) Theories. *Phys.Rev.*, D22:2227, 1980.

[42] George Lazarides, Q. Shafi, and C. Wetterich. Proton Lifetime and Fermion Masses in an SO(10) Model. *Nucl.Phys.*, B181:287, 1981.

[43] Rabindra N. Mohapatra and Goran Senjanovic. Neutrino Masses and Mixings in Gauge Models with Spontaneous Parity Violation. *Phys.Rev.*, D23:165, 1981.

[44] Robert Foot, H. Lew, X.G. He, and Girish C. Joshi. SEESAW NEUTRINO MASSES INDUCED BY A TRIPLET OF LEPTONS. *Z.Phys.*, C44:441, 1989.

[45] G. Racah. On the symmetry of particle and antiparticle. *Nuovo Cim.*, 14:322–328, 1937.

[46] S. M. Bilenky, S. Pascoli, and S. T. Petcov. Majorana neutrinos, neutrino mass spectrum, CP violation, and neutrinoless double β decay: The three-neutrino mixing case. *Phys.Rev.D*, 64(5):053010, September 2001.

[47] H.V. Klapdor-Kleingrothaus, I.V. Krivosheina, A. Dietz, and O. Chkvorets. Search for neutrinoless double beta decay with enriched Ge-76 in Gran Sasso 1990-2003. *Phys.Lett.*, B586:198–212, 2004.

[48] K. Eitel. Direct neutrino mass experiments. *Nucl.Phys.Proc.Suppl.*, 143:197–204, 2005.

[49] F. Piquemal. Future double beta decay experiments. *Nucl.Phys.B, Proc.Suppl.*, 235-236:273–280, 2013.

[50] Fedor Simkovic, Amand Faessler, Herbert Muther, Vadim Rodin, and Markus Stauf. The 0 nu bb-decay nuclear matrix elements with self-consistent short-range correlations. *Phys.Rev.*, C79:055501, 2009.

[51] Amand Faessler, G.L. Fogli, E. Lisi, V. Rodin, A.M. Rotunno, et al. QRPA uncertainties and their correlations in the analysis of 0 nu beta beta decay. *Phys.Rev.*, D79:053001, 2009.

[52] H.V. Klapdor-Kleingrothaus, A. Dietz, L. Baudis, G. Heusser, I.V. Krivosheina, et al. Latest results from the Heidelberg-Moscow double beta decay experiment. *Eur.Phys.J.*, A12:147–154, 2001.

[53] H.V. Klapdor-Kleingrothaus, A. Dietz, H.L. Harney, and I.V. Krivosheina. Evidence for neutrinoless double beta decay. *Mod.Phys.Lett.*, A16:2409–2420, 2001.

[54] M. Auger et al. Search for Neutrinoless Double-Beta Decay in ^{136}Xe with EXO-200. *Phys.Rev.Lett.*, 109:032505, 2012.

[55] A. Gando et al. Limit on Neutrinoless $\beta\beta$ Decay of Xe-136 from the First Phase of KamLAND-Zen and Comparison with the Positive Claim in Ge-76. *Phys.Rev.Lett.*, 110:062502, 2013.

[56] M. Agostini, M. Allardt, E. Andreotti, A.M. Bakalyarov, M. Balata, et al. Results on neutrinoless double beta decay of 76Ge from GERDA Phase I. 2013.

[57] A. Meroni, S.T. Petcov, and F. Simkovic. Multiple CP Non-conserving Mechanisms of $(\beta\beta)_{0\nu}$-Decay and Nuclei with Largely Different Nuclear Matrix Elements. *JHEP*, 1302:025, 2013.

[58] D.S. Delion, J. Dukelsky, and P. Schuck. Restoration of the Ikeda sum rule in selfconsistent quasiparticle random-phase approximation. *Phys.Rev.*, C55:2340–2344, 1997.

[59] Fedor Simkovic, Amand Faessler, and Petr Vogel. $0\nu\beta\beta$ nuclear matrix elements and the occupancy of individual orbits. *Phys.Rev.*, C79:015502, 2009.

[60] V.A. Rodin, Amand Faessler, F. Simkovic, and Petr Vogel. On the uncertainty in the 0 nu beta beta decay nuclear matrix elements. *Phys.Rev.*, C68:044302, 2003.

[61] V.A. Rodin, A. Faessler, F. Simkovic, and P. Vogel. Assessment of uncertainties in QRPA 0nu beta beta-decay nuclear matrix elements. *Nucl.Phys.*, A766:107–131, 2006.

[62] Fedor Simkovic, Amand Faessler, Vadim Rodin, Petr Vogel, and Jonathan Engel. Anatomy of nuclear matrix elements for neutrinoless double-beta decay. *Phys.Rev.*, C77:045503, 2008.

[63] Michael Duerr, Manfred Lindner, and Alexander Merle. On the Quantitative Impact of the Schechter-Valle Theorem. *JHEP*, 1106:091, 2011.

[64] Amand Faessler, A. Meroni, S.T. Petcov, F. Simkovic, and J. Vergados. Uncovering Multiple CP-Nonconserving Mechanisms of $(\beta\beta)_{0\nu}$-Decay. *Phys.Rev.*, D83:113003, 2011.

[65] Aurora Meroni, S.T. Petcov, and Martin Spinrath. A SUSY SU(5)xT' Unified Model of Flavour with large θ_{13}. *Phys.Rev.*, D86:113003, 2012.

[66] Claudia Hagedorn, Aurora Meroni, and Lorenzo Vitale. Mixing Patterns from the Groups Sigma (n phi). 2013.

[67] S. Pascoli and S.T. Petcov. Majorana Neutrinos, Neutrino Mass Spectrum and the $|(\beta\beta)_{0\nu}| \sim 10^{-3}$ eV Frontier in Neutrinoless Double Beta Decay. *Phys.Rev.*, D77:113003, 2008.

[68] S. Pascoli and S.T. Petcov. The SNO solar neutrino data, neutrinoless double beta decay and neutrino mass spectrum. *Phys.Lett.*, B544:239–250, 2002.

[69] S. Pascoli and S.T. Petcov. The SNO solar neutrino data, neutrinoless double beta decay and neutrino mass spectrum: Addendum. *Phys.Lett.*, B580:280–289, 2004.

[70] Samoil M. Bilenky, S. Pascoli, and S.T. Petcov. Majorana neutrinos, neutrino mass spectrum, CP violation and neutrinoless double beta decay. 2. Mixing of four neutrinos. *Phys.Rev.*, D64:113003, 2001.

[71] S. Pascoli, S. T. Petcov, and L. Wolfenstein. Searching for the CP-violation associated with Majorana neutrinos. *Physics Letters B*, 524:319–331, January 2002.

[72] Samoil M. Bilenky, C. Giunti, C.W. Kim, and S.T. Petcov. Short baseline neutrino oscillations and neutrinoless (Beta Beta) decay in schemes with an inverted mass spectrum. *Phys.Rev.*, D54:4432–4444, 1996.

[73] S. Pascoli, S.T. Petcov, and T. Schwetz. The Absolute neutrino mass scale, neutrino mass spectrum, majorana CP-violation and neutrinoless double-beta decay. *Nucl.Phys.*, B734:24–49, 2006.

[74] J. Schechter and J. W. F. Valle. Neutrinoless double-β decay in SU(2)×U(1) theories. *Pys.Rev.D*, 25:2951–2954, June 1982.

[75] E. Takasugi. Can the neutrinoless double beta decay take place in the case of Dirac neutrinos? *Physics Letters B*, 149:372–376, December 1984.

[76] Fedor Simkovic, John Vergados, and Amand Faessler. Few active mechanisms of the neutrinoless double beta-decay and effective mass of Majorana neutrinos. *Phys.Rev.*, D82:113015, 2010.

[77] A. Halprin, S.T. Petcov, and Simon Peter Rosen. EFFECTS OF LIGHT AND HEAVY MAJORANA NEUTRINOS IN NEUTRINOLESS DOUBLE BETA DECAY. *Phys.Lett.*, B125:335, 1983.

[78] Vladimir Tello, Miha Nemevsek, Fabrizio Nesti, Goran Senjanovic, and Francesco Vissani. Left-Right Symmetry: from LHC to Neutrinoless Double Beta Decay. *Phys.Rev.Lett.*, 106:151801, 2011.

[79] M. Hirsch, H.V. Klapdor-Kleingrothaus, and S.G. Kovalenko. Supersymmetry and neutrinoless double beta decay. *Phys.Rev.*, D53:1329–1348, 1996.

[80] F. Simkovic, G. Pantis, J.D. Vergados, and Amand Faessler. Additional nucleon current contributions to neutrinoless double beta decay. *Phys.Rev.*, C60:055502, 1999.

[81] R.N. Mohapatra. New Contributions to Neutrinoless Double beta Decay in Supersymmetric Theories. *Phys.Rev.*, D34:3457–3461, 1986.

[82] J.D. Vergados. NEUTRINOLESS DOUBLE BETA DECAY WITHOUT MAJORANA NEUTRINOS IN SUPERSYMMETRIC THEORIES. *Phys.Lett.*, B184:55, 1987.

[83] M. Hirsch, H.V. Klapdor-Kleingrothaus, and S.G. Kovalenko. New constraints on R-parity broken supersymmetry from neutrinoless double beta decay. *Phys.Rev.Lett.*, 75:17–20, 1995.

[84] Amand Faessler, Sergei Kovalenko, Fedor Simkovic, and Joerg Schwieger. Dominance of pion exchange in R-parity violating supersymmetry contributions to neutrinoless double beta decay. *Phys.Rev.Lett.*, 78:183–186, 1997.

[85] Amand Faessler, Sergey Kovalenko, and Fedor Simkovic. Pions in nuclei and manifestations of supersymmetry in neutrinoless double beta decay. *Phys.Rev.*, D58:115004, 1998.

[86] A. Wodecki and Wieslaw A. Kaminski. Limits on R-parity nonconservation in MSSM with gauge mediated supersymmetry breaking from the neutrinoless double beta decay. *Phys.Rev.*, C59:1232–1236, 1999.

[87] Andrzej Wodecki, Wieslaw A. Kaminski, and Fedor Simkovic. Grand unified theory constrained supersymmetry and neutrinoless double beta decay. *Phys.Rev.*, D60:115007, 1999.

[88] Gary Prezeau, M. Ramsey-Musolf, and Petr Vogel. Neutrinoless double beta decay and effective field theory. *Phys.Rev.*, D68:034016, 2003.

[89] Amand Faessler, Sergey Kovalenko, and Fedor Simkovic. Bilinear R-parity violation in neutrinoless double beta decay. *Phys.Rev.*, D58:055004, 1998.

[90] M. Hirsch, J.C. Romao, and J.W.F. Valle. Bilinear R-parity violating SUSY: Neutrinoless double beta decay in the light of solar and atmospheric neutrino data. *Phys.Lett.*, B486:255–262, 2000.

[91] M. Hirsch and J.W.F. Valle. Neutrinoless double beta decay in supersymmetry with bilinear R parity breaking. *Nucl.Phys.*, B557:60–78, 1999.

[92] M. Hirsch, H. V. Klapdor-Kleingrothaus, and S. G. Kovalenko. Erratum: On the SUSY accompanied neutrino exchange mechanism of neutrinoless double beta decay. *Physics Letters B*, 381:488, February 1996.

[93] H. Pas, M. Hirsch, and H.V. Klapdor-Kleingrothaus. Improved bounds on SUSY accompanied neutrinoless double beta decay. *Phys.Lett.*, B459:450–454, 1999.

[94] Amand Faessler, Thomas Gutsche, Sergey Kovalenko, and Fedor Simkovic. Pion dominance in RPV SUSY induced neutrinoless double beta decay. *Phys.Rev.*, D77:113012, 2008.

[95] Amand Faessler, Sergey Kovalenko, Fedor Simkovic, and Joerg Schwieger. Pion exchange currents in neutrinoless double beta decay and limits on supersymmetry. *Phys.Atom.Nucl.*, 61:1229–1235, 1998.

[96] M.K. Cheoun, A. Bobyk, A. Faessler, F. Simkovic, and G. Teneva. Neutron proton pairing in light nuclei and two neutrino double beta decay. *Nucl.Phys.*, A561:74–94, 1993.

[97] H. V. Klapdor-Kleingrothaus. Neutrino mass from laboratory: contribution of double beta decay to the neutrino mass matrix. *Nuclear Physics B Proceedings Supplements*, 100:309–313, May 2001.

[98] Alexander S. Barabash. NEMO 3 double beta decay experiment: Latest results. *J.Phys.Conf.Ser.*, 173:012008, 2009.

[99] C. Arnaboldi et al. Results from a search for the 0 neutrino beta beta-decay of Te-130. *Phys.Rev.*, C78:035502, 2008.

[100] S. M. Bilenky and S. T. Petcov. Nuclear Matrix Elements of $0\nu\beta\beta$-Decay: Possible Test of the Calculations. *ArXiv High Energy Physics - Phenomenology e-prints*, May 2004.

[101] L. Baudis, A. Dietz, G. Heusser, H.V. Klapdor-Kleingrothaus, I.V. Krivosheina, et al. Limits on the Majorana neutrino mass in the 0.1-eV range. *Phys.Rev.Lett.*, 83:41–44, 1999.

[102] A.S. Barabash and V.B. Brudanin. Investigation of double beta decay with the NEMO-3 detector. *Phys.Atom.Nucl.*, 74:312–317, 2011.

[103] H.V. Klapdor-Kleingrothaus and I.V. Krivosheina. The evidence for the observation of 0nu beta beta decay: The identification of 0nu beta beta events from the full spectra. *Mod.Phys.Lett.*, A21:1547–1566, 2006.

[104] J.D. Vergados, H. Ejiri, and F. Simkovic. Theory of Neutrinoless Double Beta Decay. *Rept.Prog.Phys.*, 75:106301, 2012.

[105] Amand Faessler, G.L. Fogli, E. Lisi, A.M. Rotunno, and F. Simkovic. Multi-Isotope Degeneracy of Neutrinoless Double Beta Decay Mechanisms in the Quasi-Particle Random Phase Approximation. *Phys.Rev.*, D83:113015, 2011.

[106] C.D. Froggatt and Holger Bech Nielsen. Hierarchy of Quark Masses, Cabibbo Angles and CP Violation. *Nucl.Phys.*, B147:277, 1979.

[107] C.S. Lam. Symmetry of Lepton Mixing. *Phys.Lett.*, B656:193–198, 2007.

[108] A. Blum, C. Hagedorn, and M. Lindner. Fermion Masses and Mixings from Dihedral Flavor Symmetries with Preserved Subgroups. *Phys.Rev.*, D77:076004, 2008.

[109] Walter Grimus and Patrick Otto Ludl. Finite flavour groups of fermions. *J.Phys.*, A45:233001, 2012.

[110] L. Wolfenstein. Oscillations Among Three Neutrino Types and CP Violation. *Phys.Rev.*, D18:958–960, 1978.

[111] P. F. Harrison, D. H. Perkins, and W. G. Scott. Tri-bimaximal mixing and the neutrino oscillation data. *Physics Letters B*, 530:167–173, March 2002.

[112] Z.-z. Xing. Nearly tri-bimaximal neutrino mixing and CP violation. *Physics Letters B*, 533:85–93, May 2002.

[113] X.-G. He and A. Zee. Some simple mixing and mass matrices for neutrinos. *Physics Letters B*, 560:87–90, May 2003.

[114] Lawrence J. Hall, Hitoshi Murayama, and Neal Weiner. Neutrino mass anarchy. *Phys.Rev.Lett.*, 84:2572–2575, 2000.

[115] David Marzocca, Serguey T. Petcov, Andrea Romanino, and Martin Spinrath. Sizeable θ_{13} from the charged lepton sector in SU(5), (tri-)bimaximal neutrino mixing and Dirac CP violation. *JHEP*, 1111:009, 2011.

[116] Stefan Antusch and Vinzenz Maurer. Large neutrino mixing angle θ_{13}^{MNS} and quark-lepton mass ratios in unified flavour models. *Phys.Rev.*, D84:117301, 2011.

[117] Stefan Antusch, Christian Gross, Vinzenz Maurer, and Constantin Sluka. $\theta_{13}^{PMNS} = \theta_C/\sqrt{2}$ from GUTs. *Nucl.Phys.*, B866:255–269, 2013.

[118] Stefan Antusch and Martin Spinrath. New GUT predictions for quark and lepton mass ratios confronted with phenomenology. *Phys.Rev.*, D79:095004, 2009.

[119] Alfredo Aranda, Christopher D. Carone, and Richard F. Lebed. Maximal neutrino mixing from a minimal flavor symmetry. *Phys.Rev.*, D62:016009, 2000.

[120] Reinier de Adelhart Toorop, Ferruccio Feruglio, and Claudia Hagedorn. Finite Modular Groups and Lepton Mixing. *Nucl.Phys.*, B858:437–467, 2012.

[121] Reinier de Adelhart Toorop, Ferruccio Feruglio, and Claudia Hagedorn. Discrete Flavour Symmetries in Light of T2K. *Phys.Lett.*, B703:447–451, 2011.

[122] Stephen F. King, Christoph Luhn, and Alexander J. Stuart. A Grand Delta(96) x SU(5) Flavour Model. *Nucl.Phys.*, B867:203–235, 2013.

[123] Shao-Feng Ge, Duane A. Dicus, and Wayne W. Repko. Residual Symmetries for Neutrino Mixing with a Large θ_{13} and Nearly Maximal δ_D. *Phys.Rev.Lett.*, 108:041801, 2012.

[124] D. Hernandez and A. Yu. Smirnov. Lepton mixing and discrete symmetries. *Phys.Rev.*, D86:053014, 2012.

[125] D. Hernandez and A. Yu. Smirnov. Discrete symmetries and model-independent patterns of lepton mixing. 2012.

[126] Bo Hu. Neutrino Mixing and Discrete Symmetries. *Phys.Rev.*, D87:033002, 2013.

[127] Guido Altarelli and Ferruccio Feruglio. Tri-bimaximal neutrino mixing, A(4) and the modular symmetry. *Nucl.Phys.*, B741:215–235, 2006.

[128] I. de Medeiros Varzielas, S.F. King, and G.G. Ross. Tri-bimaximal neutrino mixing from discrete subgroups of SU(3) and SO(3) family symmetry. *Phys.Lett.*, B644:153–157, 2007.

[129] Xiao-Gang He, Yong-Yeon Keum, and Raymond R. Volkas. A(4) flavor symmetry breaking scheme for understanding quark and neutrino mixing angles. *JHEP*, 0604:039, 2006.

[130] Ferruccio Feruglio, Claudia Hagedorn, and Robert Ziegler. Lepton Mixing Parameters from Discrete and CP Symmetries. 2012.

[131] Martin Holthausen, Manfred Lindner, and Michael A. Schmidt. CP and Discrete Flavour Symmetries. *JHEP*, 1304:122, 2013.

[132] G. A. Miller, H. F. Blichfeldt, L. E. Dickson,. "Theory and Applications of Finite Groups", John Wiley & Sons, New York, 1916, and Dover Edition, 1961; W. M. Fairbairn, T. Fulton, and W. H. Klink, J. Math. Phys. **5** (1964) 1038.

[133] I.P. Ivanov and E. Vdovin. Classification of finite reparametrization symmetry groups in the three-Higgs-doublet model. *Eur.Phys.J.*, C73:2309, 2013.

[134] P.H. Frampton, S.T. Petcov, and W. Rodejohann. On deviations from bimaximal neutrino mixing. *Nucl.Phys.*, B687:31–54, 2004.

[135] Andrea Romanino. Charged lepton contributions to the solar neutrino mixing and theta(13). *Phys.Rev.*, D70:013003, 2004.

[136] K.A. Hochmuth, S.T. Petcov, and W. Rodejohann. U(PMNS) = U**dagger (l) U(nu). *Phys.Lett.*, B654:177–188, 2007.

[137] P.H. Frampton and T.W. Kephart. Simple nonAbelian finite flavor groups and fermion masses. *Int.J.Mod.Phys.*, A10:4689–4704, 1995.

[138] Ferruccio Feruglio, Claudia Hagedorn, Yin Lin, and Luca Merlo. Tri-bimaximal Neutrino Mixing and Quark Masses from a Discrete Flavour Symmetry. *Nucl.Phys.*, B775:120–142, 2007.

[139] Gui-Jun Ding. Fermion Mass Hierarchies and Flavor Mixing from T-prime Symmetry. *Phys.Rev.*, D78:036011, 2008.

[140] J.-Q. Chen and P.-D. Fan. Algebraic expressions of the Clebsch-Gordon coefficients of the point group $T^{\dagger}$. *Journal of Mathematical Physics*, 39:5519–5535, October 1998.

[141] Mu-Chun Chen and K.T. Mahanthappa. Group Theoretical Origin of CP Violation. *Phys.Lett.*, B681:444–447, 2009.

[142] Mu-Chun Chen and K.T. Mahanthappa. CKM and Tri-bimaximal MNS Matrices in a $SU(5) \times^{(d)} T$ Model. *Phys.Lett.*, B652:34–39, 2007.

[143] Mu-Chun Chen, Kalyana T. Mahanthappa, Aurora Meroni, and S.T. Petcov. Predictions for Neutrino Masses, $\beta\beta_{0\nu}$-Decay and Lepton Flavor Violation in a SUSY $SU(5) \times T'$ Model of Flavour. 2011.

[144] Mu-Chun Chen and K.T. Mahanthappa. From CKM matrix to MNS matrix: A Model based on supersymmetric SO(10) x U(2)(F) symmetry. *Phys.Rev.*, D62:113007, 2000.

[145] S. Antusch, S. F. King, M. Malinský, and M. Spinrath. Quark mixing sum rules and the right unitarity triangle.

[146] Howard Georgi and C. Jarlskog. A New Lepton - Quark Mass Relation in a Unified Theory. *Phys.Lett.*, B86:297–300, 1979.

[147] M. Carena, M. Olechowski, S. Pokorski, and C. E. M. Wagner. Electroweak symmetry breaking and bottom-top Yukawa unification. *Nuclear Physics B*, 426:269–300, September 1994.

[148] L. J. Hall, R. Rattazzi, and U. Sarid. Top quark mass in supersymmetric SO(10) unification.

[149] R. Hempfling. Yukawa coupling unification with supersymmetric threshold corrections.

[150] T. Blavzek, S. Raby, and S. Pokorski. Finite supersymmetric threshold corrections to CKM matrix elements in the large tan β regime. *prd*, 52:4151–4158, October 1995.

[151] Stefan Antusch and Martin Spinrath. Quark and lepton masses at the GUT scale including SUSY threshold corrections. *Phys.Rev.*, D78:075020, 2008.

[152] Stefano Profumo. Neutralino dark matter, b tau Yukawa unification and nonuniversal sfermion masses. *Phys.Rev.*, D68:015006, 2003.

[153] Stefan Antusch, Lorenzo Calibbi, Vinzenz Maurer, and Martin Spinrath. From Flavour to SUSY Flavour Models. *Nucl.Phys.*, B852:108–148, 2011.

[154] Zhi-zhong Xing, He Zhang, and Shun Zhou. Updated Values of Running Quark and Lepton Masses. *Phys.Rev.*, D77:113016, 2008.

[155] H. Leutwyler. Nonlattice determinations of the light quark masses. *Nucl.Phys.Proc.Suppl.*, 94:108–115, 2001.

[156] Stefan Antusch, Joern Kersten, Manfred Lindner, Michael Ratz, and Michael Andreas Schmidt. Running neutrino mass parameters in see-saw scenarios. *JHEP*, 0503:024, 2005.

[157] J. Charles, A. Höcker, H. Lacker, S. Laplace, F. R. Diberder, J. Malclés, J. Ocariz, M. Pivk, and L. Roos. CP violation and the CKM matrix: assessing the impact of the asymmetric B factories. *European Physical Journal C*, 41:1–131, May 2005.

[158] M. Bona, M. Ciuchini, E. Franco, V. Lubicz, G. Martinelli, F. Parodi, M. Pierini, P. Roudeau, C. Schiavi, L. Silvestrini, V. Sordini, A. Stocchi, and V. Vagnoni. Improved determination of the CKM angle α from $B \to \pi\pi$ decays. *Phys.Rev.D*, 76(1):014015, July 2007.

[159] C. Hagedorn, E. Molinaro, and S. T. Petcov. Majorana phases and leptogenesis in see-saw models with A_4 symmetry. *Journal of High Energy Physics*, 9:115, September 2009.

[160] C. Jarlskog. Commutator of the quark mass matrices in the standard electroweak model and a measure of maximal CP nonconservation. *Physical Review Letters*, 55:1039–1042, September 1985.

[161] C. Jarlskog. A basis independent formulation of the connection between quark mass matrices, CP violation and experiment. *Zeitschrift fur Physik C Particles and Fields*, 29:491–497, September 1985.

[162] P. I. Krastev and S. T. Petcov. Resonance amplification and T-violation effects in three-neutrino oscillations in the earth. *Physics Letters B*, 205:84–92, April 1988.

[163] S. Antusch, J. Kersten, M. Lindner, and M. Ratz. Running neutrino masses, mixings and CP phases: analytical results and phenomenological consequences. *Nuclear Physics B*, 674:401–433, December 2003.

[164] Ivo de Medeiros Varzielas and Luca Merlo. Ultraviolet Completion of Flavour Models. *JHEP*, 1102:062, 2011.

[165] S. Antusch, S. F. King, C. Luhn, and M. Spinrath. Right unitarity triangles and tri-bimaximal mixing from discrete symmetries and unification. *Nuclear Physics B*, 850:477–504, September 2011.

[166] C.S. Lam. Finite Symmetry of Leptonic Mass Matrices. *Phys.Rev.*, D87:013001, 2013.

[167] Roman Zwicky and Thomas Fischbacher. On discrete Minimal Flavour Violation. *Phys.Rev.*, D80:076009, 2009.

[168] Martin Holthausen, Kher Sham Lim, and Manfred Lindner. Lepton Mixing Patterns from a Scan of Finite Discrete Groups. *Phys.Lett.*, B721:61–67, 2013.

[169] Martin Holthausen and Kher Sham Lim. Quark and Leptonic Mixing Patterns from the Breakdown of a Common Discrete Flavor Symmetry. 2013.

[170] Stephen F. King, Thomas Neder, and Alexander J. Stuart. Lepton Mixing Predictions from Delta($6n^2$) Family Symmetry. 2013.

[171] E. O'Brien H.U. Besche, B. Eick. GAP, "GAP – Groups, Algorithms, and Programming, Version 4.5.5", (2012), `http://www.gap-system.org`; H. U. Besche, B. Eick, E. O'Brien, "SmallGroups- library of all 'small' groups, GAP package, Version included in GAP 4.5.5", (2002), `http://www.gap-system.org/Packages/sgl.html`.

[172] W. Grimus and P.O. Ludl. Principal series of finite subgroups of SU(3). *J.Phys.*, A43:445209, 2010.

[173] Alexander Merle and Roman Zwicky. Explicit and spontaneous breaking of SU(3) into its finite subgroups. *JHEP*, 1202:128, 2012.

[174] C.C. Nishi. Generalized CP symmetries in $\Delta(27)$ flavor models. 2013.

[175] Amihay Hanany and Yang-Hui He. NonAbelian finite gauge theories. *JHEP*, 9902:013, 1999.

[176] P. M. van Den Broek and J. F. Cornwell. Clebsch-Gordan coefficients of symmetry groups. *physica status solidi (b)*, 90 part 1:211224, 1978.